Naval Research Laboratory
Washington, DC 20375-5320

NRL/MR/7130--94-7623

Sonar Dome Reliability XIX: Data Analysis of the USS Kauffman Sonar Rubber Dome

J. F. COVEY

Physical Acoustics Branch
Acoustics Division

D. WEAVER

SFA, Inc.

November 14, 1994

Approved for public release; distribution unlimited.

REPORT DOCUMENTATION PAGE

Form Approved
OMB No. 0704-0188

1. AGENCY USE ONLY *(Leave Blank)*

2. REPORT DATE

Noveber 14, 1994

3. REPORT TYPE AND DATES COVERED

Memo 5-1-94 to 9-14-94

4. TITLE AND SUBTITLE

Sonar Dome Reliability XIX: Data Analysis of the USS Kauffman Sonar Rubber Dome

5. FUNDING NUMBERS

6. AUTHOR(S)

J. F. Covey and D. B. Weaver*

7. PERFORMING ORGANIZATION NAME(S) AND ADDRESS(ES)

Naval Research Laboratory
Washington, DC 20375-5320

8. PERFORMING ORGANIZATION REPORT NUMBER

NRL/MR/7130--94-7623

9. SPONSORING/MONITORING AGENCY NAME(S) AND ADDRESS(ES)

Naval Sea Systems Command
Code 91W4D
Washington, DC 20362-5000

10. SPONSORING/MONITORING AGENCY REPORT NUMBER

11. SUPPLEMENTARY NOTES

*SFA, Inc.

12a. DISTRIBUTION/AVAILABILITY STATEMENT

Approved for public release; distribution unlimited.

12b. DISTRIBUTION CODE

13. ABSTRACT *(Maximum 200 words)*

In August of 1992, a new Sonar Rubber Dome (SRD), instrumented with sensors for the Sonar Dome Acoustic Deflection Measurement System, was installed aboard the USS Kauffman (FFG-59). The modification and deployment of the Sonar Dome Acoustic Deflection Measurement System to measure the deflection behavior of the SRD was an ambitious first time effort intended to provide calibration data for the University of Washington Applied Physics Laboratory's SRD finite element model. The purpose of this report is to relate the findings of the data taken from FFG-59's SRD. This will include a comparison between the predictions of University of Washington Applied Physics Laboratory's finite element model and NRL's measurements. While the results from this comparison cannot be considered conclusive, they do suggest, from a dynamic perspective, that the SRD may be more rigid than initially predicted.

14. SUBJECT TERMS

Acoustic	Sonar domes
Time-of-Flight	Keel domes
Deflection measurement	

15. NUMBER OF PAGES

159

16. PRICE CODE

17. SECURITY CLASSIFICATION OF REPORT	18. SECURITY CLASSIFICATION OF THIS PAGE	19. SECURITY CLASSIFICATION OF ABSTRACT	20. LIMITATION OF ABSTRACT
UNCLASSIFIED	UNCLASSIFIED	UNCLASSIFIED	UL

NSN 7540-01-280-5500

Standard Form 298 (Rev. 2-89)
Prescribed by ANSI Std 239-18
298-102

CONTENTS

Sonar Dome Reliability XIX: Data Analysis of the USS Kauffman Sonar Rubber Dome

1.0 Introduction

In August of 1992, a new Sonar Rubber Dome (SRD), serial #022, instrumented with sensors for the Sonar Dome Acoustic Deflection Measurement System (SDADMS), was installed aboard the USS Kauffman (FFG–59). This marked the third ship–board deployment of the SDADMS, but in a highly modified configuration. This was the first time that it would be used to test a SRD, since the two previous deployments of the SDADMS had been to test Sonar Dome Rubber Windows (SDRW's).

The purpose of this report is to relate the findings of the data taken from FFG–59's SRD. This will include a comparison between the predictions of the University of Washington Applied Physics Laboratory's (UW/APL) Finite Element Model (FEM) and NRL's measurements.

1.1 Maine Shakedown Test

In October and November of 1992, two sea tests were performed on FFG–59's SRD, as previously documented[1]. The first of these sea tests occurred on October 21–22, 1992, during a post dry–dock shakedown. It was intended that this first sea test serve as a training cruise for the new SRD test personnel. As such the test was an unqualified success.

Among the many data runs taken, the most informative were acquired between 0856 and 1430, on October 21. Fourteen data runs were taken during this period as FFG–59 performed independent maneuvers in rough seas. The exact sea conditions are not known, since the environmental data acquisition program, "SEAB7"[2], was not ready for use, and since FFG–59 has been unresponsive to our requests to provide the necessary quartermaster's log information from this time period. It is known that the seas were quite rough and that the ship was probably traveling at low speed.

The data runs from the Maine Shakedown test, that will be referred to in this report, are MAXL1– MAXL6 and MAXRUF1–MAXRUF8. All fourteen data runs use the same 125 transducer scan pattern. As previously noted, there was no environmental data recorded. As such, this limits the usefulness of the information provided by these data runs. The most salient feature of this series of data runs is that they provide the most comprehensive information about the FFG–59 SRD's characteristic deflection behavior.

This data has been used in an in–house developed, animated 3-dimensional visualization program, called "srdvwr"[2], which reveals some of the SRD's modal movement patterns

Manuscript approved October 5, 1994.

(see Figure 12). In this report, the Maine Shakedown data will be used to contrast observations from the following Antigua sea test.

1.2 Antigua Sea Test

During the period of November 15–25, 1992, deflection measurements were made on FFG–59's SRD as the ship transited from Newport, R.I. to Antigua in the British West Indies (see Table 1). During this period, 27 data runs were taken, from numerous scan groups which variously include 65 of the 128 total deflection measurement transducers installed. Most data runs scanned from 8 to 16 transducers, with two data runs using up to 24 unique transducers.

As previously documented[1], the acoustic deflection measurement equipment behaved irregularly. This made the data acquisition process quite challenging. During the brief periods when FFG–59's SQS–56 sonar was not active, NRL test personnel acquired as much data as possible. Much of this time, though, was spent diagnosing equipment problems and creating new transducer scan groups.

It wasn't known until much later, after careful data screening and iterative processing, that nearly all of the data contained anomalies that are difficult to explain. It was further discovered that the sample rate of the environmental data was much lower than had been expected (see Appendix H). This would later prove to be a problem when UW/APL used the environmental data to test the accuracy of their SRD FEM. The data analysis challenge, then, was to recover as much meaningful data as possible from this apparently contaminated data set.

2.0 Data Processing

Before discussing data run specifics, it is essential to review the methodology used for data collection and data reduction.

2.1 Data Collection

The acoustic deflection measurement process involves the measurement of an acoustic signal's propagation, in time, through water. In particular, this refers to measuring the elapsed time from when a driver transducer, which is mounted on the inner surface of an SRD, is excited, to the time when the acoustic wave from this driver transducer is sensed by a fixed array of receiving hydrophones (see Figure 1).

These "time–of–flight" or time–interval events are measured by a group of four interval timers, which individually relay their readings to the system computer through their own private interfaces. The system computer stores the time–interval measurements in temporary memory, called buffers. Each interval timer has a separate buffer allocated to it. When the buffer memories fill with time–interval measurements, the computer flushes the buffers into a program array and continues to store incoming time–interval measurements in the appropriate buffers.

Table 1: Antigua Sea Trial Data Summary

File Name	Transducer Scan Pattern	Approx Sea State	Date: Nov. 1992	Time	Course Change (deg)	Ship Speed (knots)	Max. Roll (deg)	Sound Velocity (m/s)
ANT_16D1	ANT16	1	15	22:01	0	0.0	1	1450.00
ANT16_D2	ANT16	1	15	22:17	0	0.0	1	1450.00
ANT16_2_D1	ANT16_2	1	16	10:45	1	20.0	2	1457.17
A16_3D1	ANT16_3	1	17	13:32	1	14.0	1	1466.49
ANT_16_3D2	ANT16_3	1	18	1:24	0	8.0	3	1471.78
SM00_16D1	SM00	1	18	1:32	0	8.0	2	1471.50
SM01_16D1	SM01	1	18	1:35	1	8.0	3	1471.48
SM02_16D1	SM02	1	18	1:46	0	8.0	3	1471.41
SM120_7D1	SM120_7	1	18	1:53	4	6.5	1	1471.19
LAST16_D1	LAST16	1	18	1:56	1	6.5	1	1471.19
SM00_16D2	SM00	1	18	8:16	0	3.3	1	1470.96
ANT_16_3D3	ANT16_3	2	18	9:18	4	18.3	4	1470.74
ANT16_3D5	ANT16_3	1	18	13:03	0	18.0	2	1469.23
ANT16_2D2	ANT16_2	1	18	16:29	3	14-20.0	2	1468.86
ANT16D1	ANT16	1	18	16:45	1	13.6	1	1468.69
BANT16_4D1	ANT16_4	2	19	22:11	1	6.3	4	1491.65
BASM02_16D1	SM02	1	20	8:41	1	2.4	3	1493.70
BANT16_4D2	ANT16_4	3	20	12:19	4	5.0	9	1491.87
BANT16_4D3	ANT16_4	3	20	12:24	5	5.0	11	1491.87
BA0001_16D1	A0001_16	2	20	12:50	2	3.0	5	1491.82
BA0001_16D2	A0001_16	3	20	15:52	5	5.6	12	1491.74
BA16_2D3	ANT16_2	3	20	18:26	7	4.2	10	1492.63
CA2_27D1	CA2_27	3	20	22:42	74	2.8	9	1494.19
CFA2_27D1	FA2_27	4	21	8:45	6	4.4	14	1498.08
CFA3_27D7	FA3_27	4	21	22:40	10	5.5	16	1499.34
CFA2_27D8	FA2_27	3	21	23:16	8	4.0	9	1499.77
DF3_27D9	FA3_27	4	22	20:40	7	6.4	15	1503.67
EANT_4_16D1	ANT16_4	3	23	6:33	7	6.0	12	1504.94
FFA3_27D10	FA3_27	3	23	15:54	21	2.0	7	1506.18

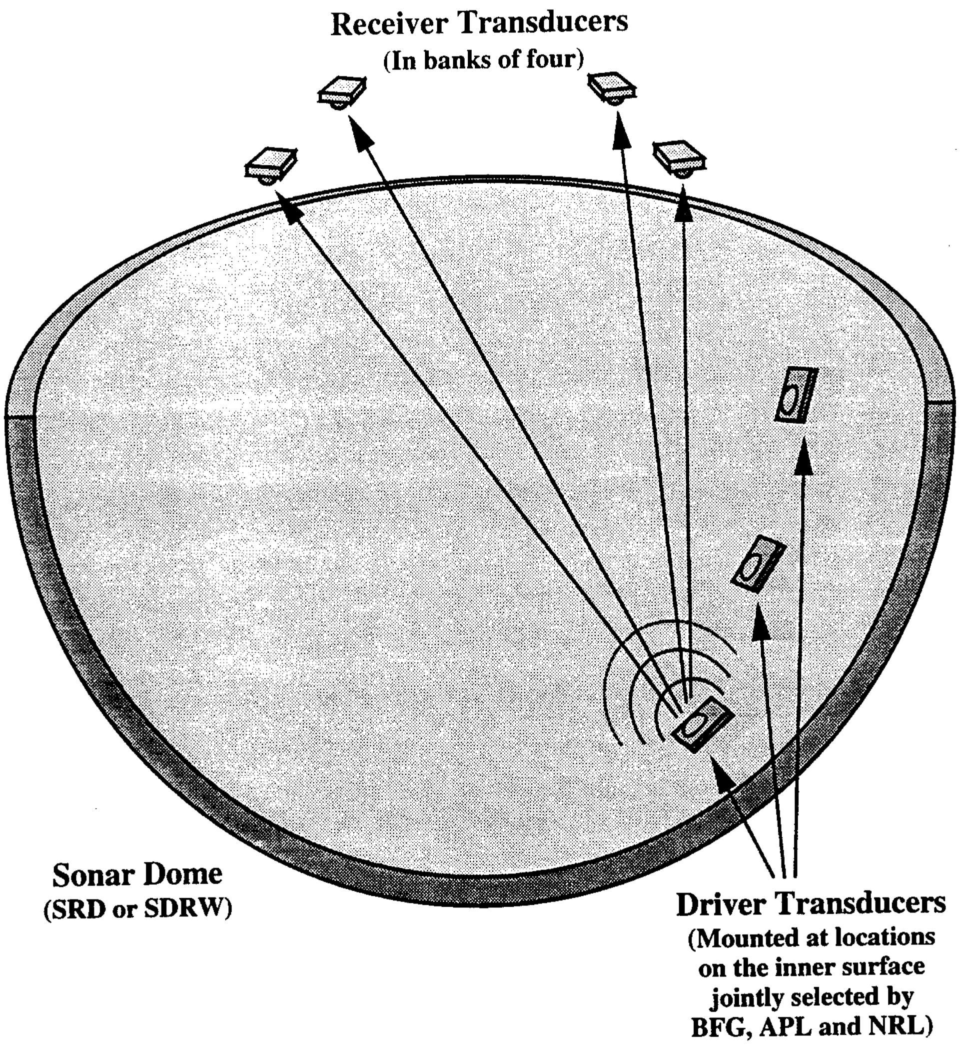

FIGURE 1. Ultrasonic Time–of–Flight Measurement

One of the error monitoring features of the data acquisition process involves checking the buffers to ensure that they all hold the same number of readings. Infrequently, one or more of the four interval timers will miss a timing event, usually due to a drop in received acoustic signal intensity. If such an event occurs, the computer must abort the data acquisition run. This is necessary because the timers must be run asynchronously to obtain the high data throughput required. This means that if one timer misses an event, the missed event cannot be backtracked through buffer memory, and the entire data run therefore becomes unintelligible.

This condition occurred a few times during the Maine Shakedown test and was thought, at that time, to be due to the rough seas. From a system operator's perspective, the situation would call for re–initiating the data run. If the condition became persistent, the system operator would be required to run a diagnostic routine to determine which driver transducer was dropping out. The system operator would then create a new scan pattern that either increased the associated receiver hydrophone amplifier gain for that driver transducer, or completely cull the troublesome driver transducer from the scan pattern.

During the Antigua sea test, driver transducer drop–out was a chronic condition, which necessitated creating numerous scan patterns based upon a predecessor. Table 2 illustrates this with scan patterns ANT16, ANT16_2, ANT16_3 and ANT16_4. Scan pattern LAST16 is identical to ANT16 with the exception that different gain settings were assigned to the computer controlled amplifier for certain driver transducers in the scan pattern.

Once data had been successfully collected, the system operator could then run a data continuity checking routine, in the main data acquisition program "SEADUAL16Y"[2], that would provide several statistical graphs that showed the degree of dispersion in the "time–of–flight" data. This program served as a good diagnostic for determining a confidence level for the data. As such, the Antigua data showed a lot of dispersion, giving an immediate indication that the deflection measurement system was not performing in a reliable manner. This early indication initiated a sequence of actions that focused on correcting the system performance.

2.2 Data Reduction

With the commencement of the SDRW deflection measurement test on the USS Yorktown (CG–48) in July, 1989, it was quickly understood that data–reduction would become a significant, time consuming task. Commercial data processing programs, such as DSP Development Corporation's DADiSP®, were investigated but they lacked the ability to perform specific tasks that were unique to deflection measurement data processing. General purpose data processing programs are primarily intended for processing entire data records and are not conducive to the manipulation of individual data points which may be corrupted. With this understanding, an in–house data screening program was developed, called "GROOM" (see Figure 13).

The primary feature of "GROOM" was that it permitted data outliers to be identified and corrected by a human operator. Outliers in deflection measurement data are represented by unexpected trigger events. This might mean that the system interval timer in question was not triggered by the intended acoustic signal.

Outliers typically occur individually and can be corrected by averaging the two nearest neighbor data points. Outliers can also occur in groups. It has been found that group outliers often contain deflection information that is displaced by a fixed time constant. Correction of group outliers consists of determining the beginning and end of the group and shifting the outlying data by the fixed time constant.

After the FFG–59 SRD tests, "GROOM"[2] was significantly enhanced and modified. New semi–automated routines were added to help find and correct outliers with minimal human intervention. Several criteria for outlier correction still required human input. The primary criterion was in determining the base line from which outliers were identified. This was aided by the addition of a sample coordinate conversion routine which, on demand, con-

Table 2: Transducer Scan Pattern Index

Scan Pattern	1	2	3	4	5	6	7	8	9	10	11	12	13	14	15	16	17	18	19	20	21	22	23	24	25	26	27
ANT16	50	92	15	71	29	66	65	75	51	79	83	86	70	99	85	108											
ANT16_2	50	92	15	71	29	66	65	75	76	51	79	83	86	70	85	108											
ANT16_3	50	92	15	71	29	66	65	75	4	51	70	85	108	50	92	15											
SM00	60	21	44	41	59	40	24	31	23	58	45	22	7	42	68	43											
SM01	9	105	116	114	61	82	106	74	118	78	69	101	32	115	46	98											
SM02	50	72	87	67	92	15	128	71	29	66	65	80	75	76	4	51											
SM120	117	57	16	39	17	18	53	55	117	57	16	39	17	18	53	55											
LAST16	50	92	15	71	29	66	65	75	51	79	83	86	70	99	85	108											
ANT16_4	50	92	71	29	66	75	92	66	79	83	70	79	79	79	79	79											
A0001_16	21	59	40	31	42	68	82	106	74	118	78	69	115	46	98	50											
CA2_27	50	72	87	67	92	15	67	71	29	66	65	75	67	51	95	79	127	83	86	70	67	85	108	67	67	67	67
FA2_27	50	72	87	67	92	15	71	29	66	50	75	51	95	79	50	83	86	70	85	108	21	50	58	42	43	82	106
FA3_27	50	72	87	67	92	15	71	29	66	50	75	51	67	79	50	67	86	70	85	108	67	50	67	67	67	67	67

Note: The numeric values in the table refer to the SRD sensor location number as established by B.F. Goodrich and modified by NRL.

verted the "time–of–flight" information, from a specified data sample of the four interval timer records, into four sets of Cartesian coordinates.

There were many cases in the Antigua data runs where there were as many outliers in a given record as there were "good" data points. It became ambiguous as to which data points were outliers and which data points were not. With the introduction of displayed reference coordinates to "GROOM", the sample coordinate conversion provided an indispensable guide to correcting what might have been hopelessly garbled data records.

As the post processing of data continued, it was repeatedly discovered that "GROOM" had to be modified to enable correction of increasingly subtle anomalies in the data.

2.2.1 Coordinate Conversions

To explain the coordinate conversion process, it is necessary to review some of the preparations that led to the FFG–59 sea tests. B. F. Goodrich was tasked, by NAVSEA 91W4D, to produce a CAD data base of an ideal SRD, and a Cartesian coordinate set of the proposed driver transducer locations.

It was important to establish an ideal set of driver transducer location coordinates, via CAD software, to serve as a starting point for equipment installation planning, and post sea test data processing. Unfortunately, these ideal coordinates could not completely translate into physical reality. This was due, in part, to small variances between the hand–fabricated SRD and the CAD model. Other variances with the ideal coordinate base came from the process of installing the driver transducers on the inner surface of the SRD.

This process involved meticulously drawing a coordinate grid on the inner surface of the SRD to facilitate accurate placement of the driver transducers. The compound curvature of the SRD's surface made drawing straight lines a distinct challenge. It was also discovered, during the grid layout process, that the ends of the SRD drooped by approximately one half inch, while the SRD was installed in its shipping fixture. This half inch droop translated into as much as one inch of error in grid placement on the fore and aft sloped surfaces.

2.2.2 Receiver Positioning

The accuracy of the deflection measurements were heavily dependent upon the accurate positioning of the deflection measurement system's receiver arrays. A total of ten, 4 hydrophone, receiver arrays were installed in FFG–59's SRD to accommodate deflection measurements of over 75% of the SRD's entire inner surface (see Figures 14 and 15). An in–house computer visualization package, called "srd"[2], was developed to determine the optimal placement and angle of focus for each of the ten receiver arrays (see Figures 16 and 17).

Unfortunately, when it came to the actual installation of the receiver arrays on FFG–59, dry–dock scheduling restrictions limited the equipment installation personnel to the use of measuring tape and line–of–sight estimates while working under very *unfavorable* conditions. This situation caused an undetermined amount of error in receiver placement.

In 1988, NRL, developed a triangulation algorithm that permitted reliable conversion of time–of–flight measurements into Cartesian coordinates (See Appendix F). This algorithm, formulated by Dr. Kin W. Ng, of SFA, Inc., under NRL contract, used a flexible relative origin scheme to accommodate the irregular geometry of the SDRW compartment on CG–48.

Dr. Ng's routine was later adapted to the SRD geometry. The adaptation of the algorithm was heavily dependent upon *accurate* physical placement of the receiver arrays, since each array had its own relative origin that had to be translated by a *known* distance to the SRD's common origin. When the receiver arrays were finally installed on FFG–59, the uncertainty in their placement introduced coordinate transformation problems that caused significant complications, leading to delays in the subsequent post sea test data conversion process.

The best method for minimizing the receiver array positioning uncertainties was to measure SRD deflections with respect to a "zero deflection" pierside data run, rather than the ideal coordinate set established by B. F. Goodrich. The "zero deflection" pierside data run, MAXD1000, became the default pierside reference basis. The B.F. Goodrich ideal reference coordinates were later used as a basis in the in–house developed computer animated 3–D visualization program, "srdvwr"[2], with the differential pierside reference–based deflection values superimposed over these points.

The pierside reference basis worked quite well with the Maine Shakedown data. However, the Antigua data exhibited significant anomalies for which the pierside reference basis couldn't account.

3.0 Deflection Data

After processing several Antigua deflection data files, it became apparent that the data exhibited many anomalies. The most notable anomalies were static offsets, suggesting that the SRD had permanently shifted to starboard by 1 to 3 inches and aft by 1 to 2 inches, with respect to the pierside "zero deflection" reference.

This eventually led to the creation of the transducer specific summary graphs which plotted a given transducer's average deflection, in Cartesian coordinates, with respect to the pierside reference, for each data run in which the transducer was used (see Appendix A). The most remarkable feature in the graph was the disparity in behavior between the Maine Shakedown and the Antigua sea tests. The Maine Shakedown data, as well as the pierside data runs, are all well correlated with the pierside reference. Virtually all of the Antigua data runs exhibit a marked divergence from the pierside reference.

3.1 Cause of the Disparity

It is thought that the *disparity* exhibited in the Antigua data may be due to a combination of two effects. The first effect would be *water intrusion* into underwater electrical cable connections. This may have severely degraded the excitation pulse to the driver transducers, or it may have severely degraded the received signal from the receiver hydrophones. The second possible effect may have been *electromagnetic interference* from shipboard systems, such as the SQS–56 sonar.

3.1.1 Water Intrusion

The possibility of water intrusion into electrical connections in the SRD is very likely. When final connections were being made in dry–dock, the SDADMS underwater electronic modules had been exposed to grit from sand–blasting and paint droplets from the nearby spray–painting of epoxy based paint on FFG–59's hull.

Every reasonable precaution had been taken to prevent contamination of the electrical connectors, from sealing the exposed connections with duct tape, to complete replacement of all water–proofing o–rings at the last possible moment. However, the dry–dock schedule was very tight with spray–painting and sand–blasting continuing, round the clock, even during the final cable connection process at 0300 in the morning.

It is very difficult to predict what the effects of water intrusion can be without knowing the degree of pervasiveness. Slight intrusion, affecting one circuit can lead to corrosive build–up between contacts, and therefore degradation of signal transmission. Large scale intrusion can lead to the establishment of ground loops and even short circuits.

If a short circuit were the case then no data could be acquired from the affected circuit. A ground loop would add a DC bias to the circuit, which may have happened. However, if the DC bias were persistent then no data could be acquired from the affected circuit. An intermittent ground loop would cause random DC shifts in the affected circuit which could cause spurious interval–timer trigger events. Some of the Antigua data exhibited this property. In this case the affected data record would have been eliminated in "GROOM", and therefore would have no further effect in the data conversion process.

A corrosive build–up would cause increasing signal attenuation, which would necessitate higher amplifier gain settings. This may also have happened. In this case, a steadily degrading signal would cause a time shift from the expected trigger point. This will be discussed in section 3.2.

3.1.2 Electro–Magnetic Interference

When the deflection measurement system's custom electronics were being developed and tested, the work could only be realistically performed off ship. This limited the range of conditions which the developer could simulate. After the deflection measurement system was installed on FFG–59, it was discovered that when the SQS–56 sonar was energized, even in the passive mode, a considerable amount of electrical interference was detected from the deflection measurement system's sensitive electronics. The deflection measurement personnel tried to filter out as much of the electronic interference as possible but it is somewhat likely that the SQS–56 sonar did disturb the sea test measurements by causing periodic electromagnetically coupled noise spikes that may have resulted in unexpected interval–timer trigger events.

This is only a somewhat likely case since the deflection measurement system performed nominally during the Maine Shakedown even while the SQS–56 sonar was energized. What is unknown is the cumulative effects of the SQS–56 sonar operating in the active mode. When FFG–59's SQS–56 sonar went active, often without prior warning, the deflection measurement personnel would shutdown the deflection measurement system to minimize permanent equipment damage. It is difficult to quantify what, if any, long term effect the SQS–56 sonar, or any of FFG–59's other electronic equipment may have had on the SRD deflection measurements.

3.2 Time Shifts

Under normal operating conditions, the intensity of the received signal does not vary significantly. There are certain circumstances that can perturb the acquired data, even when the deflection measurement system electronics are functioning properly.

Regardless of the cause, one observed result was the appearance of *time shifts* in some received signals. These may also have been caused by an increase in receiver hydrophone pre–amplifier gain. The input to each interval timer had a computer controlled pre–amplifier associated with it. During a data acquisition run, the deflection measurement system's computer controller would set the pre–amplifier gain to a pre–defined level associated with a given driver–transducer/receiver–hydrophone combination.

As the Antigua sea test progressed, deflection measurement system personnel found that it was frequently necessary to increase the assigned pre–amplifier gain for many driver–transducer/receiver–hydrophone combinations, to ensure continuous acquisition of data. These changes to pre–amplifier gain settings often caused the system interval timers to trigger at a different point on a received acoustic wave packet than what was originally recorded in the pier–side zero–deflection reference data set. These pre–amplifier gain changes therefore often caused *time shifts* in the Antigua data runs.

Figure 2 illustrates these two cases

- In the case of a signal attenuated by contact corrosion, the associated interval–timer could trigger off a later peak in the received waveform packet. This could cause a delayed trigger of a multiple of approximately 5 micro seconds.
- In the case of increased computer controlled amplifier gain, the associated interval timer might trigger off an earlier peak in the received waveform packet. This could cause a premature trigger of a multiple of approximately 5 micro seconds.

Figure 2 illustrates the analog waveform processing that takes place between a receiver hydrophone and the input to the associated interval timer. The received signal passes

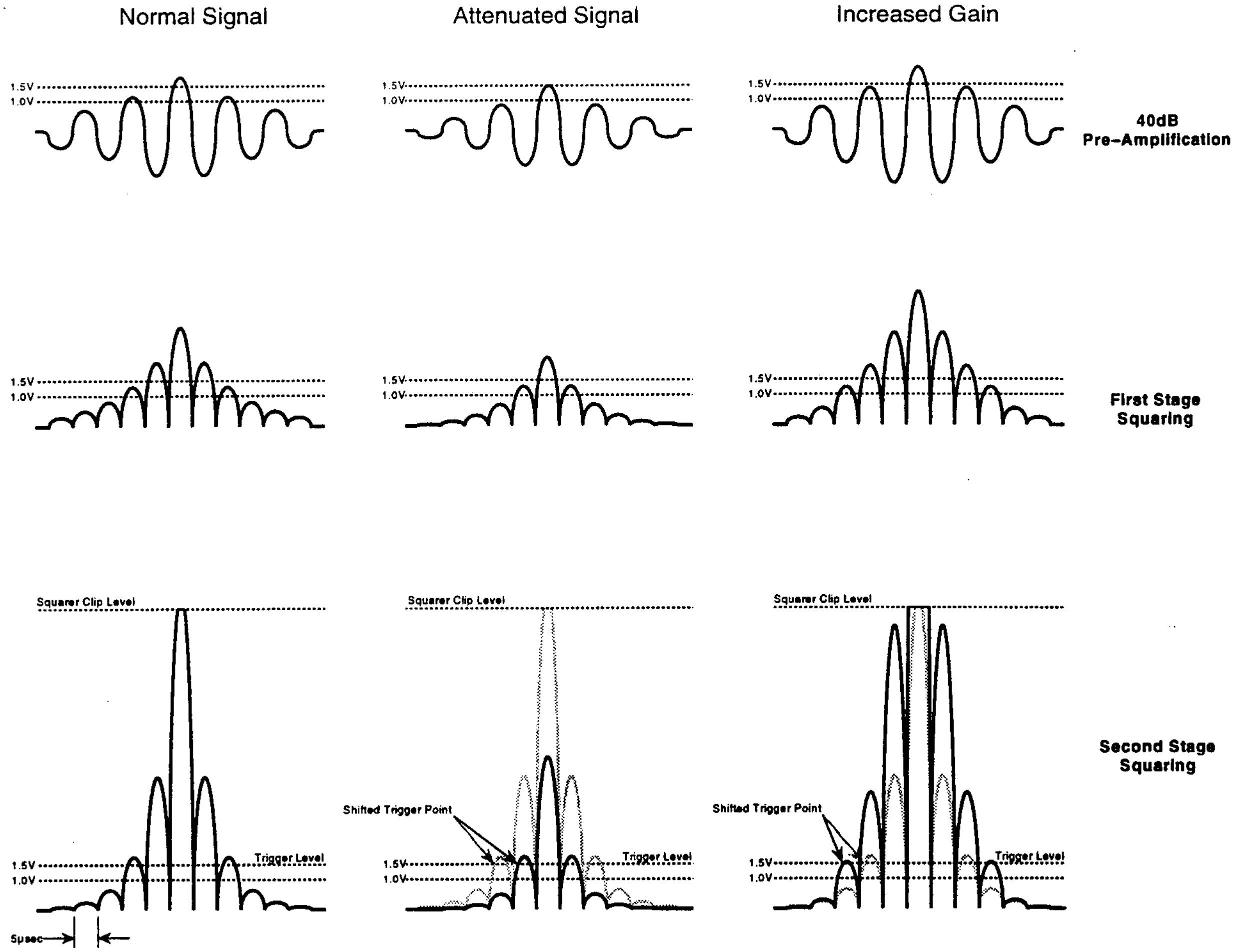

FIGURE 2. Time Shift Concepts

through a fixed 40dB pre–amplifier and is then further amplified by a computer gain controlled amplifier. The output signal from the amplifier then passes through a two stage analog squaring circuit that rectifies the signal and increases the magnitude of the signals above 1.0 Volts, and attenuates the signal magnitudes below 1.0 Volts. The double squaring process effectively reduces the possibility of an unexpected interval timer trigger event that would be caused by a border line signal peak.

After exhaustive manipulation of the Antigua sea test data, it was discovered that, in some cases, the time–of–flight data showed an offset of five micro seconds, or a multiple thereof, from the pierside zero deflection reference data. This is the expected time shift for the above mechanism. A spreadsheet analysis was generated that graphed the performance of a given transducer over the entirety of the FFG–59 sea tests.

Of the 65 transducers used in the Antigua sea test, transducer 50, located in the forward starboard portion of the SRD, was used more than any other. The graphs in Appendix A illustrate the performance of transducer 50, as well as a number of other transducers, from the Maine Shakedown, which includes the "MAX..." Series of data runs, through the end of the Antigua sea test. The most apparent feature in the graphs is how the data diverges on and after data run "A16_3D1". This data set was the second run taken after FFG–59 had gotten underway for Antigua on November 16, 1992. The time intervening between, when the deflection measurement system was apparently acquiring *good* data in "ANT16_2_D1", on November 16, and when driver transducers started returning divergent values, in "A16_3D1", on November 17, was approximately 27 hours.

It is still unknown what mechanism caused the deflection measurements to become skewed as the graphs indicate. It was thought that the data could be adjusted by shifting the time–of–flight records by multiples of 5 micro seconds to bring them into convergence with the pierside zero deflection reference and the Maine Shakedown sea test data. This process was applied to the data run "ANT_16_3D3", which was one of the data runs used to test UW/APL's SRD FEM.

4.0 Comparison with UW/APL Predictions

The graphs in Figures 4–11 summarize the results of the UW/APL predictions for the 12 transducers mutually used in data runs "ANT16_2D1" and "ANT_16_3D3". The graphs depict the deflection results in terms of movement perpendicular, or *normal*, to the inner surface of the SRD, and movement along, or *tangential*, to the inner surface of the SRD, as shown in Figure 3.

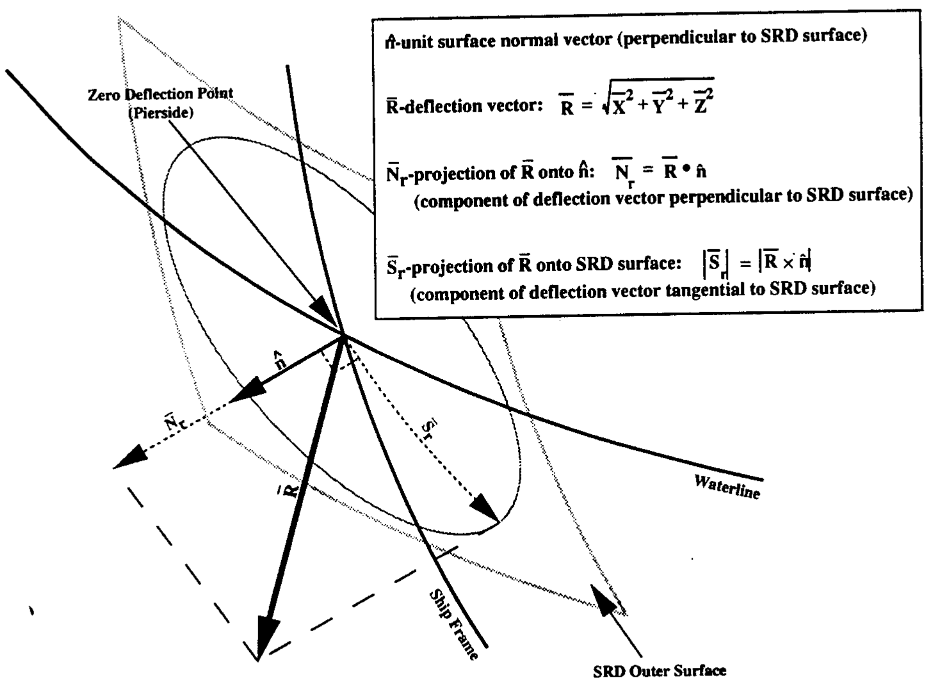

FIGURE 3. Deflection Components

Surface normal deflection components are expressed in both positive (outward movement) and negative (inward movement) terms, relative to the pierside zero deflection reference location for NRL measurements, and the theoretical BFG CAD coordinates for the UW/APL predictions. The tangential components are magnitude only quantities and therefore are directionless.

4.1 Data Run ANT16_2_D1

Data run "ANT16_2_D1" did not show the divergence anomalies present in later Antigua data runs, and was therefore not adjusted with the 5 micro second multiple time shifts. The scope of this analysis encompasses ten samples from the data run time point, 7.47 seconds, to time point, 19.85 seconds. In this data run, the seas were calm, at sea state 1 or less, and FFG–59 was travelling at approximately 20 knots.

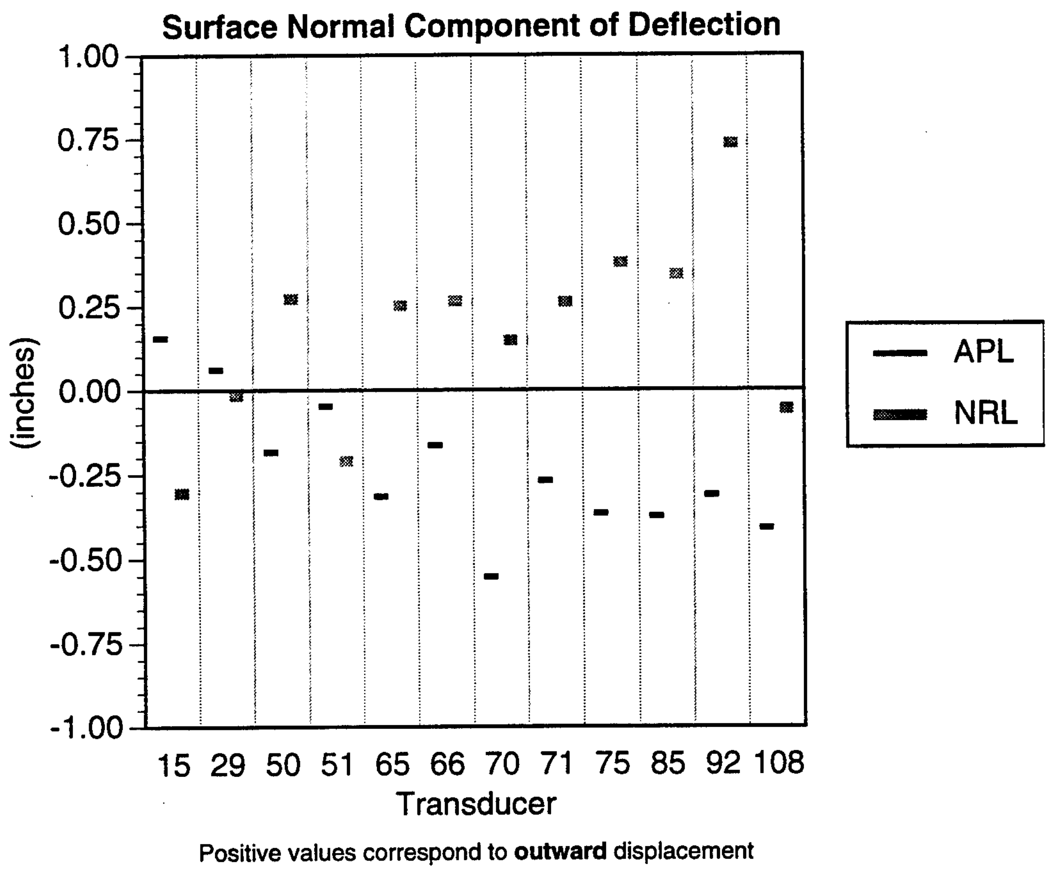

FIGURE 4. ANT16_2_D1 Static Surface Normal Displacement

These first two comparison graphs show *static* or average deflections for the analysis time window. In Figure 4, the Static Surface Normal Displacement graph shows that the magnitudes of the APL predictions and the NRL measurements are similar but are near mirror images of each other. In most cases where APL has predicted inward movement of the SRD, the NRL data indicates that the opposite occurred.

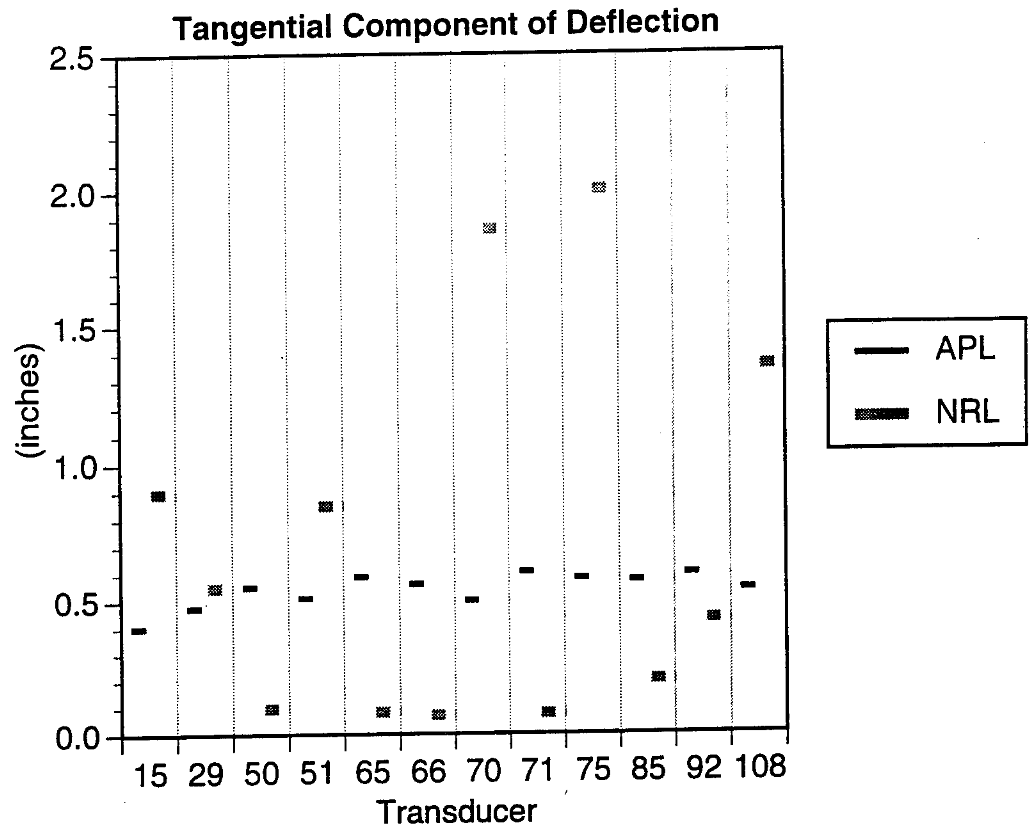

FIGURE 5. ANT16_2_D1 Static Tangential Displacement

In Figure 5, the Tangential Component of Deflection graph shows that APL has consistently predicted deflections along the surface of the SRD of approximately 0.5 inches. Seven of the NRL transducers show small tangential movement of 0.5 inches or less. Five of the NRL measurements indicate larger tangential deflections from nearly one inch to two inches. This group of transducers may be showing symptoms of the large anomalous offsets that affected later data runs, and may have therefore returned flawed data.

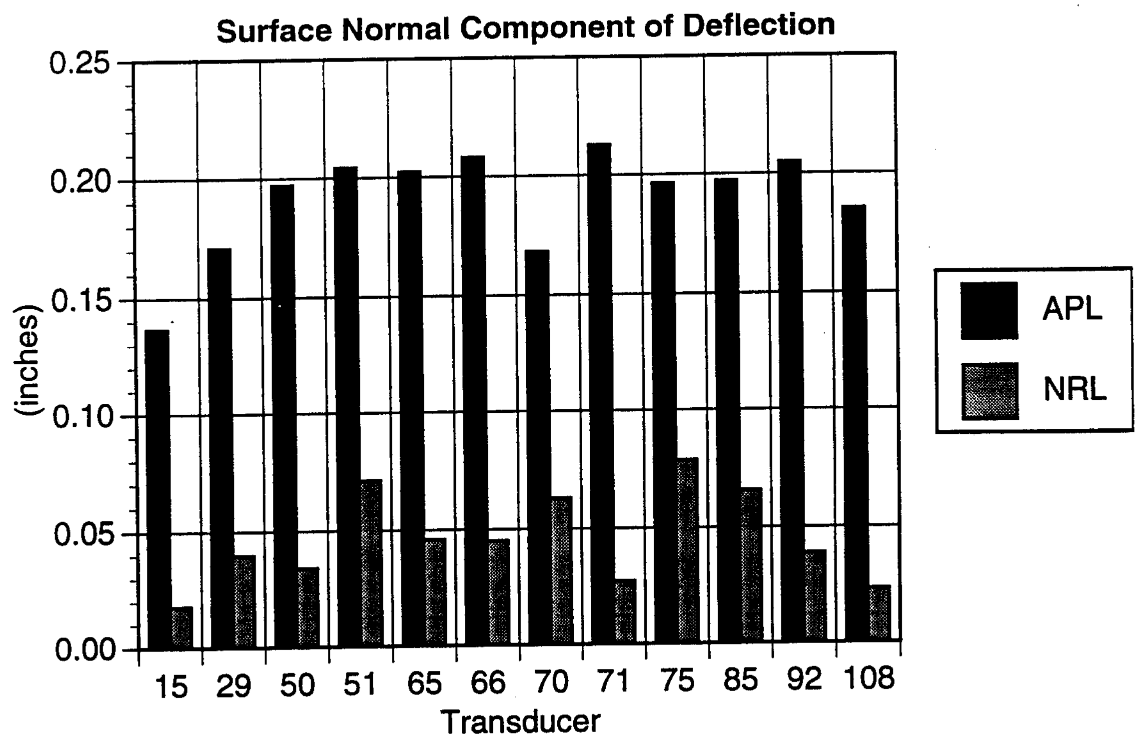

FIGURE 6. ANT16_2_D1 Dynamic Surface Normal Movement

The next two graphs depict the *dynamic* or time varying component of the deflections in the analysis time window. The Dynamic Surface Normal Component graph, in Figure 6, shows that APL has predicted dynamic surface normal movements of approximately 0.15 to 0.20 inches. The NRL measurements show smaller movements of approximately 0.02 to 0.08 inches. This indicates the APL FEM predicts dynamic surface normal movements that are nearly three times what NRL has measured.

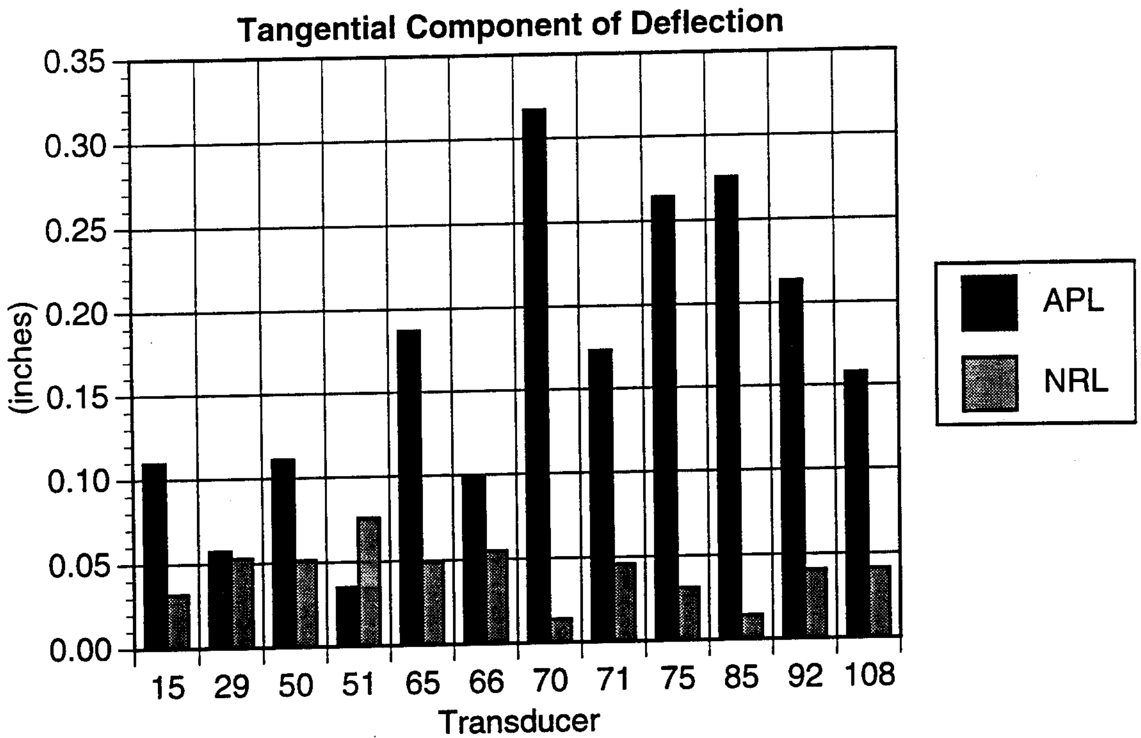

FIGURE 7. ANT16_2_D1 Dynamic Tangential Movement

The Dynamic Tangential Movement graph, in Figure 7, shows that APL's predictions vary between 0.03 inches and 0.32 inches. NRL's measurements show dynamic tangential movements of approximately 0.08 inches or less.

4.2 Data Run ANT_16_3D3

Data run "ANT_16_3D3" did show the divergence anomalies present in most of the Antigua data runs. This data run was adjusted with the 5 micro second multiple time shift but did not yield the improvements that were anticipated. The graphs that follow show both the unadjusted NRL measurements as well as the 5 micro second multiple time shift adjustments of the same NRL data. This analysis encompasses ten samples from the data run time point, 104.92 seconds, to time point, 117.28 seconds. The environmental conditions for this data run, were slightly rougher seas, at sea state 2, with FFG–59 was travelling at approximately 18 knots.

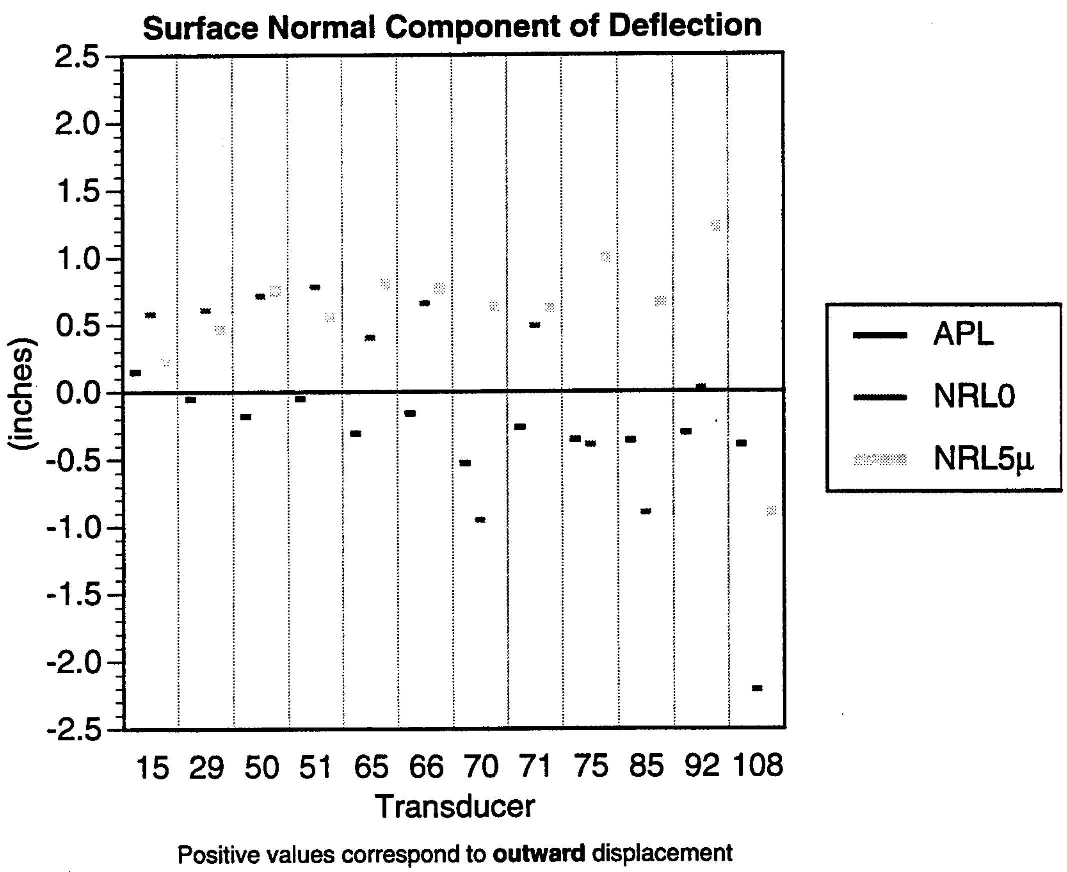

FIGURE 8. ANT_16_3D3 Static Surface Normal Displacement

This first *static* comparison graph of the Surface Normal Component of Deflection in Figure 8, shows that the magnitude of the NRL measurements are somewhat greater than the APL predictions. The unadjusted NRL data (NRL0) shows deflection components that vary from 0.75 inches to approximately -2.2 inches. The diversity in the range of these measurements suggest that this data may be flawed. The NRL 5 micro second multiple adjusted data (NRL5μ) shows more consistent results with values that are nearly twice what APL has predicted but generally indicate SRD displacement in the opposite direction.

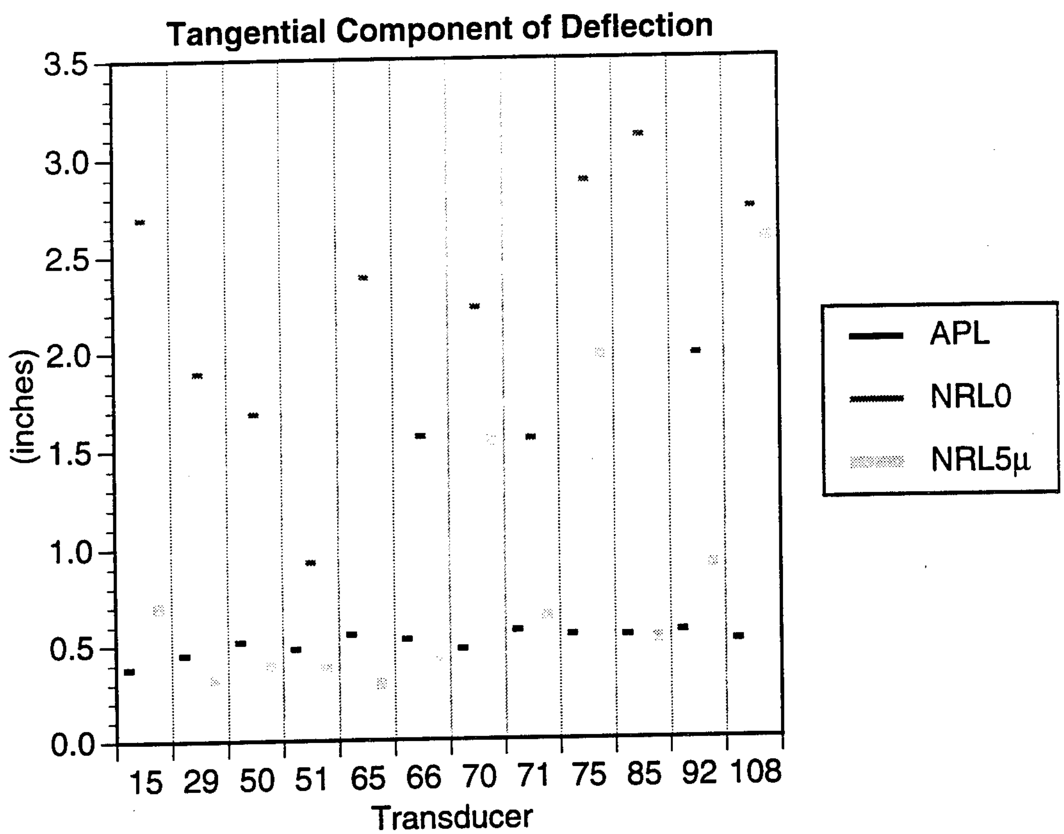

FIGURE 9. ANT_16_3D3 Static Tangential Displacement

In Figure 9, the *static* Tangential Component of Displacement graph shows that APL has consistently predicted SRD surface displacements of approximately 0.5 inches. The unadjusted NRL measurements (NRL0) fluctuate from nearly one inch to greater than three inches. This again suggests that this dataset may be flawed. The NRL 5 micro second multiple adjusted data (NRL5μ) generally shows good agreement with APL's predictions.

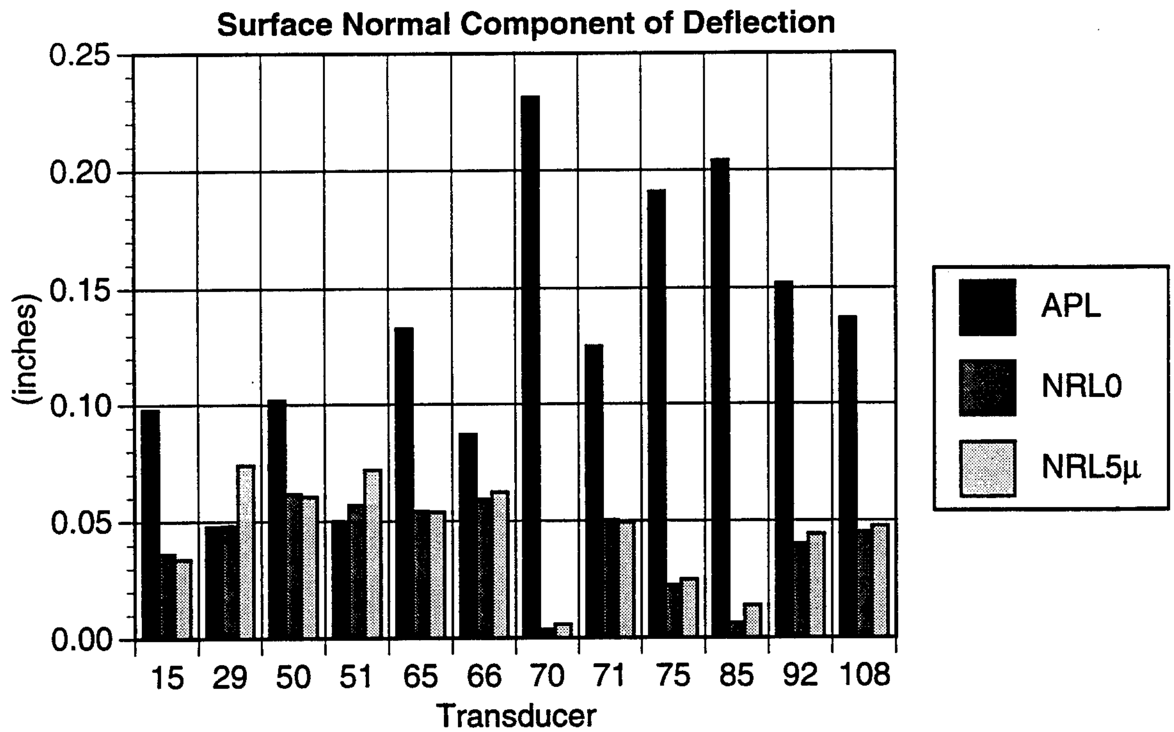

FIGURE 10. ANT_16_3D3 Dynamic Surface Normal Movement

The *dynamic* Surface Normal Component of Deflection graph, in Figure 10, shows the APL predictions varying from nearly 0.05 inches to as much as 0.23 inches. The NRL 5 micro second multiple adjusted data closely follows the NRL unadjusted data, which indicate a smaller range of SRD surface perpendicular movements of 0.07 inches or less.

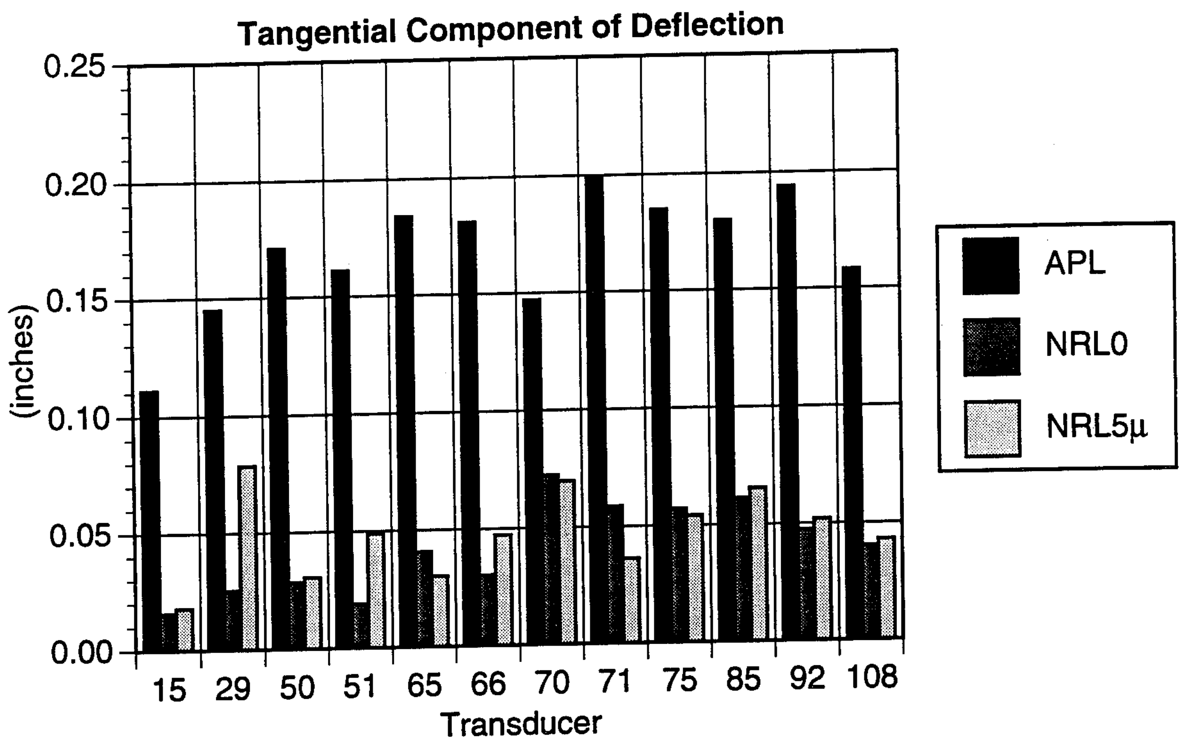

FIGURE 11. ANT_16_3D3 Dynamic Tangential Movement

In Figure 11, the *dynamic* Tangential Component of Displacement graph shows that APL predicts SRD surface movements ranging from more than 0.1 inches to 0.2 inches. The NRL 5 micro second multiple adjusted data again generally follows the NRL unadjusted data which indicates SRD tangential movements of approximately 0.7 inches or less.

5.0 Conclusion

The modification and deployment of the SDADMS to measure the deflection behavior of the SRD was an *ambitious* effort intended to provide calibration data for UW/APL's SRD FEM. This first time effort was partially successful in that a large amount of dynamic deflection data *was* collected and *was* used for comparison with the predictions from UW/APL.

While the results from this comparison cannot be considered conclusive, they do suggest, from a *dynamic* perspective, that the SRD *may* be <u>more rigid</u> than initially predicted by UW/APL's Finite Element Model. Due to unexpected difficulties associated with the data collection process, primarily with the collection of environmental data (see Appendix H), the necessary dynamic SRD pressure data was not obtainable, which UW/APL needed to provide accurate dynamic deflection predictions. The results of the comparison cannot therefore be considered to be the final word on the subject.

Unlike in the SDRW, where installed test equipment is relatively accessible, the physical ship–board configuration of the SRD prevents the correction of system problems that may arise after SRD installation. This first deployment of the SDADMS in an SRD necessitated a two fold increase in system complexity. The deployment of the SDADMS aboard FFG–59 went well when these facts are taken into account. Unfortunately the test was only partially successful.

For the future, it is recommended that another test be conducted on a SRD to confirm the findings of the UW/APL comparison.

References

[1] "Sonar Dome Reliability XVIII: Measured Deflections of the USS KAUFFMAN Sonar Rubber Dome, 15–25 Nov 1992". NRL Memorandum Report 7436. By J. F. Covey (Code 7135), D. B. Weaver (SFA, Inc.), and L. J. Levenberry (GeoCenters). January 7, 1994

[2] "Sonar Dome Reliability XX: Software Developments in the Acoustic Sonar Dome Deflection Measurement System". NRL Memorandum Report 7611. By D. B. Weaver (SFA, Inc.) and J. F. Covey (Code 7135). August 1, 1994

Figure 12: SDADMS Maine Shakedown Test Frame From Animated Data Display "srdvwr"

- Deformations Exagerated 75 Times For Illustrative Purposes
  - Deflection colors correspond to movement on the X-axis

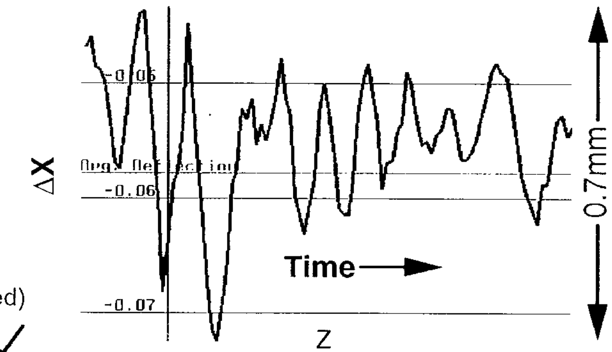

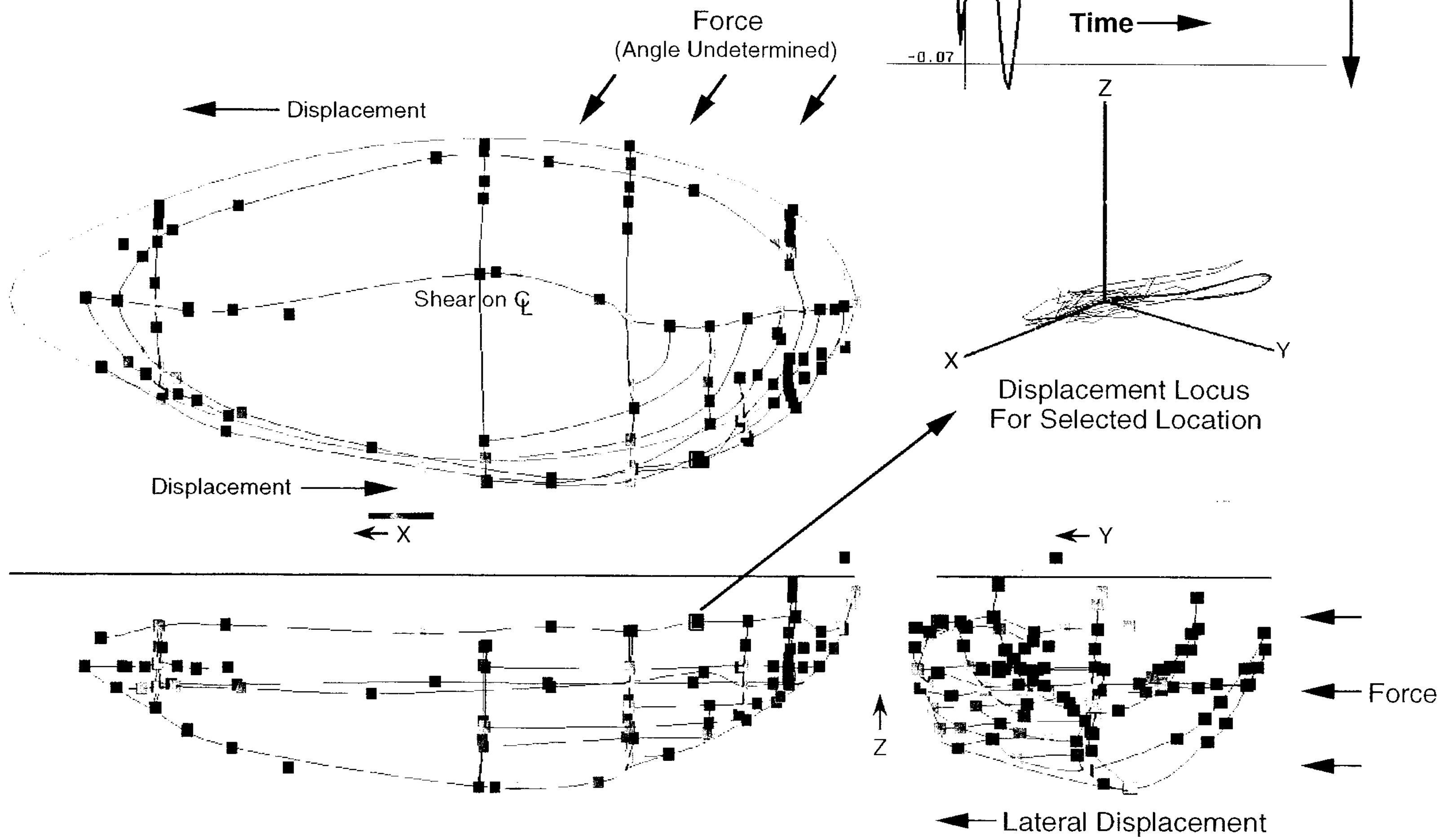

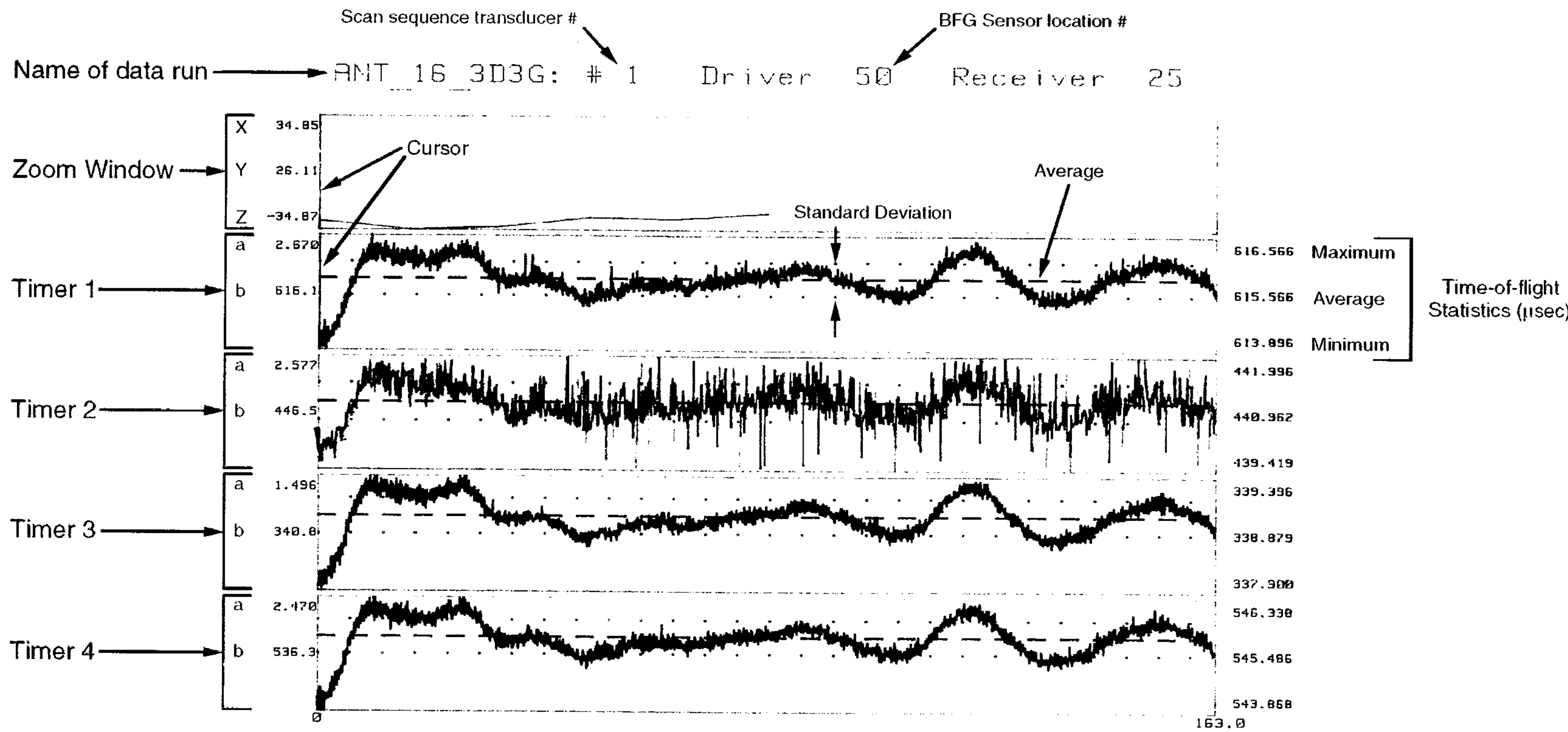

X) Zero Deflection X-coordinate (inches)
Y) Zero Deflection Y-coordinate (inches)
Z) Zero Deflection Z-coordinate (inches)
a) Vertical Scale (μsec)
b) Average time-of-flight from Zero Deflection run (μsec)

Note: In All graphs, the Vertical axis represents Time-of-flight (μsec) and the Horizontal axis represents Linear Elapsed Time (sec).

Figure 13: Elements of the 'Groom' Window

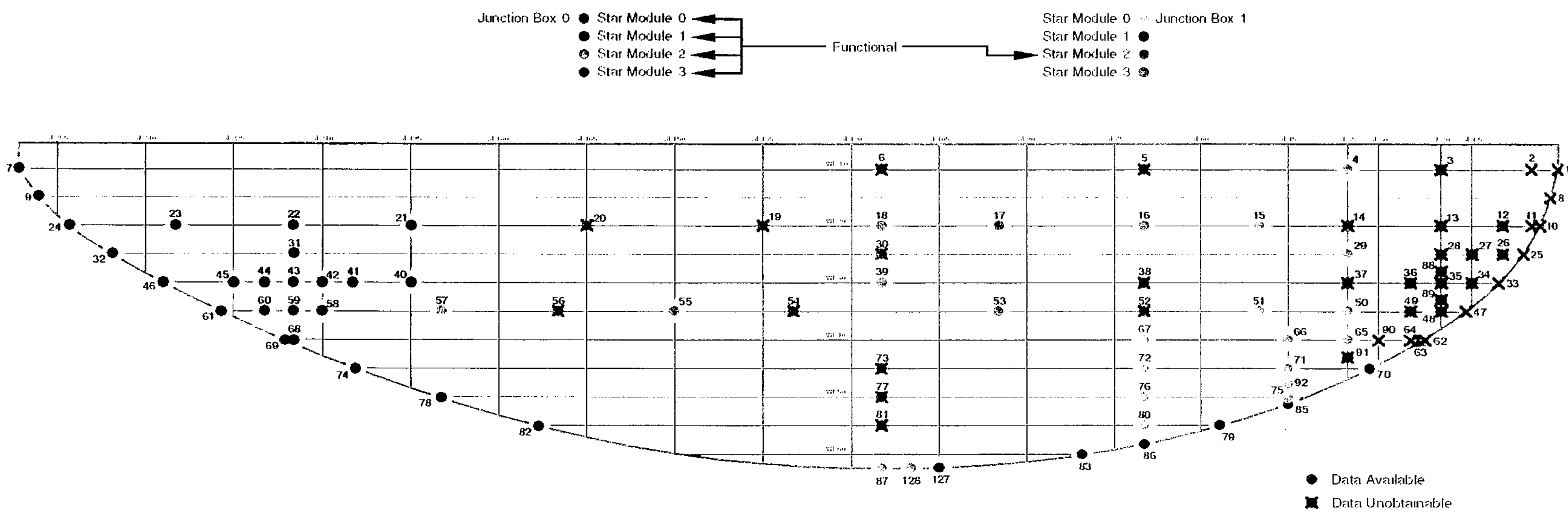

Note: All transducers, except #1, #7, #8, #9, #10, #24, #25, #32, #33, #46, #47, #61, #63, #69, #70, #74, #78, #79, #82, #83, #85, #86 and #87 are located on the starboard side. Transducers #1, #7, #8, #9, #10, #24, #25, #32, #33, #46, #47, #61, #63, #69, #70, #74, #78, #79, #82, #83, #85, #86 and #87 are on the centerline.

Figure 14: SRD Starboard Side

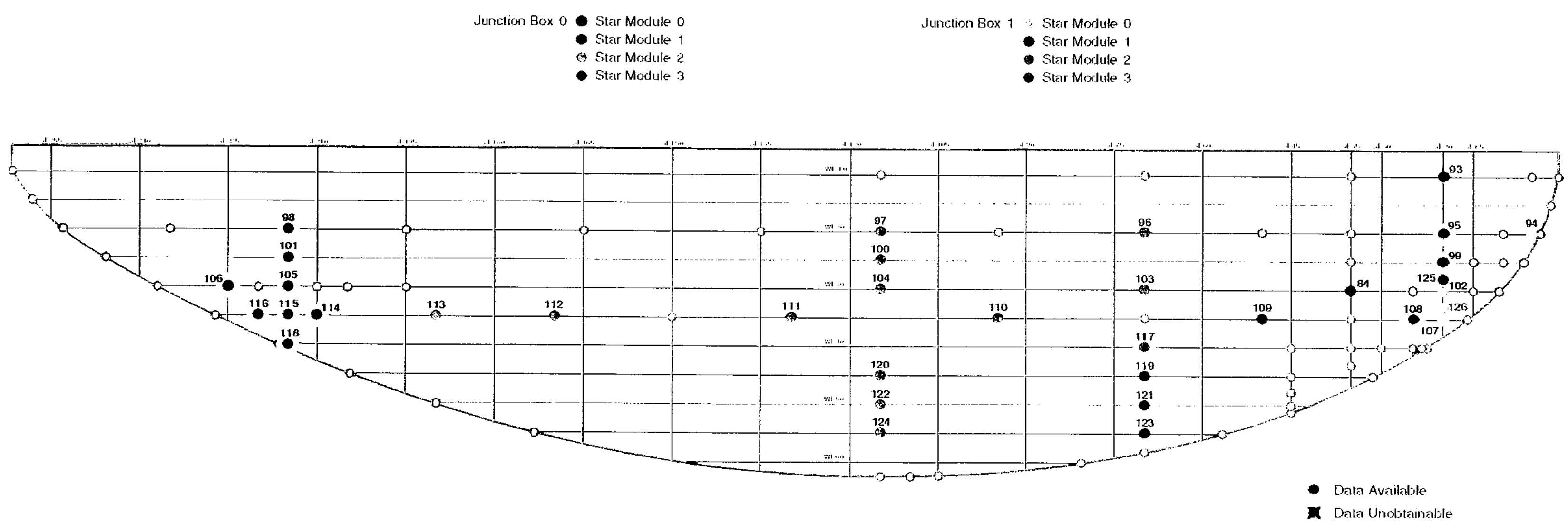

Figure 15: SRD Port Side

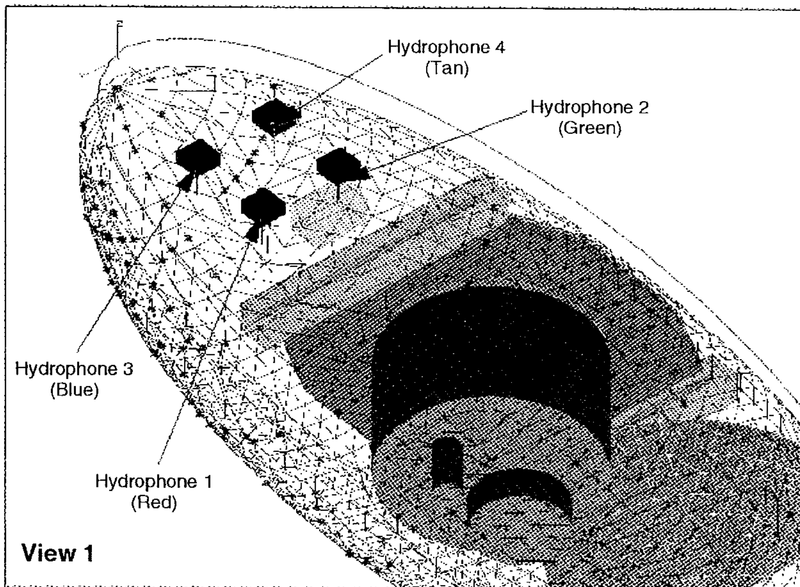

Figure 16: Hydrophone Positioning with "srd"

These three views illustrate the positioning and adjustment of hydrophone receivers mounted on the underside of the four forward Star Module boxes, as in **View 1.**

View 2 illustrates how the four hydrophone receivers' main lobes of receptivity would overlap if each hydrophone were pointed downward, perpendicular to the plane of the pressure plate. The colored areas on the SRD surface show the individual influences of each hydrophone. The areas on the SRD surface where **all** four hydrophones overlap are shown in a greyish–white. Maximizing this *overlap* is the objective of this study.

View 3 illustrates how reorienting each of the four hydrophone receivers, by tilt and rotation, can maximize the receptivity lobe overlap, while maintaining the hydrophones in their original respective locations. This is shown by the larger greyish–white area of maximum lobe overlap.

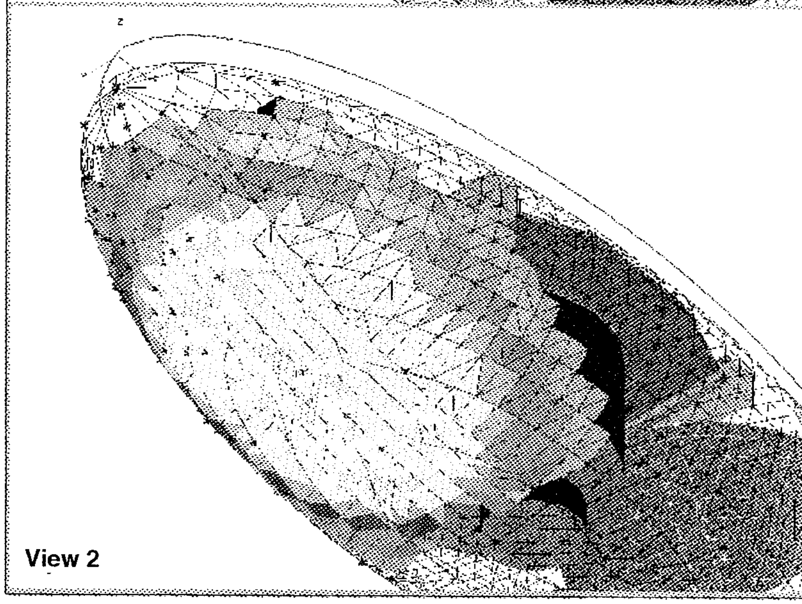

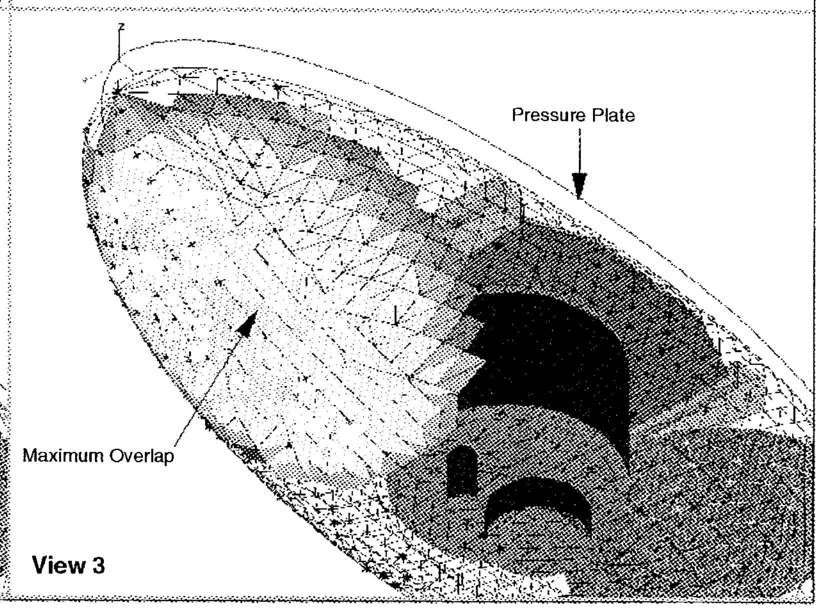

View 4

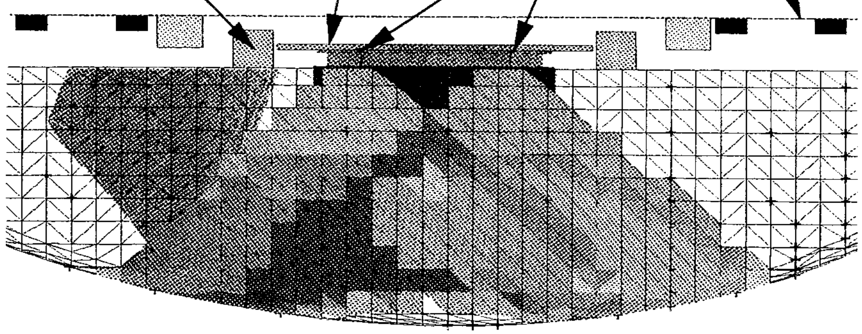

Figure 17: Other Possible Hydrophone Mounting Locations

View 4 shows how mounting four hydrophones, pointing downward, attached to the bottom of the Adapter Plate, initially will achieve little overlap.

View 5 illustrates a similar non–overlap problem for an array of downward pointing hydrophones mounted on the bottom of the SQS–56 Sonar Array.

Both non–overlap problems are due to the close proximity of the SRD to the hydrophones. Without use of the NRL computer model, hydrophones would probably have been mounted in this manner with poor results.

View 6 shows the aft section of the SRD. This view demonstrates that a single hydrophone array mounted on the bottom of the Junction Box can be optimzed to cover the entire area of interest.

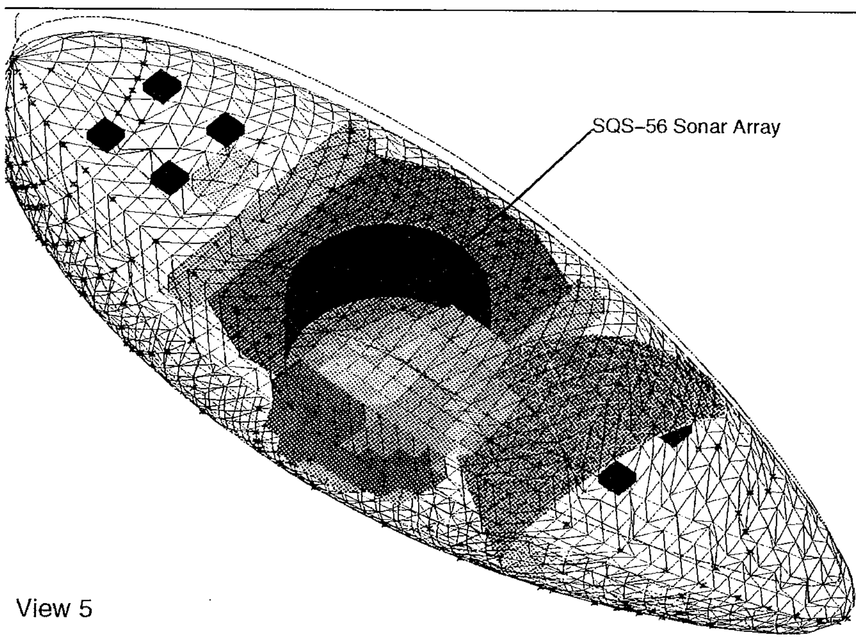

View 5

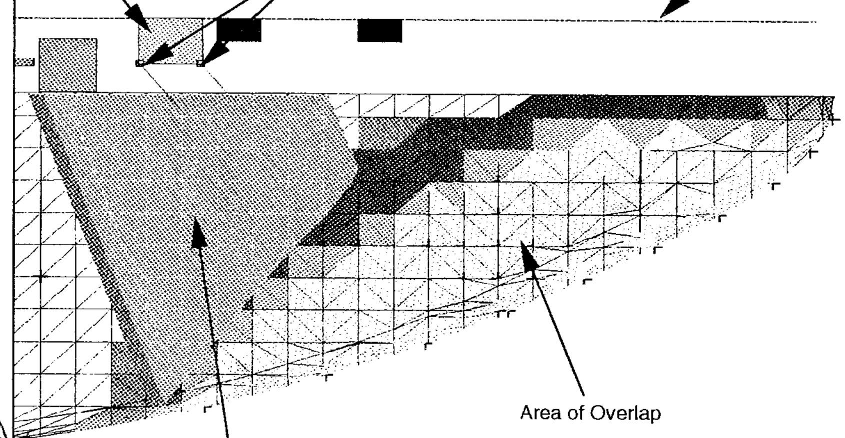

View 6

Appendix A: Transducer Specific Performance Summaries

The graphs in this section review the *average* deflection behavior of a subgroup of driver transducers that were used in the Maine Shakedown and Antigua sea tests. This subgroup consists of the 21 driver transducers that were used *most* frequently.

The X-axis of each graph represents a consistent set of data runs presented in chronological order. This group include the 14 Maine Shakedown data runs, as noted on page 1 in the body of this report, two Antigua pre–departure pierside data runs and 26 Antigua underway data runs. The two Antigua pre–departure pierside data runs, ANT_16D1 and ANT16_D2, consist of the driver transducers grouped in scan pattern ANT_16.

The Y-axis of each graph represents the *average* or static deflection of a transducer over the duration of a given data run with respect to that transducer's zero deflection pierside reference.

For each driver transducer, two graphs are presented. The lower graph displays how each of the four system interval timers responded to the driver transducer in question. In situations where the time–of–flight data from a given timer was unrecoverable, its data points have been eliminated.

The upper graph represents the triangulated deflection measurements in Cartesian coordinates. X-axis measurements are aligned with the ship's keel, where positive values represent displacements in the aft direction. Y-axis measurements are aligned athwartships, where positive values indicate starboard displacements. Z-axis measurements are aligned vertically, where positive values represent upward displacements.

These graphs typically show how the transducers behaved during each of the two sea tests. During the Maine Shakedown most transducers exhibit a uniform behavior pattern, whereas in the Antigua underway data runs, they show a deflection behavior that diverges from the zero deflection pierside reference.

Transducer 15 Performance Summary
(Relative to Pierside Zero Deflection Reference)

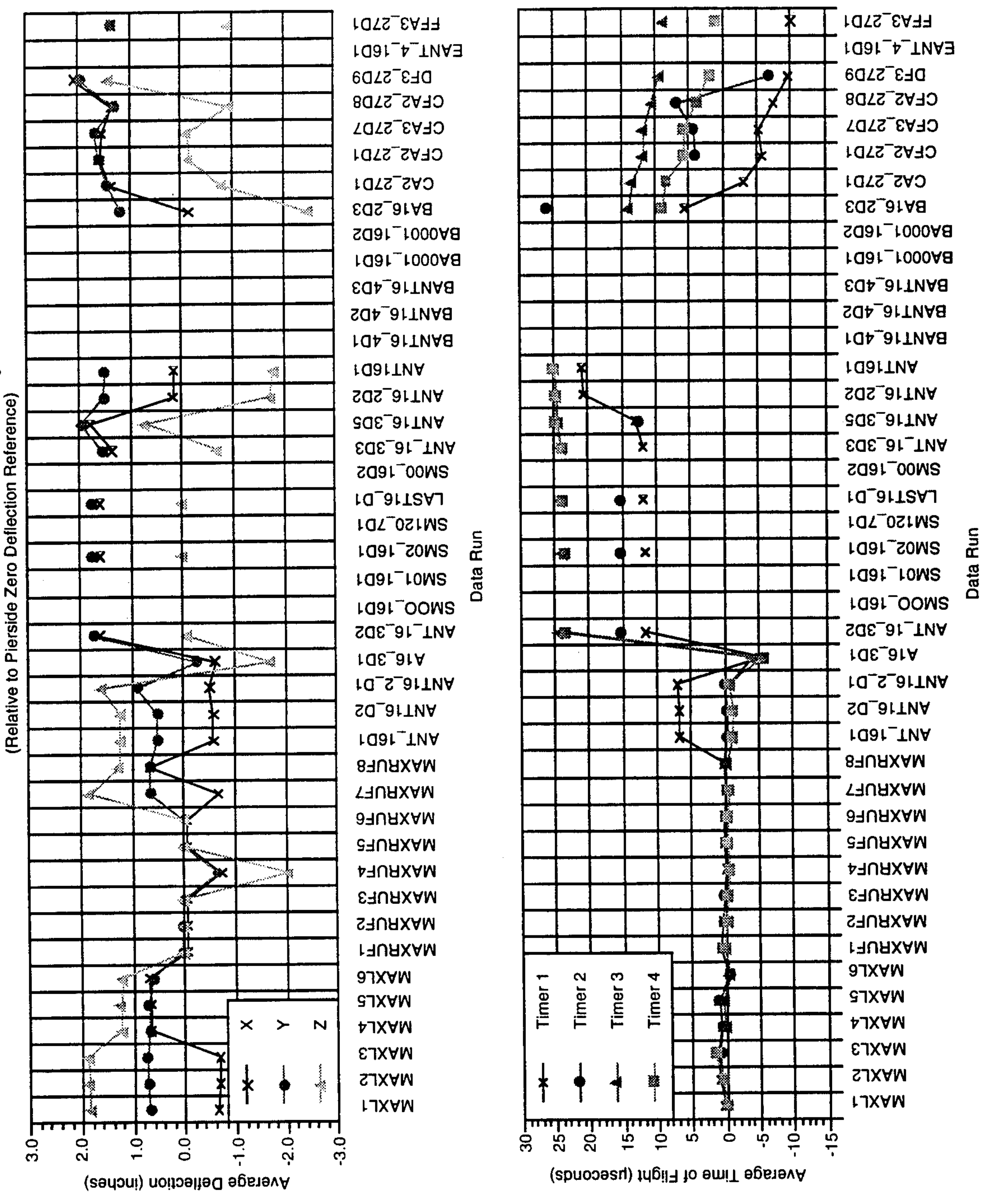

Transducer 21 Performance Summary
(Relative to Pierside Zero Deflection Reference)

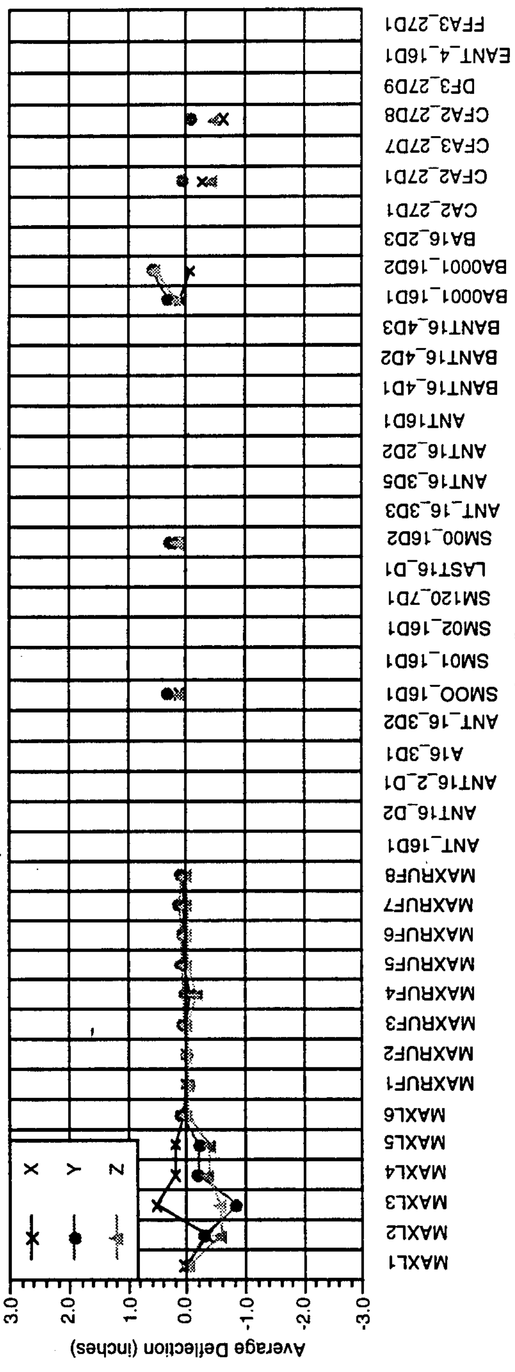

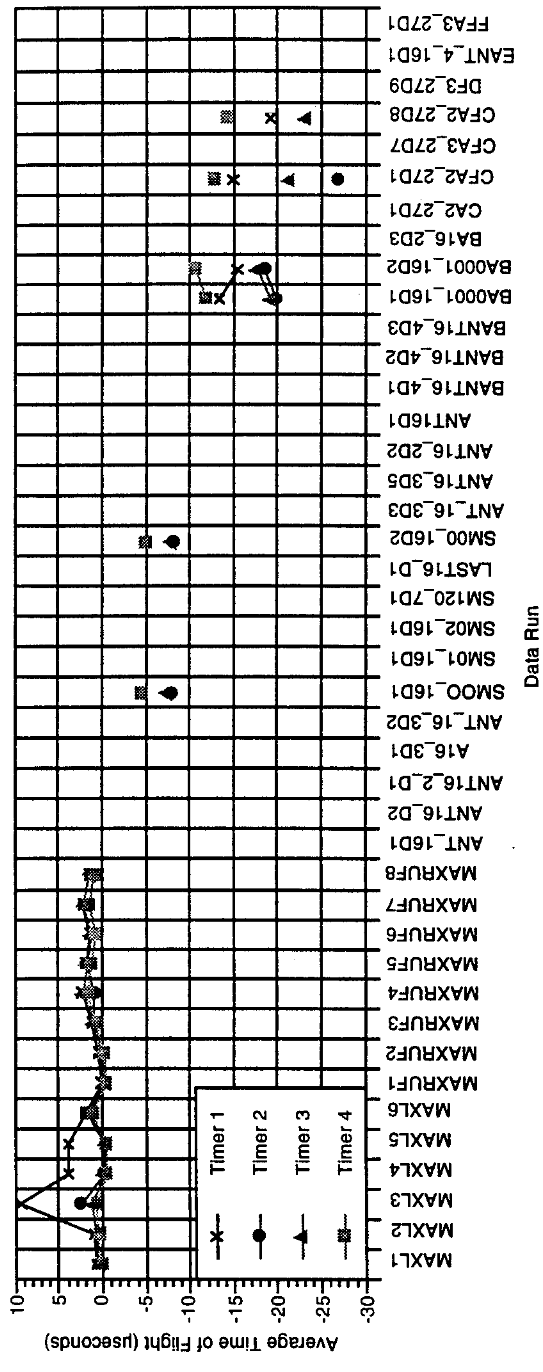

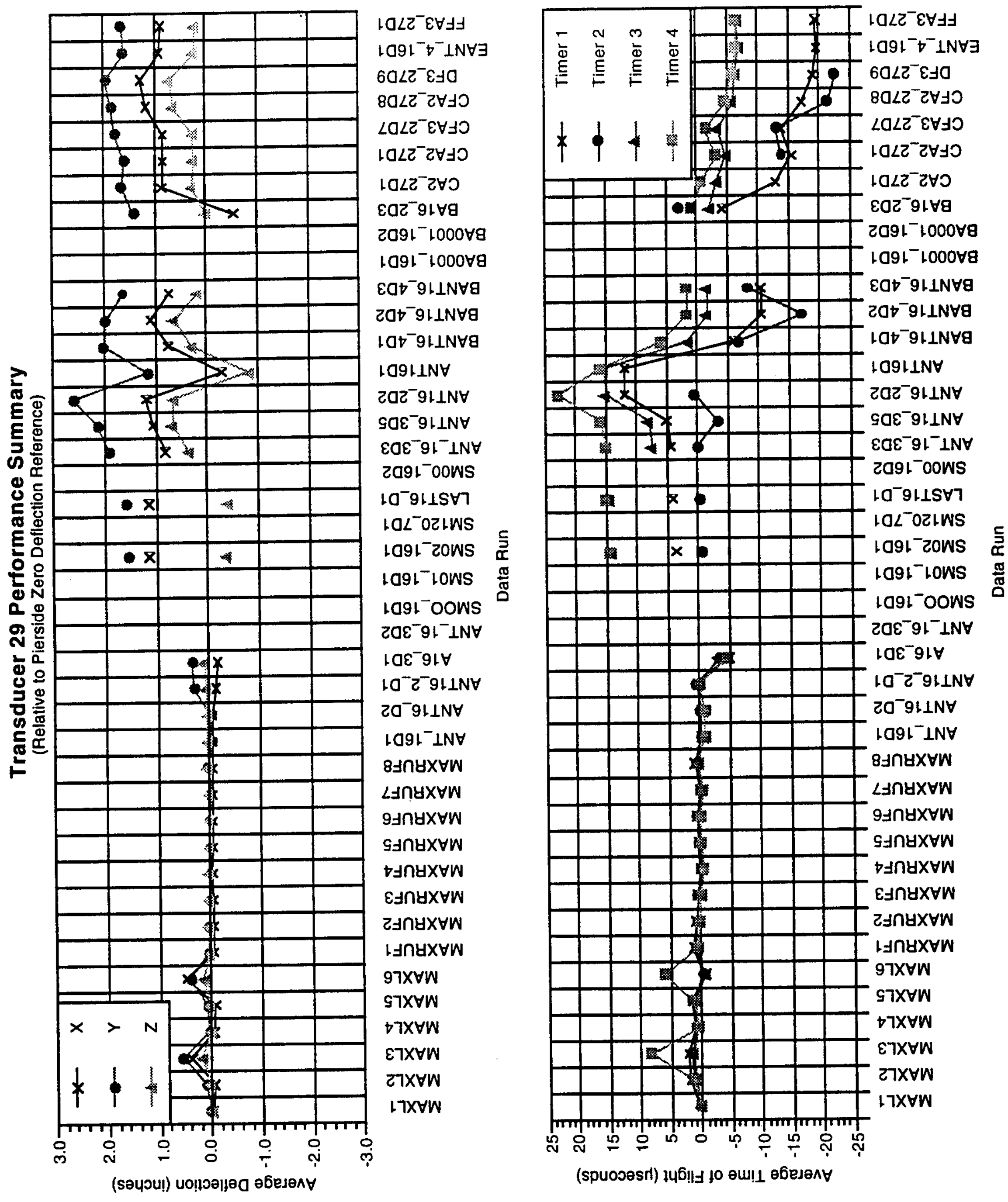
Transducer 29 Performance Summary
(Relative to Pierside Zero Deflection Reference)
X
Y
Z
Average Deflection (inches)
3.0
2.0
1.0
0.0
-1.0
-2.0
-3.0
Data Run
MAXL1
MAXL2
MAXL3
MAXL4
MAXL5
MAXL6
MAXRUF1
MAXRUF2
MAXRUF3
MAXRUF4
MAXRUF5
MAXRUF6
MAXRUF7
MAXRUF8
ANT_16D1
ANT16_D2
ANT16_2_D1
A16_3D1
ANT_16_3D2
SMOO_16D1
SM01_16D1
SM02_16D1
SM120_7D1
LAST16_D1
SM00_16D2
ANT_16_3D3
ANT16_3D5
ANT16_2D2
ANT16D1
BANT16_4D1
BANT16_4D2
BANT16_4D3
BA0001_16D1
BA0001_16D2
BA16_2D3
CA2_27D1
CFA2_27D1
CFA3_27D7
CFA2_27D8
DF3_27D9
EANT_4_16D1
FFA3_27D1
Timer 1
Timer 2
Timer 3
Timer 4
Average Time of Flight (μseconds)
25
20
15
10
5
0
-5
-10
-15
-20
-25
Data Run

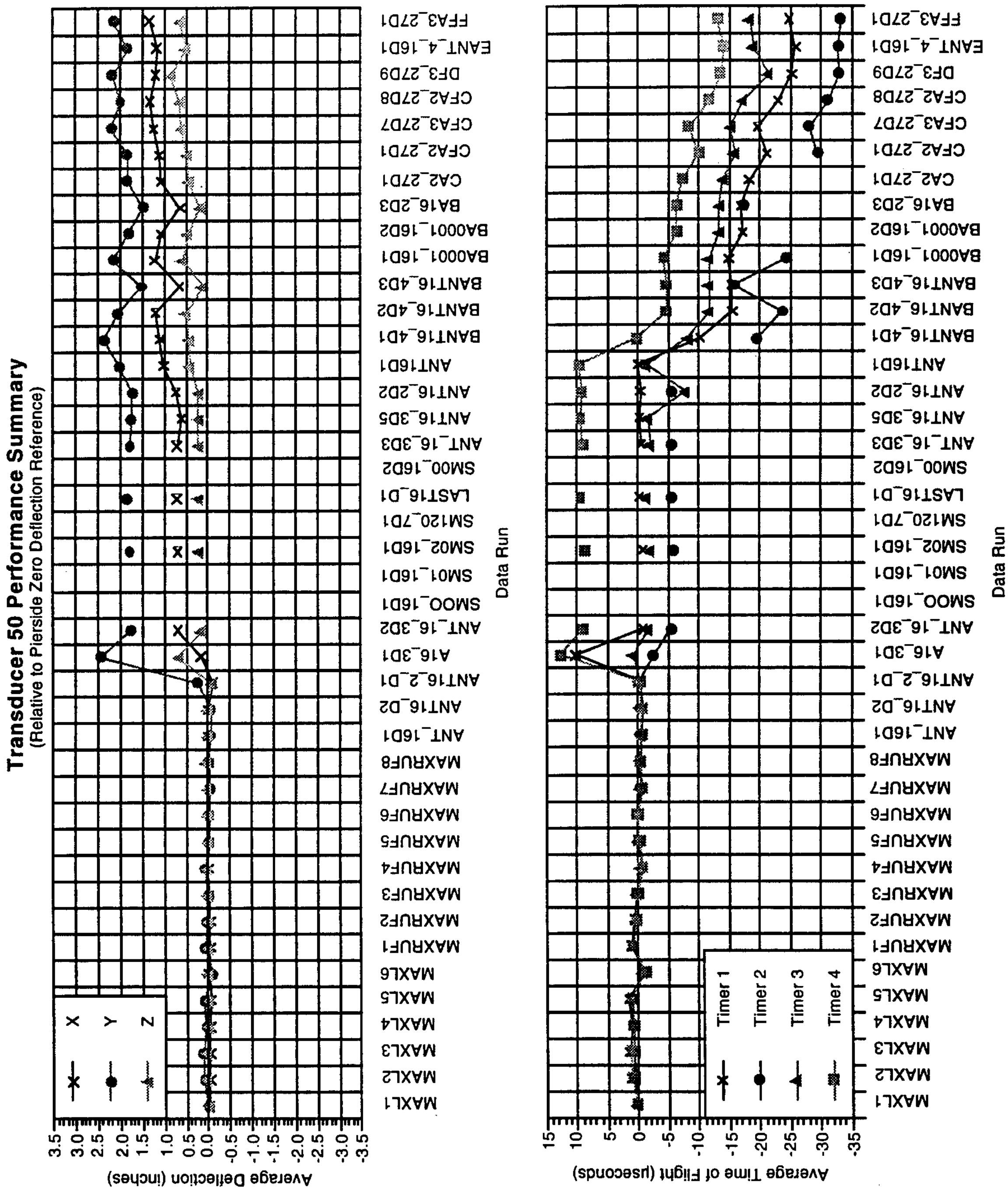
Transducer 50 Performance Summary
(Relative to Pierside Zero Deflection Reference)
Average Deflection (inches)
X
Y
Z
Data Run
Average Time of Flight (μseconds)
Timer 1
Timer 2
Timer 3
Timer 4
Data Run

Transducer 51 Performance Summary

(Relative to Pierside Zero Deflection Reference)

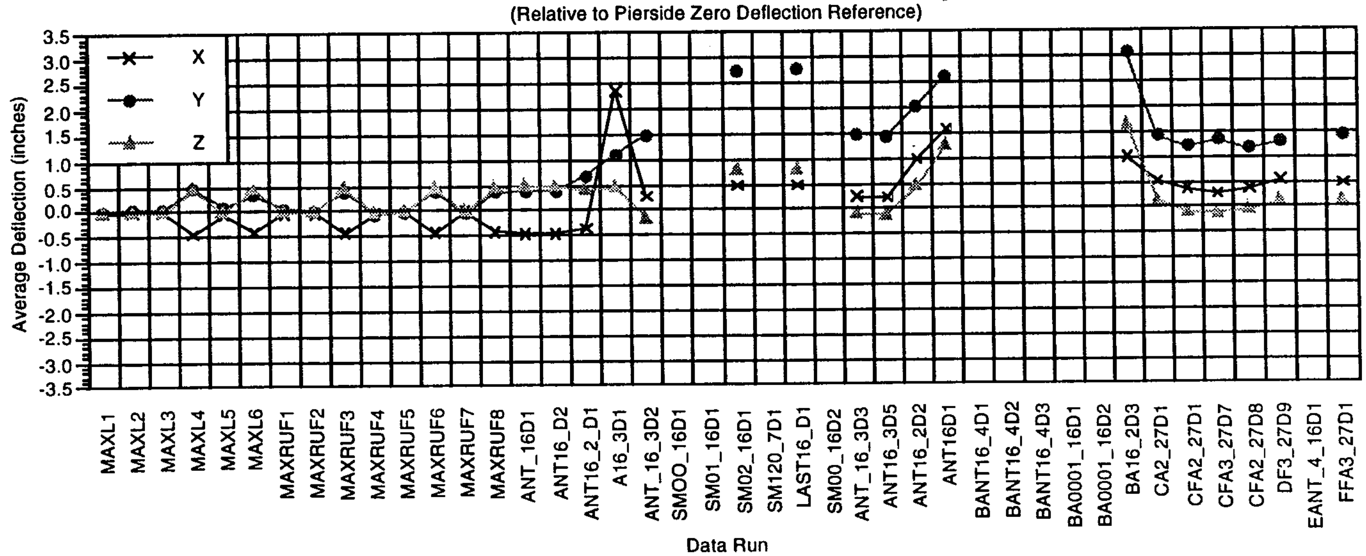

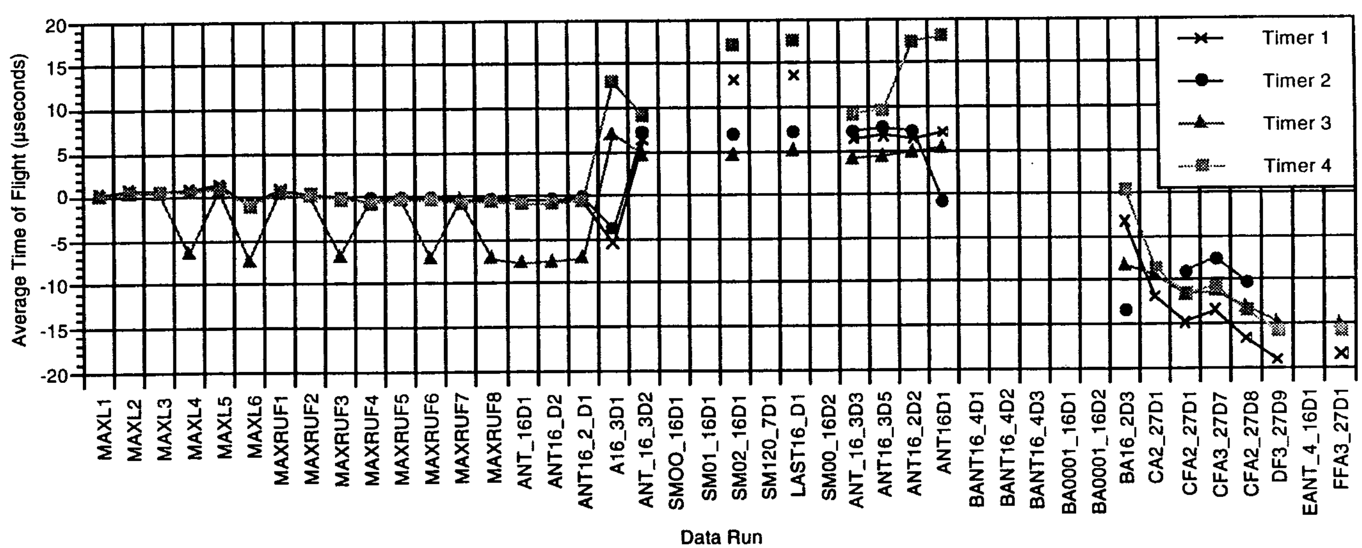

Transducer 65 Performance Summary
(Relative to Pierside Zero Deflection Reference)

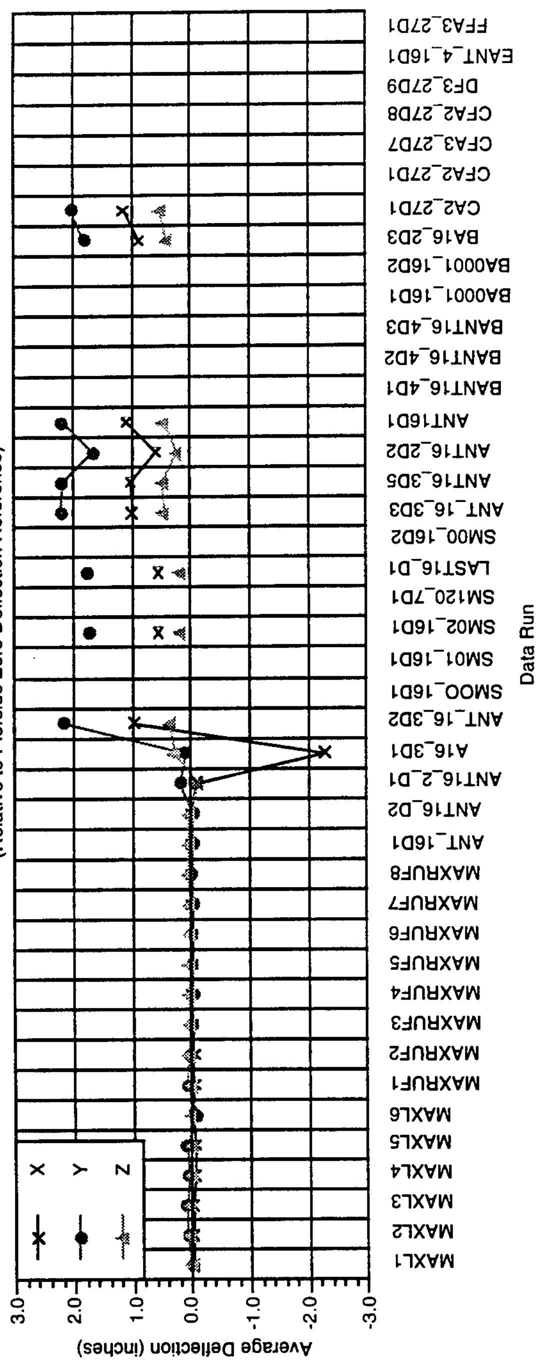

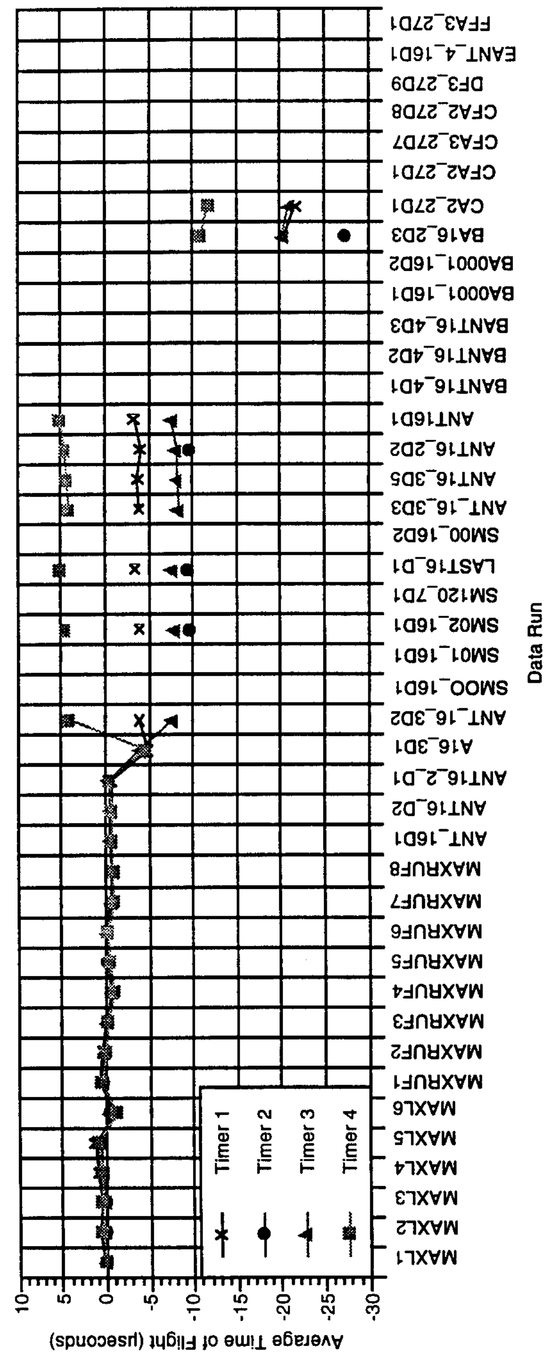

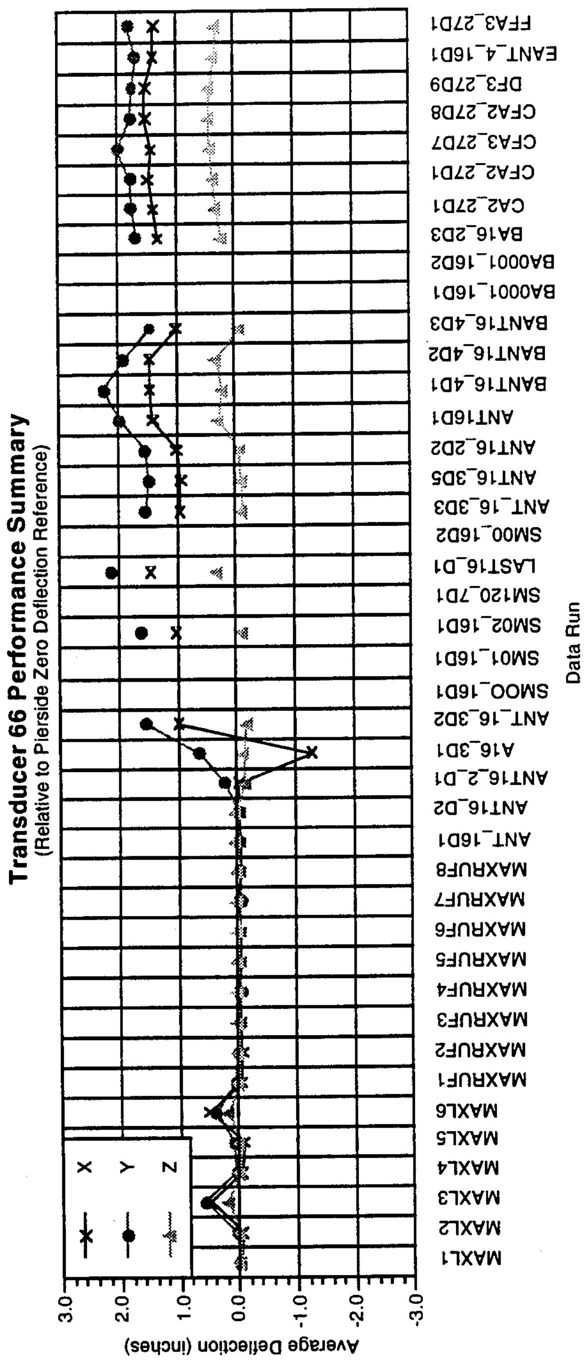
Transducer 66 Performance Summary
(Relative to Pierside Zero Deflection Reference)
Average Deflection (inches)
Data Run
X
Y
Z

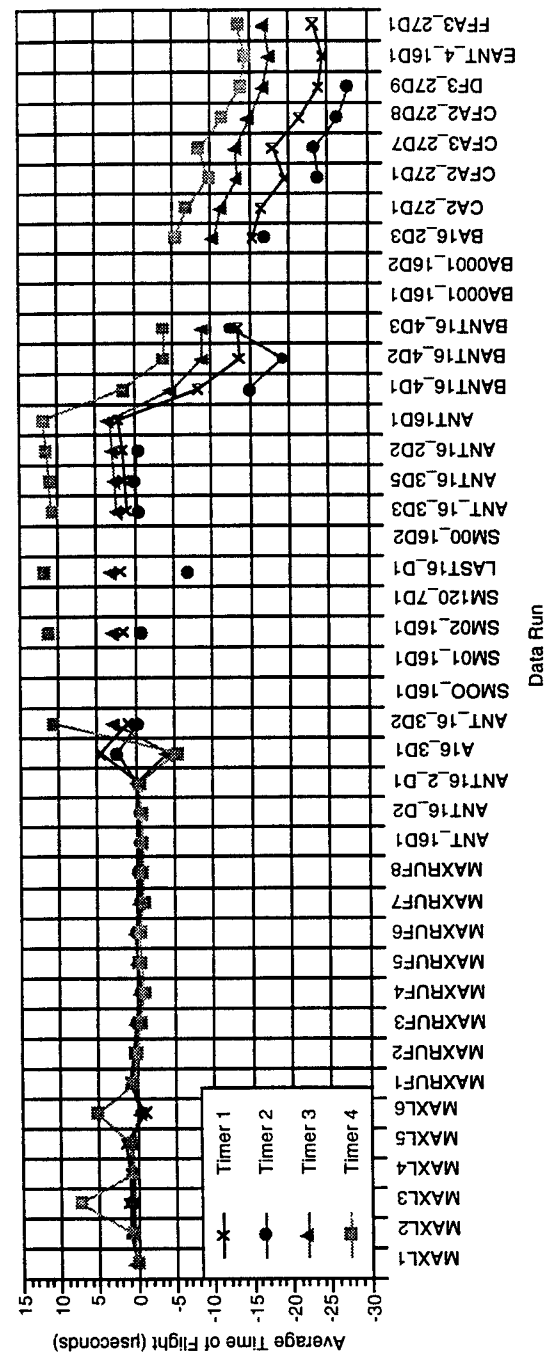
Average Time of Flight (μseconds)
Data Run
Timer 1
Timer 2
Timer 3
Timer 4

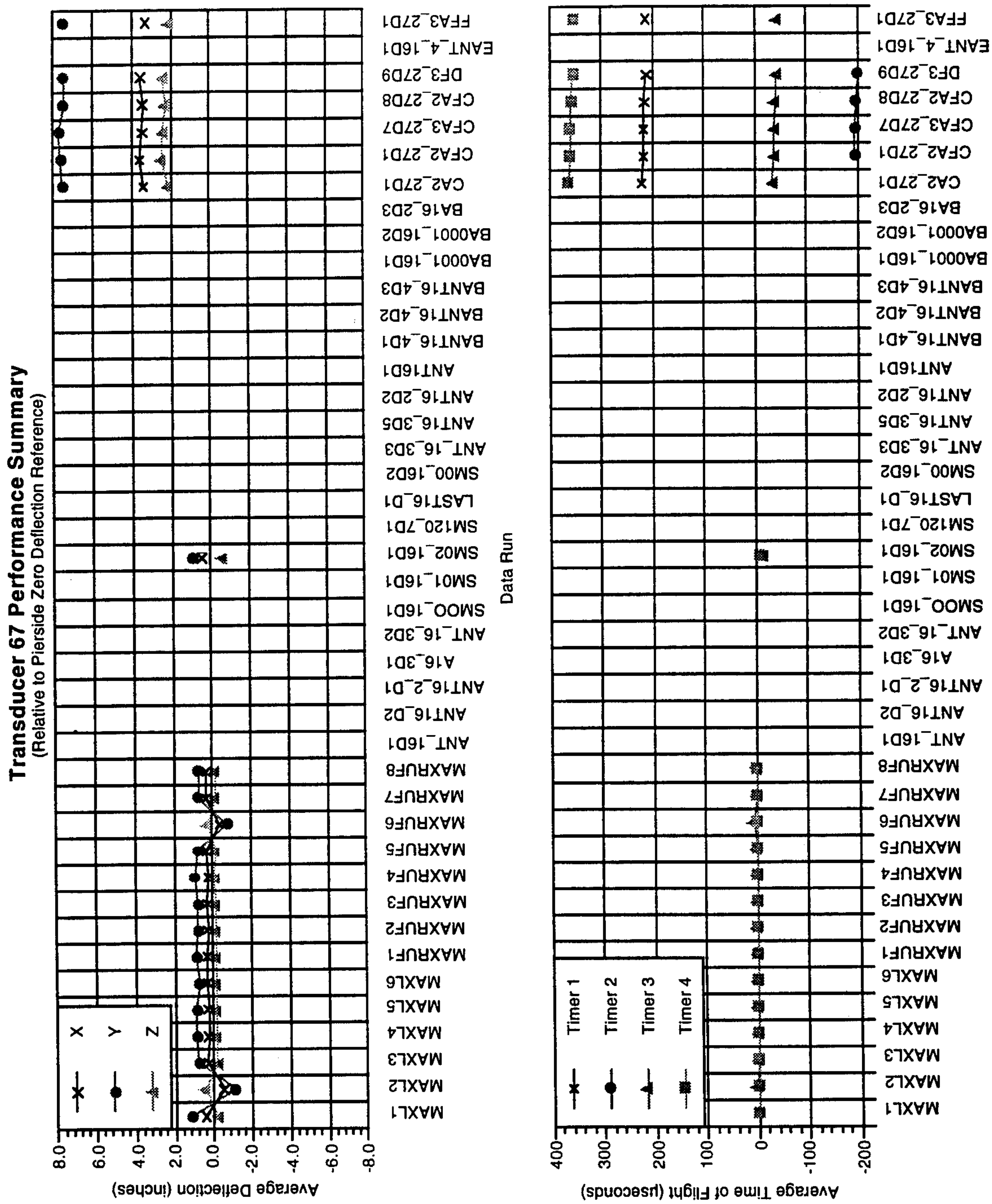
Transducer 67 Performance Summary
(Relative to Pierside Zero Deflection Reference)
Average Deflection (inches)
Data Run
X
Y
Z
Average Time of Flight (µseconds)
Data Run
Timer 1
Timer 2
Timer 3
Timer 4
FFA3_27D1
EANT_4_16D1
DF3_27D9
CFA2_27D8
CFA3_27D7
CFA2_27D1
CA2_27D1
BA16_2D3
BA0001_16D2
BA0001_16D1
BANT16_4D3
BANT16_4D2
BANT16_4D1
ANT16D1
ANT16_2D2
ANT16_3D5
ANT_16_3D3
SM00_16D2
LAST16_D1
SM120_7D1
SM02_16D1
SM01_16D1
SMOO_16D1
ANT_16_3D2
A16_3D1
ANT16_2_D1
ANT16_D2
ANT_16D1
MAXRUF8
MAXRUF7
MAXRUF6
MAXRUF5
MAXRUF4
MAXRUF3
MAXRUF2
MAXRUF1
MAXL6
MAXL5
MAXL4
MAXL3
MAXL2
MAXL1

Transducer 70 Performance Summary
(Relative to Pierside Zero Deflection Reference)

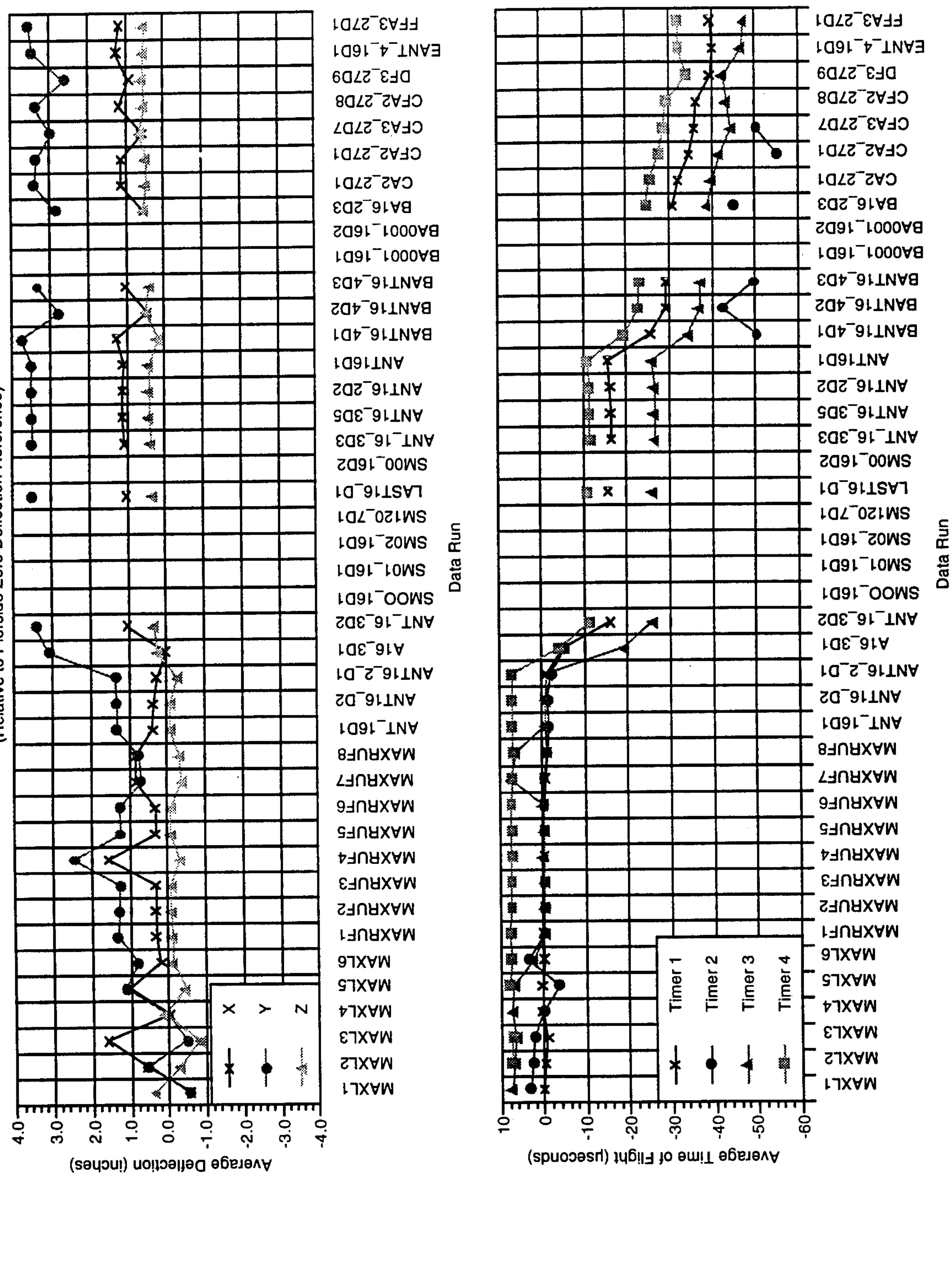

Transducer 71 Performance Summary
(Relative to Pierside Zero Deflection Reference)

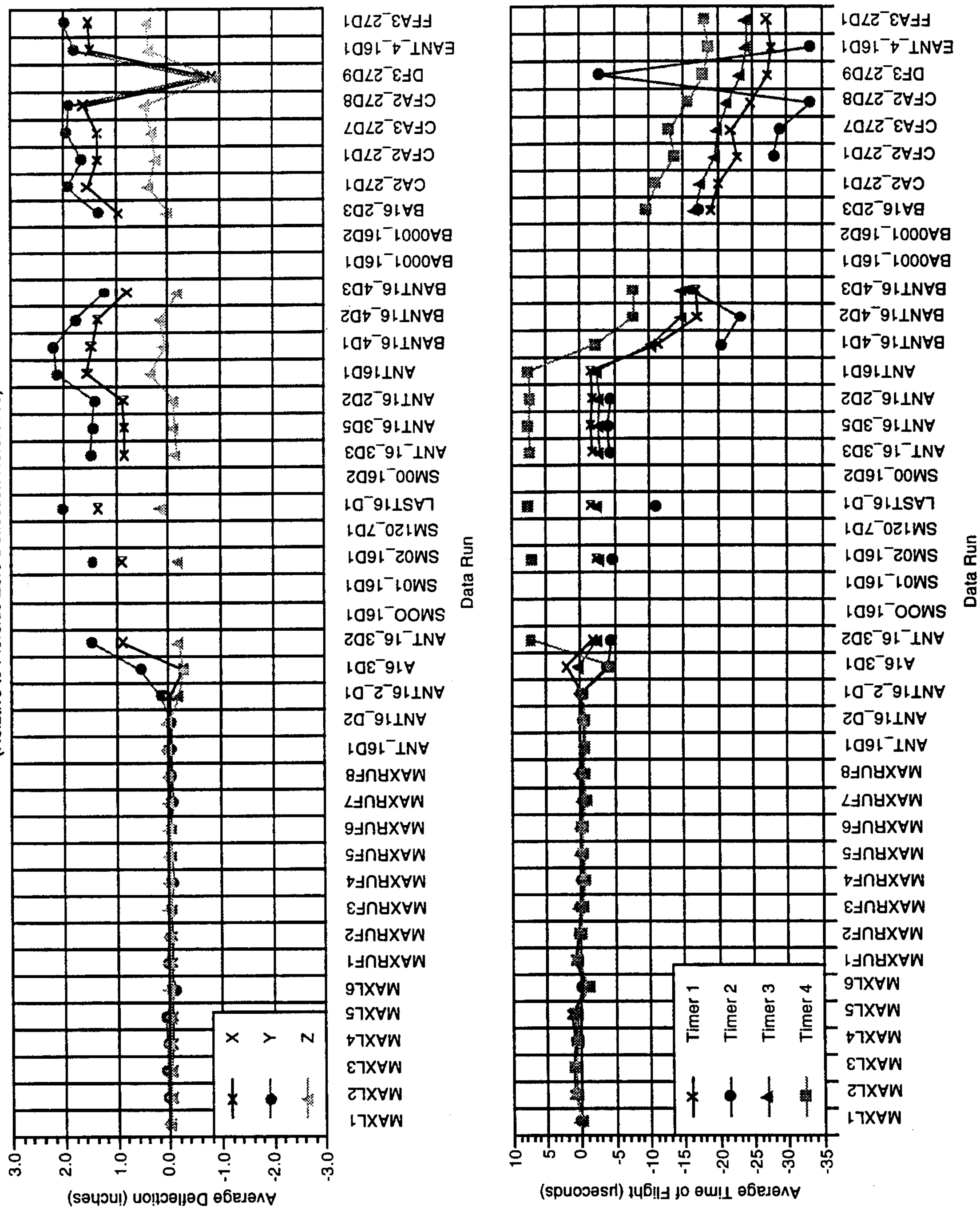

Transducer 72 Performance Summary
(Relative to Pierside Zero Deflection Reference)

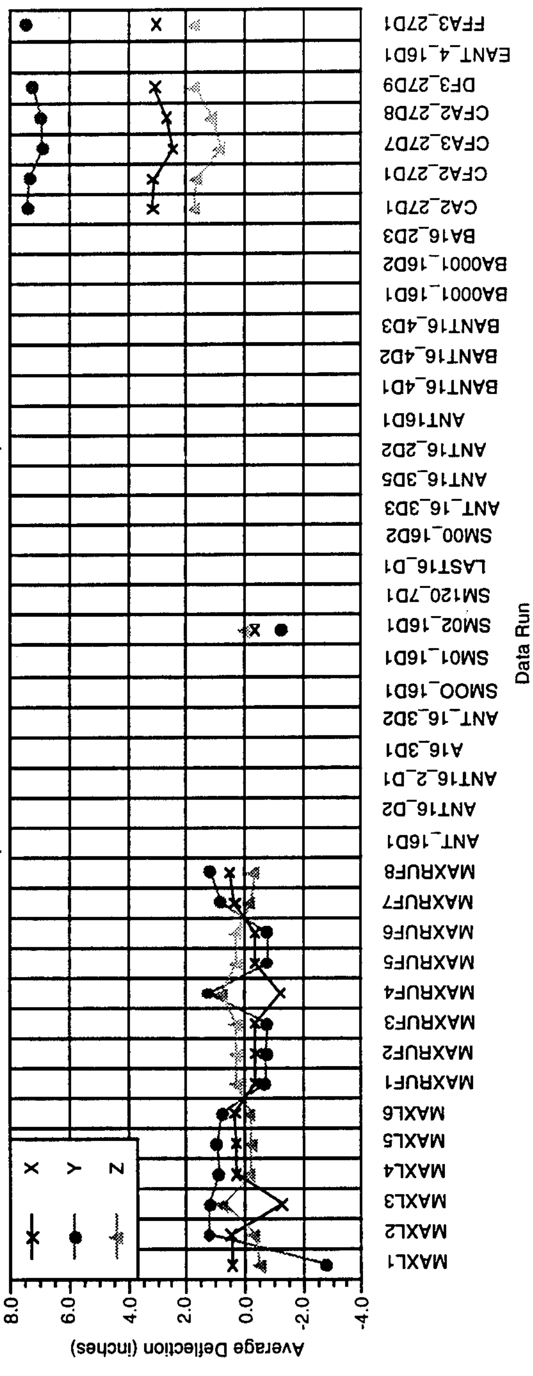

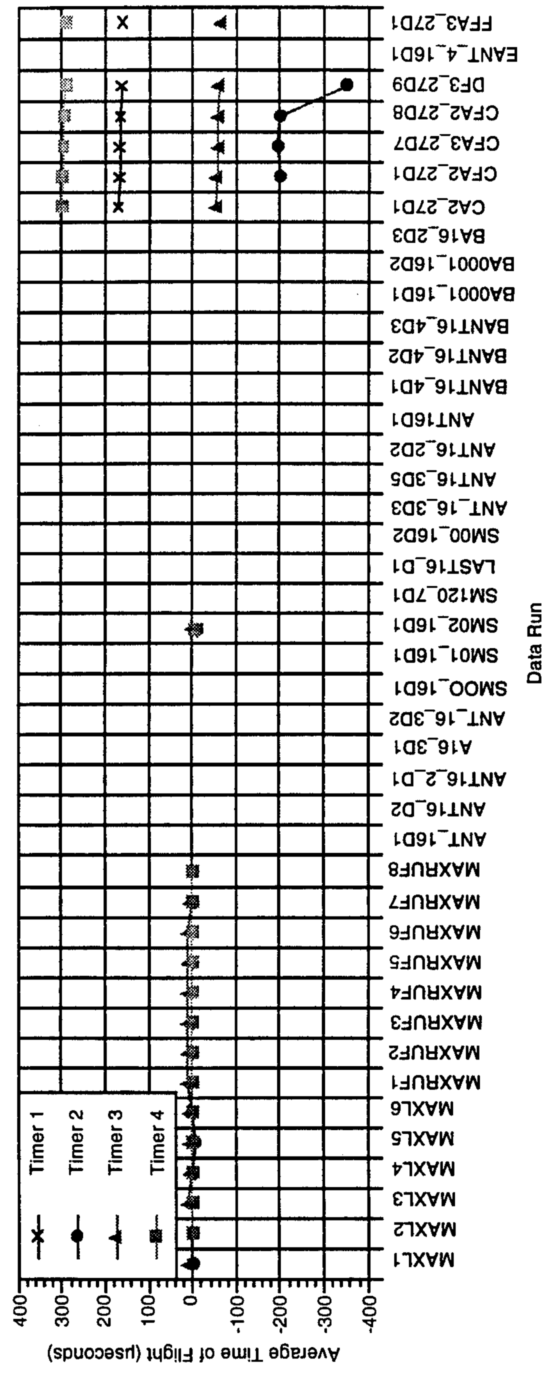

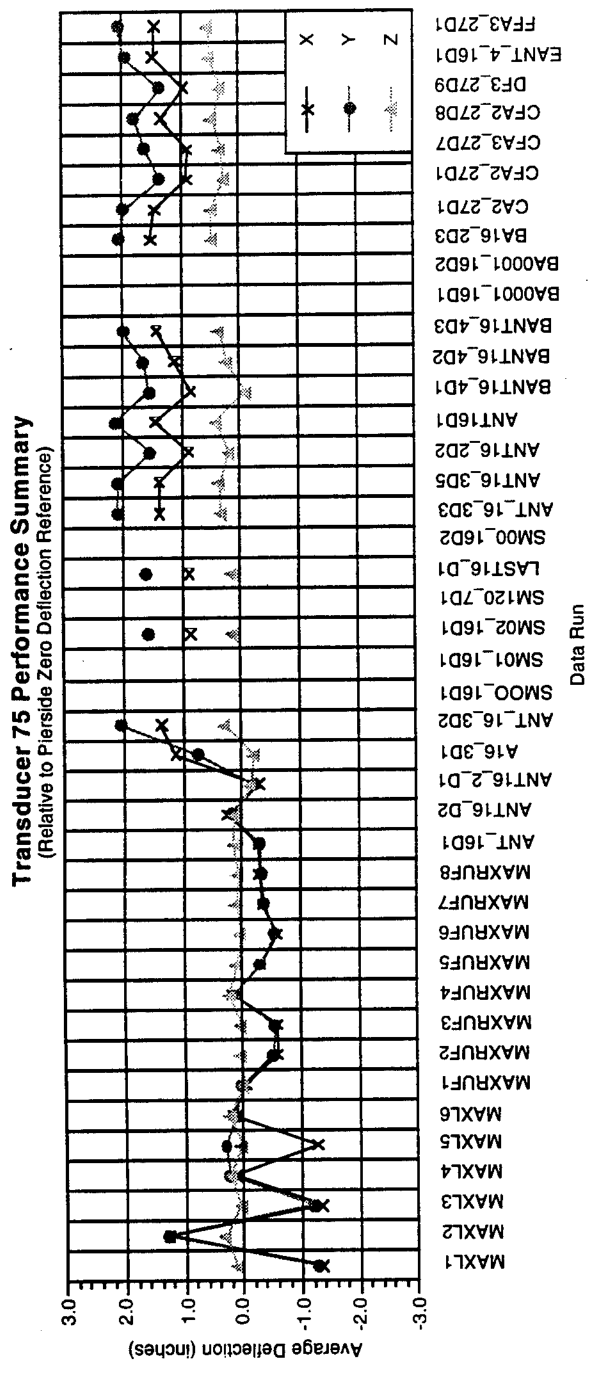
Transducer 75 Performance Summary
(Relative to Pierside Zero Deflection Reference)
Average Deflection (inches)
Data Run
X
Y
Z

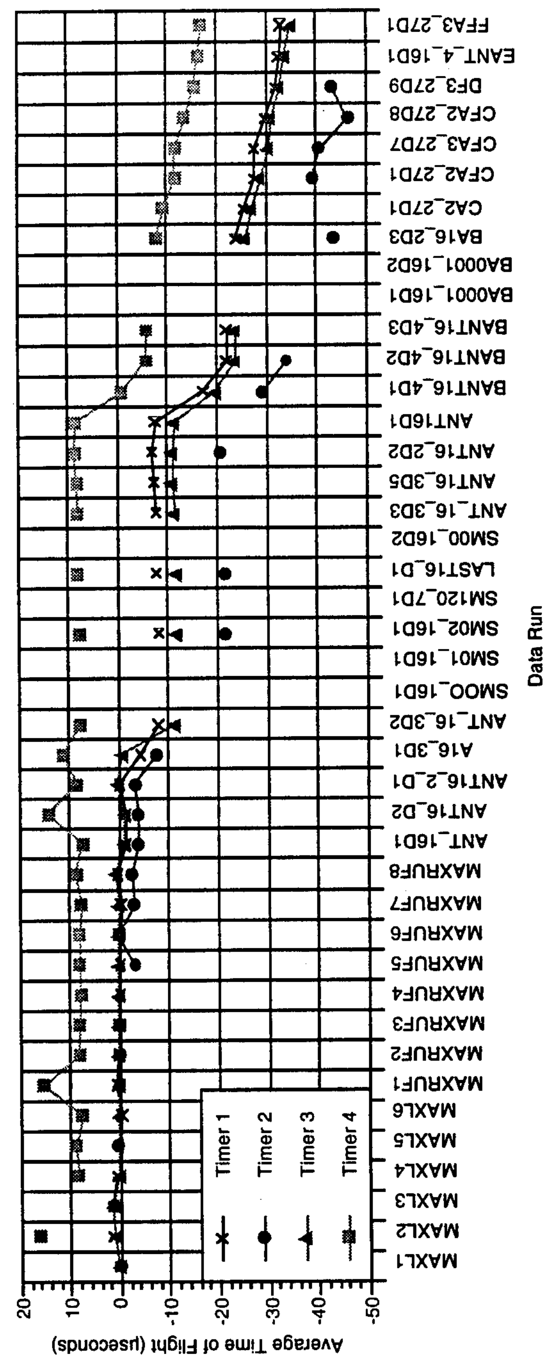
Average Time of Flight (μseconds)
Data Run
Timer 1
Timer 2
Timer 3
Timer 4

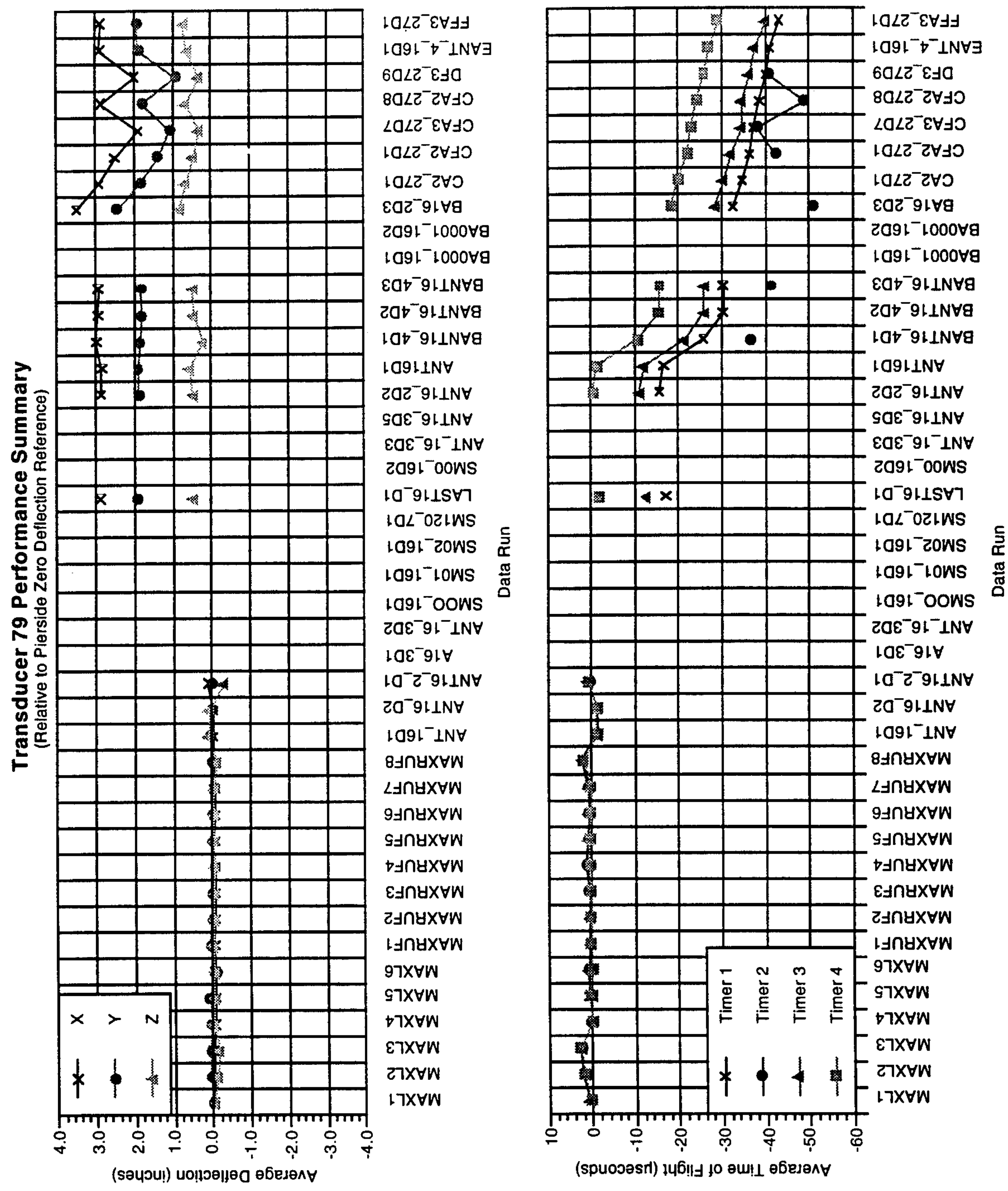
Transducer 79 Performance Summary
(Relative to Pierside Zero Deflection Reference)
Average Deflection (inches)
Average Time of Flight (µseconds)
Data Run
X
Y
Z
Timer 1
Timer 2
Timer 3
Timer 4

Transducer 82 Performance Summary
(Relative to Pierside Zero Deflection Reference)

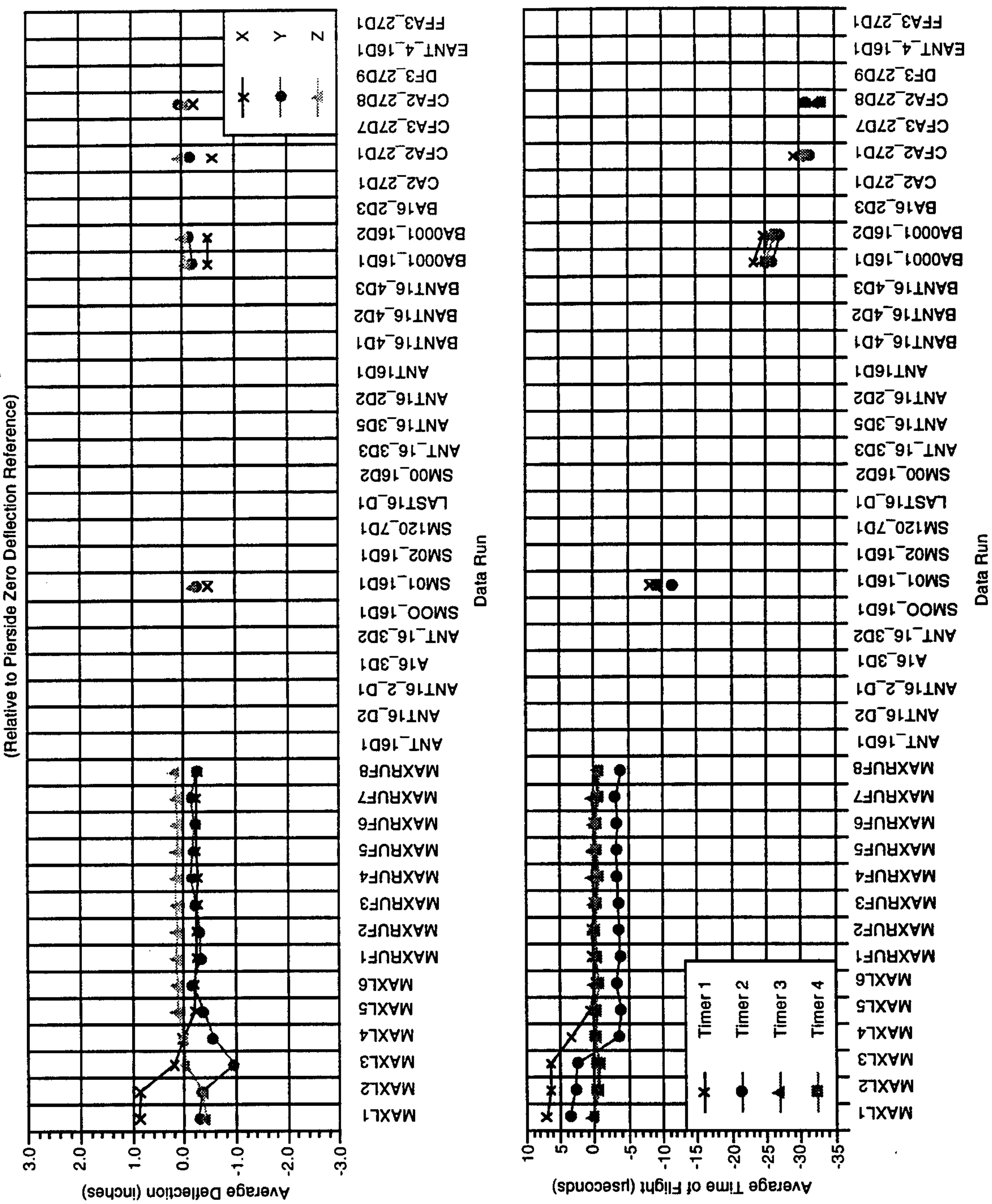

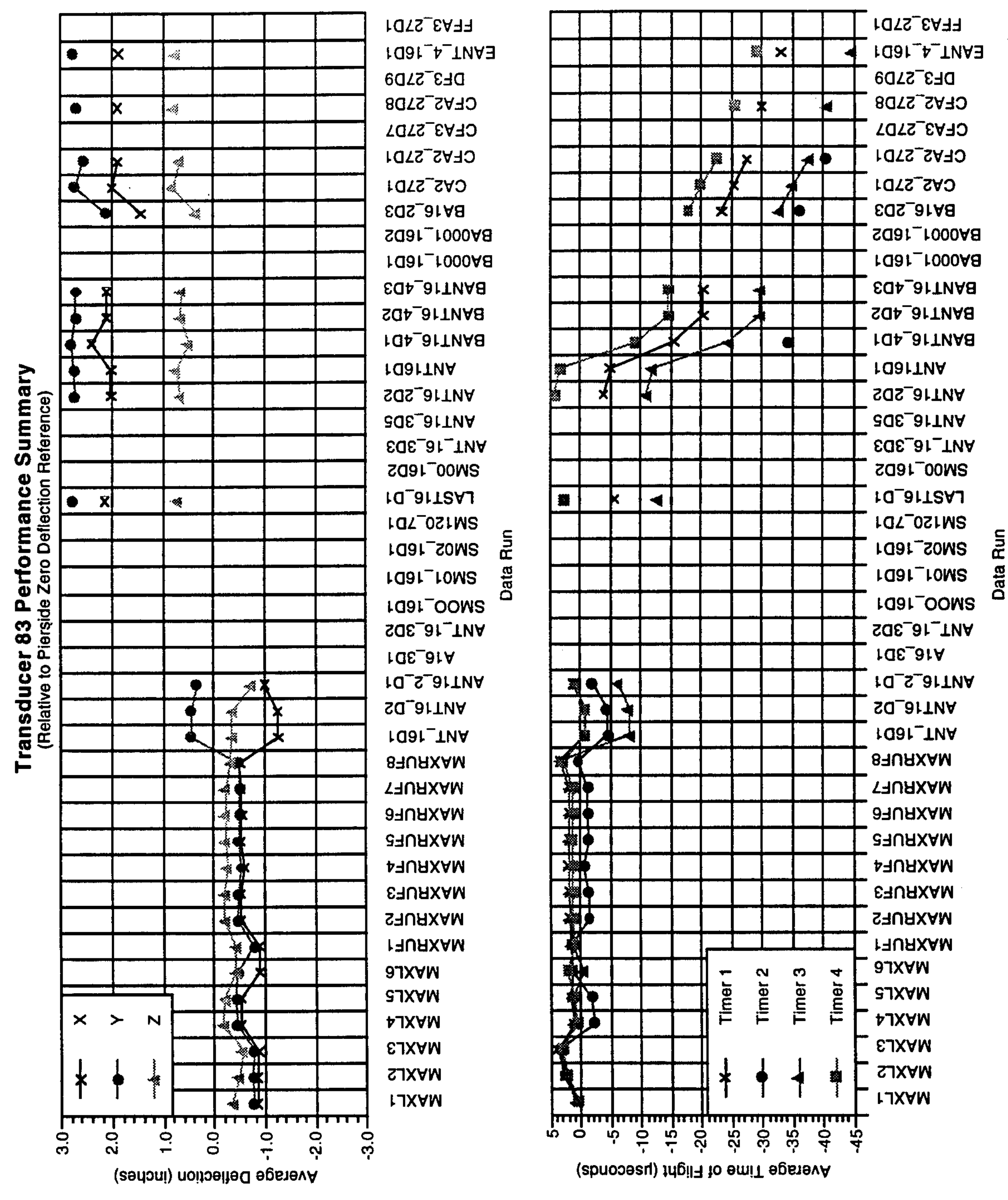
Transducer 83 Performance Summary
(Relative to Pierside Zero Deflection Reference)
Average Deflection (inches)
Data Run
X
Y
Z
Average Time of Flight (µseconds)
Data Run
Timer 1
Timer 2
Timer 3
Timer 4

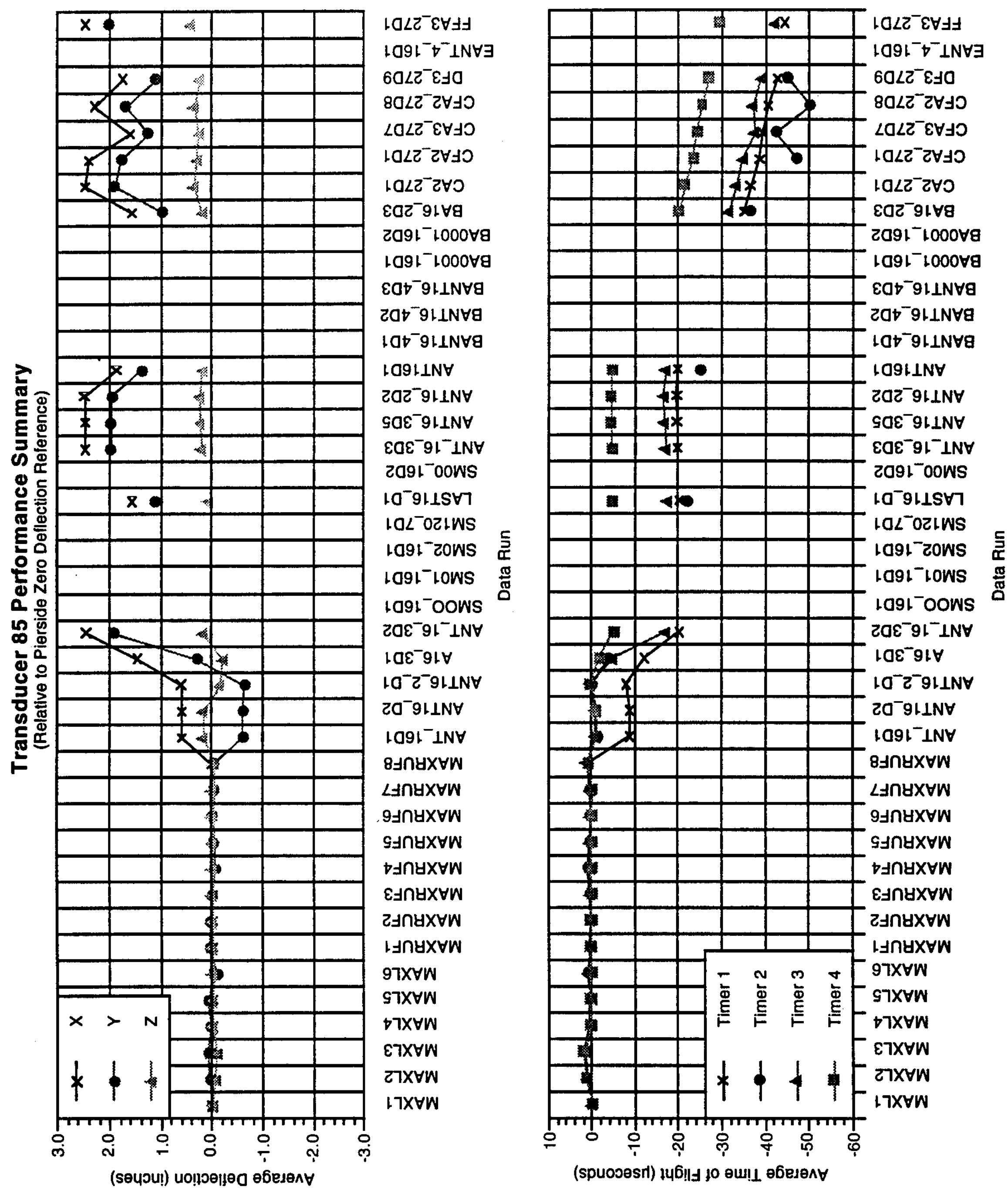
Transducer 85 Performance Summary
(Relative to Pierside Zero Deflection Reference)
Average Deflection (inches)
Average Time of Flight (µseconds)
Data Run
X
Y
Z
Timer 1
Timer 2
Timer 3
Timer 4

Transducer 86 Performance Summary
(Relative to Pierside Zero Deflection Reference)

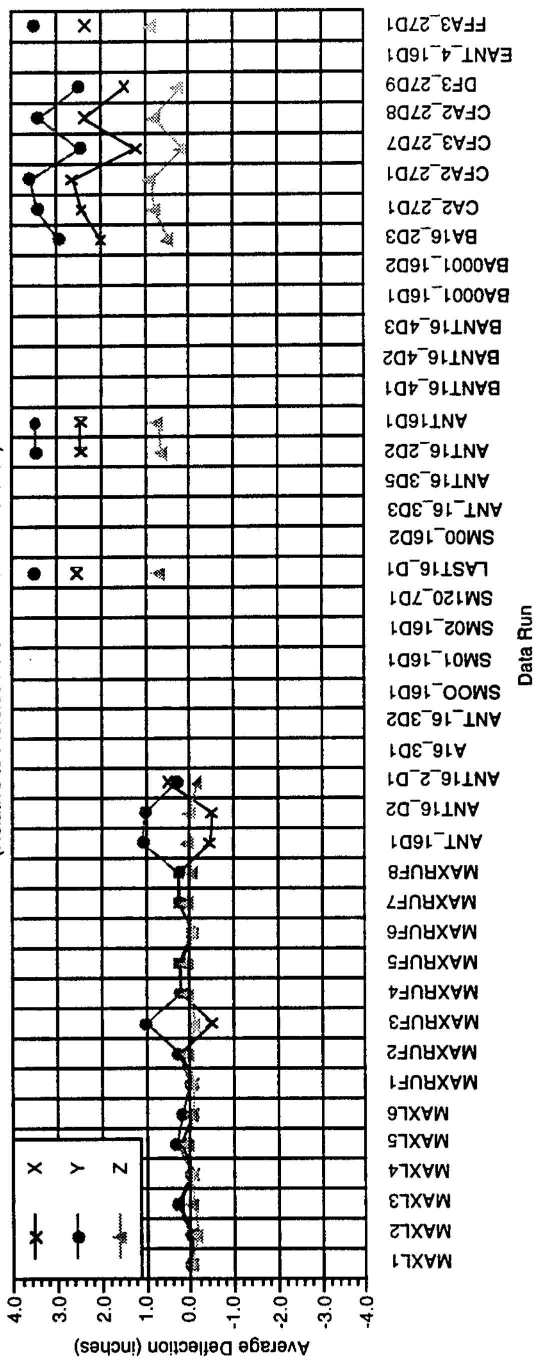

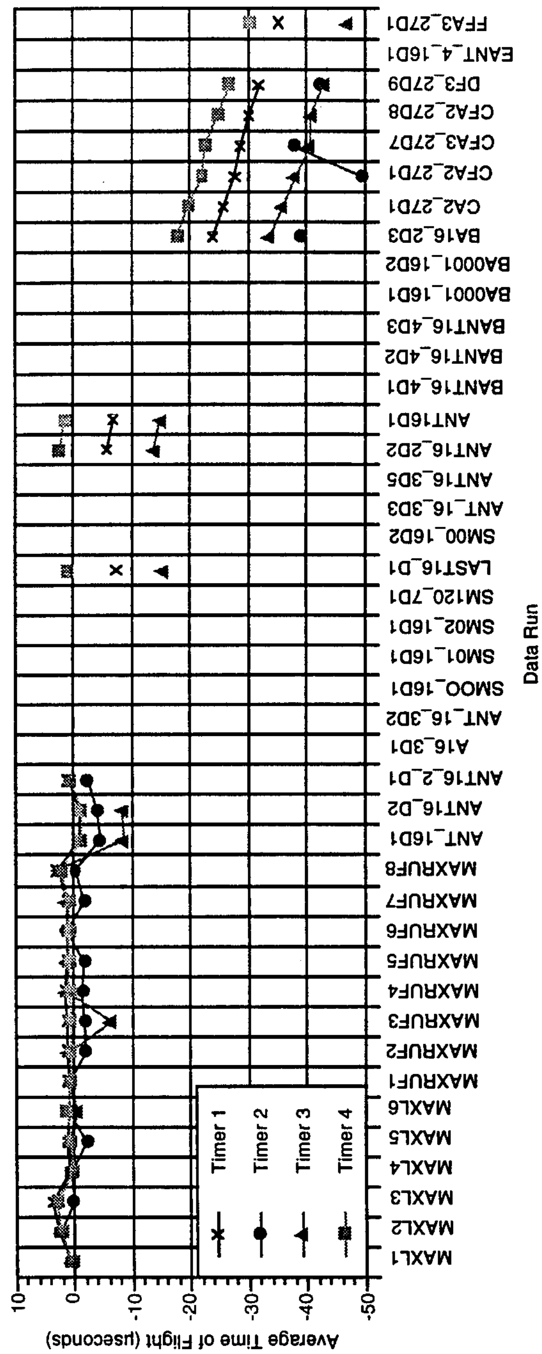

Transducer 87 Performance Summary

(Relative to Pierside Zero Deflection Reference)

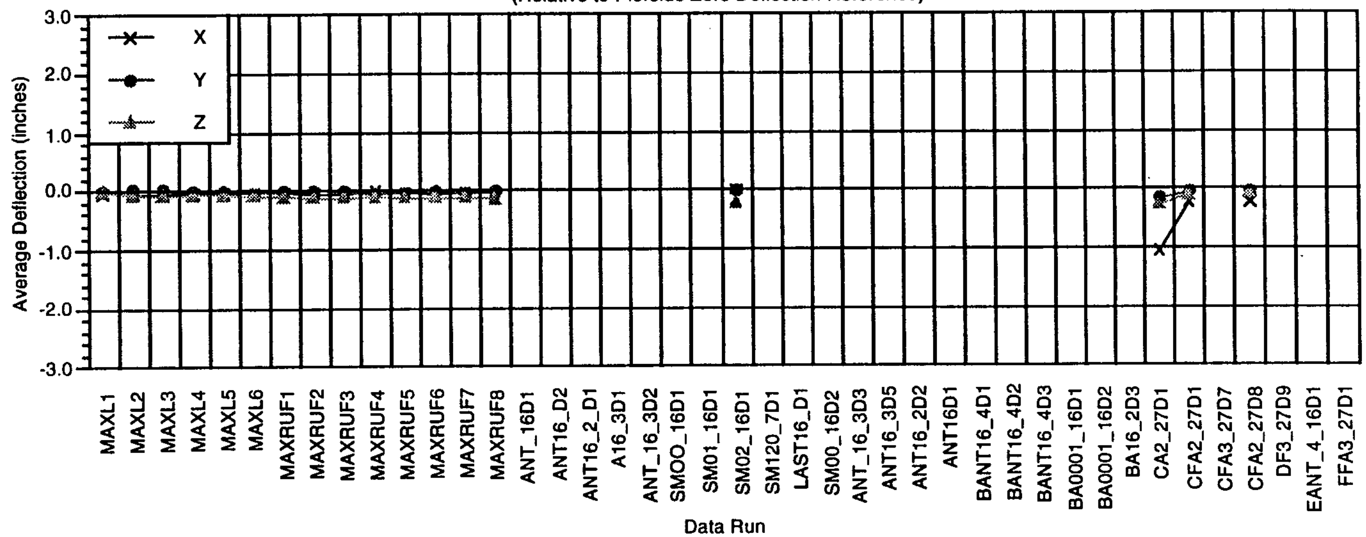

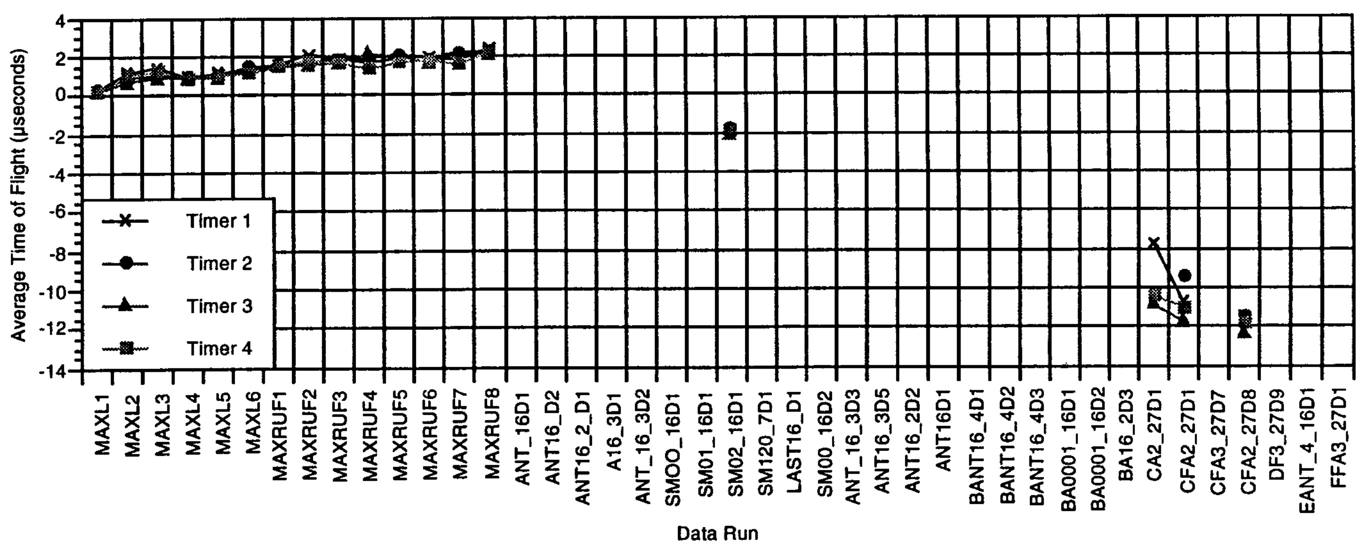

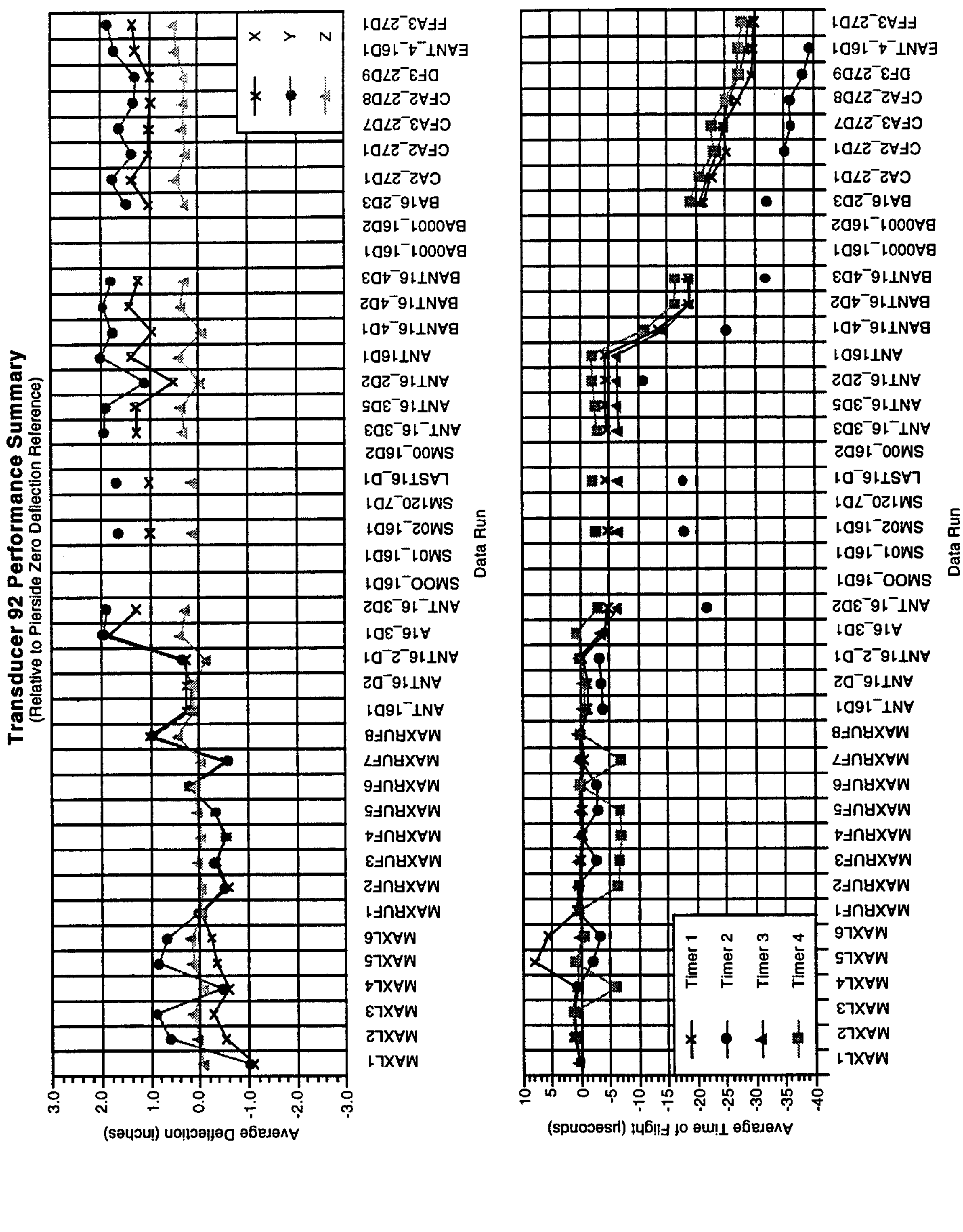
Transducer 92 Performance Summary
(Relative to Pierside Zero Deflection Reference)
Average Deflection (inches)
Average Time of Flight (µseconds)
Data Run
X
Y
Z
Timer 1
Timer 2
Timer 3
Timer 4

Transducer 95 Performance Summary
(Relative to Pierside Zero Deflection Reference)

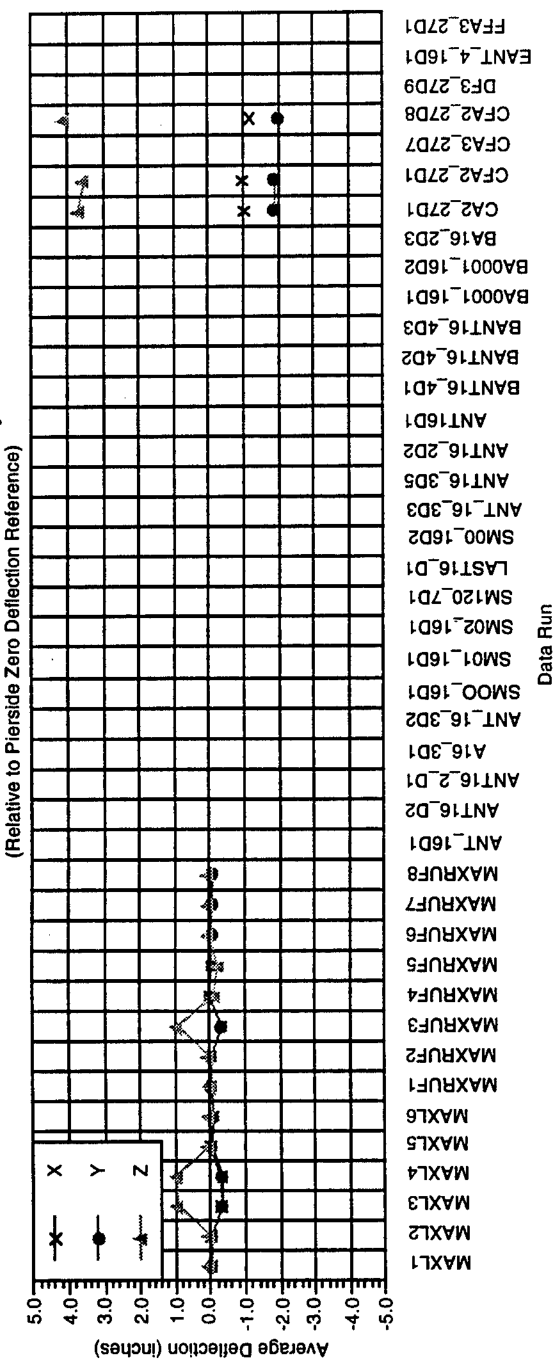

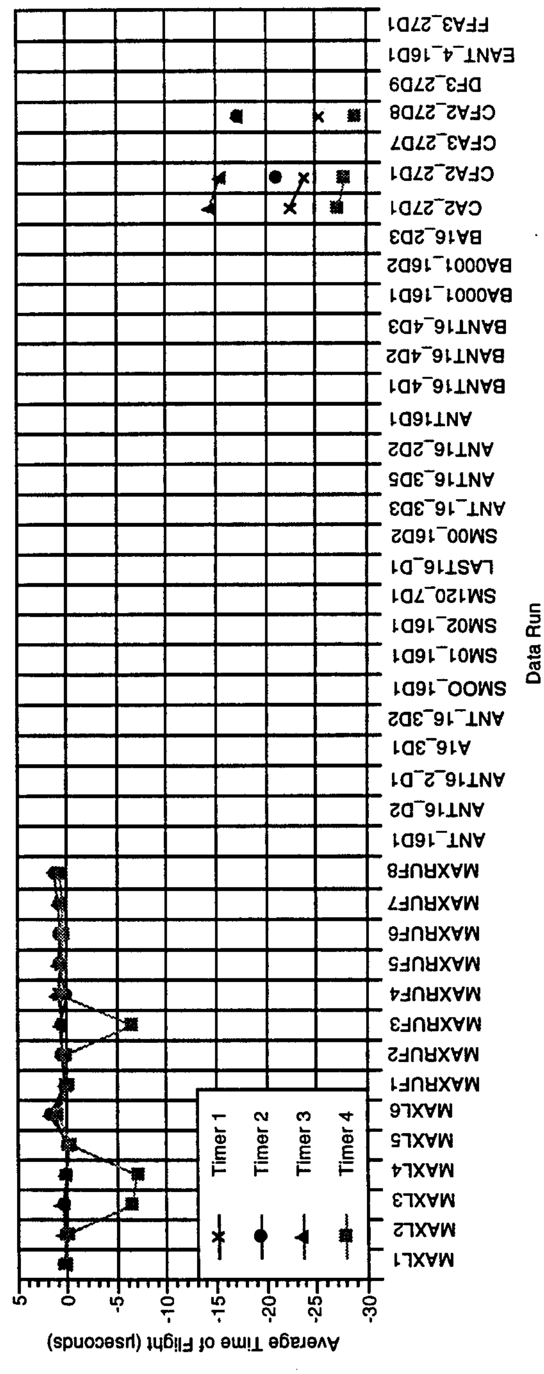

Transducer 108 Performance Summary
(Relative to Pierside Zero Deflection Reference)

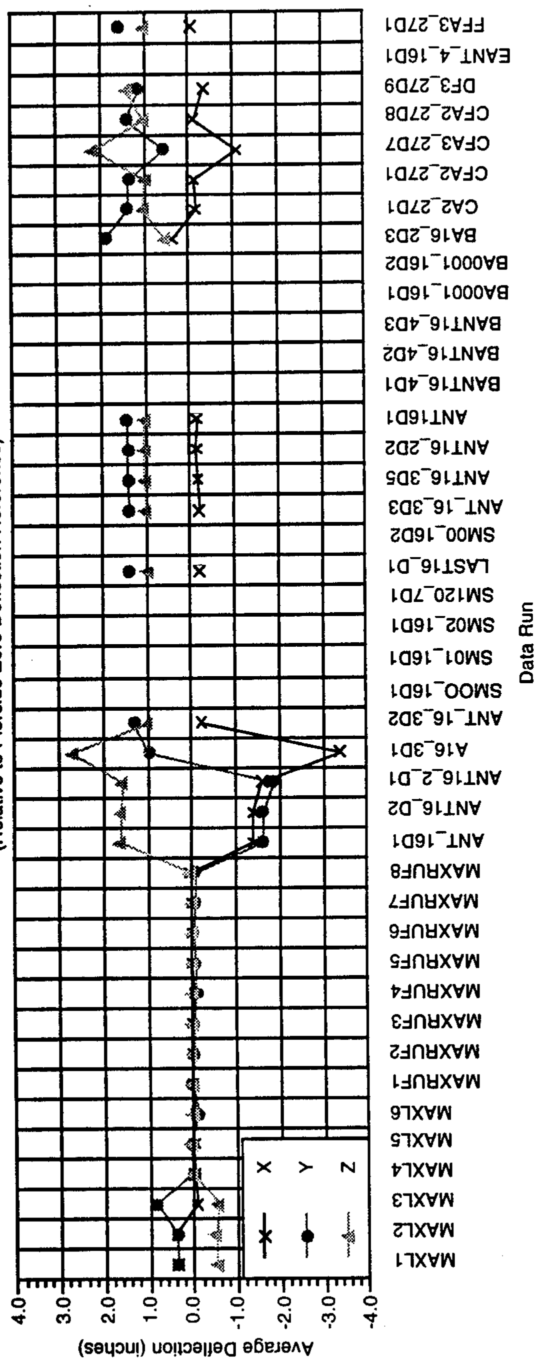

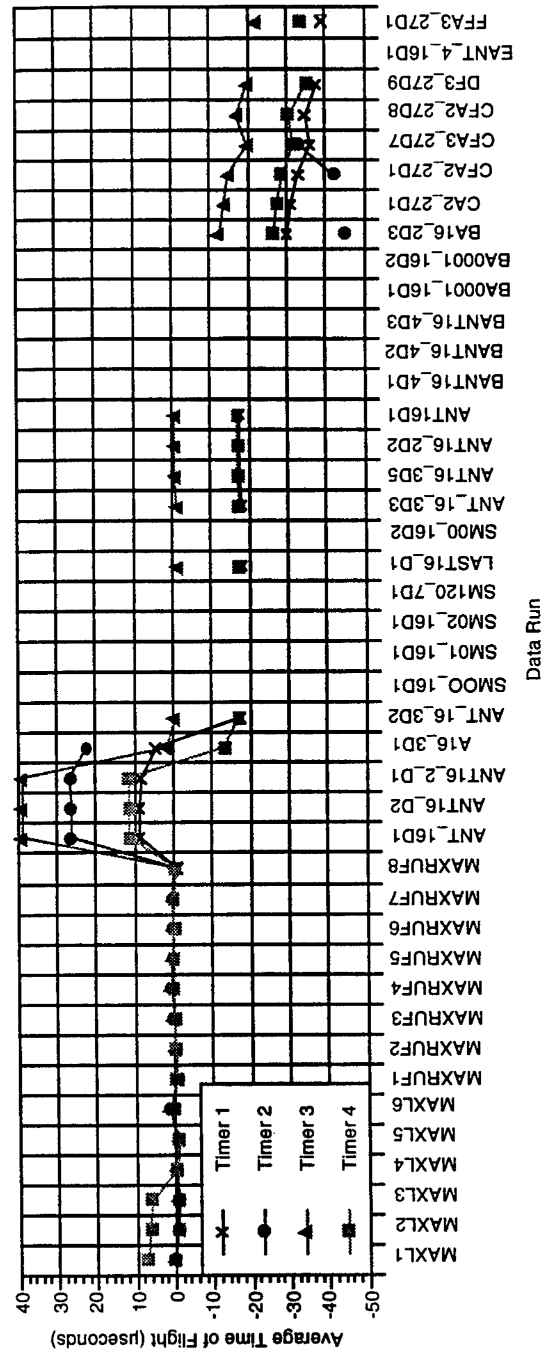

Appendix B: Data Run Range Summaries

The graphs presented in this appendix represent the *dynamic* behavior of most of the driver transducers used in the 26 Antigua underway data runs. Some driver transducers were removed from the graphs because they exhibited such extreme offsets from the zero deflection pierside reference that they skewed the vertical scaling on the graphs to the point where the dynamic ranges of some other driver transducers became too small to register on the graph.

The graphs are chronologically arranged by data run. Each page displays three graphs, each graph representing an axis in the Cartesian coordinate system. The X-axis of each graph represents a subset of driver transducers from a given data run. The Y-axis of each graph represents the range of deflections measured in a given data run, with reference to the zero deflection pierside reference. The data for each transducer is represented by a vertical bar which depicts the minimum and maximum measured deflections.

Some transducers exhibit a wide range of deflections while most others show a very small range of deflections. The transducers that yield what seems to be a disproportionately wide deflection range, may contain data with a large amount of noise.

Data Run ANT16_2_D1

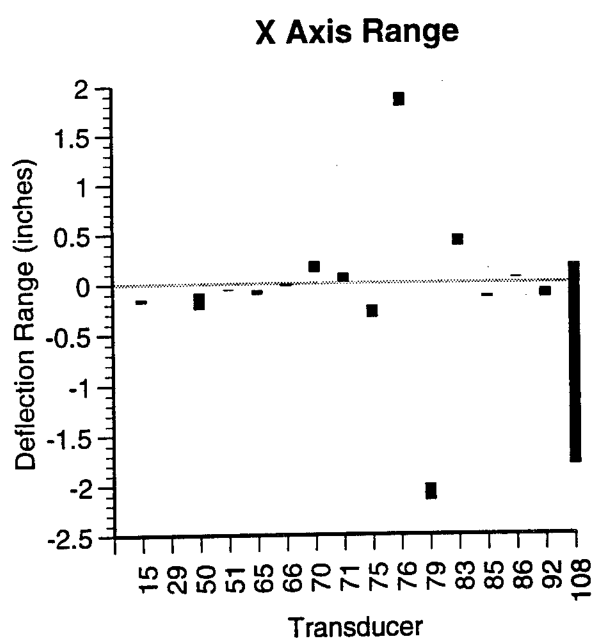

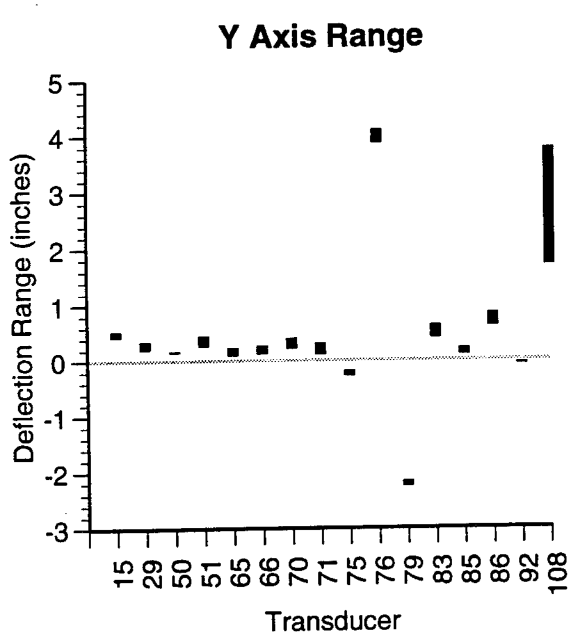

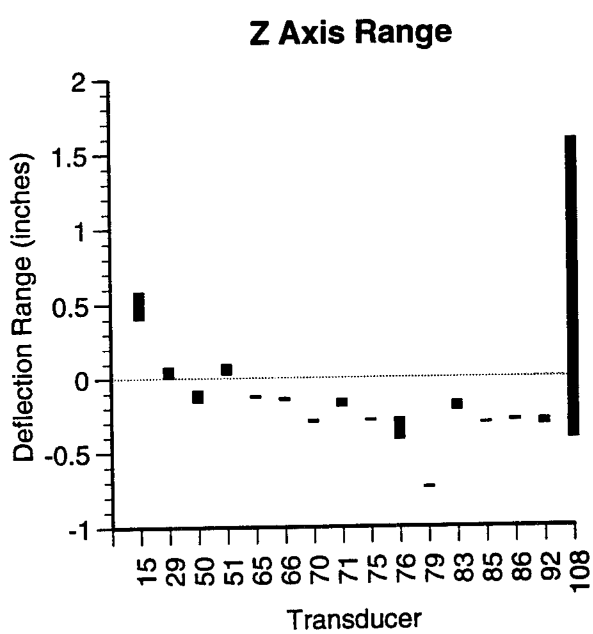

Data Run A16_3D1

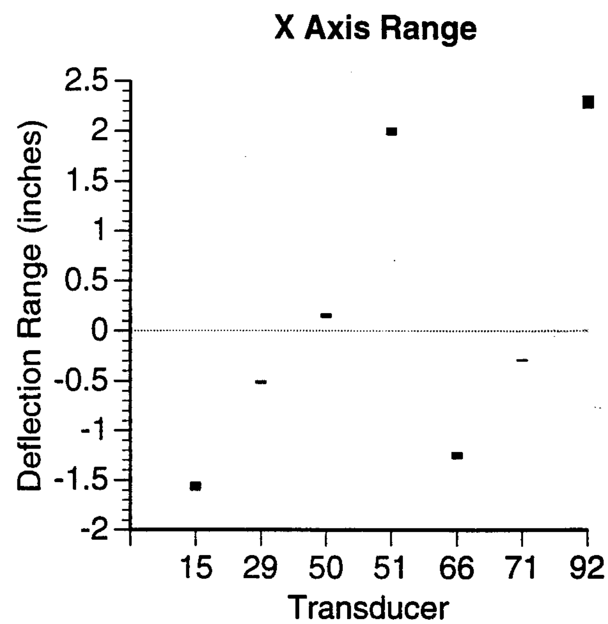

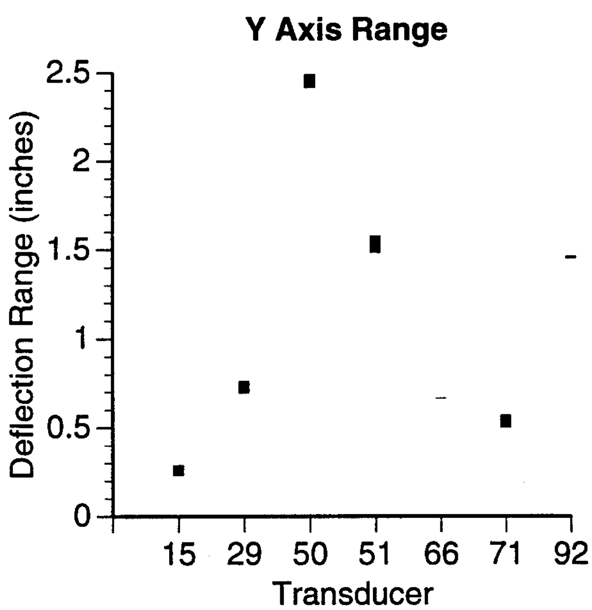

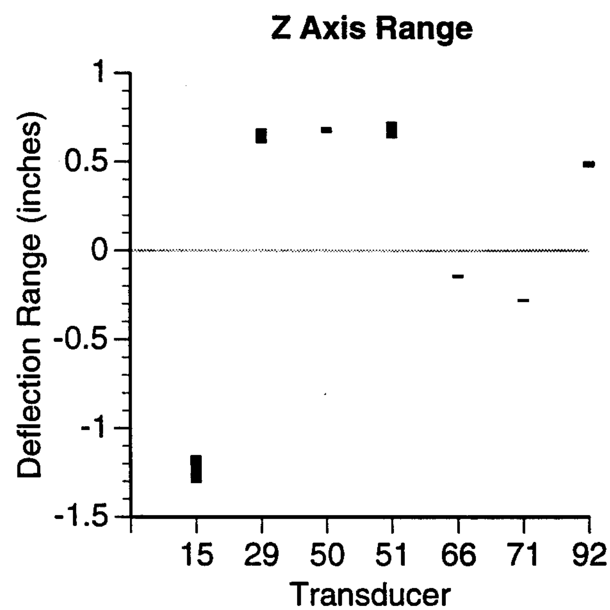

Data Run ANT_16_3D2

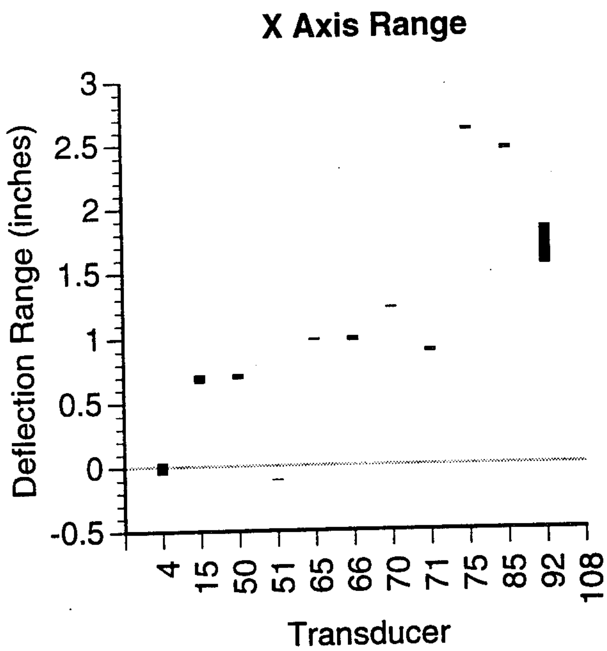

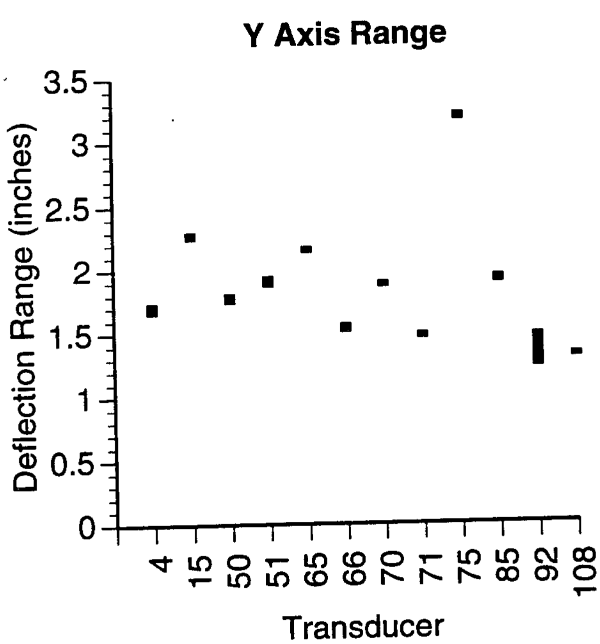

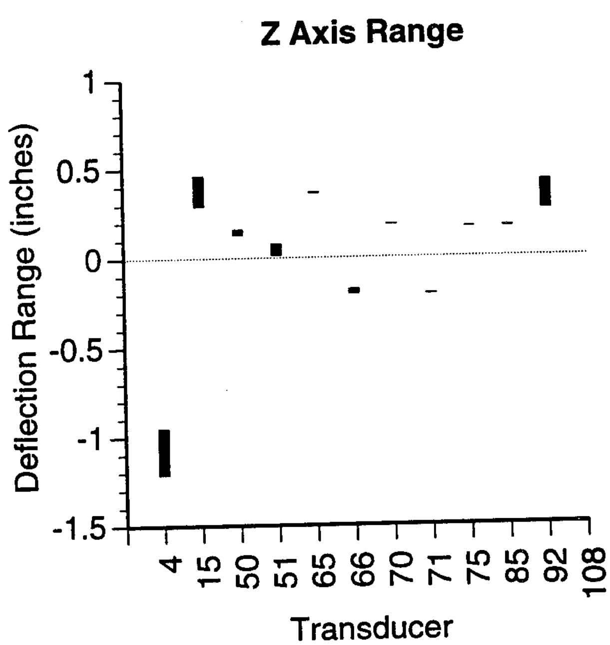

Data Run SM00_16D1

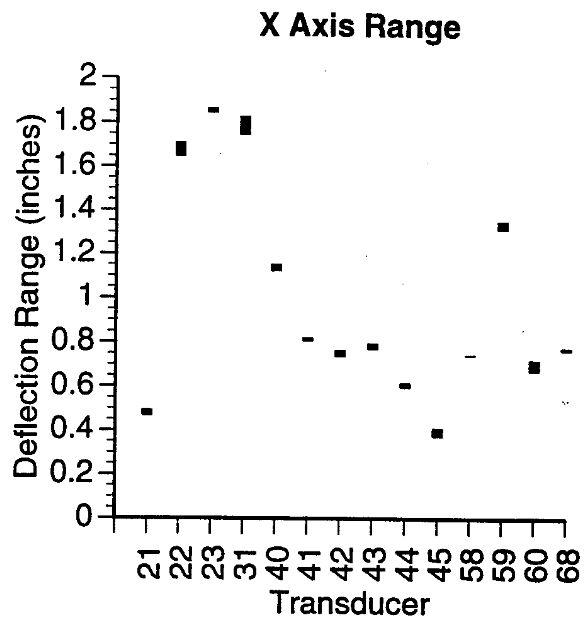

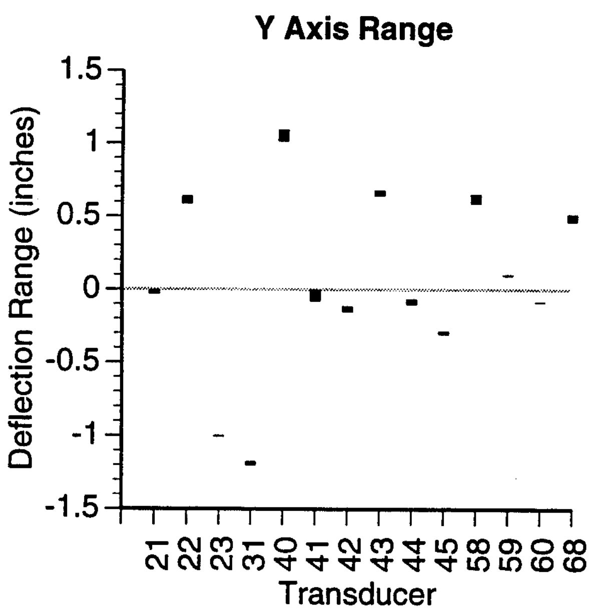

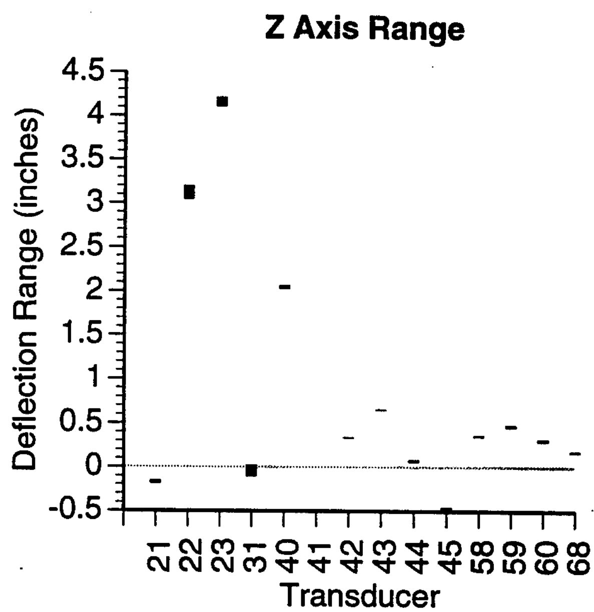

Data Run SM01_16D1

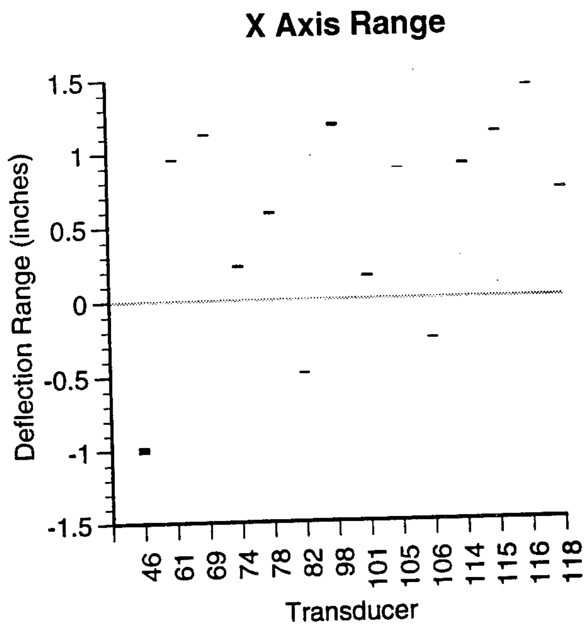

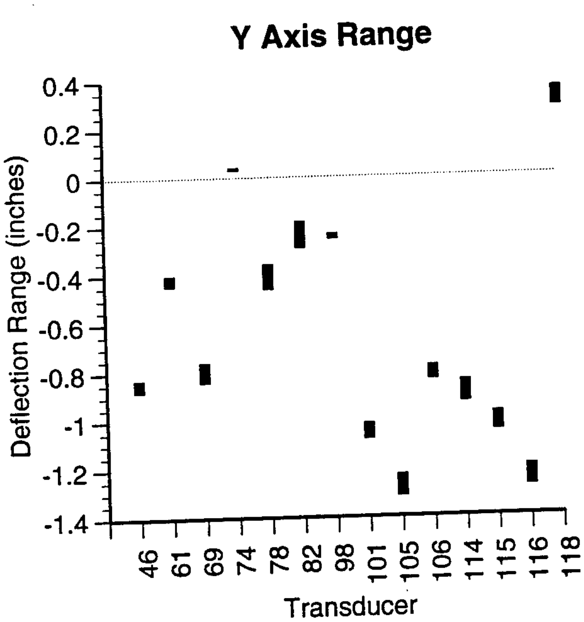

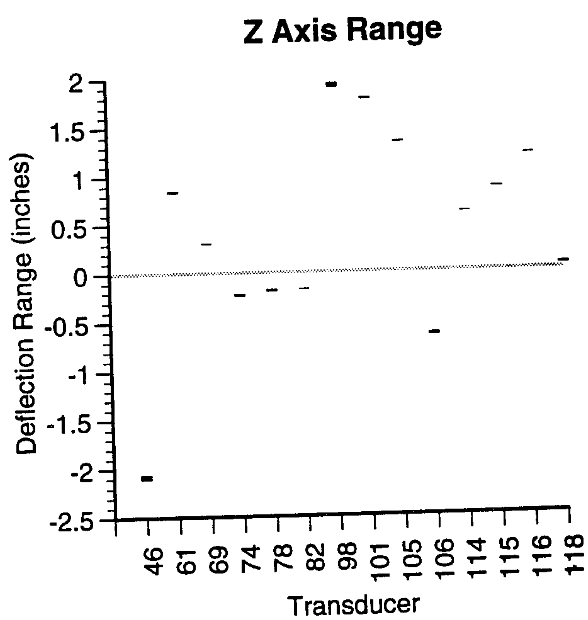

Data Run SM02_16D1

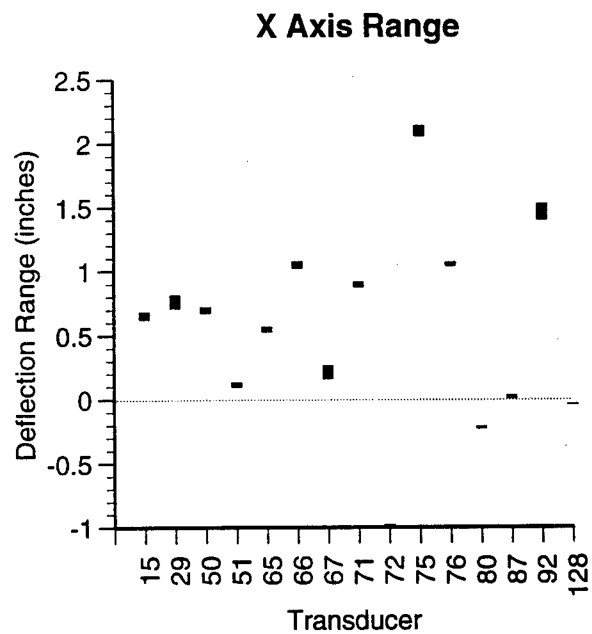

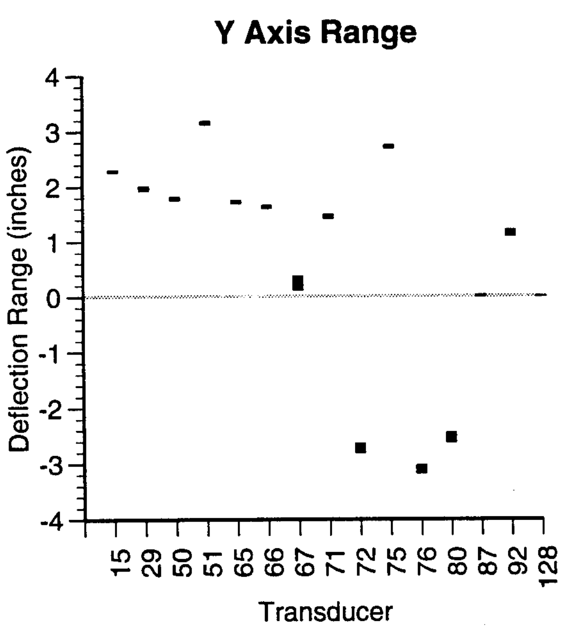

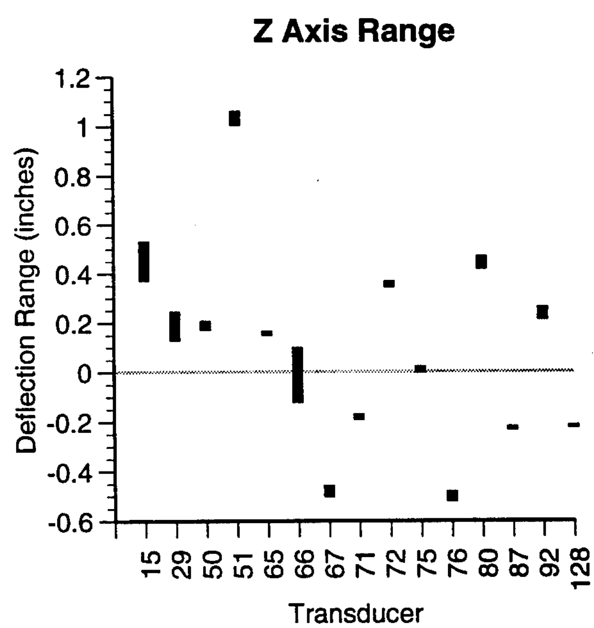

Data Run SM120_7D1

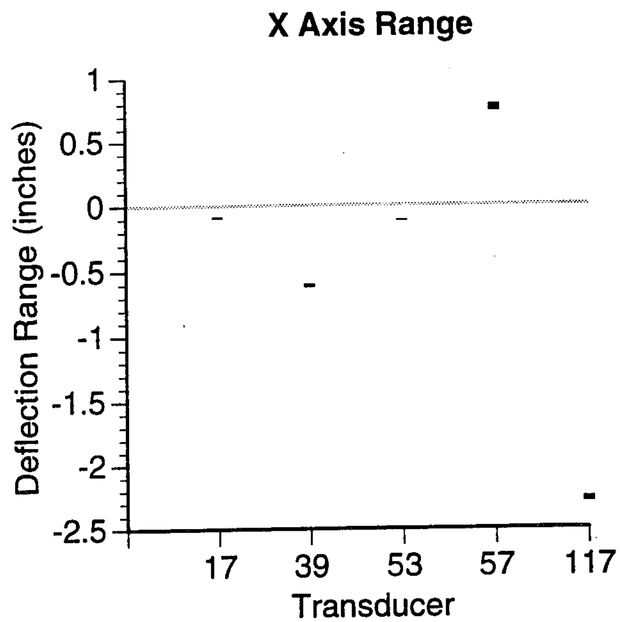

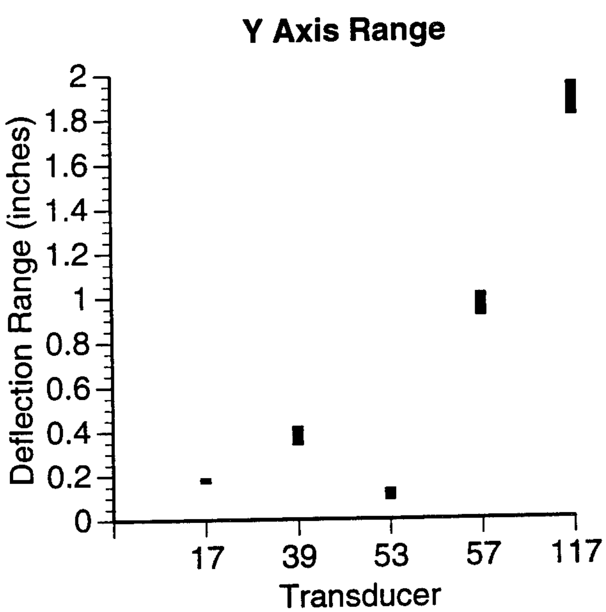

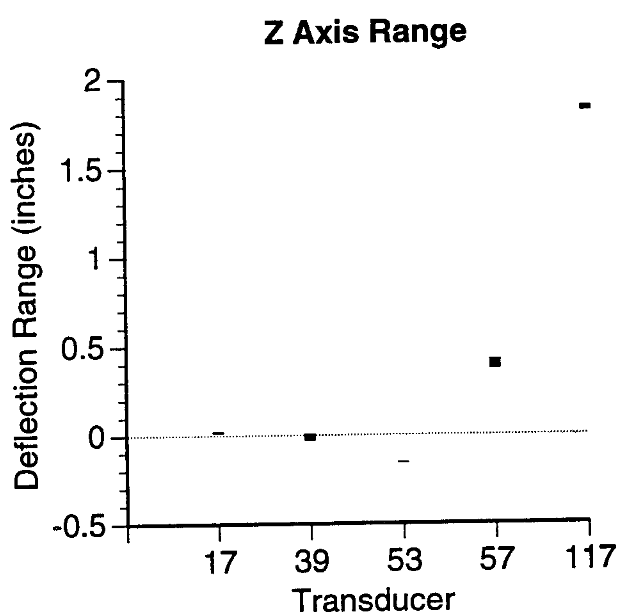

Data Run LAST16_D1

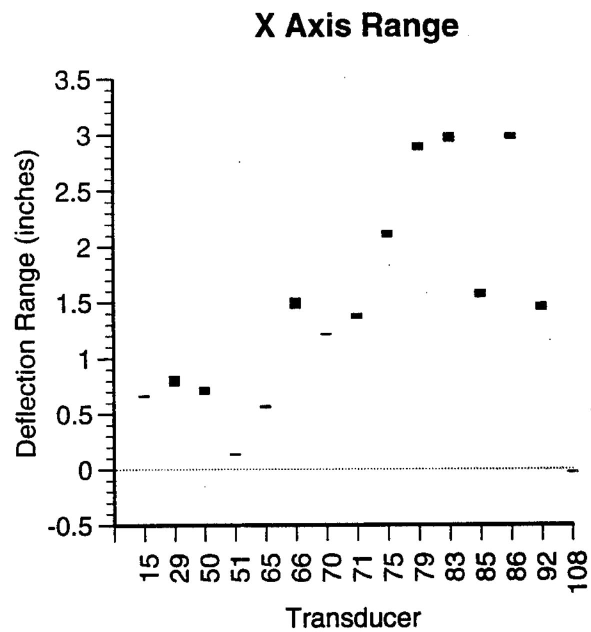

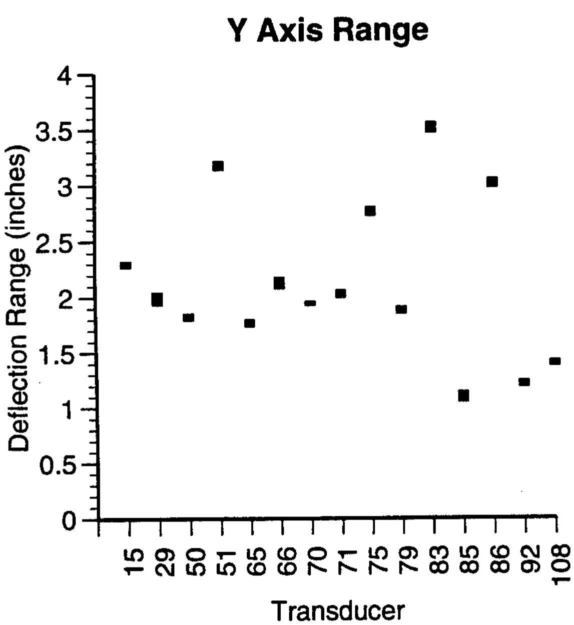

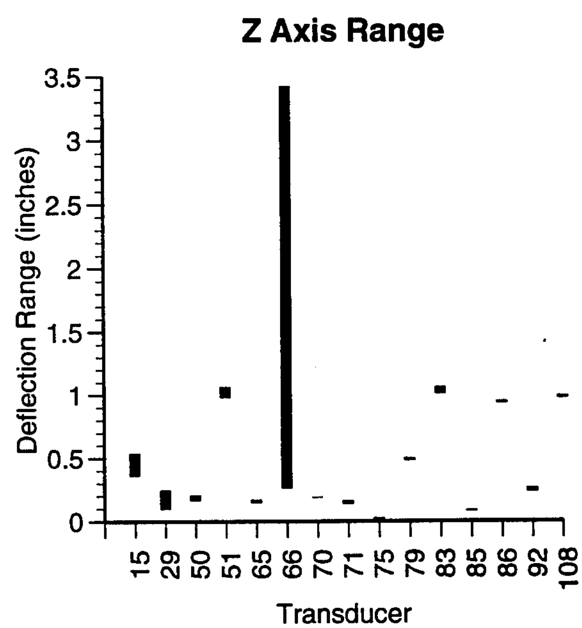

Data Run SM00_16D2

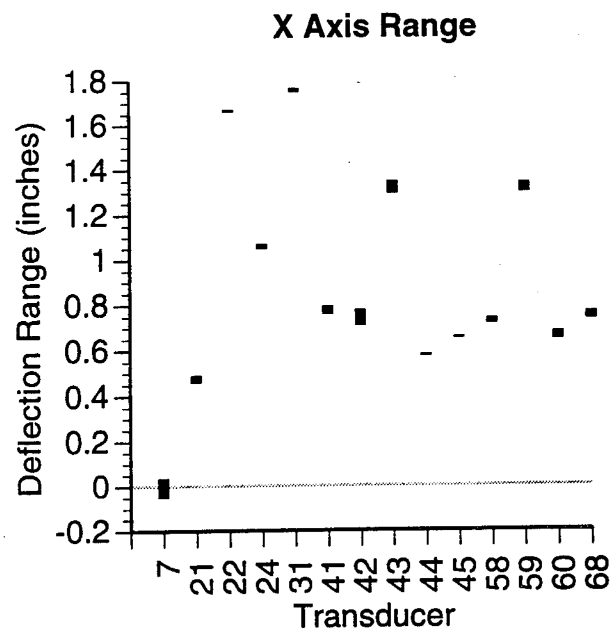

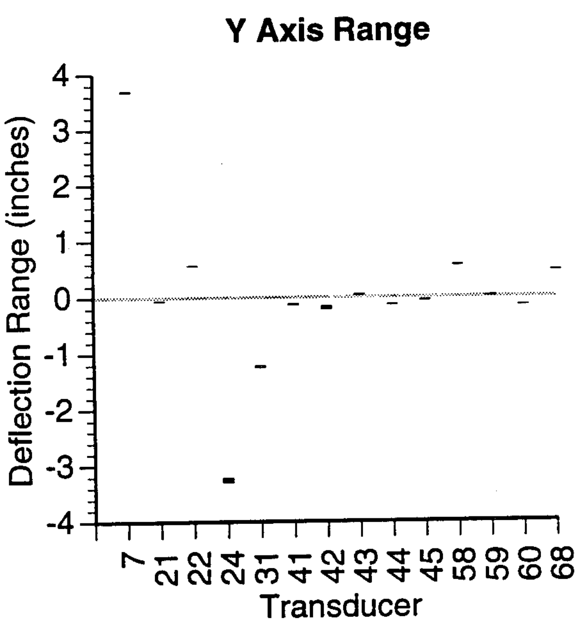

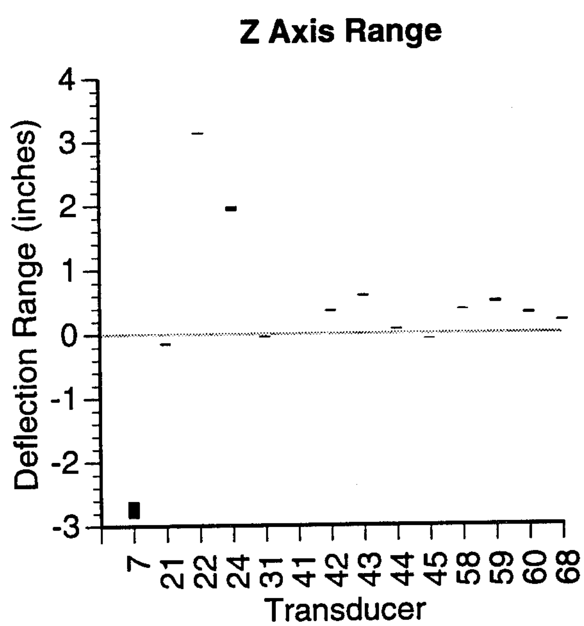

Data Run ANT_16_3D3

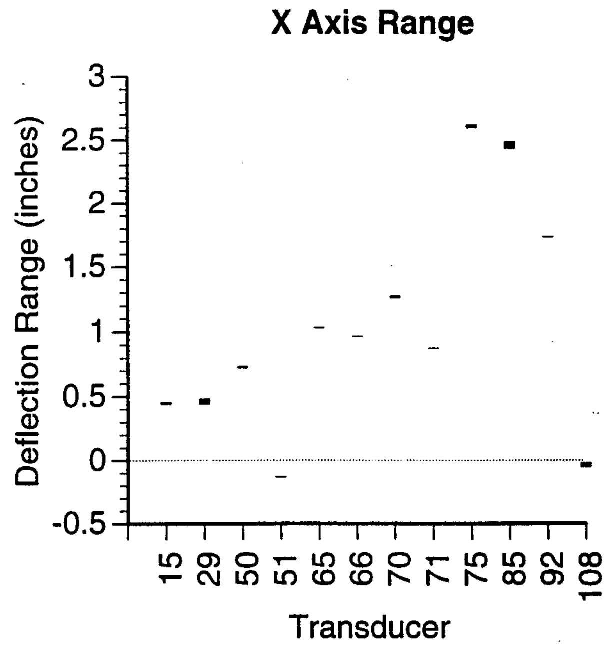

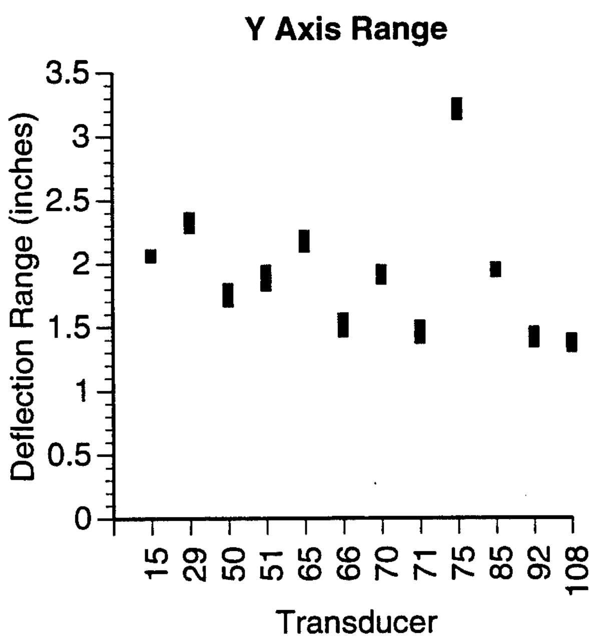

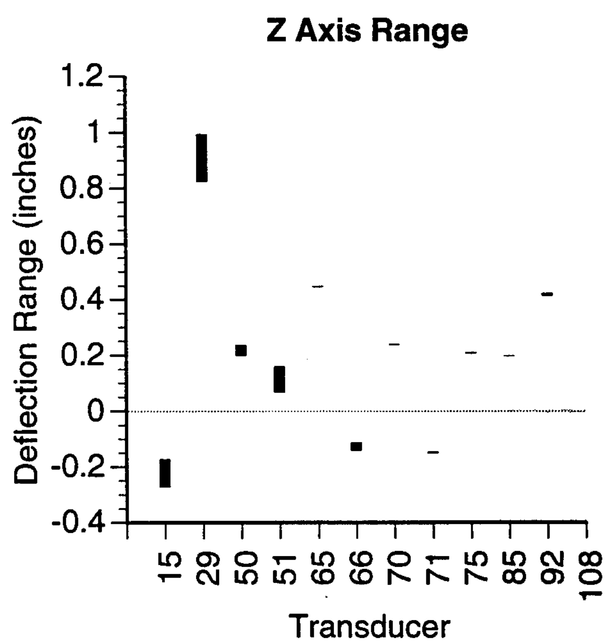

Data Run ANT16_3D5

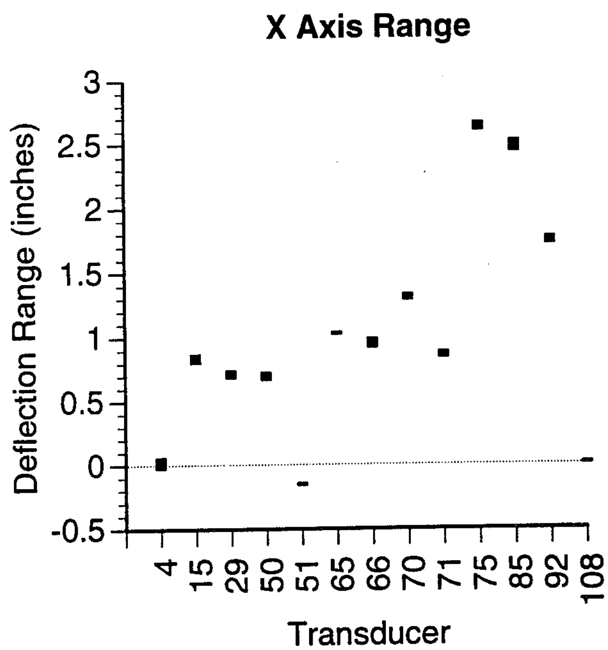

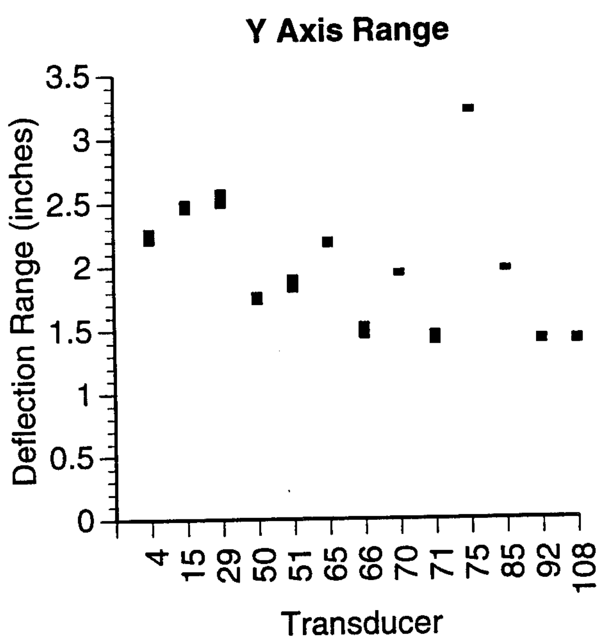

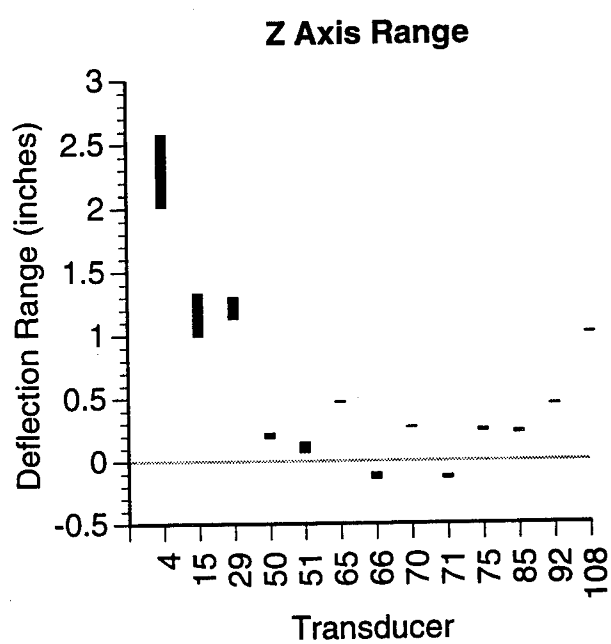

Data Run ANT16_2D2

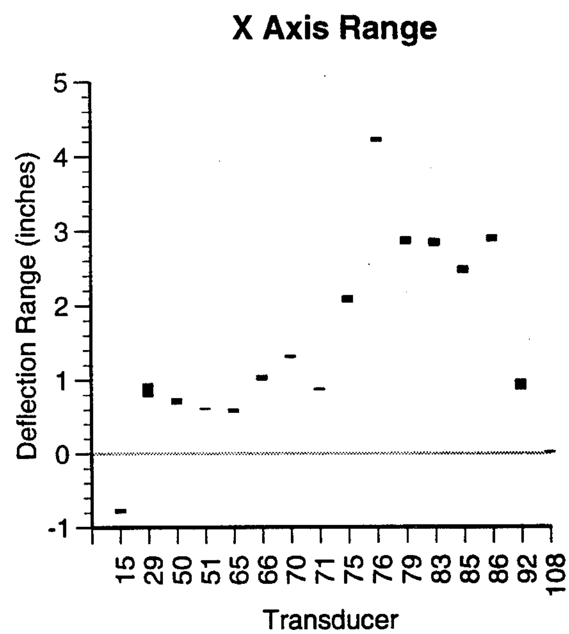

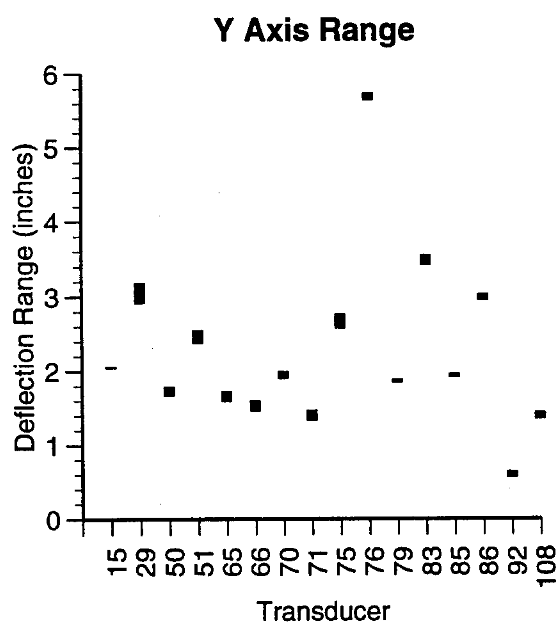

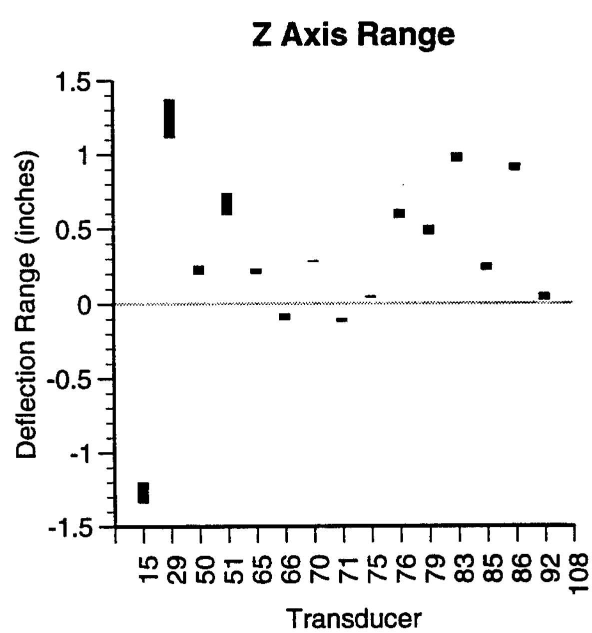

Data Run ANT16D1

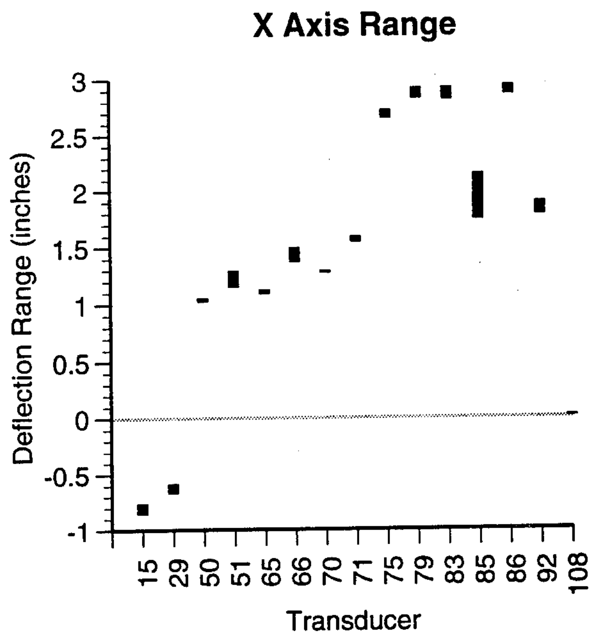

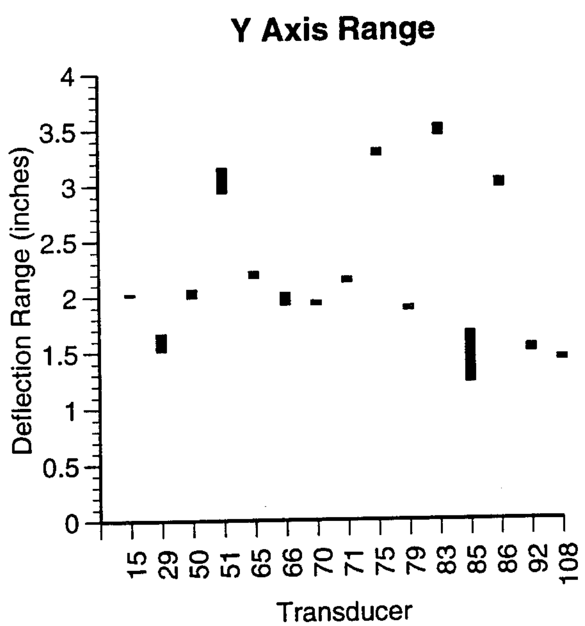

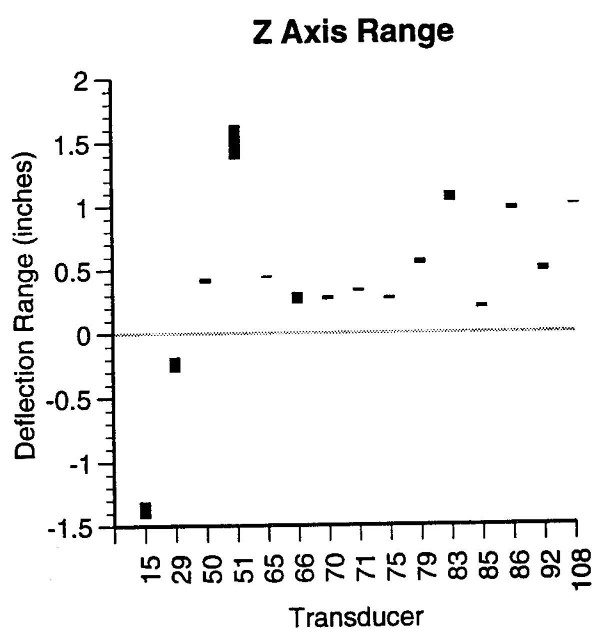

Data Run BANT16_4D1

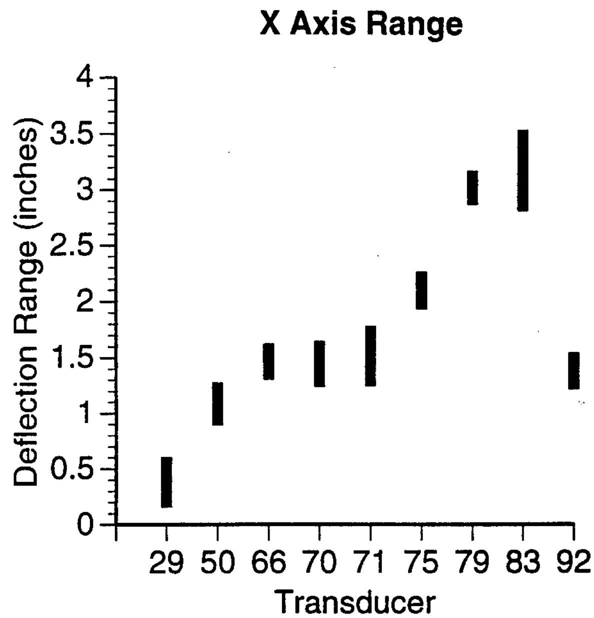

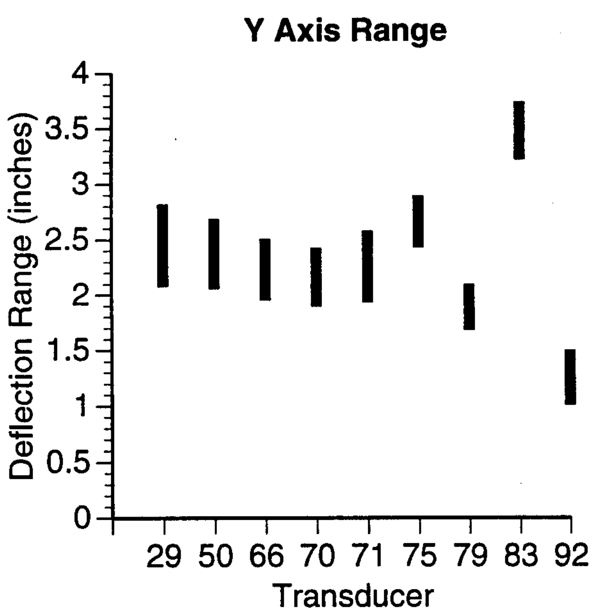

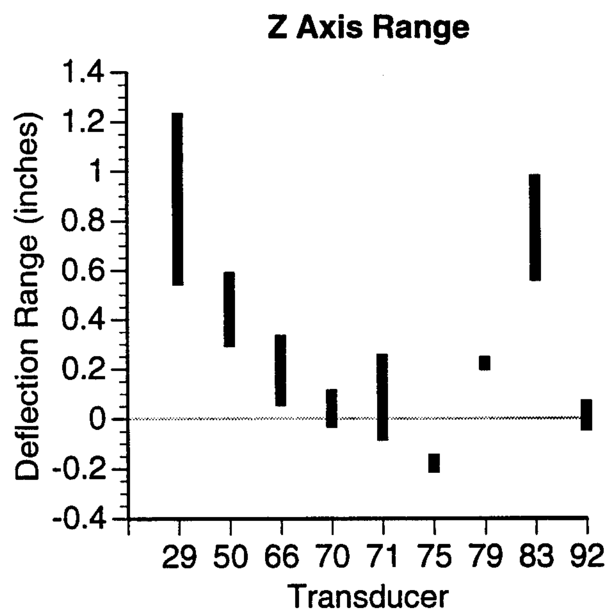

Data Run BANT16_4D2

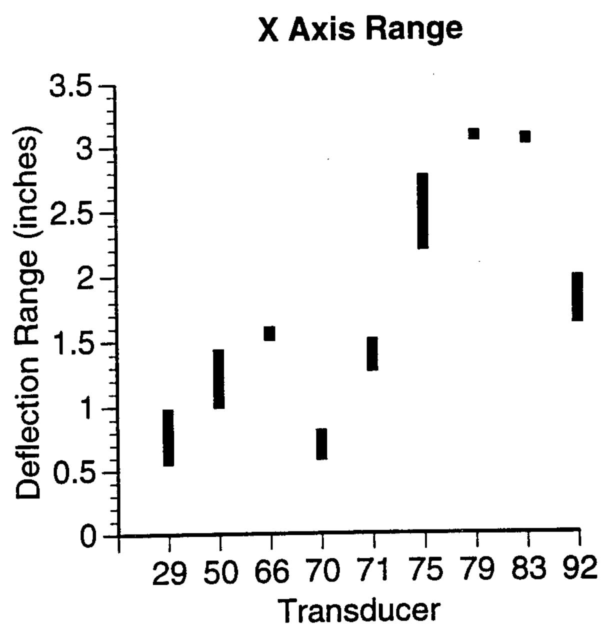

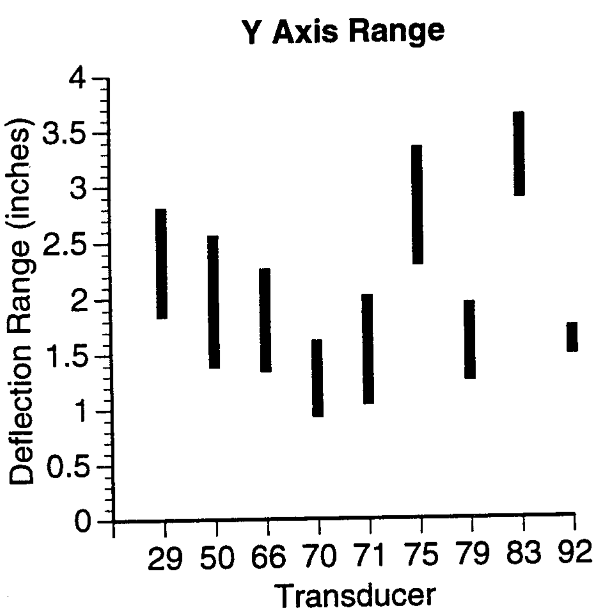

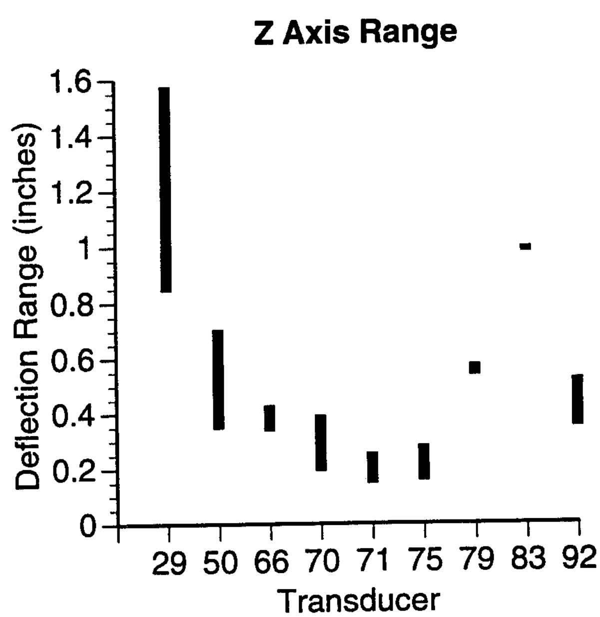

Data Run BANT16_4D3

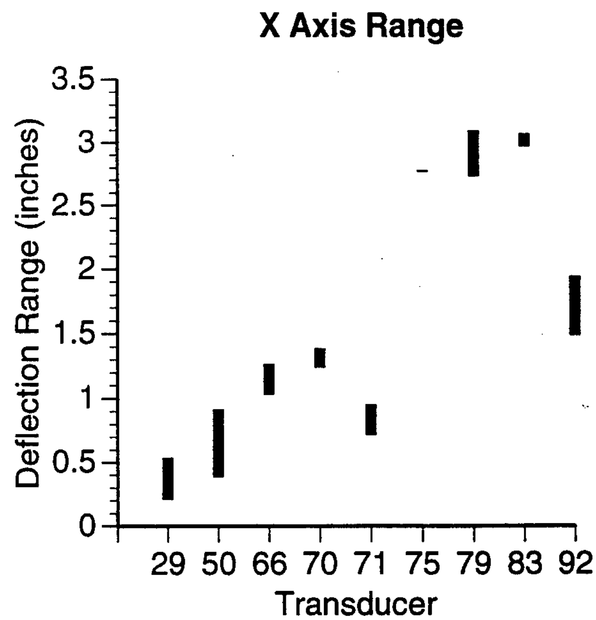

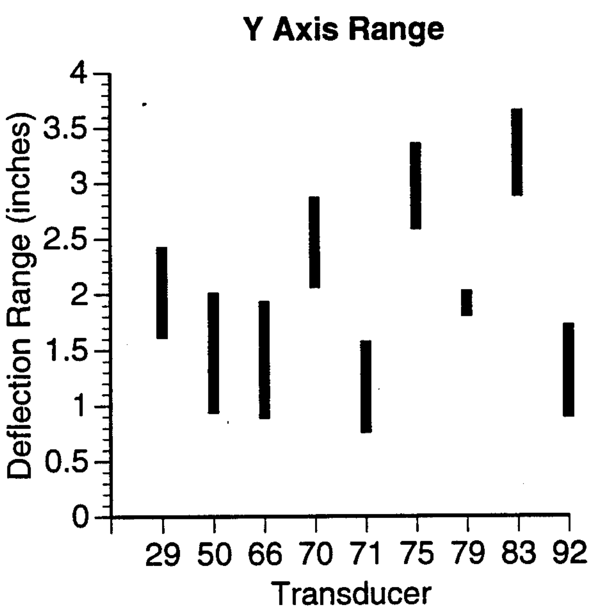

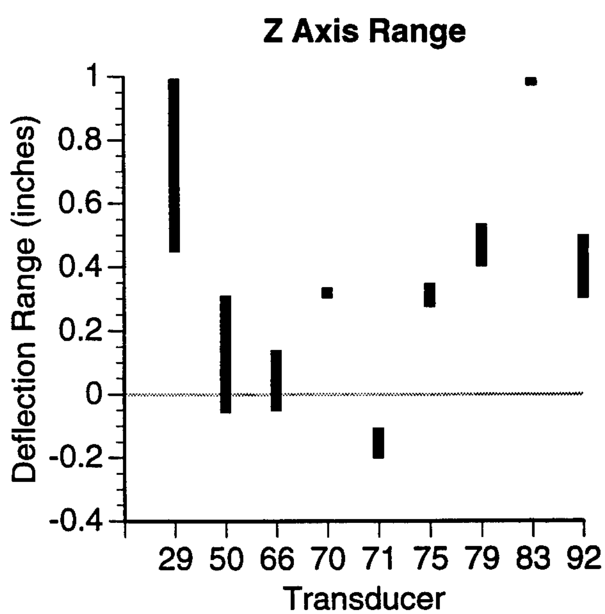

Data Run BA0001_16D1

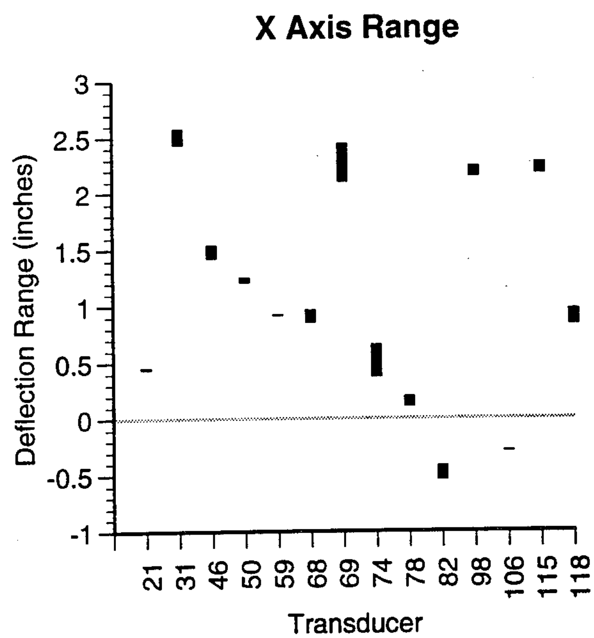

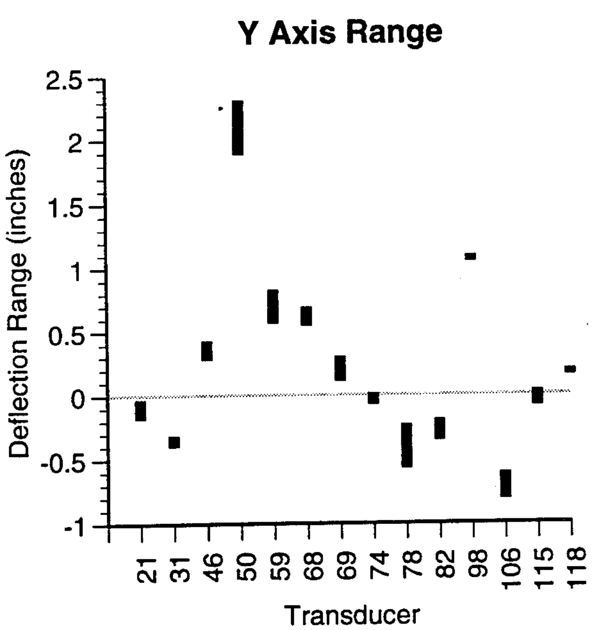

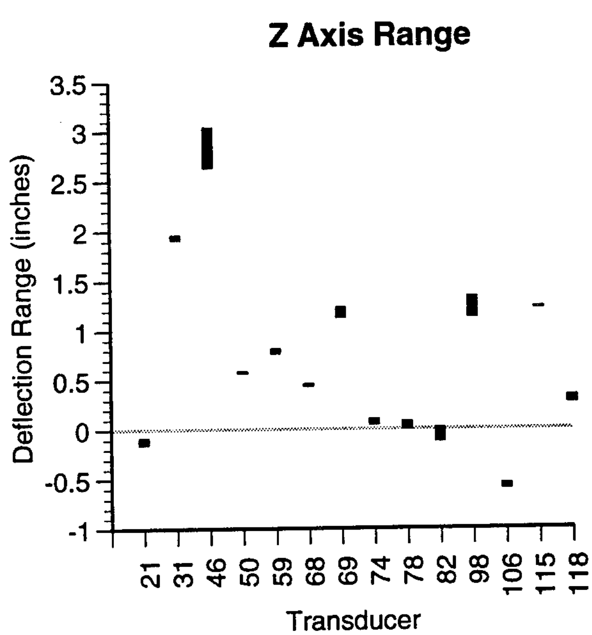

Data Run BA0001_16D2

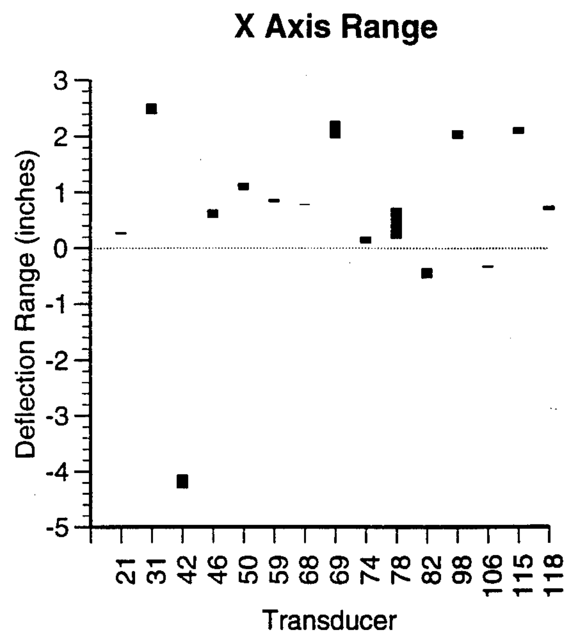

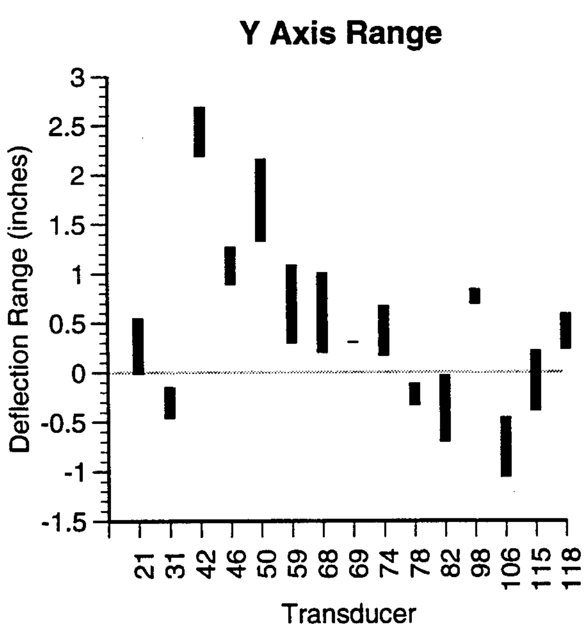

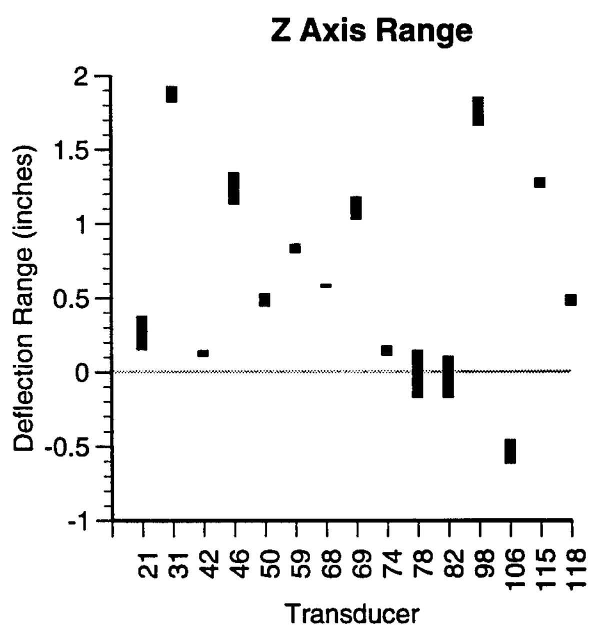

Data Run BA16_2D3

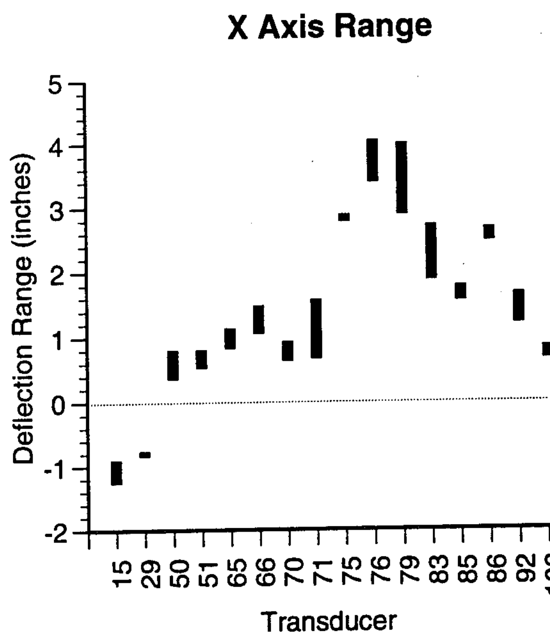

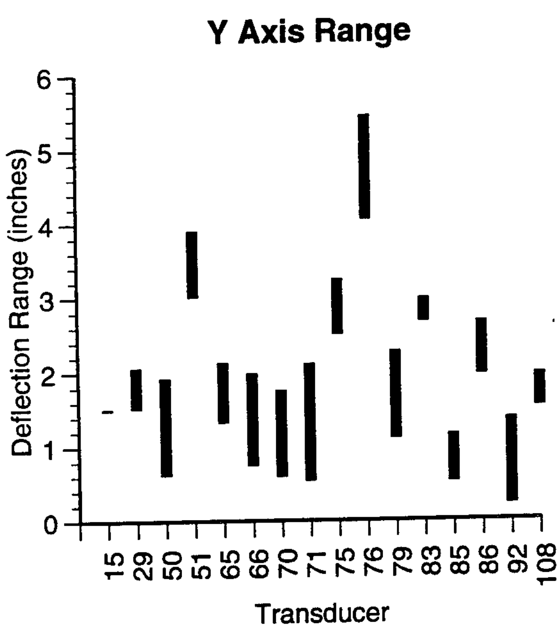

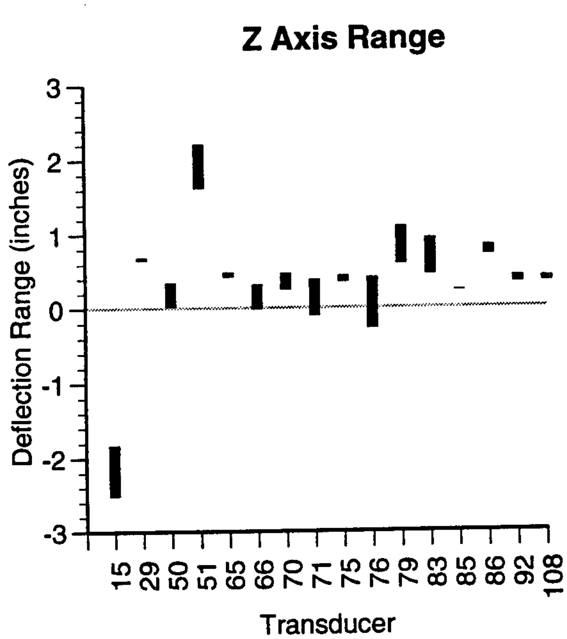

Data Run CA2_27D1

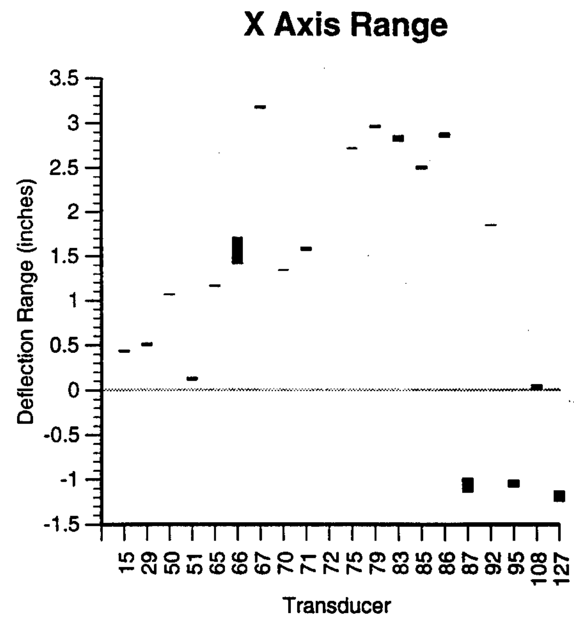

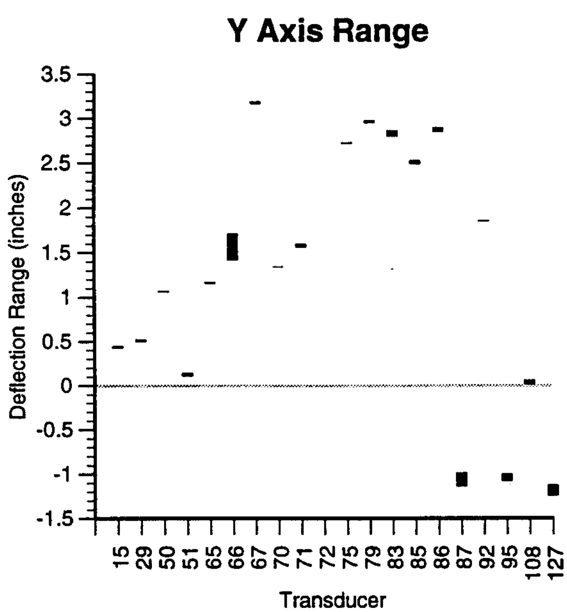

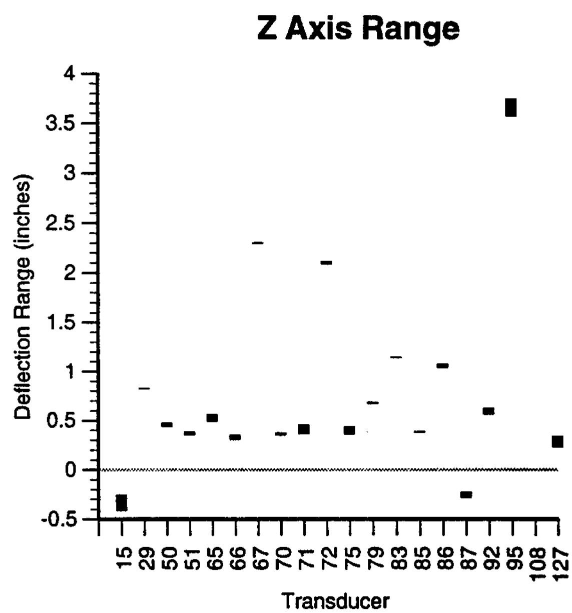

Data Run CFA2_27D1

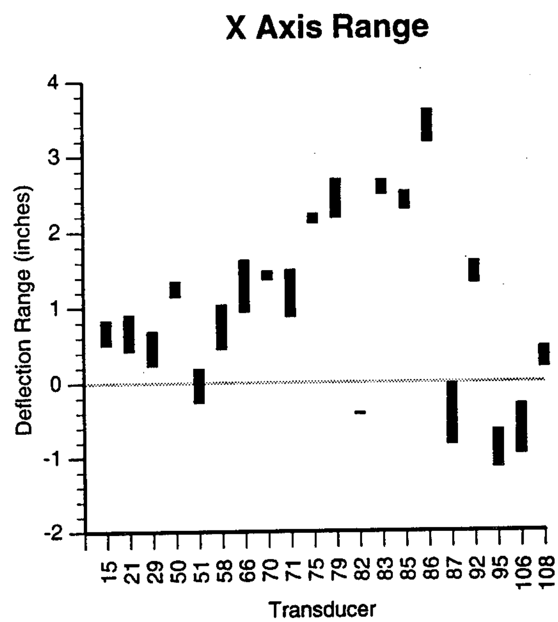

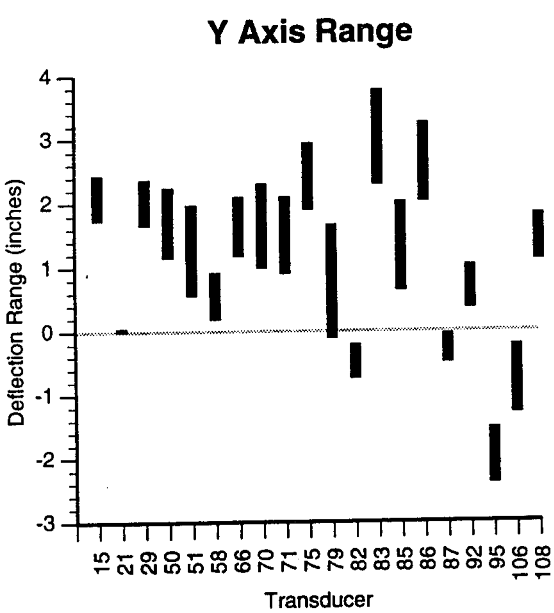

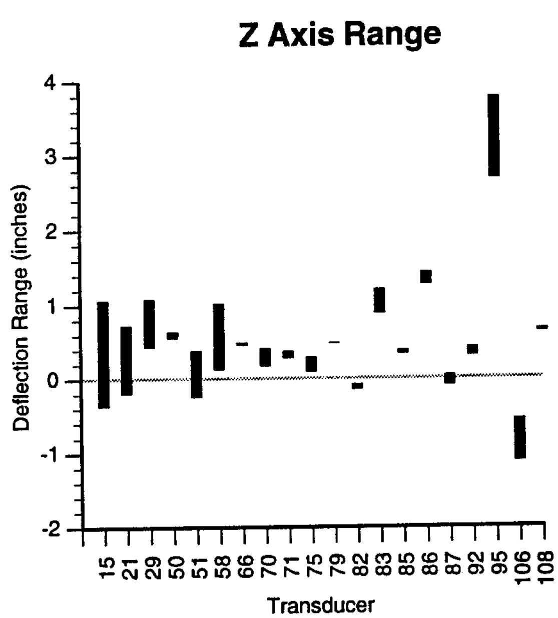

Data Run CFA3_27D7

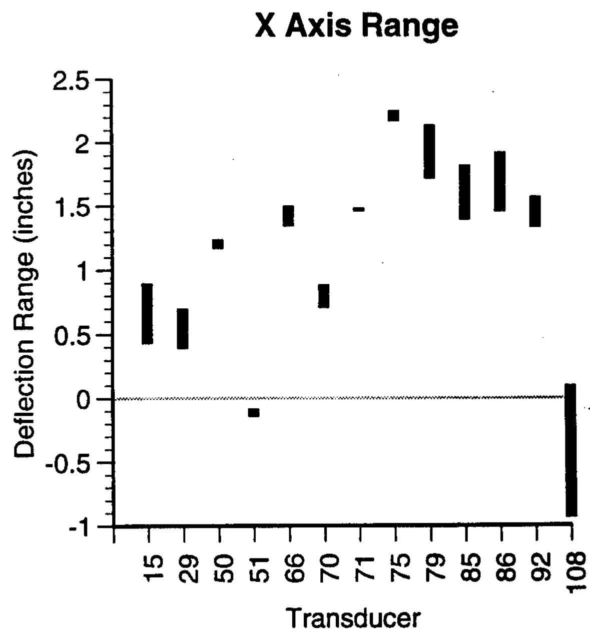

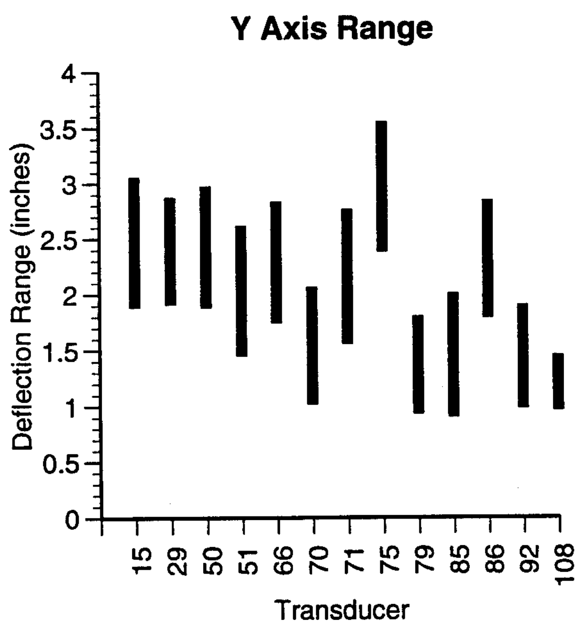

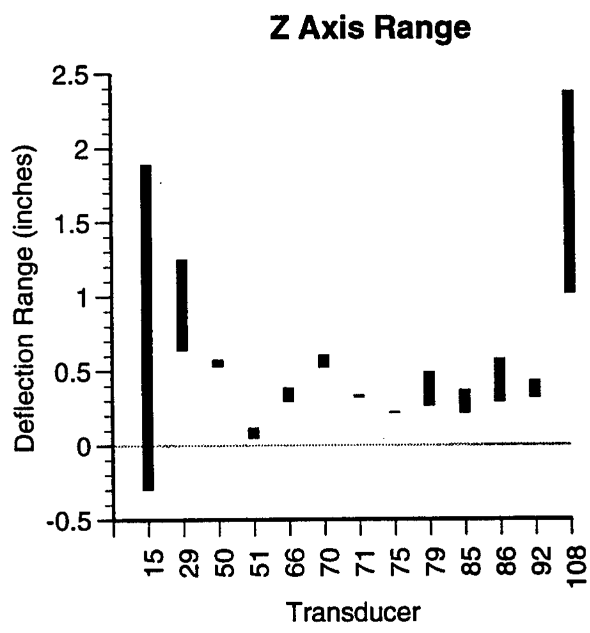

Data Run CFA2_27D8

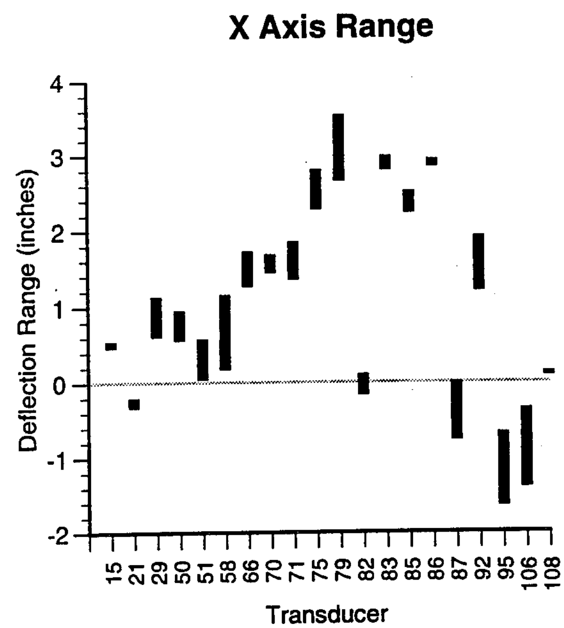

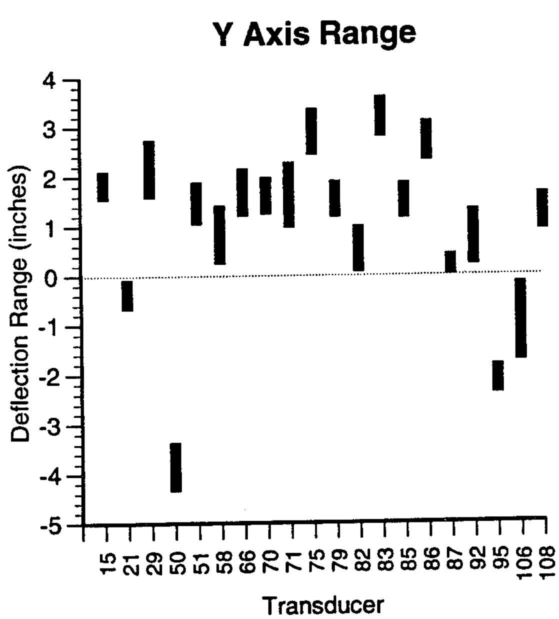

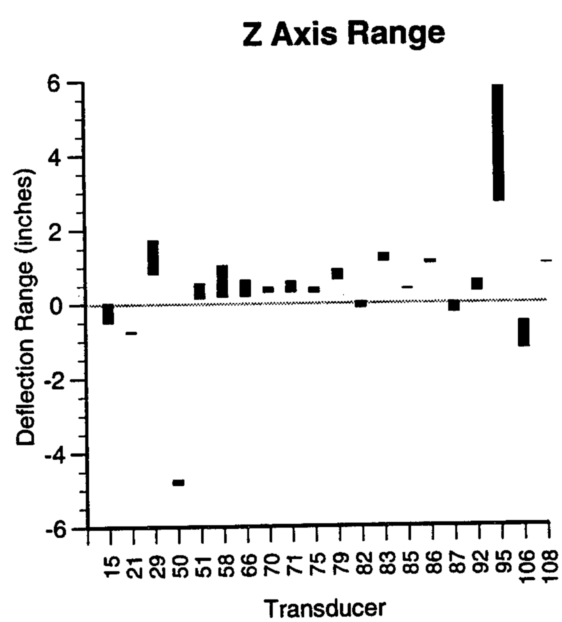

Data Run DF3_27D9

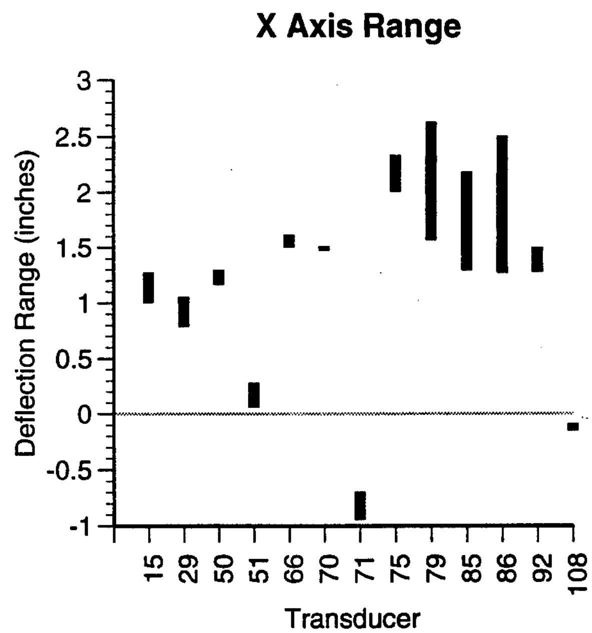

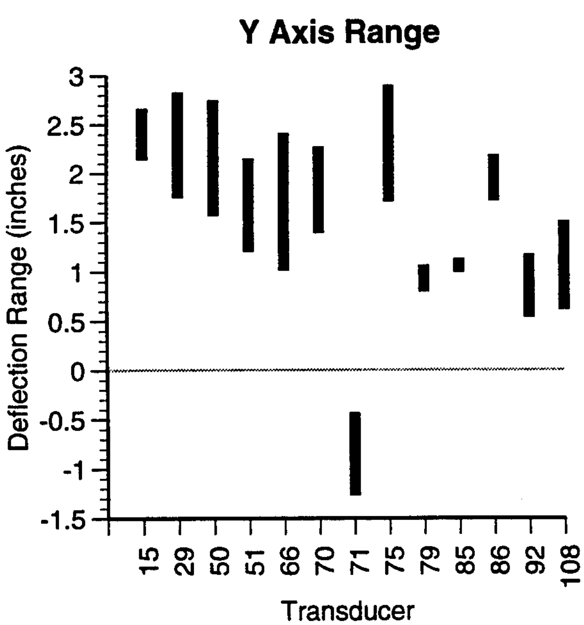

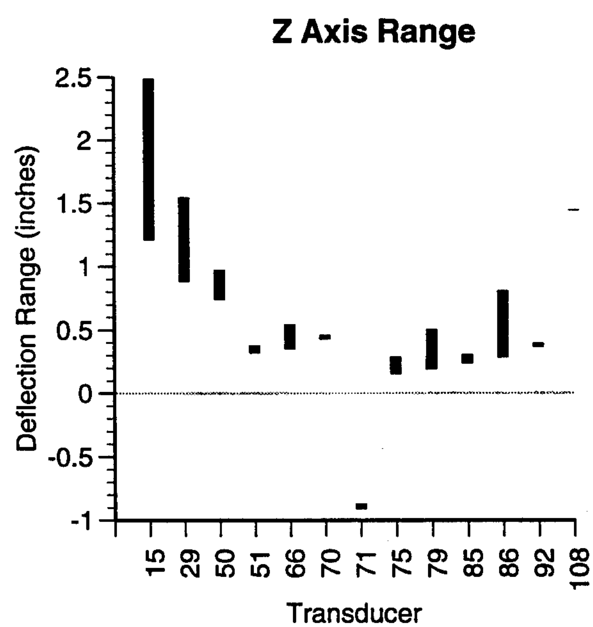

Data Run EANT_4_16D1

X Axis Range

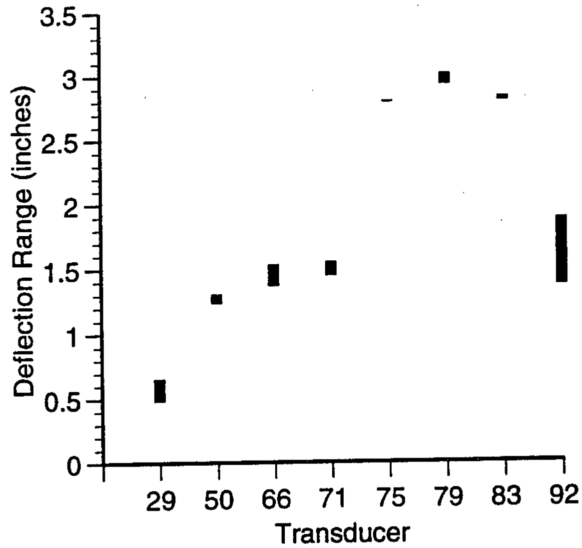

Y Axis Range

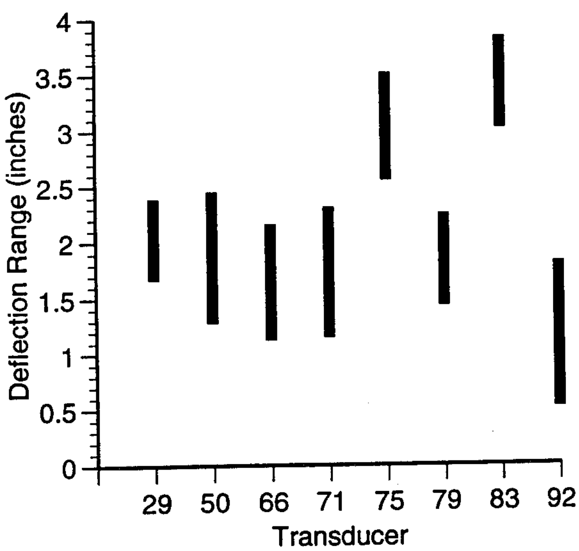

Z Axis Range

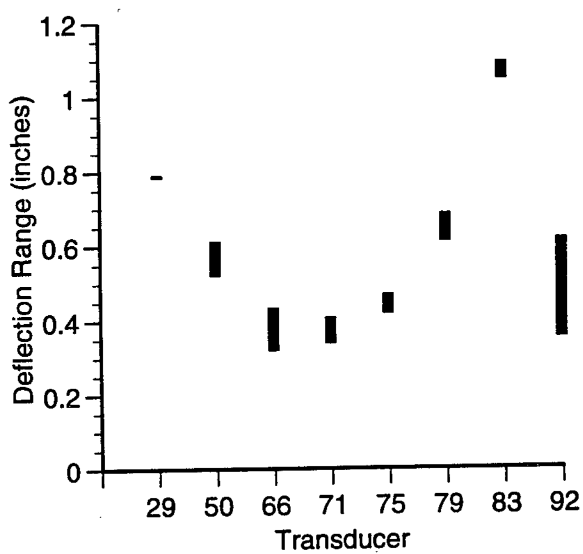

Data Run FFA3_27D10

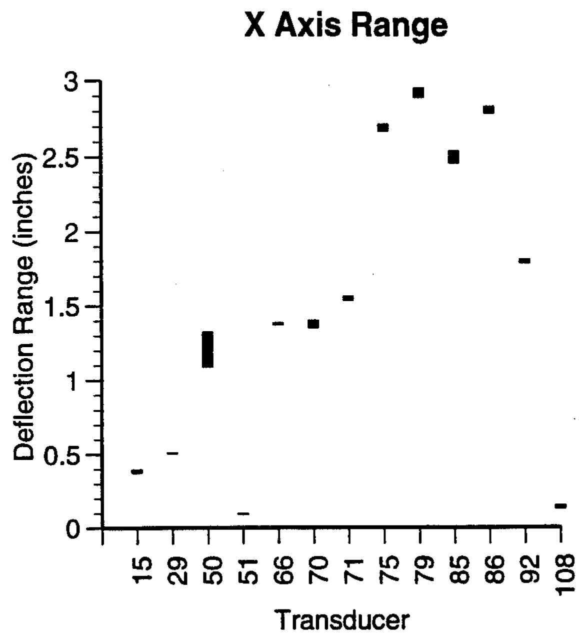

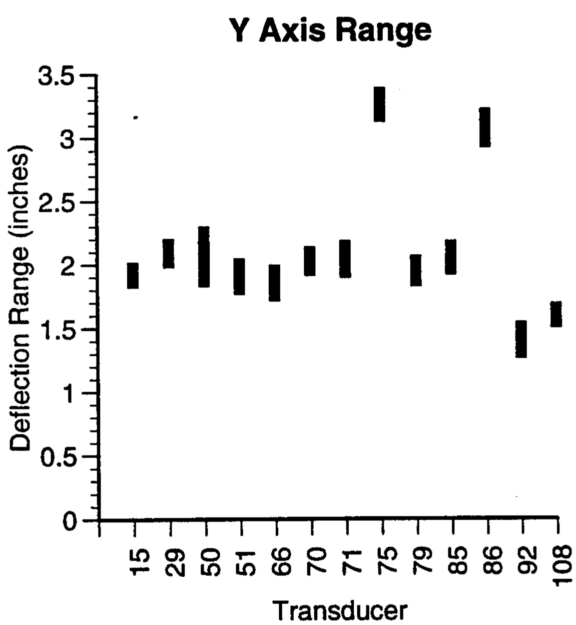

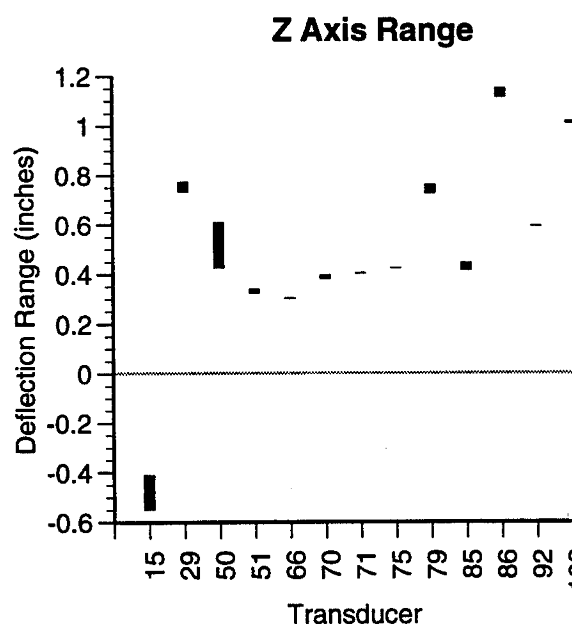

Appendix C: ANT_16_3D3 Cartesian Plots

This section contains plots of deflection data from ANT_16_3D3 which was the first data run used for comparison with predictions from UW/APL's FEM of an SRD.

Each driver transducer is represented by two pages of plots. The first page shows three graphs, each of which represents measured deflections on an axis in the Cartesian coordinate system. The X-axis of each of these graphs represents elapsed time from the beginning of the data run. The Y-axis represents absolute deflection measurements with respect to the SRD's Cartesian origin (in the forward end of the SRD).

The second page consists of four scatter plots that depict deflection measurements, over the duration of the data run, in Cartesian coordinate space. The upper left scatter plot shows deflection measurements on the X–Y plane. The lower left plot shows deflections in the Y–Z plane. The lower right scatter plot shows deflections in the X–Z plane. The upper right plot is a 3 dimensional oblique rendering of the same data.

The scatter plots from the second page are useful in determining if the SRD exhibits dynamic movement in a dominant direction.

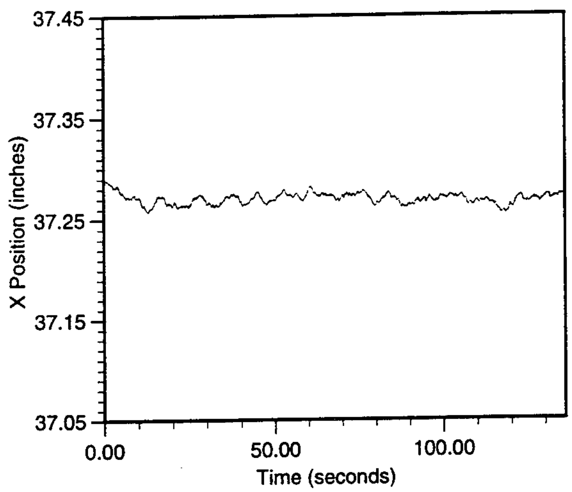

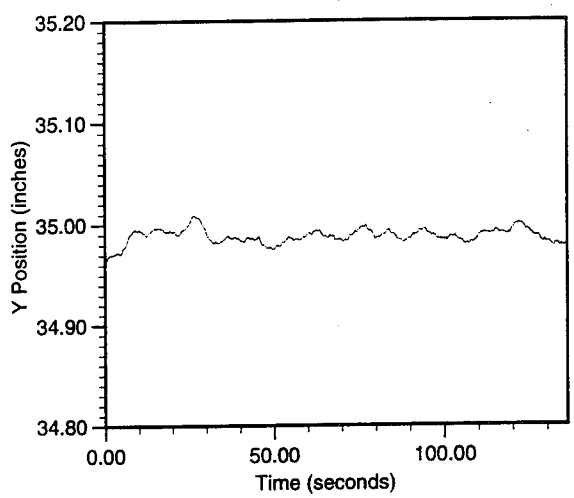

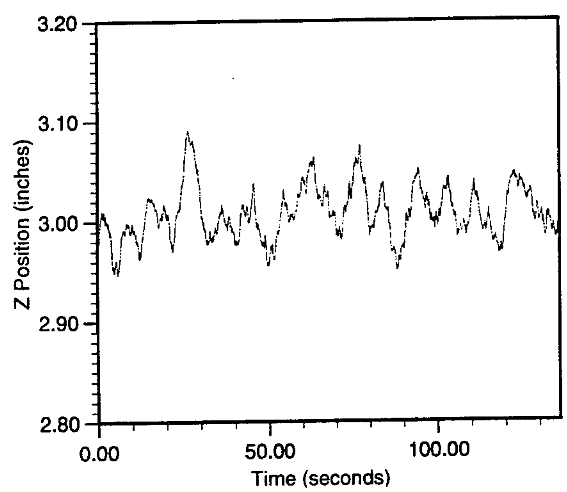

Data Run: ANT_16_3D3
Transducer: 4

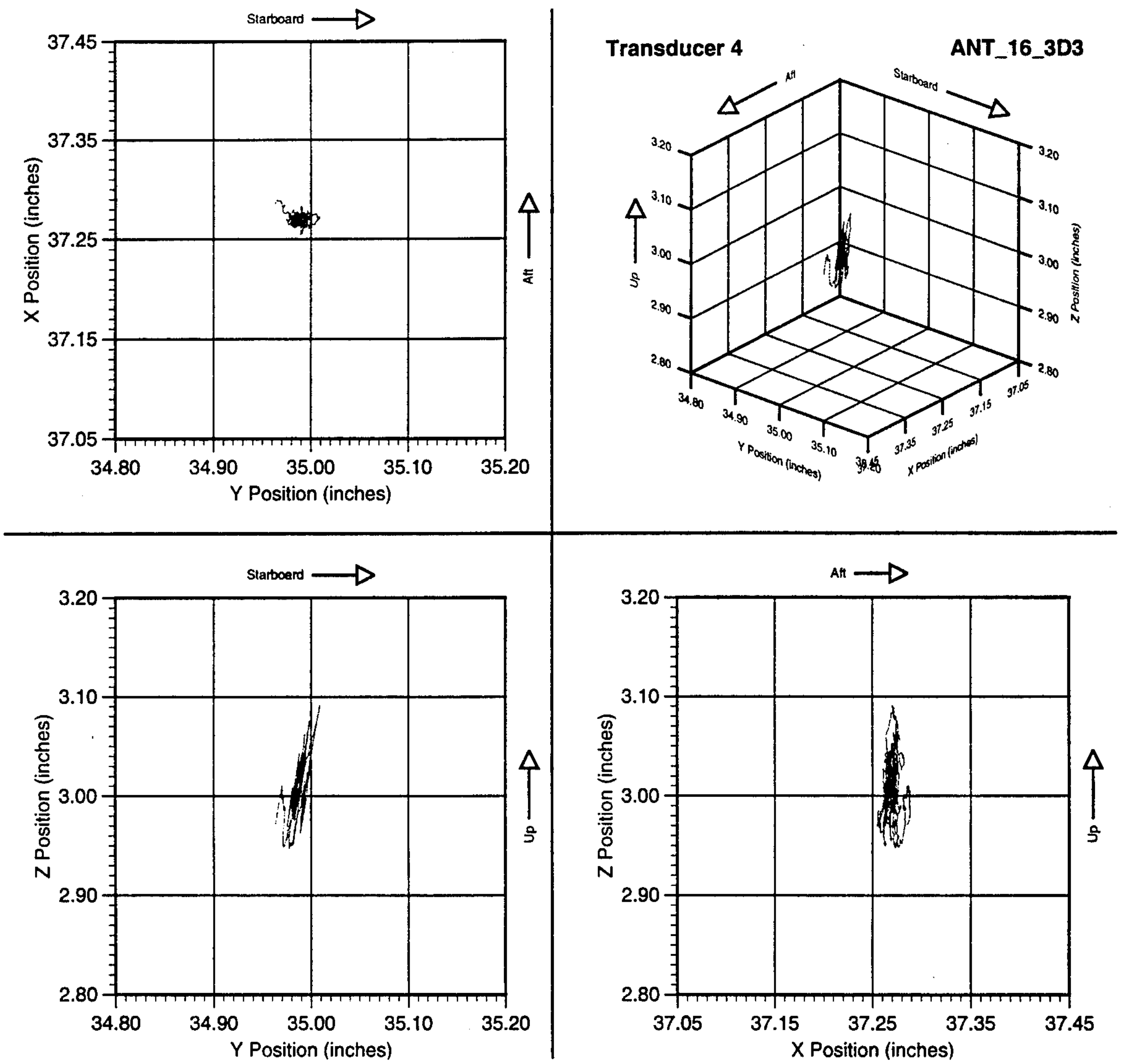
Transducer 4
ANT_16_3D3
Starboard
Aft
Up
X Position (inches)
Y Position (inches)
Z Position (inches)
37.05
37.15
37.25
37.35
37.45
34.80
34.90
35.00
35.10
35.20
2.80
2.90
3.00
3.10
3.20

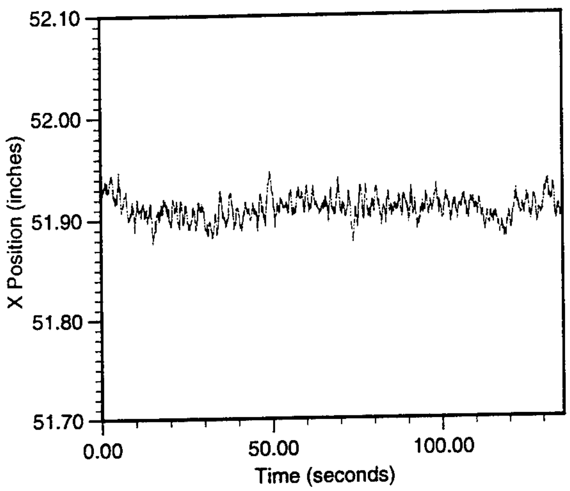

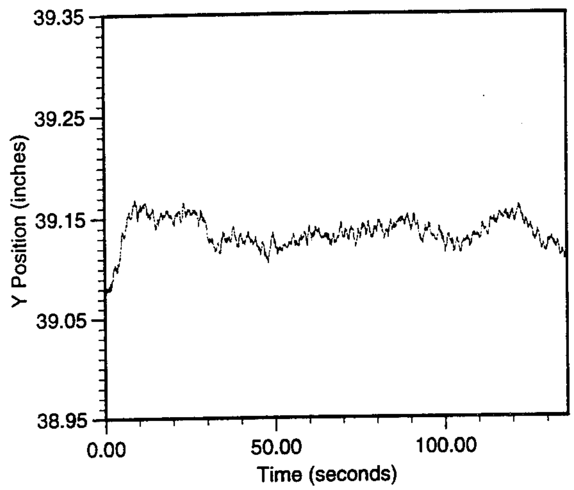

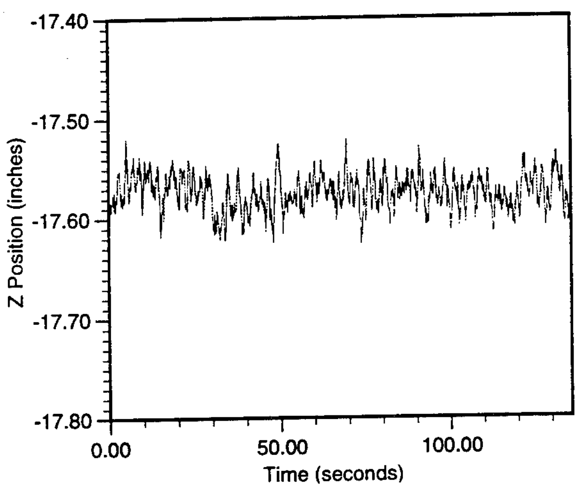

Data Run: ANT_16_3D3
Transducer: 15

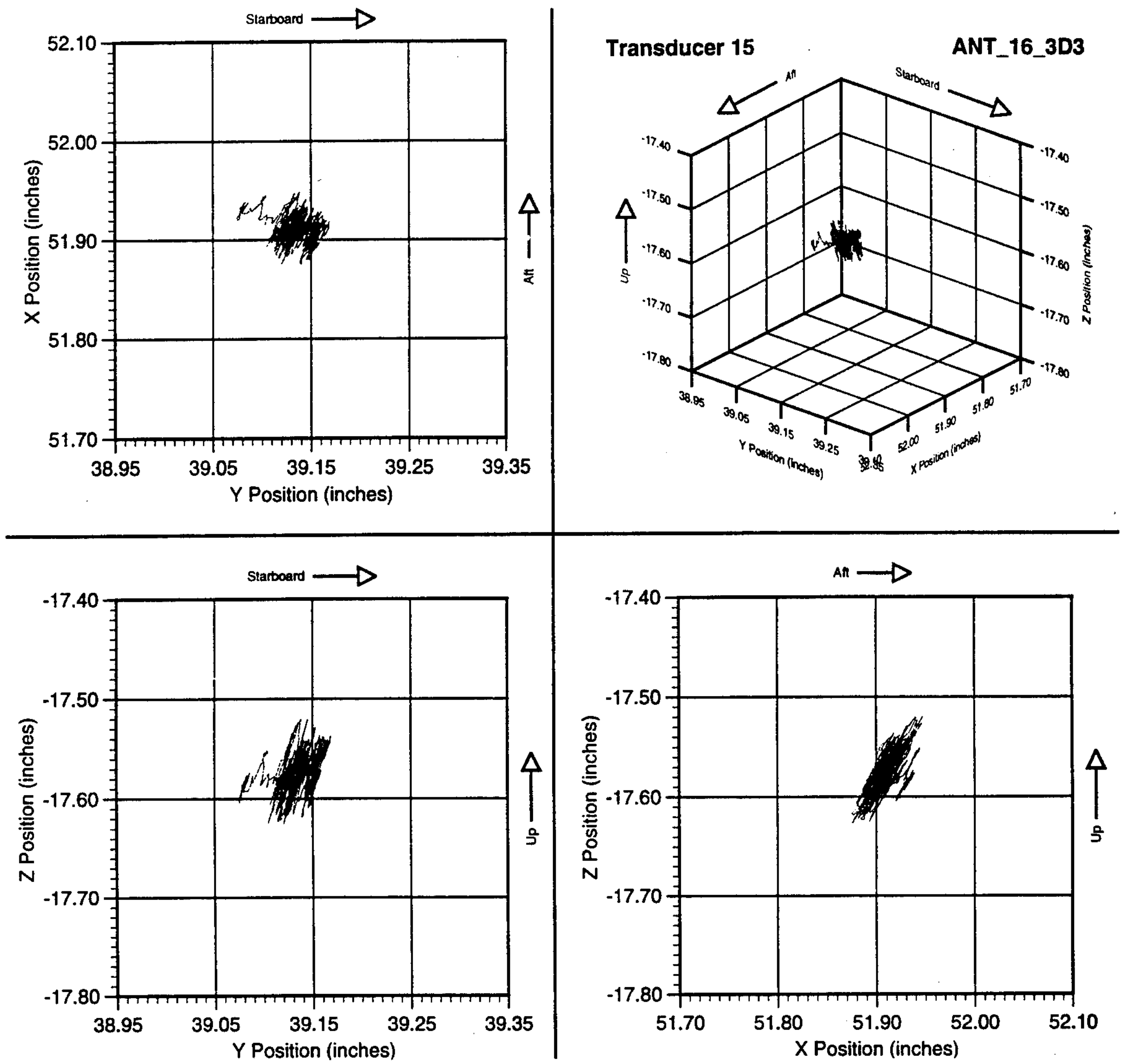

Transducer 15
ANT_16_3D3
Starboard
Aft
Up
X Position (inches)
Y Position (inches)
Z Position (inches)
52.10
52.00
51.90
51.80
51.70
38.95
39.05
39.15
39.25
39.35
-17.40
-17.50
-17.60
-17.70
-17.80

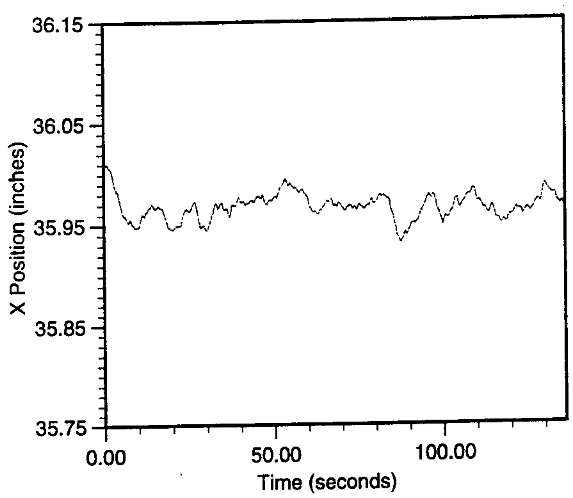

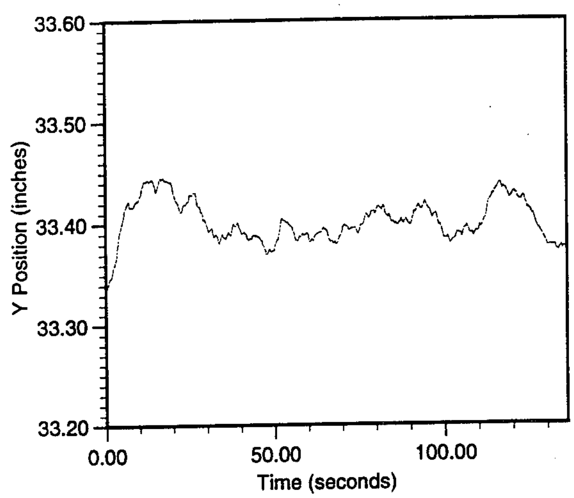

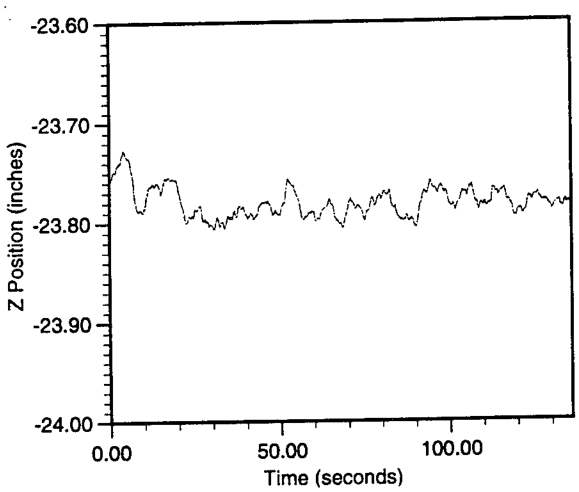

Data Run: ANT_16_3D3
Transducer: 29

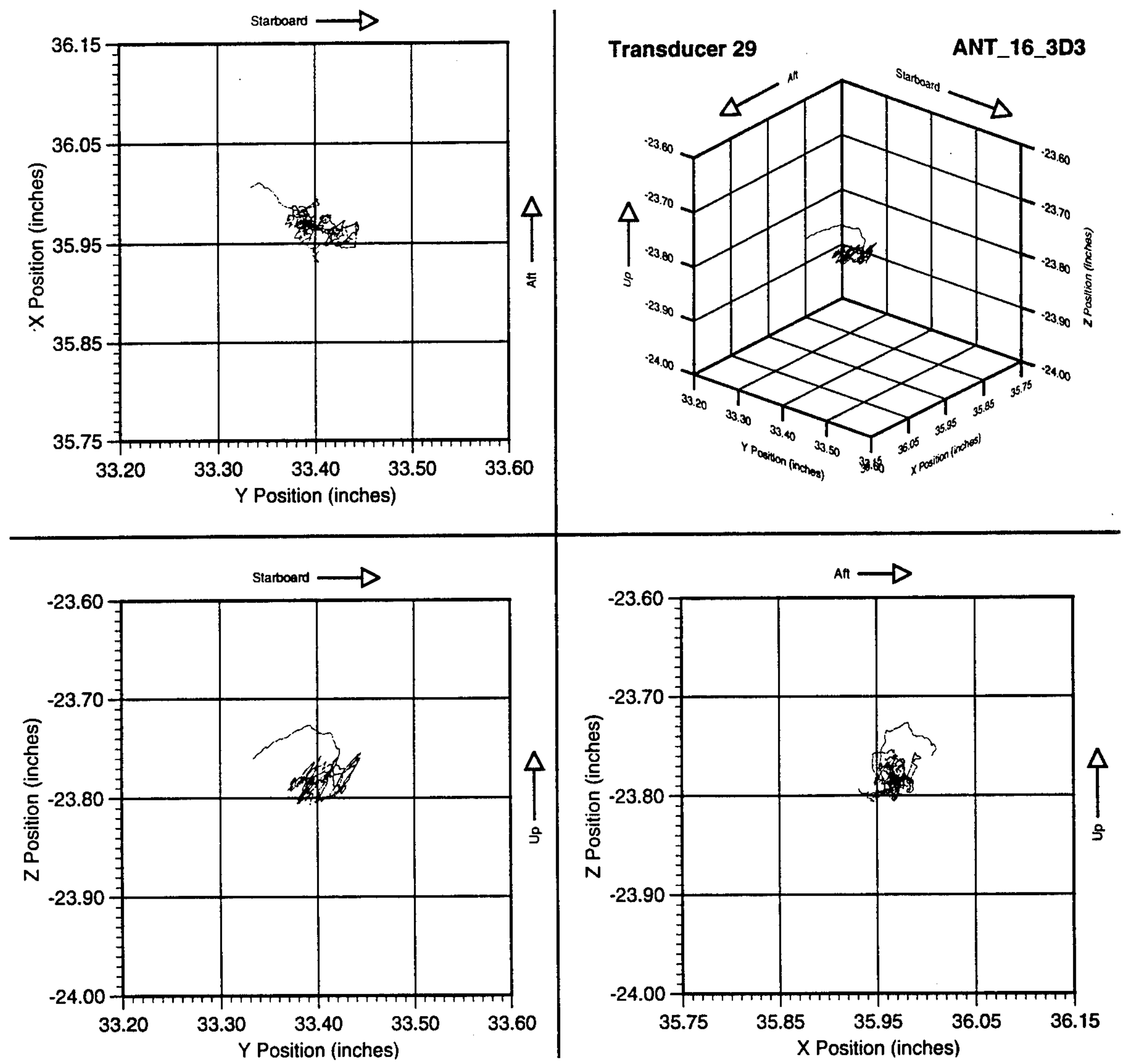
Transducer 29
ANT_16_3D3
Starboard
Aft
Up
X Position (inches)
Y Position (inches)
Z Position (inches)
36.15
36.05
35.95
35.85
35.75
33.20
33.30
33.40
33.50
33.60
-23.60
-23.70
-23.80
-23.90
-24.00
36.05
36.15

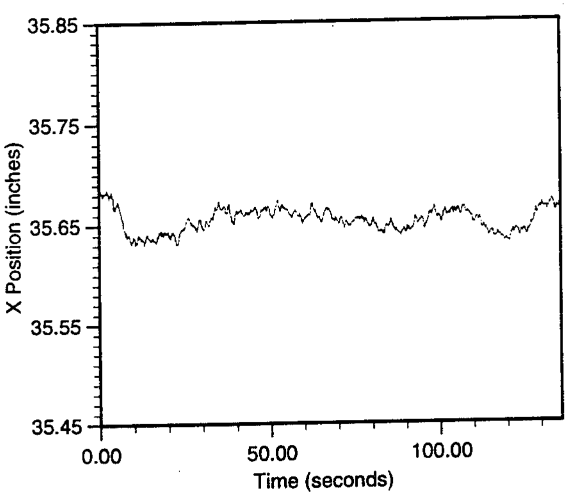

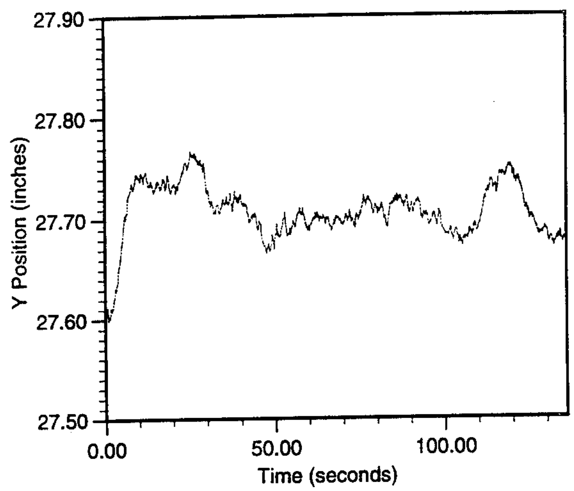

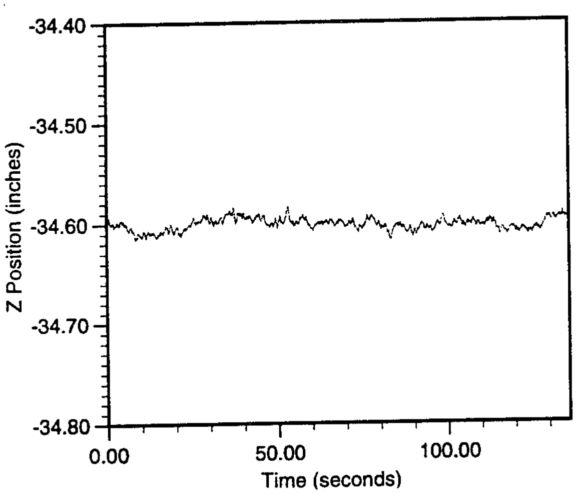

Data Run: ANT_16_3D3
Transducer: 50

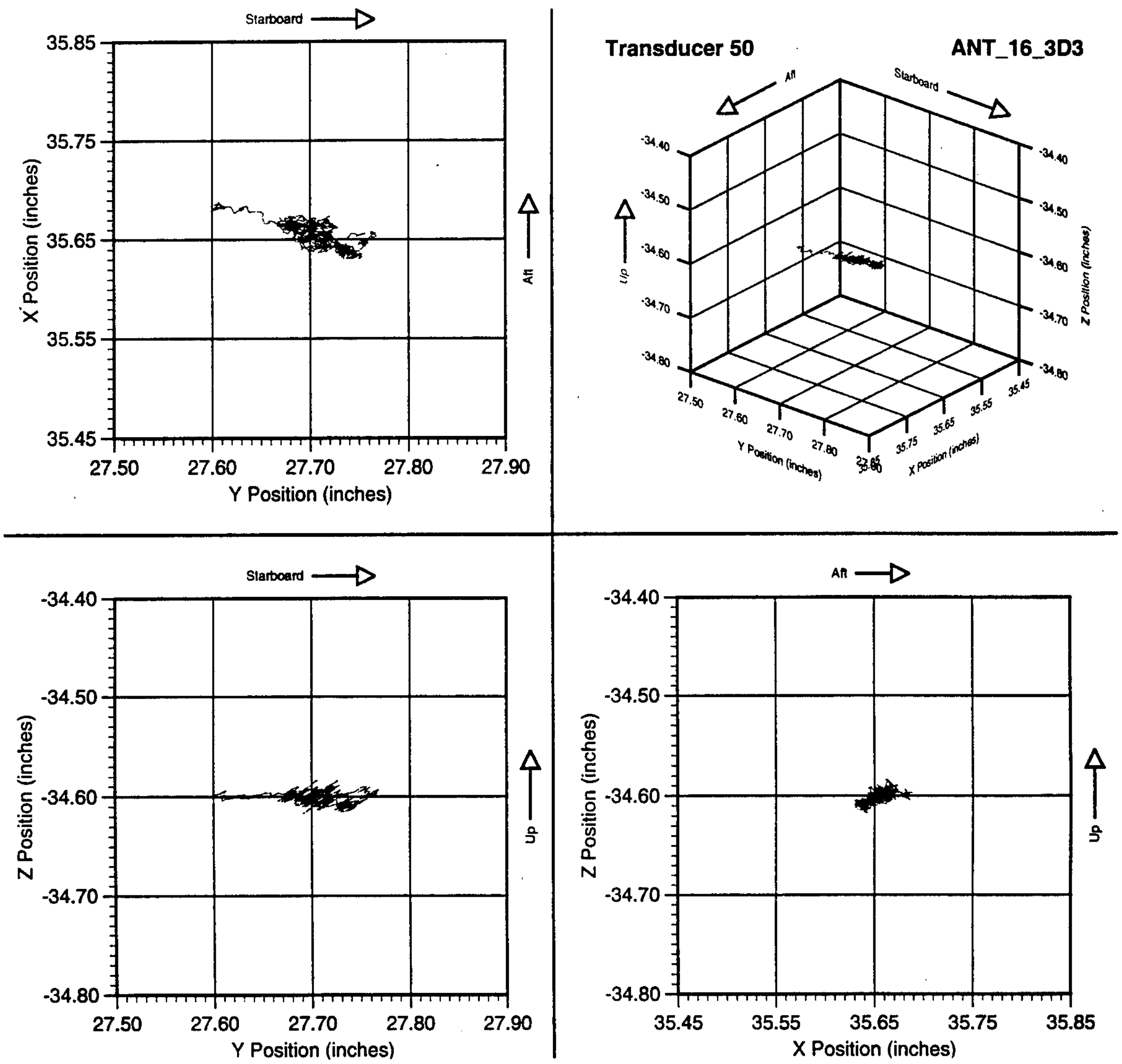
Transducer 50
ANT_16_3D3
Starboard
Aft
Up
X´ Position (inches)
Y Position (inches)
Z Position (inches)
X Position (inches)
35.85
35.75
35.65
35.55
35.45
27.50
27.60
27.70
27.80
27.90
-34.40
-34.50
-34.60
-34.70
-34.80

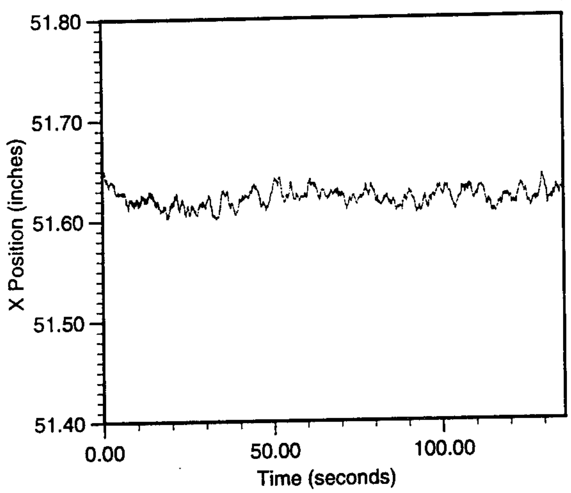

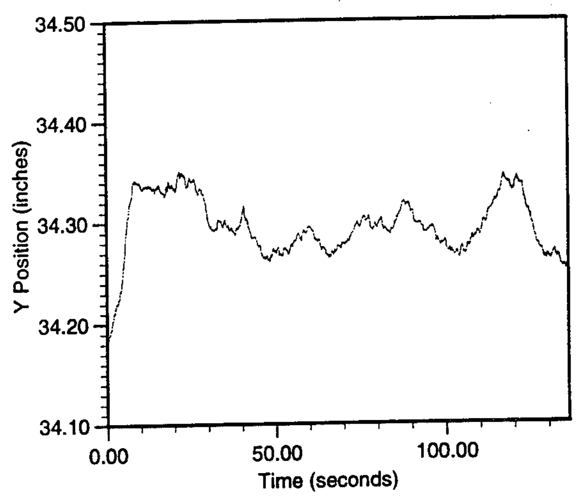

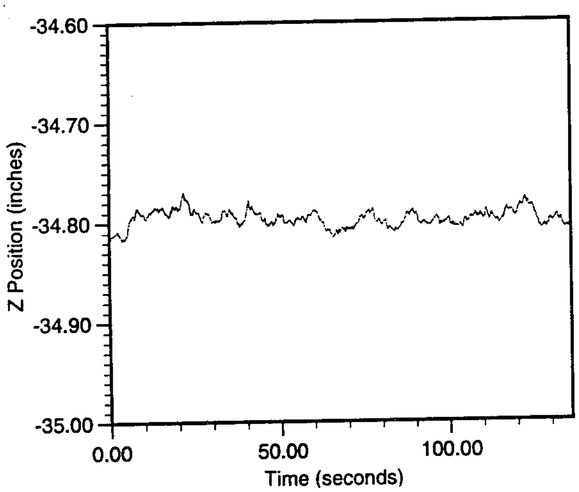

Data Run: ANT_16_3D3
Transducer: 51

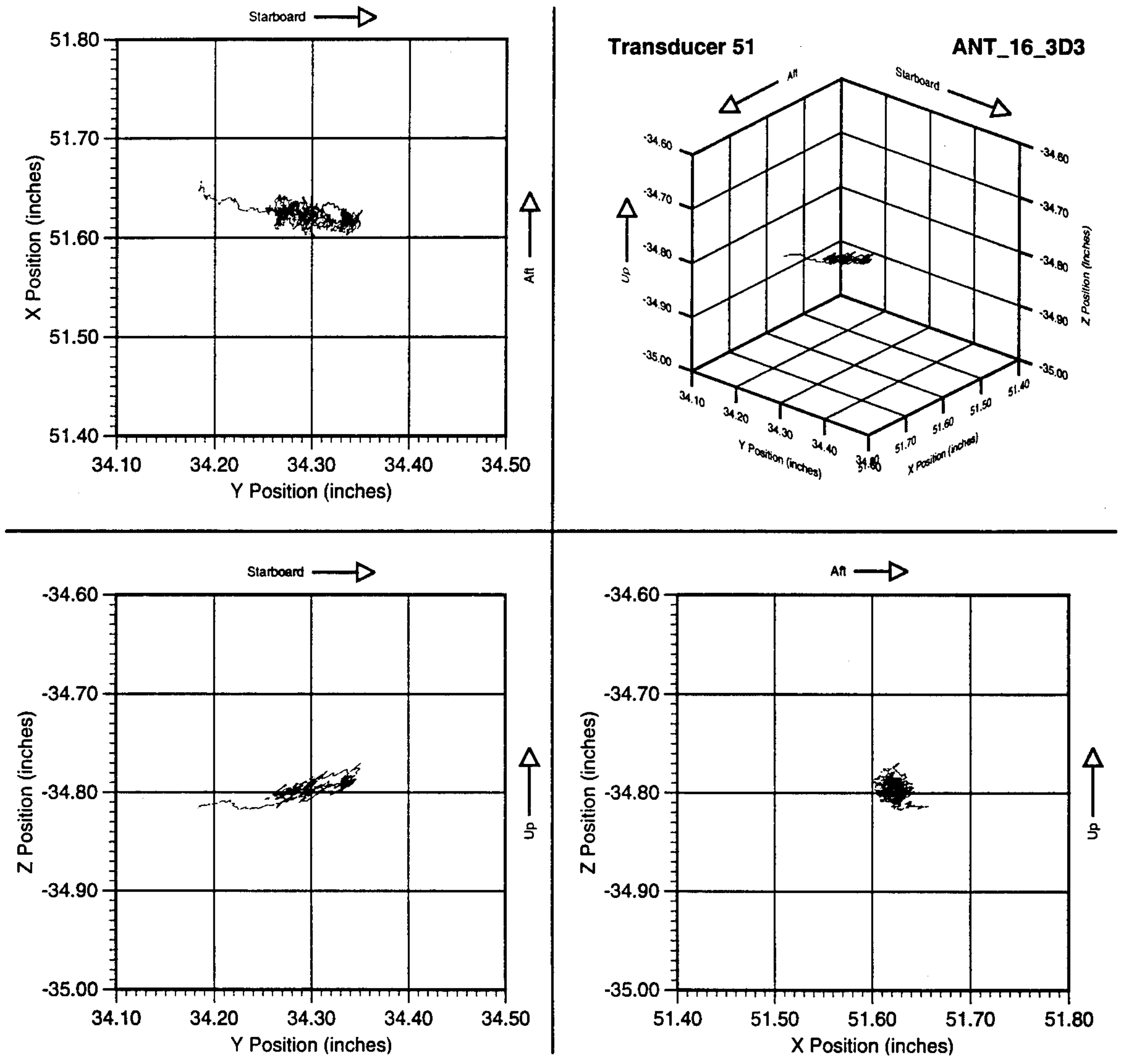
Transducer 51
ANT_16_3D3
Starboard
Aft
Up
X Position (inches)
Y Position (inches)
Z Position (inches)
51.80
51.70
51.60
51.50
51.40
34.10
34.20
34.30
34.40
34.50
-34.60
-34.70
-34.80
-34.90
-35.00

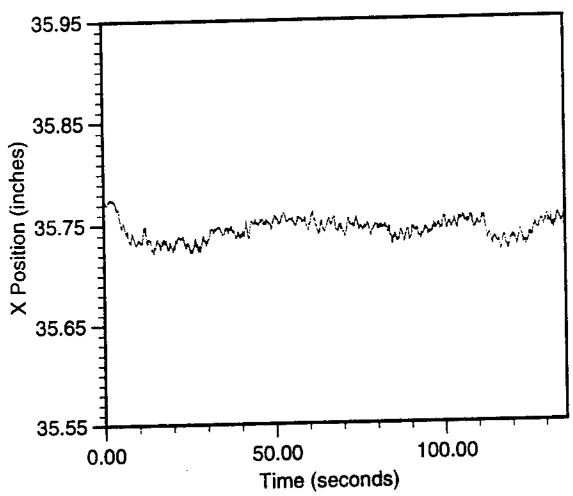

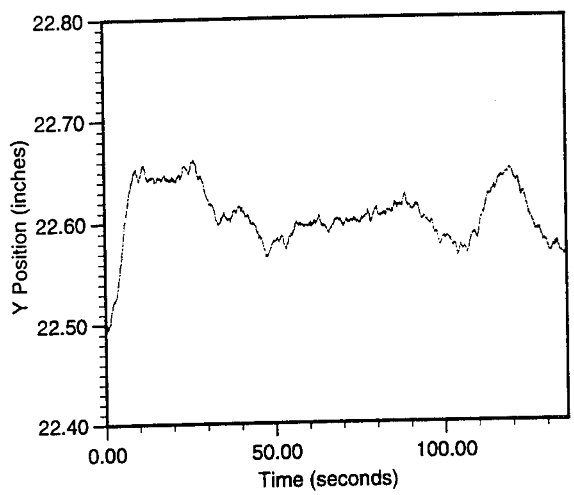

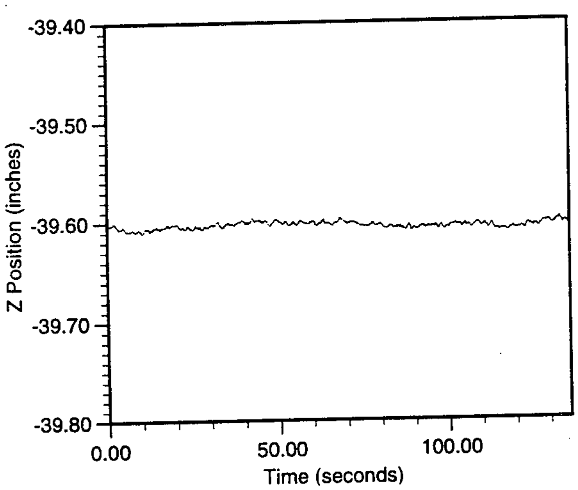

Data Run: ANT_16_3D3
Transducer: 65

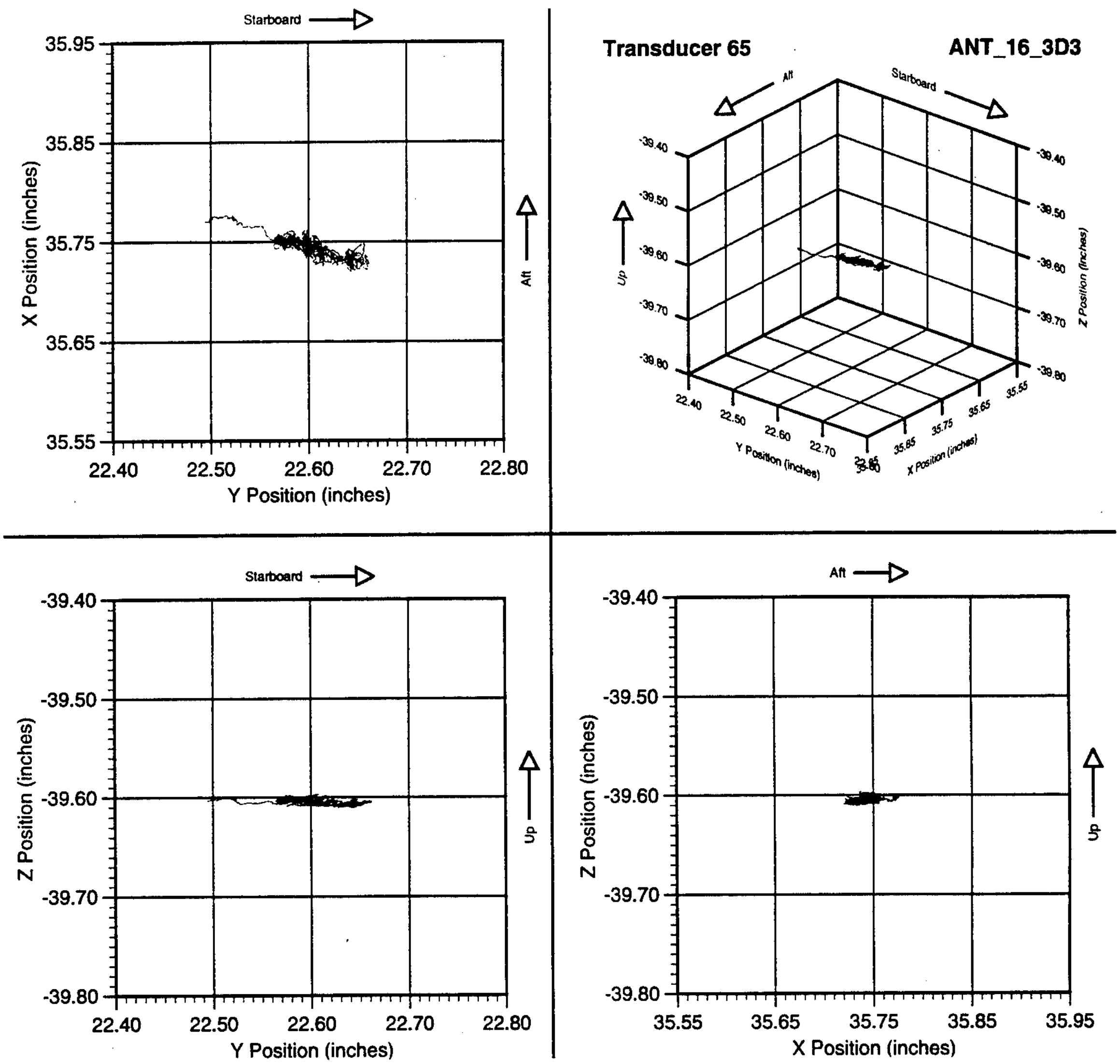
Transducer 65
ANT_16_3D3
Starboard
Aft
Up
X Position (inches)
Y Position (inches)
Z Position (inches)
35.95
35.85
35.75
35.65
35.55
22.40
22.50
22.60
22.70
22.80
-39.40
-39.50
-39.60
-39.70
-39.80

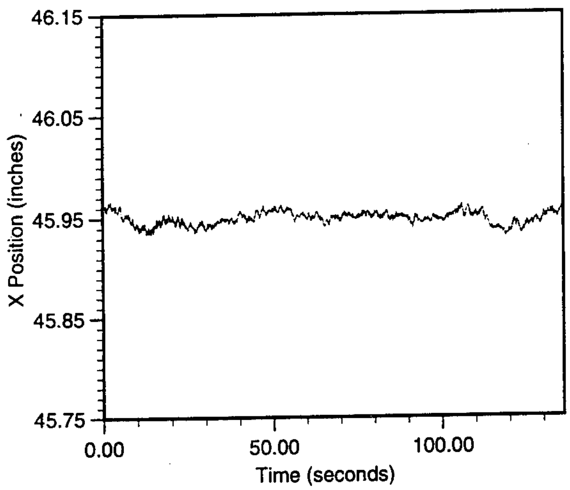

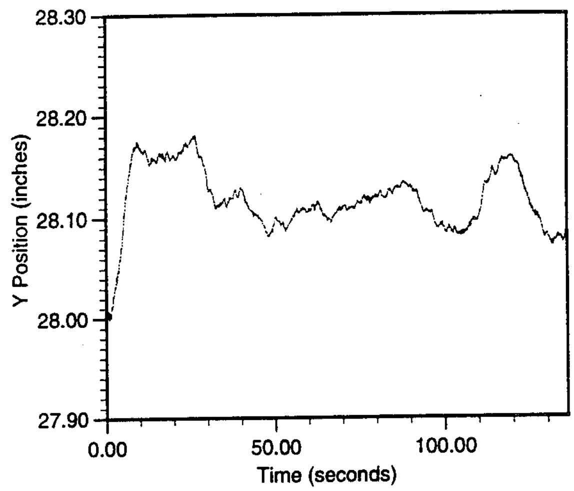

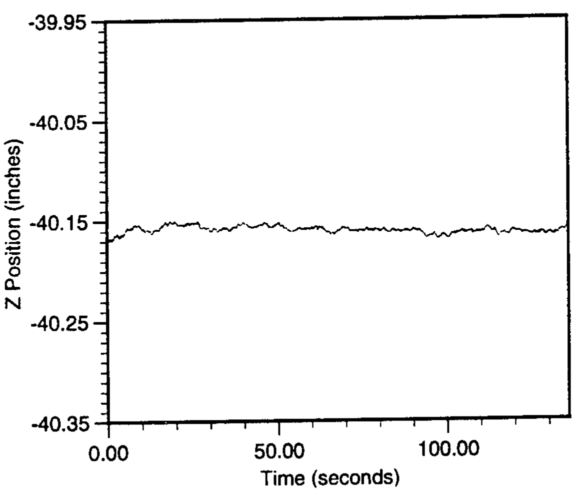

Data Run: ANT_16_3D3
Transducer: 66

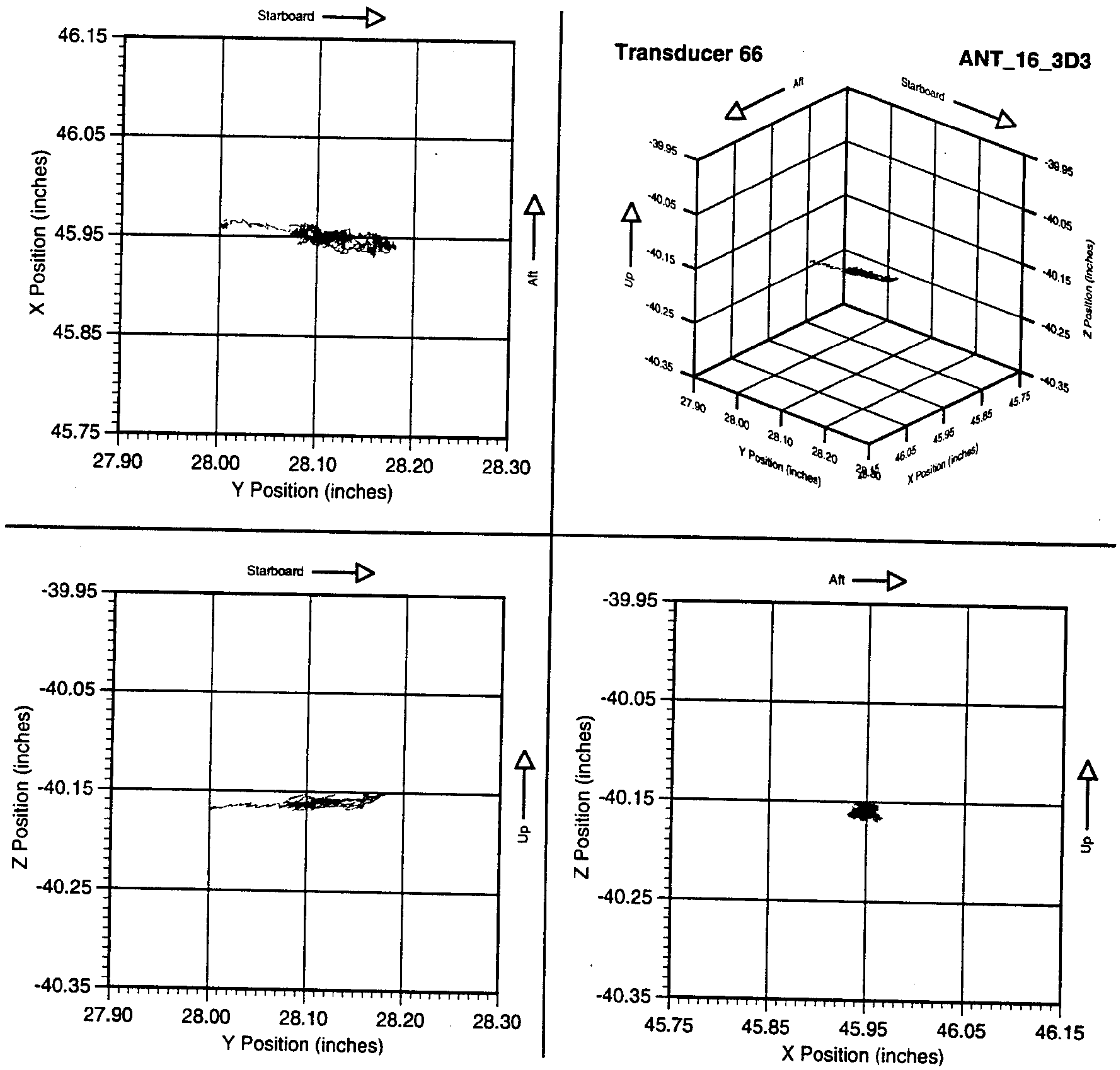
Transducer 66
ANT_16_3D3
Starboard
Aft
Up
X Position (inches)
Y Position (inches)
Z Position (inches)
46.15
46.05
45.95
45.85
45.75
27.90
28.00
28.10
28.20
28.30
-39.95
-40.05
-40.15
-40.25
-40.35

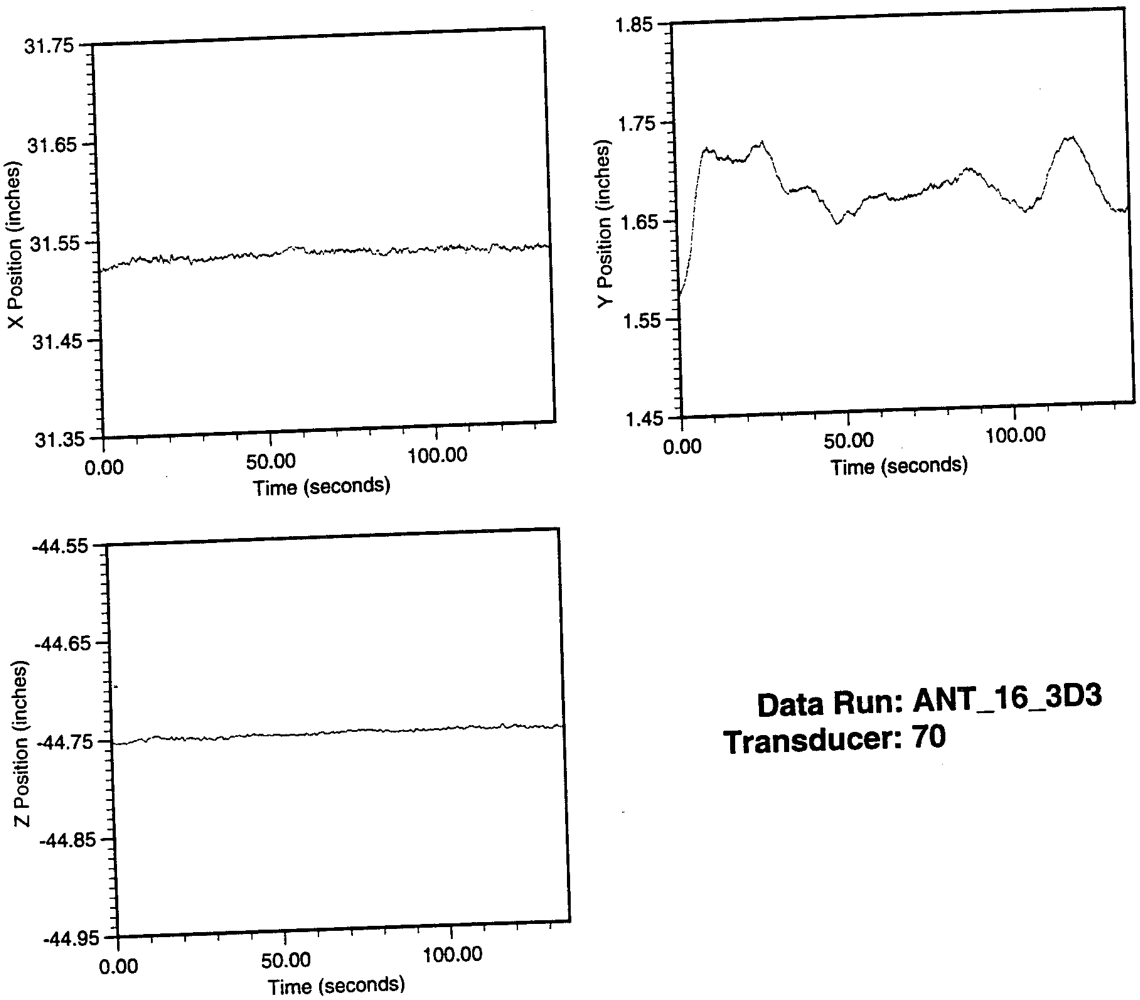

Data Run: ANT_16_3D3
Transducer: 70

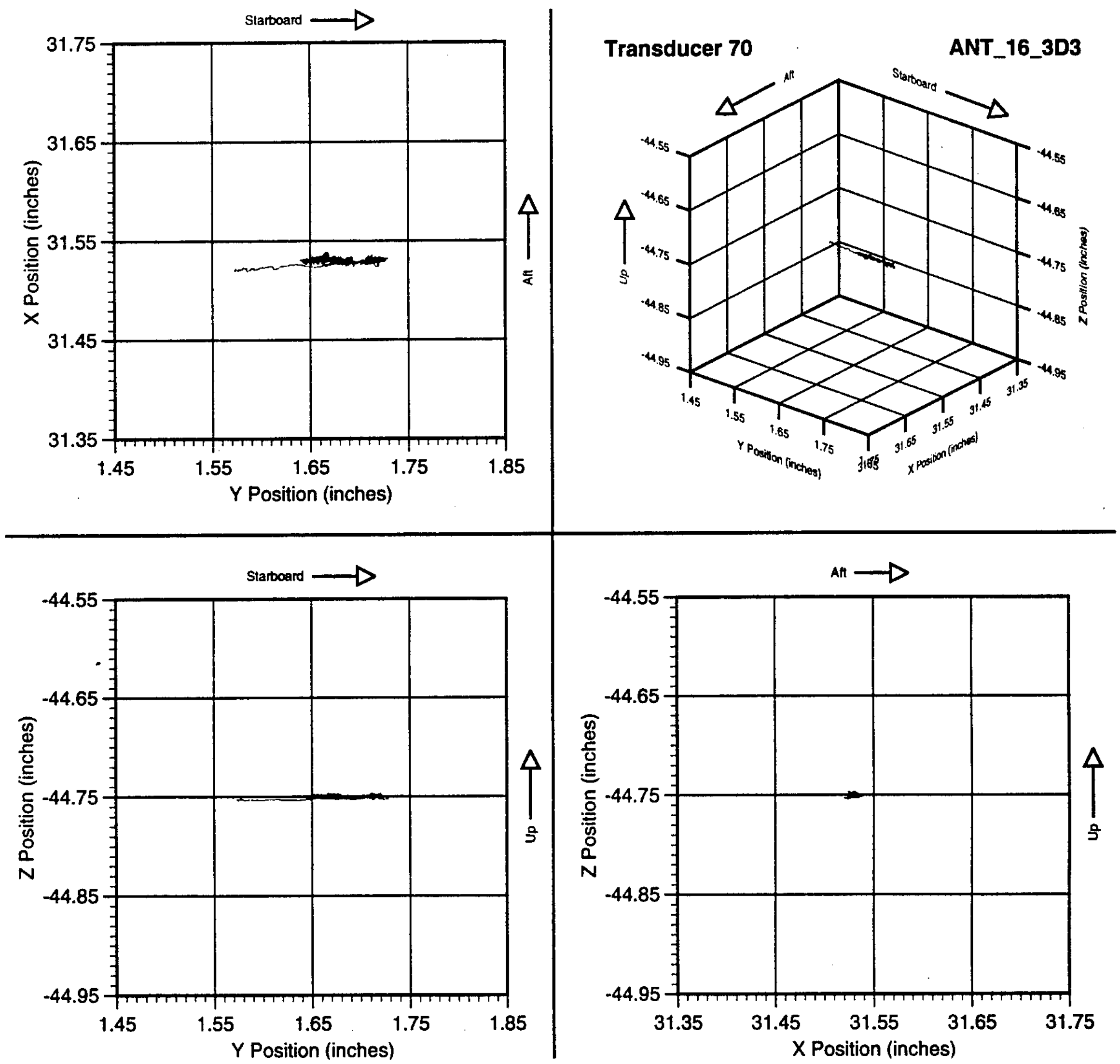
Transducer 70
ANT_16_3D3
Starboard
Aft
Up
X Position (inches)
Y Position (inches)
Z Position (inches)
31.75
31.65
31.55
31.45
31.35
1.45
1.55
1.65
1.75
1.85
-44.55
-44.65
-44.75
-44.85
-44.95

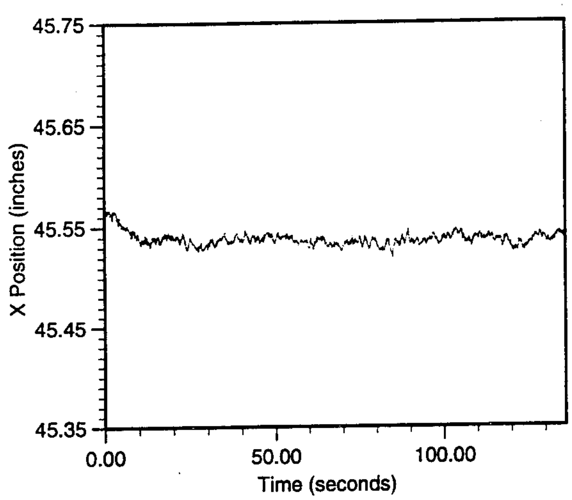

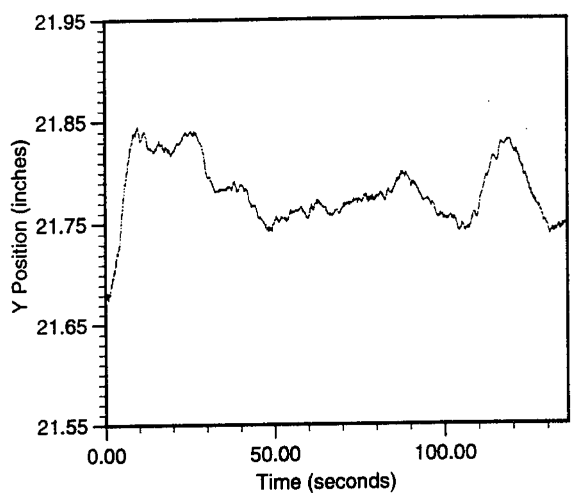

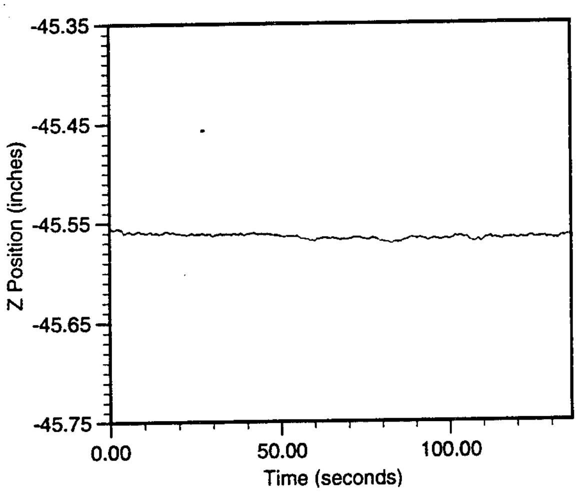

Data Run: ANT_16_3D3
Transducer: 71

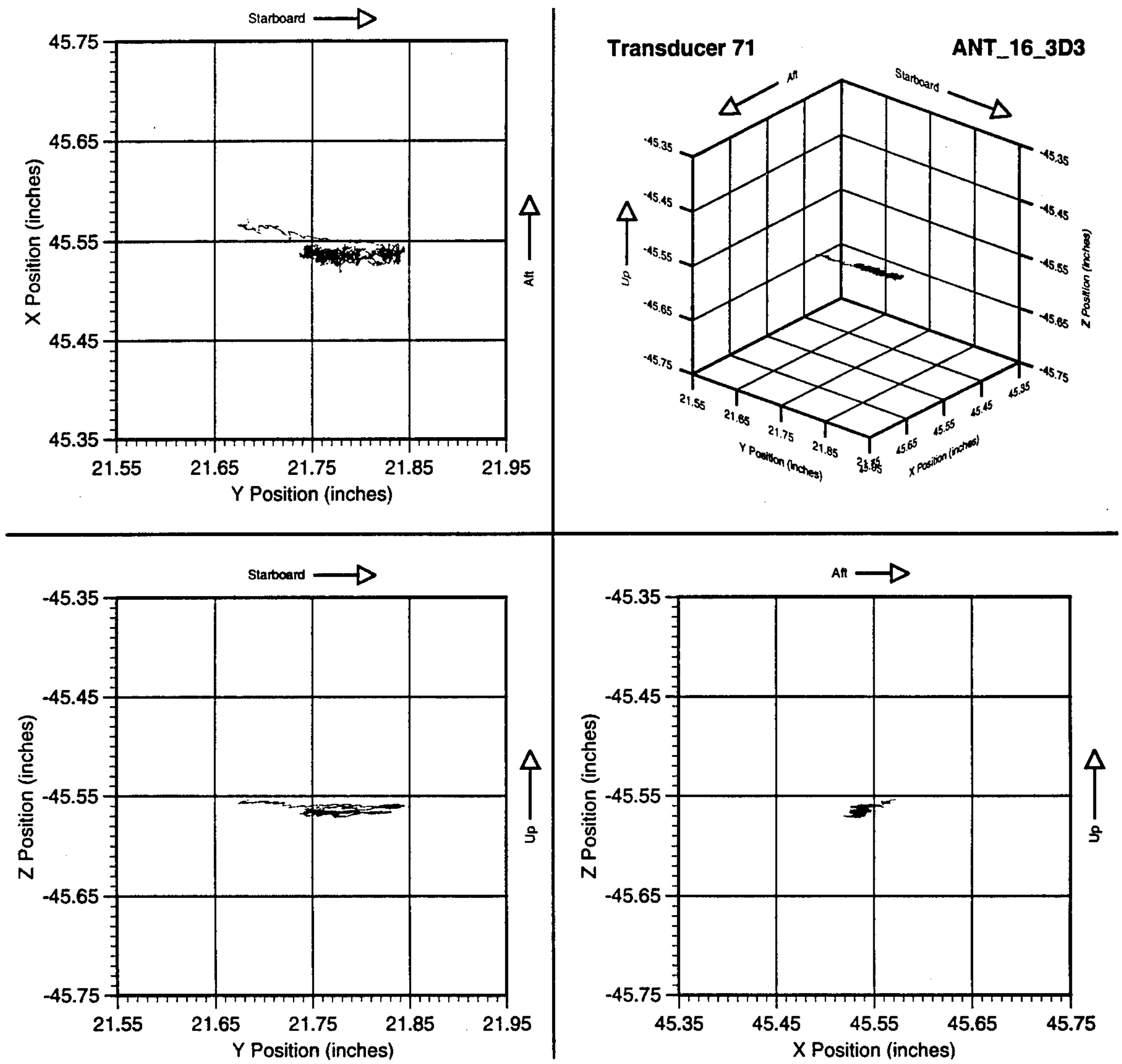
Starboard
45.75
45.65
45.55
45.45
45.35
X Position (inches)
21.55
21.65
21.75
21.85
21.95
Y Position (inches)
Aft
Transducer 71
ANT_16_3D3
Aft
Starboard
Up
Z Position (inches)
Y Position (inches)
X Position (inches)
Starboard
-45.35
-45.45
-45.55
-45.65
-45.75
Z Position (inches)
Up
Aft
X Position (inches)
45.35
45.45
45.55
45.65
45.75

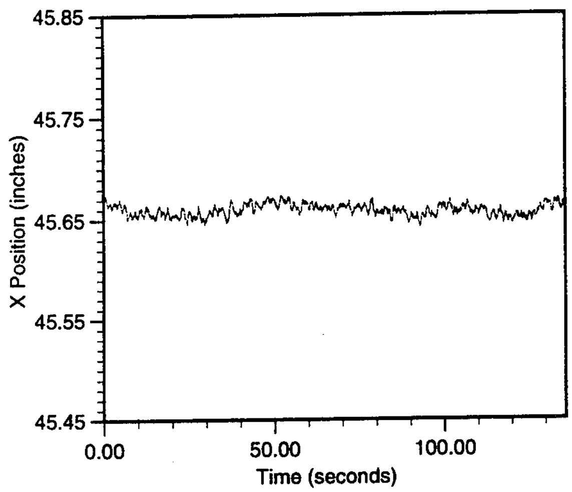

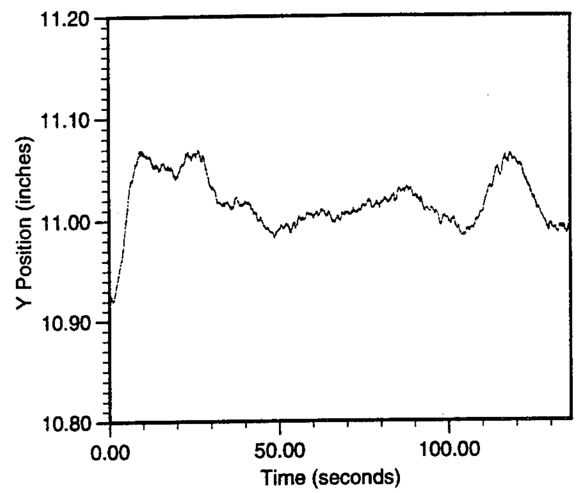

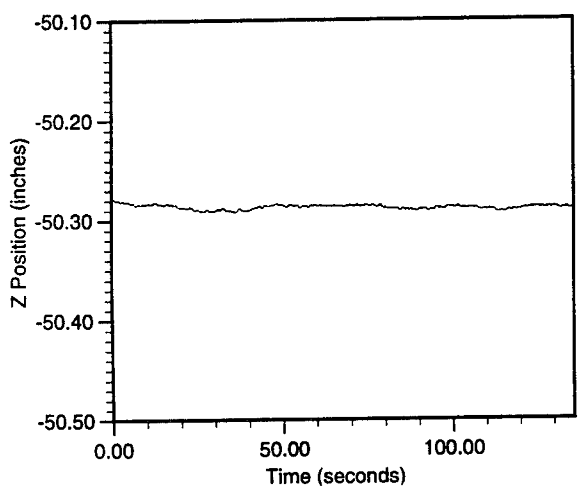

Data Run: ANT_16_3D3
Transducer: 75

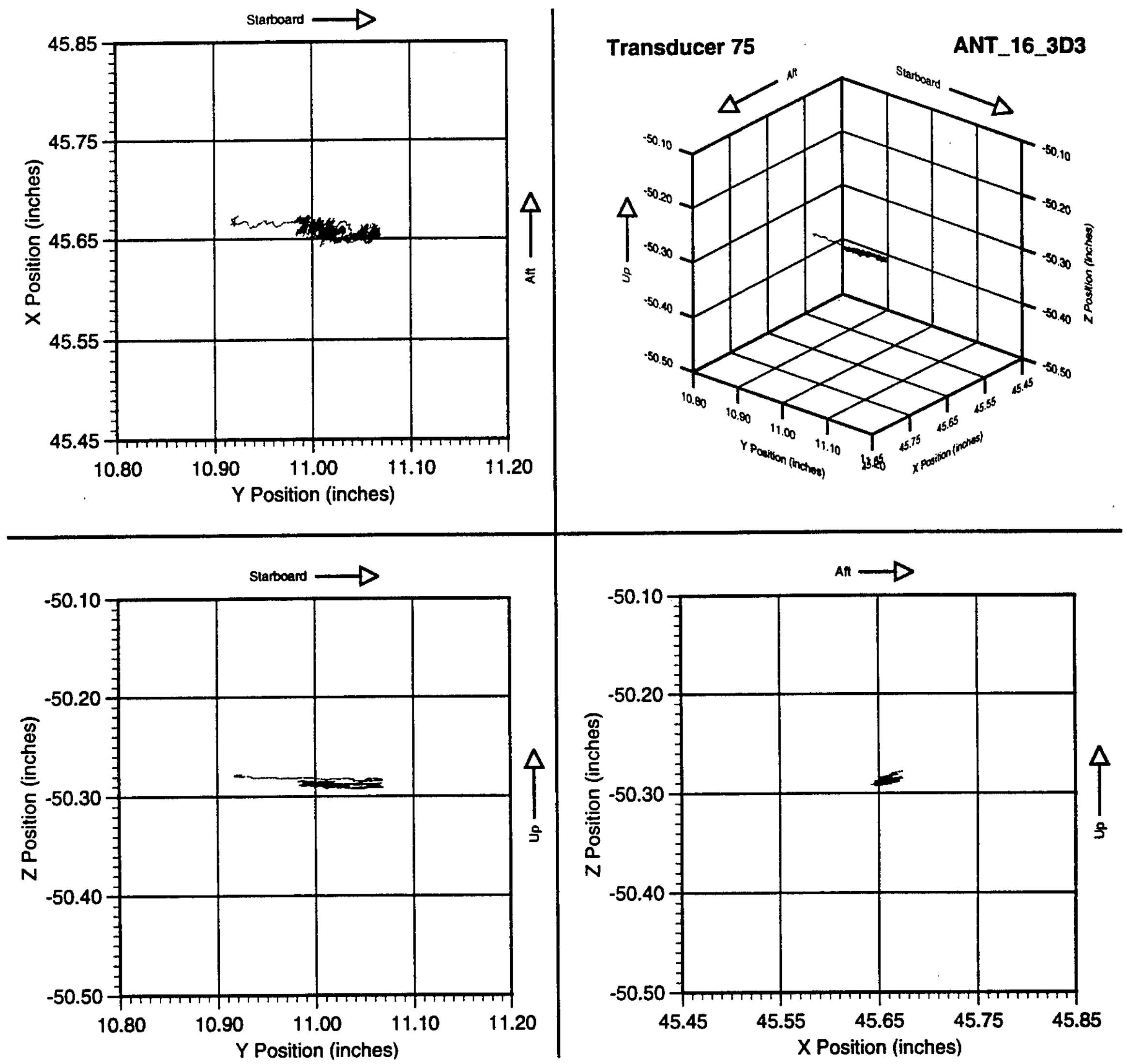
Transducer 75
ANT_16_3D3
Starboard
Aft
Up
X Position (inches)
Y Position (inches)
Z Position (inches)
45.85
45.75
45.65
45.55
45.45
10.80
10.90
11.00
11.10
11.20
-50.10
-50.20
-50.30
-50.40
-50.50

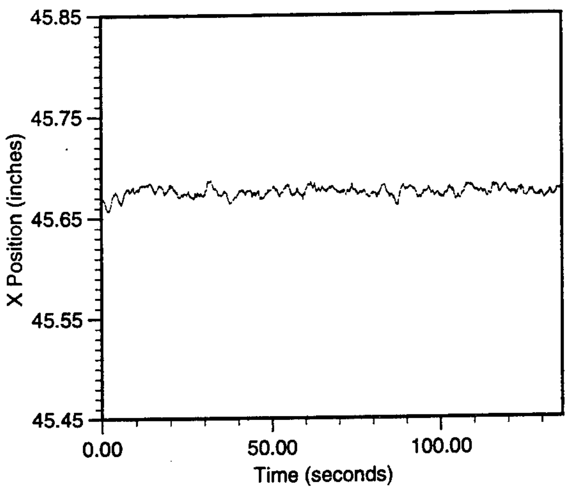

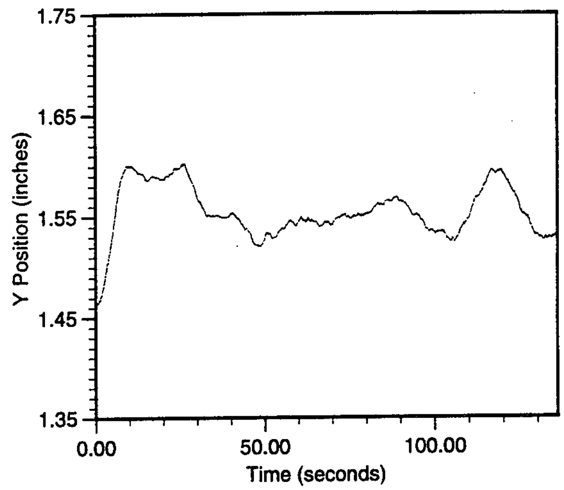

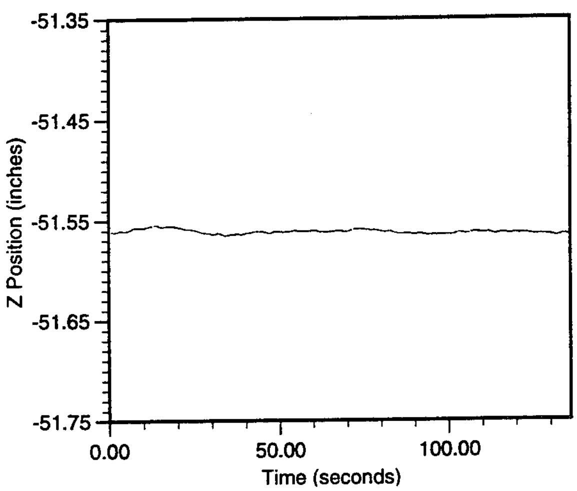

Data Run: ANT_16_3D3
Transducer: 85

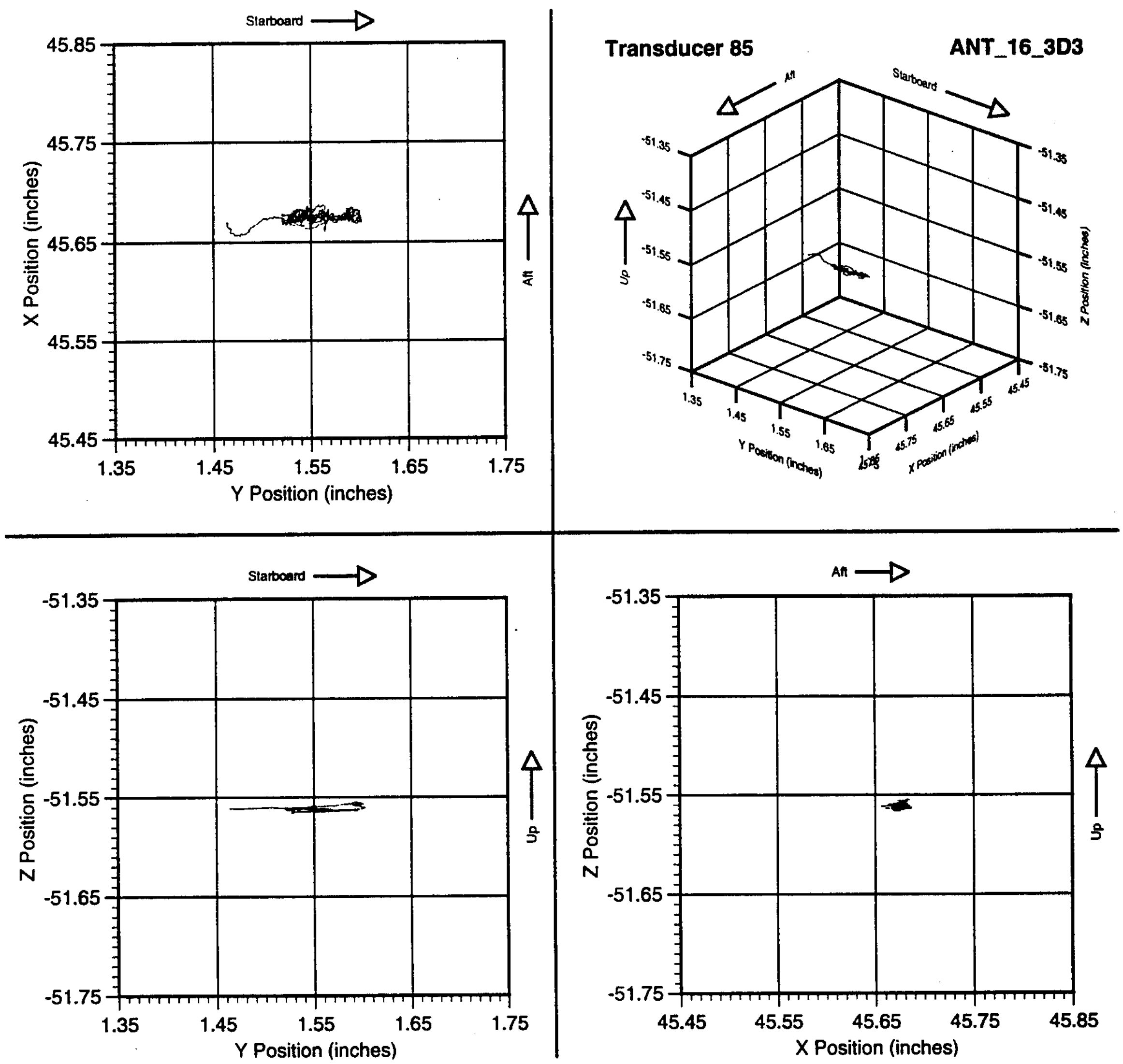
Starboard
45.85
45.75
45.65
45.55
45.45
X Position (inches)
1.35
1.45
1.55
1.65
1.75
Y Position (inches)
Aft
Transducer 85
ANT_16_3D3
Aft
Starboard
Up
Z Position (inches)
Y Position (inches)
X Position (inches)
-51.35
-51.45
-51.55
-51.65
-51.75
Starboard
Z Position (inches)
Up
Aft
45.45
45.55
45.65
45.75
45.85
X Position (inches)

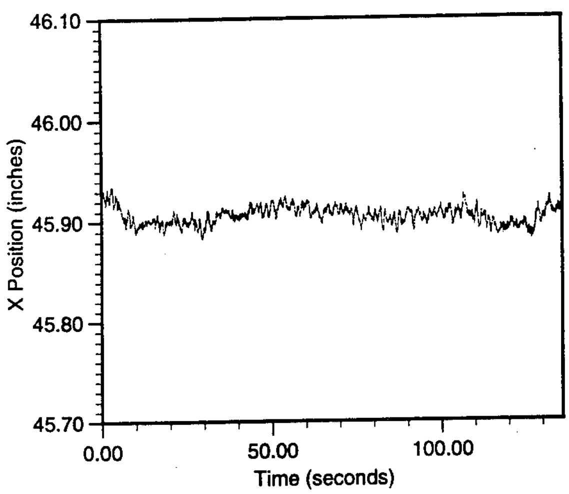

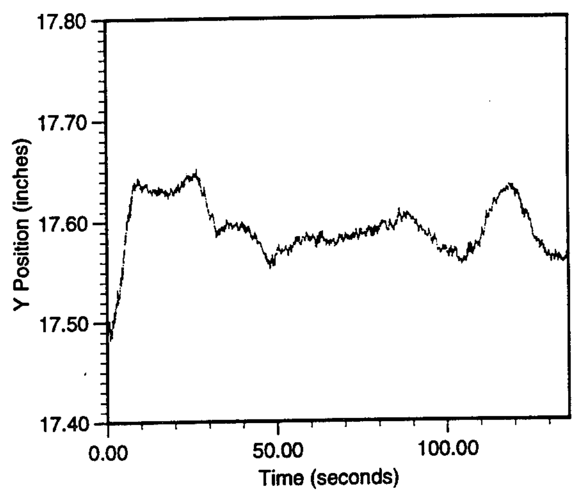

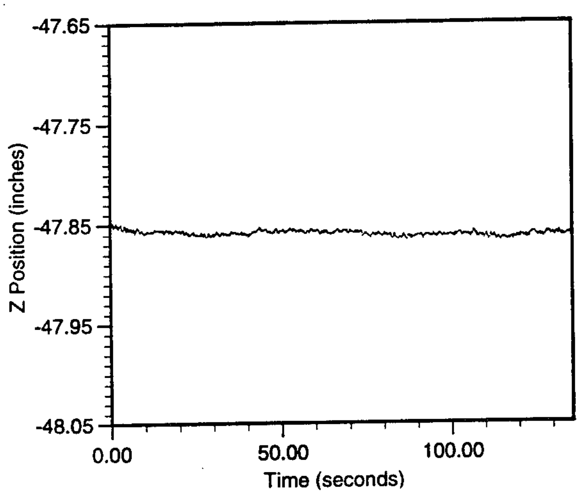

Data Run: ANT_16_3D3
Transducer: 92

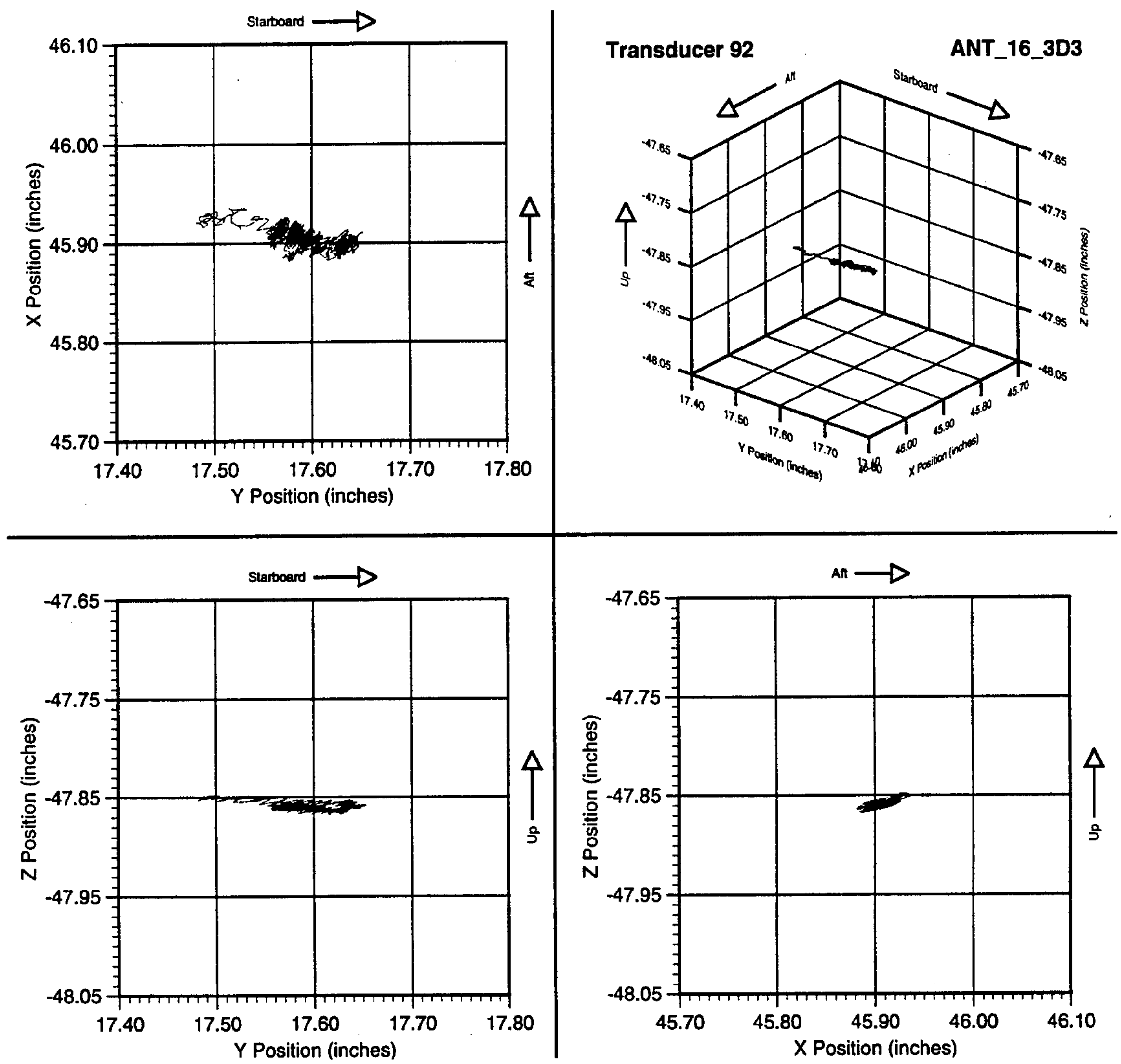
Transducer 92
ANT_16_3D3
Starboard
Aft
Up
X Position (inches)
Y Position (inches)
Z Position (inches)
46.10
46.00
45.90
45.80
45.70
17.40
17.50
17.60
17.70
17.80
-47.65
-47.75
-47.85
-47.95
-48.05
46.10

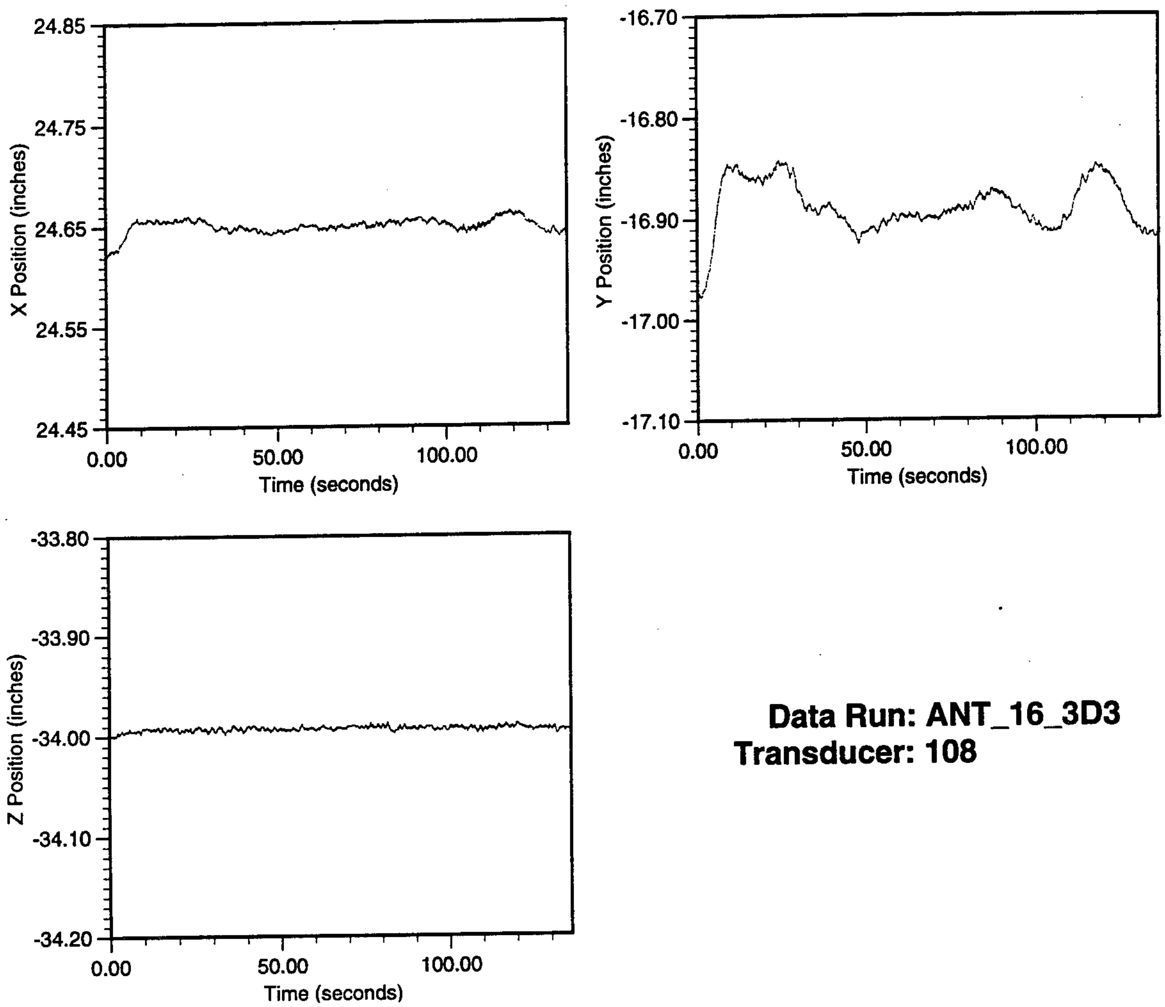

Data Run: ANT_16_3D3
Transducer: 108

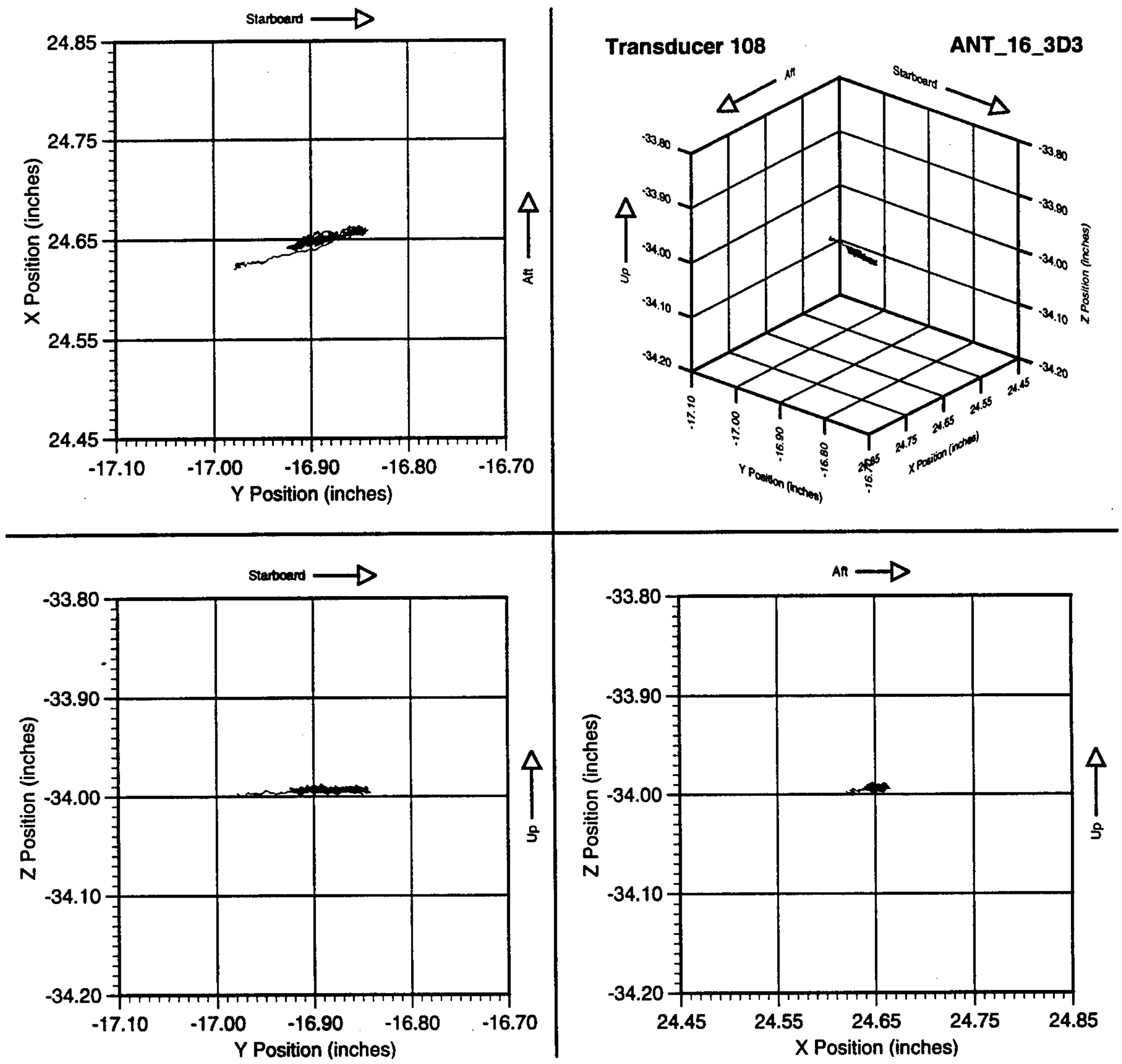

Starboard
24.85
24.75
24.65
24.55
24.45
X Position (inches)
-17.10
-17.00
-16.90
-16.80
-16.70
Y Position (inches)
Aft
Transducer 108
ANT_16_3D3
Aft
Starboard
Up
Z Position (inches)
-33.80
-33.90
-34.00
-34.10
-34.20
Y Position (inches)
X Position (inches)
Z Position (inches)
-33.80
-33.90
-34.00
-34.10
-34.20
-17.10
-17.00
-16.90
-16.80
-16.70
Y Position (inches)
Up
Aft
Z Position (inches)
24.45
24.55
24.65
24.75
24.85
X Position (inches)
Up

Appendix D: ANT16_2_D1 Cartesian Plots

This section contains plots of deflection data from ANT16_2_D1 which was the second data run used for comparison with predictions from UW/APL's FEM of an SRD.

Each driver transducer is represented by two pages of plots. The first page shows three graphs, each of which represents measured deflections on an axis in the Cartesian coordinate system. The X-axis of each of these graphs represents elapsed time from the beginning of the data run. The Y-axis represents absolute deflection measurements with respect to the SRD's Cartesian origin (in the forward end of the SRD).

The second page consists of four scatter plots that depict deflection measurements, over the duration of the data run, in Cartesian coordinate space. The upper left scatter plot shows deflection measurements on the X–Y plane. The lower left plot shows deflections in the Y–Z plane. The lower right scatter plot shows deflections in the X–Z plane. The upper right plot is a 3 dimensional oblique rendering of the same data.

The scatter plots from the second page are useful in determining if the SRD exhibits dynamic movement in a dominant direction.

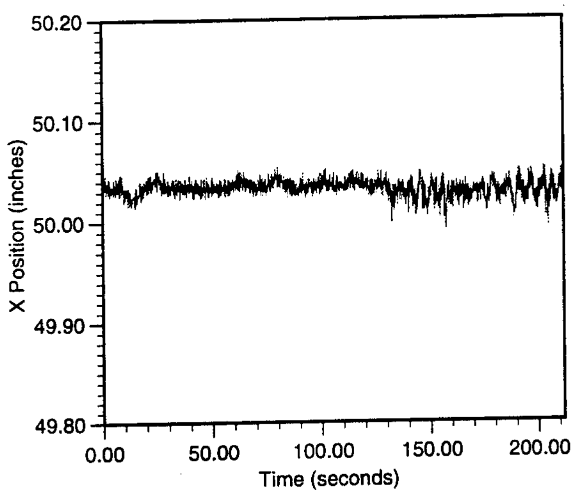

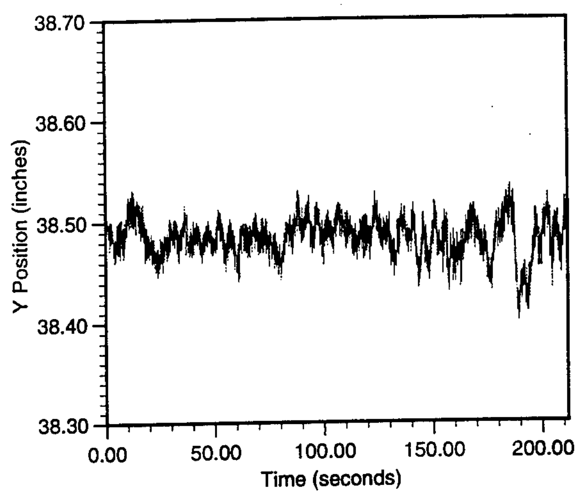

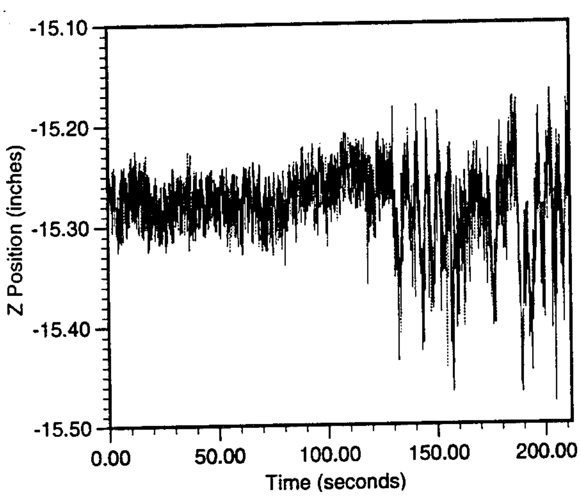

Data Run: ANT16_2_D1
Transducer: 15

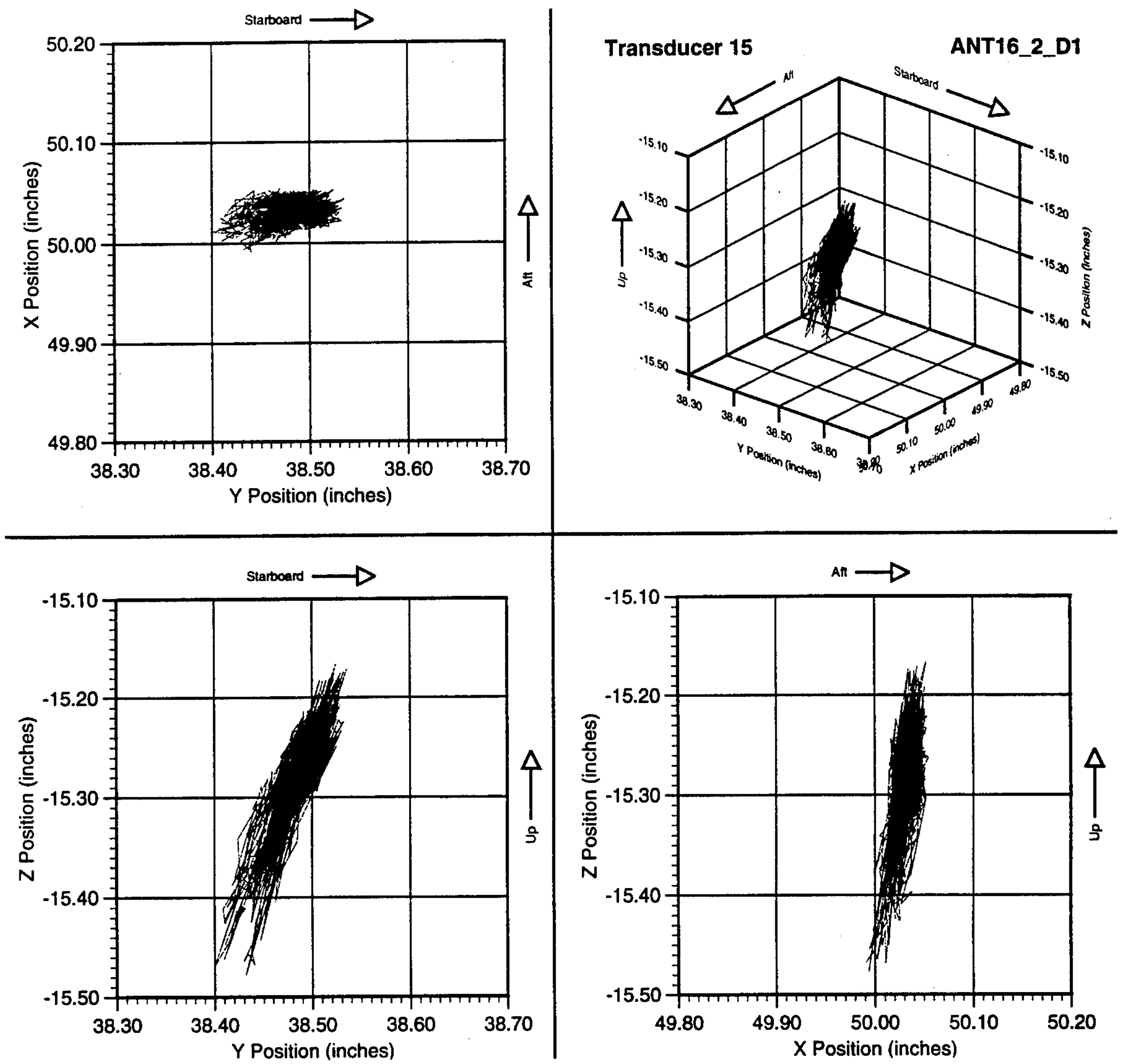
Transducer 15
ANT16_2_D1
Starboard
Aft
Up
X Position (inches)
Y Position (inches)
Z Position (inches)
50.20
50.10
50.00
49.90
49.80
38.30
38.40
38.50
38.60
38.70
-15.10
-15.20
-15.30
-15.40
-15.50
50.20

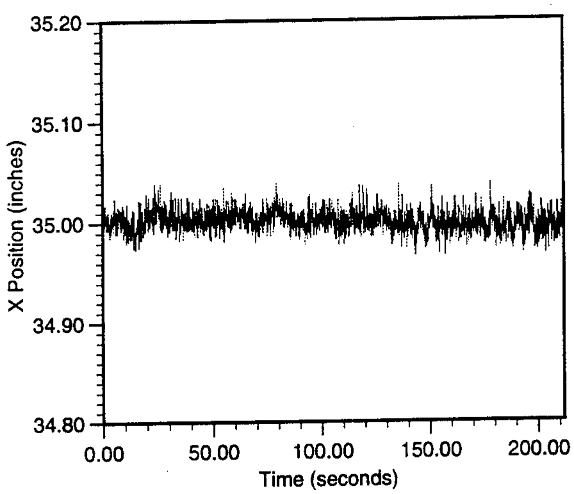

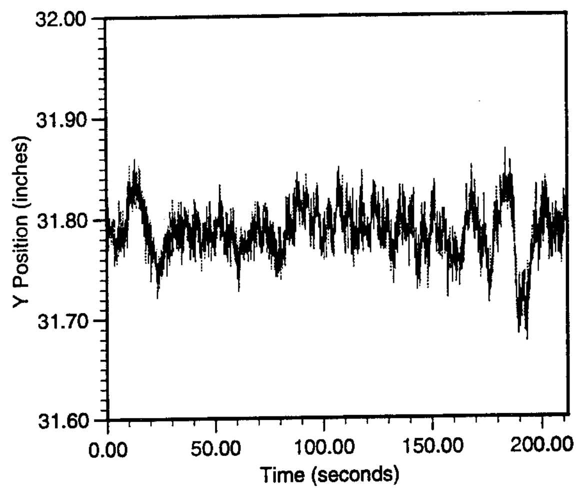

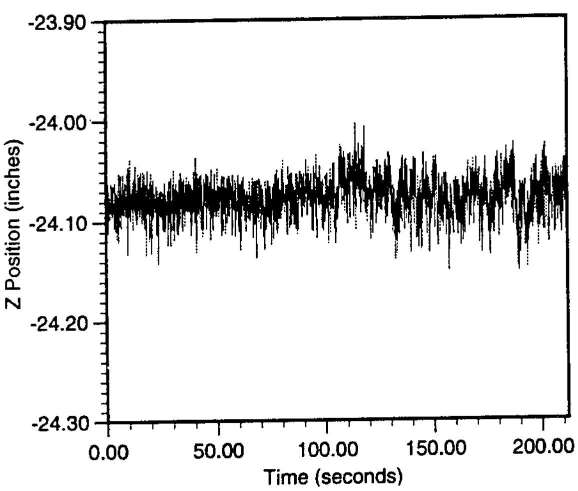

Data Run: ANT16_2_D1
Transducer: 29

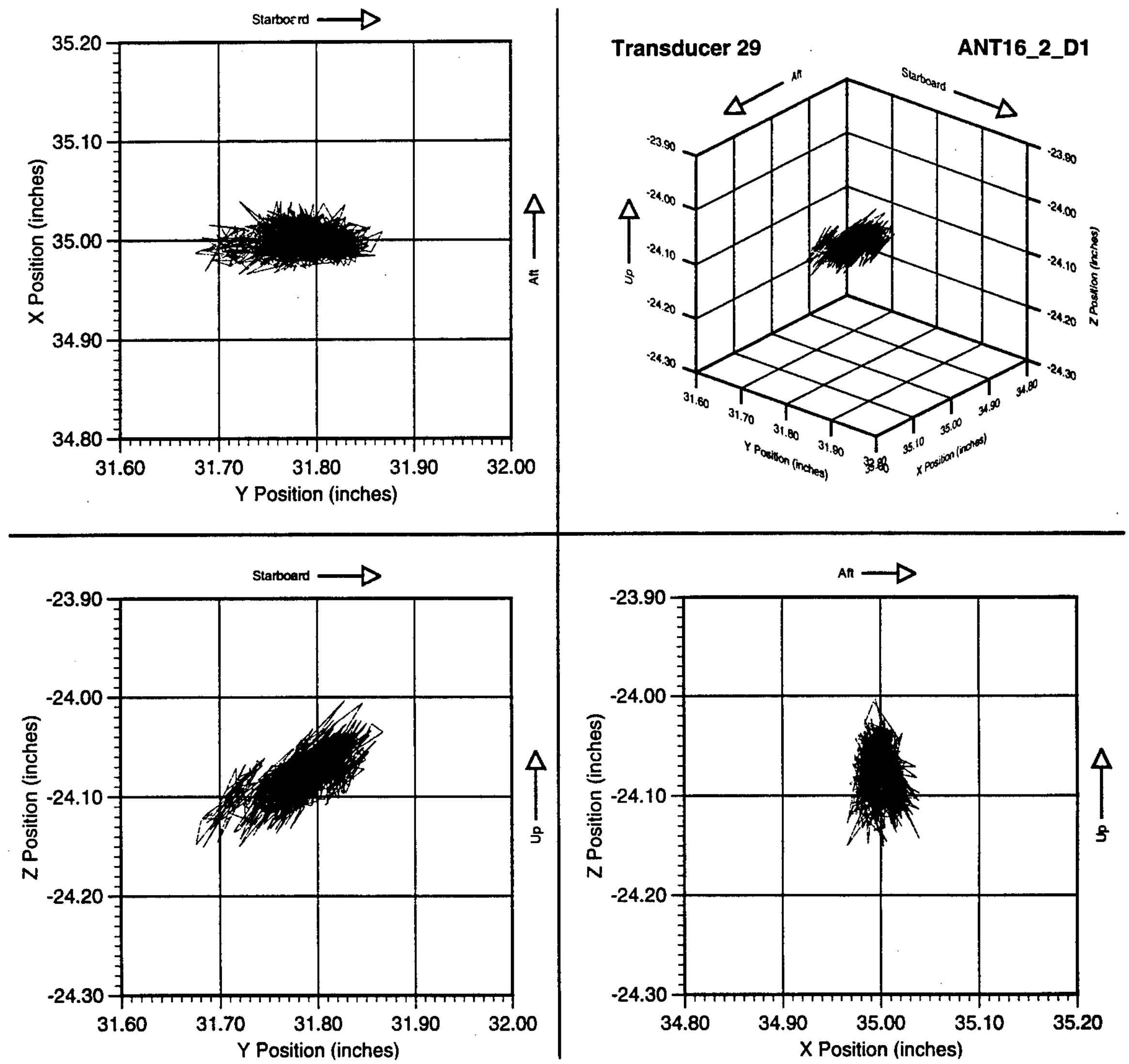
Transducer 29
ANT16_2_D1
Starboard
Aft
Up
X Position (inches)
Y Position (inches)
Z Position (inches)
35.20
35.10
35.00
34.90
34.80
31.60
31.70
31.80
31.90
32.00
-23.90
-24.00
-24.10
-24.20
-24.30
35.00
35.10
35.20

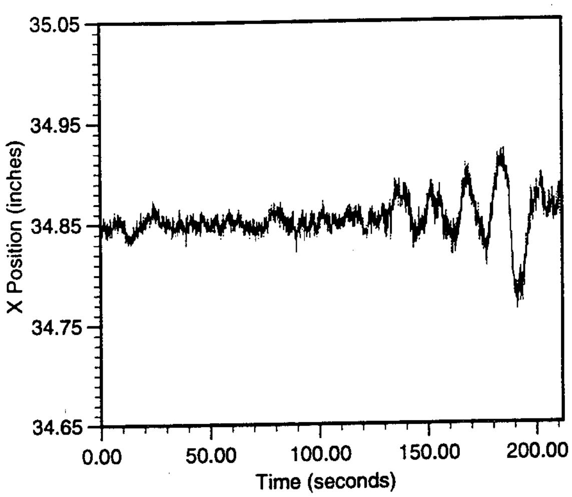

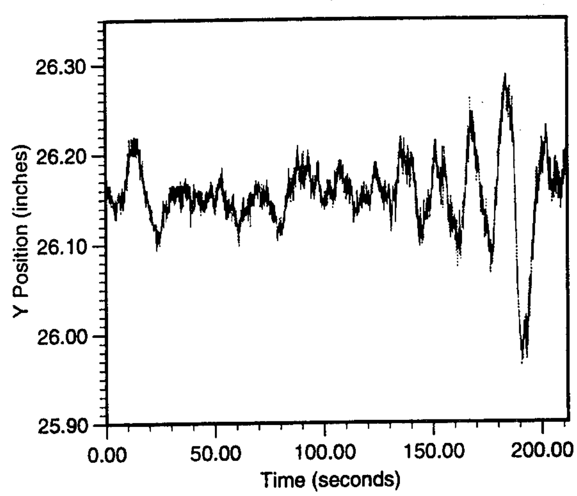

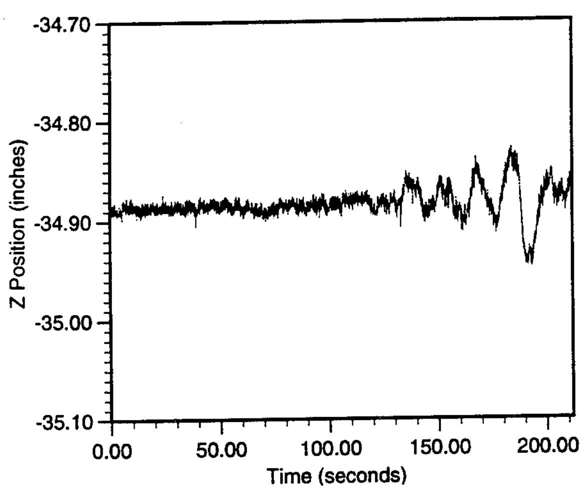

Data Run: ANT16_2_D1
Transducer: 50

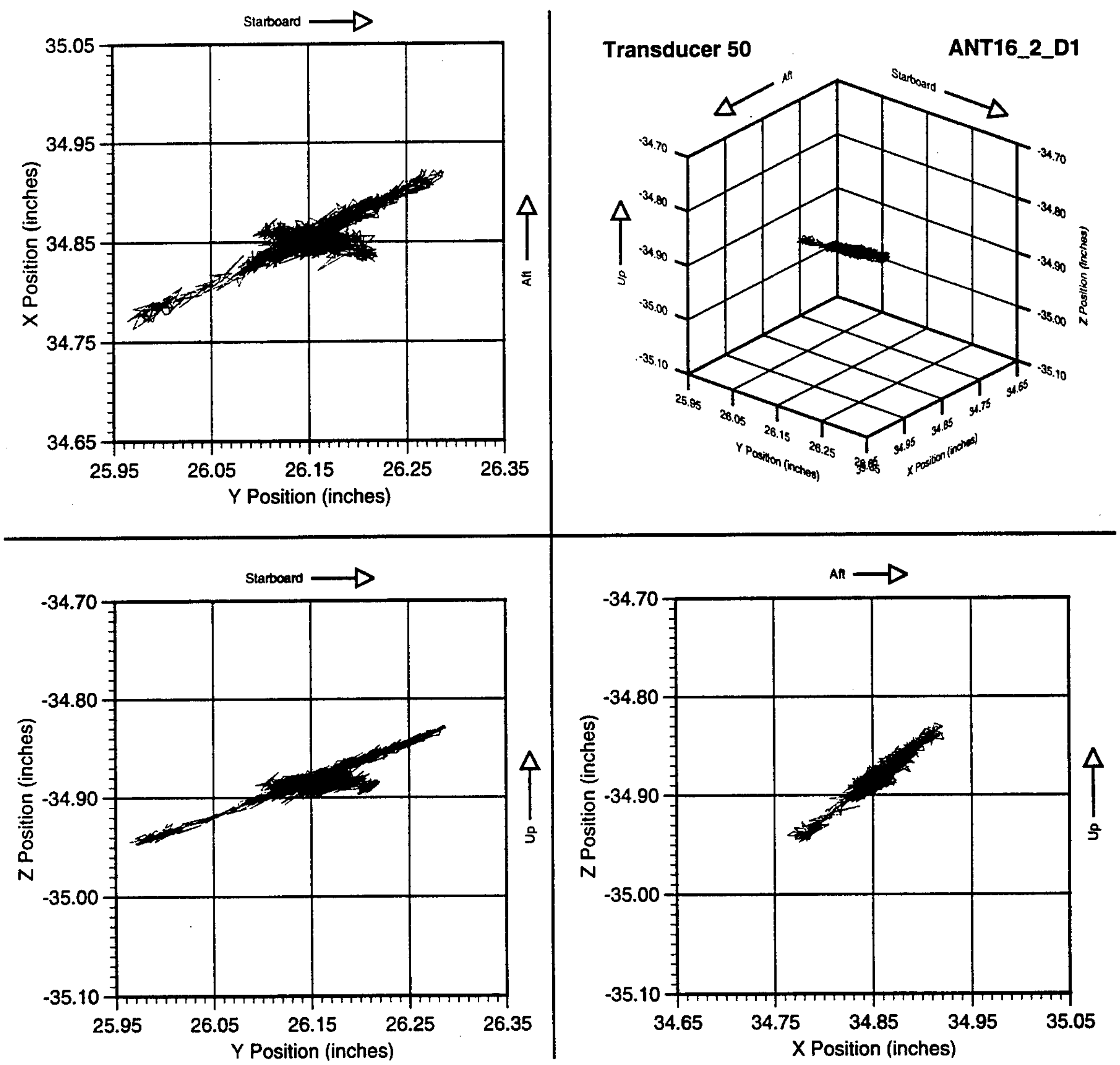
Transducer 50
ANT16_2_D1
Starboard
Aft
Up
X Position (inches)
Y Position (inches)
Z Position (inches)

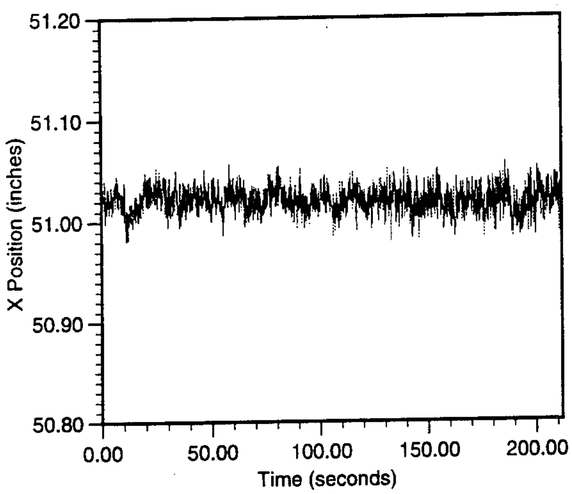

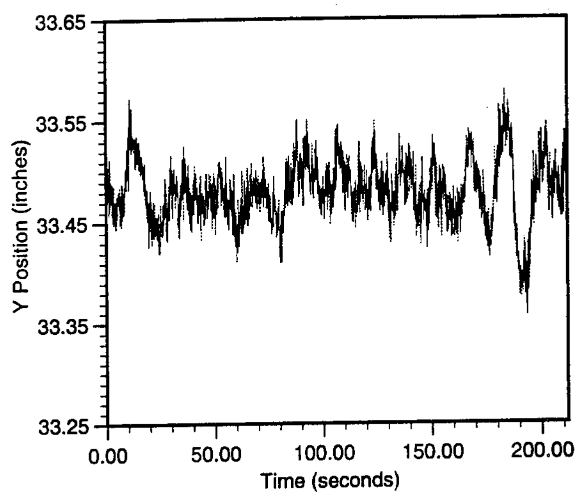

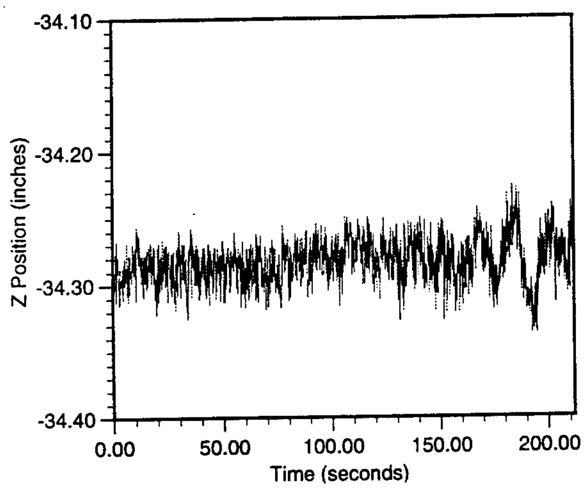

Data Run: ANT16_2_D1
Transducer: 51

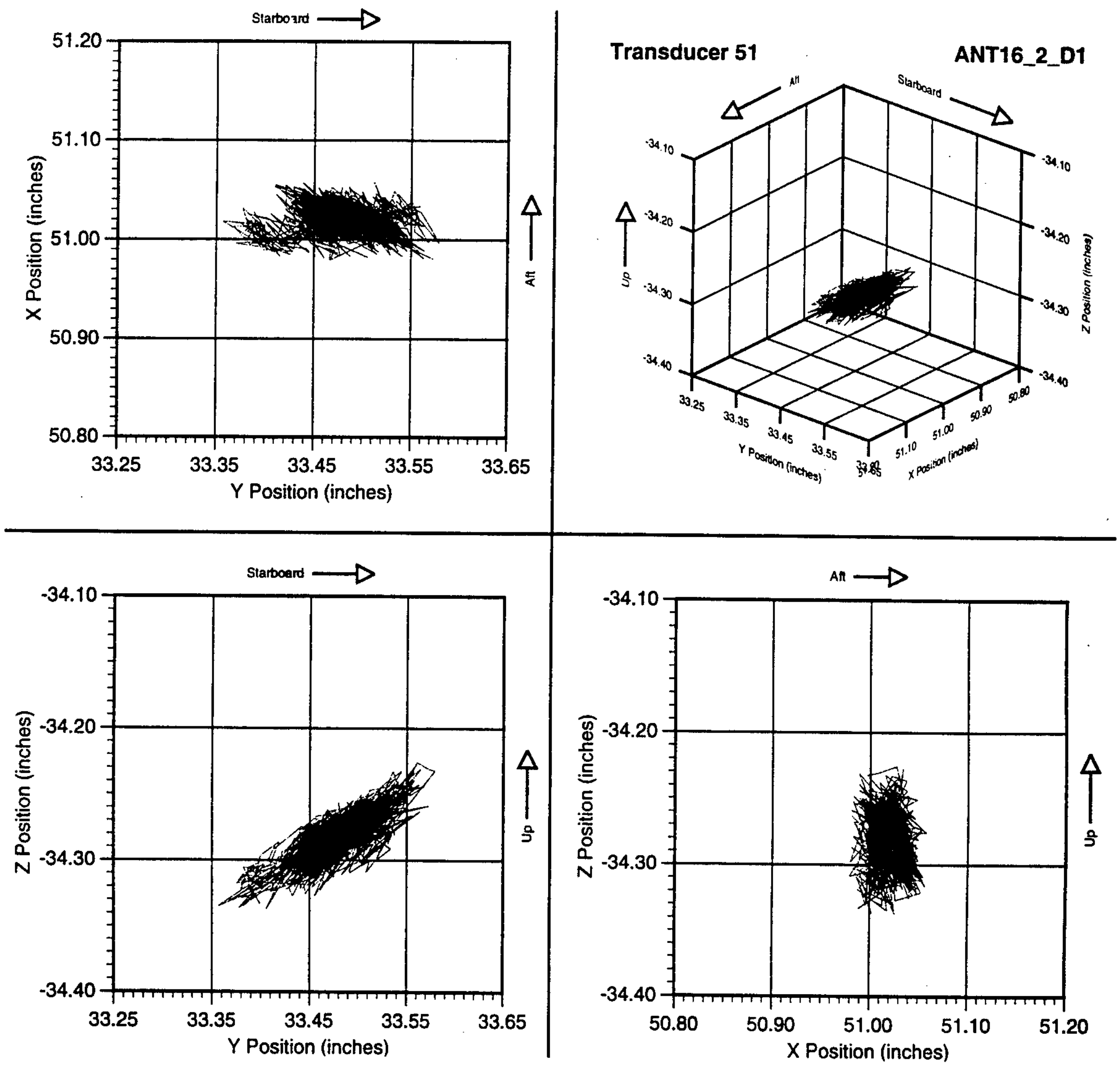

Transducer 51
ANT16_2_D1
Starboard
Aft
Up
X Position (inches)
Y Position (inches)
Z Position (inches)
51.20
51.10
51.00
50.90
50.80
33.25
33.35
33.45
33.55
33.65
-34.10
-34.20
-34.30
-34.40

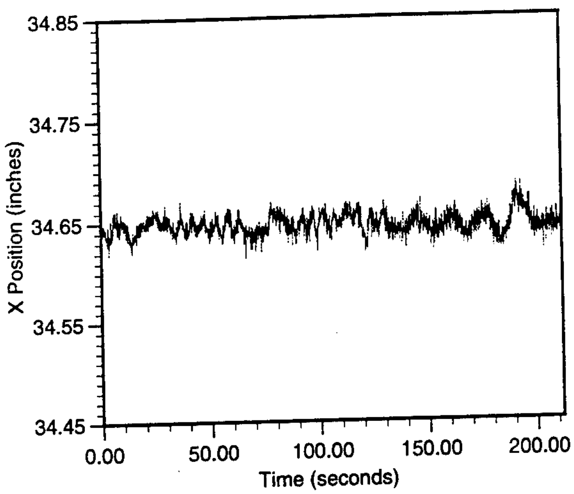

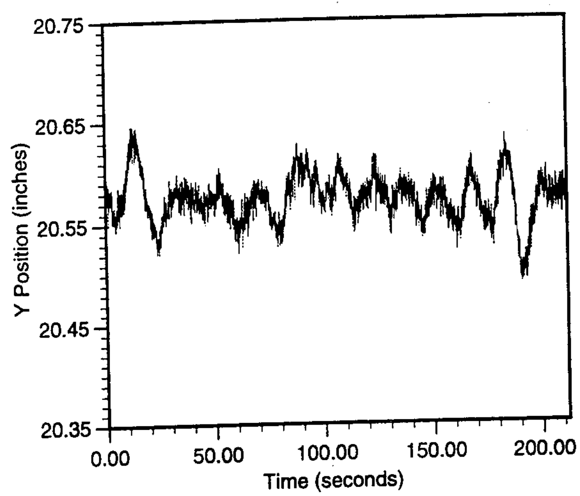

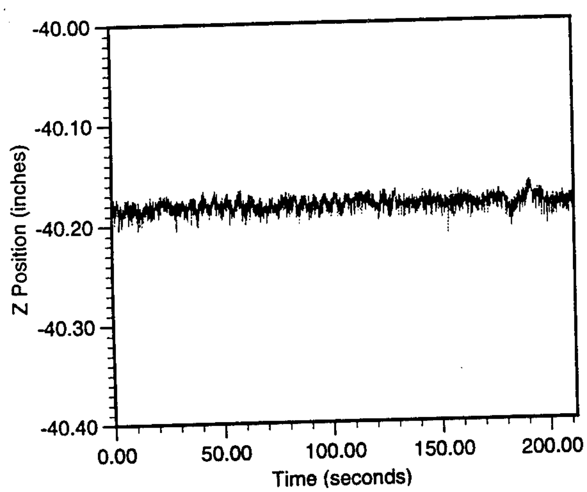

Data Run: ANT16_2_D1
Transducer: 65

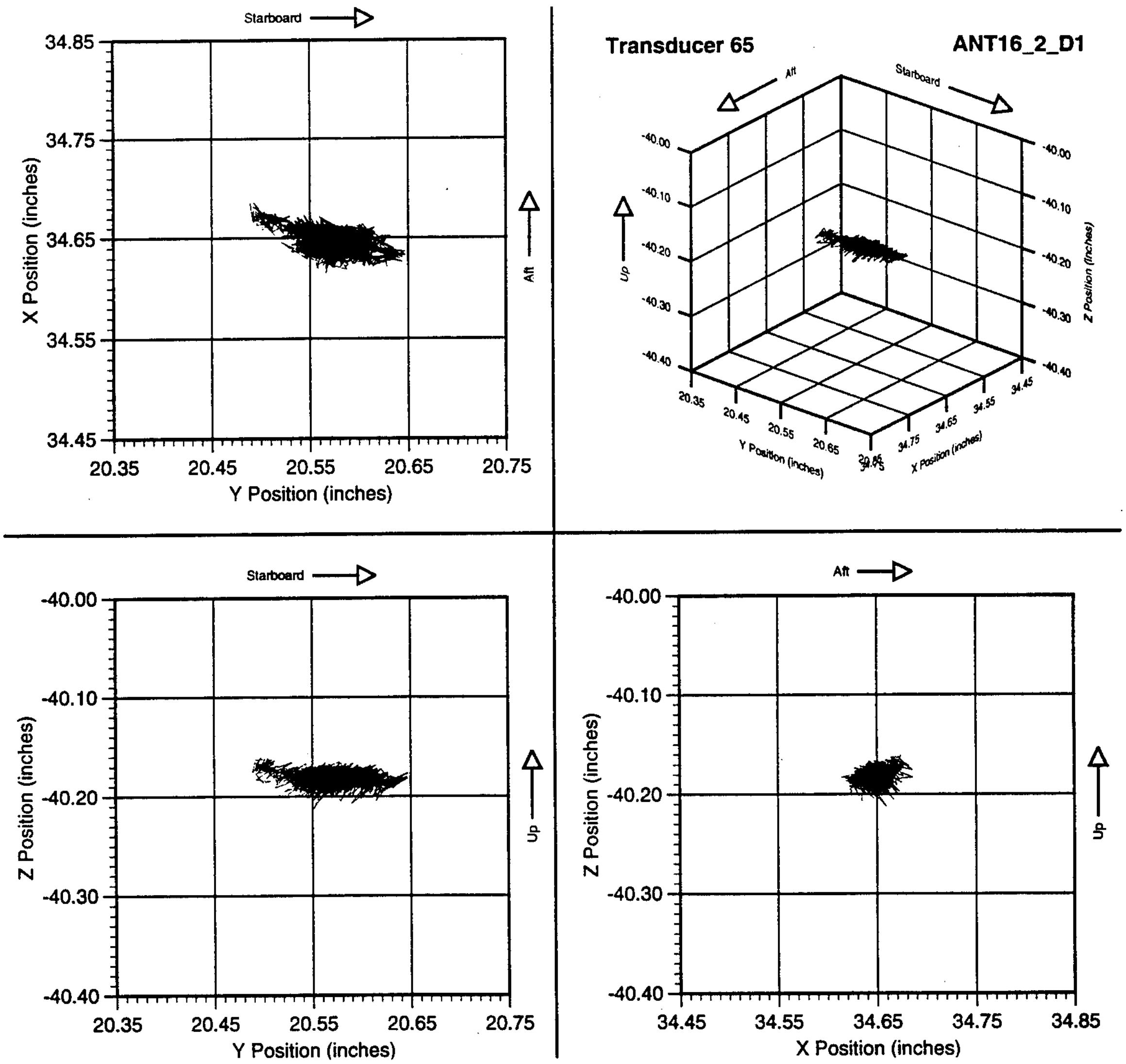
Transducer 65
ANT16_2_D1
Starboard
Aft
Up
X Position (inches)
Y Position (inches)
Z Position (inches)
34.85
34.75
34.65
34.55
34.45
20.35
20.45
20.55
20.65
20.75
-40.00
-40.10
-40.20
-40.30
-40.40

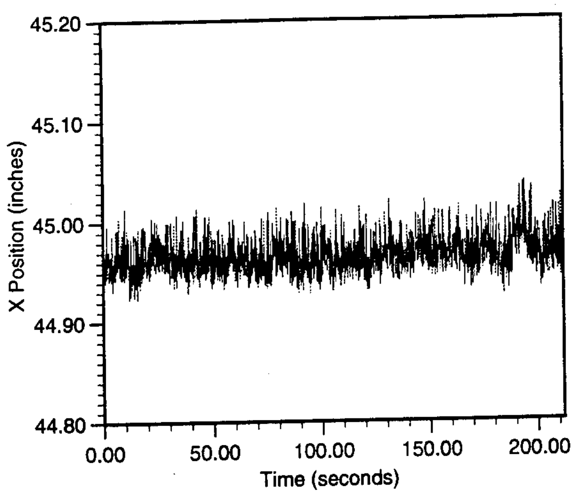

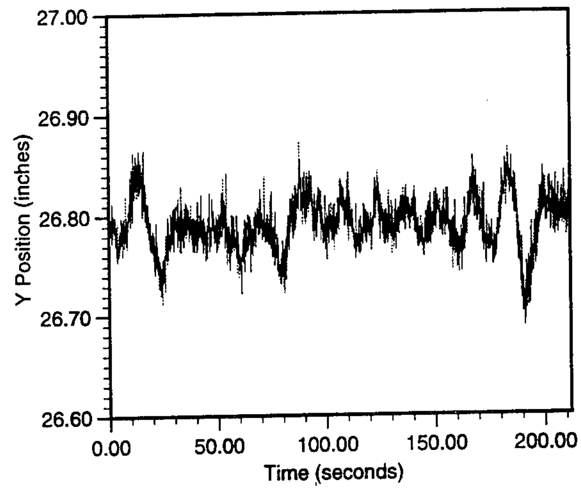

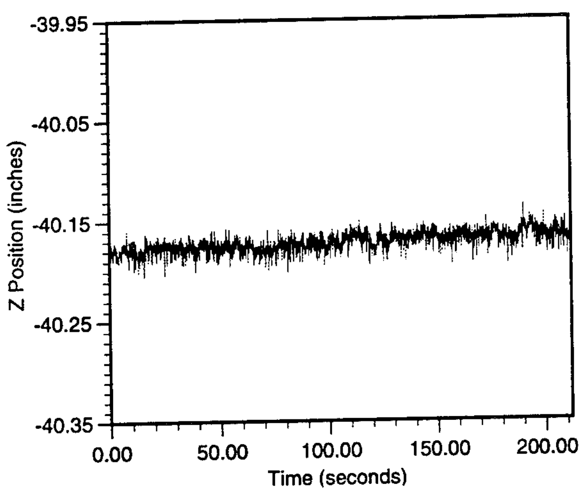

Data Run: ANT16_2_D1
Transducer: 66

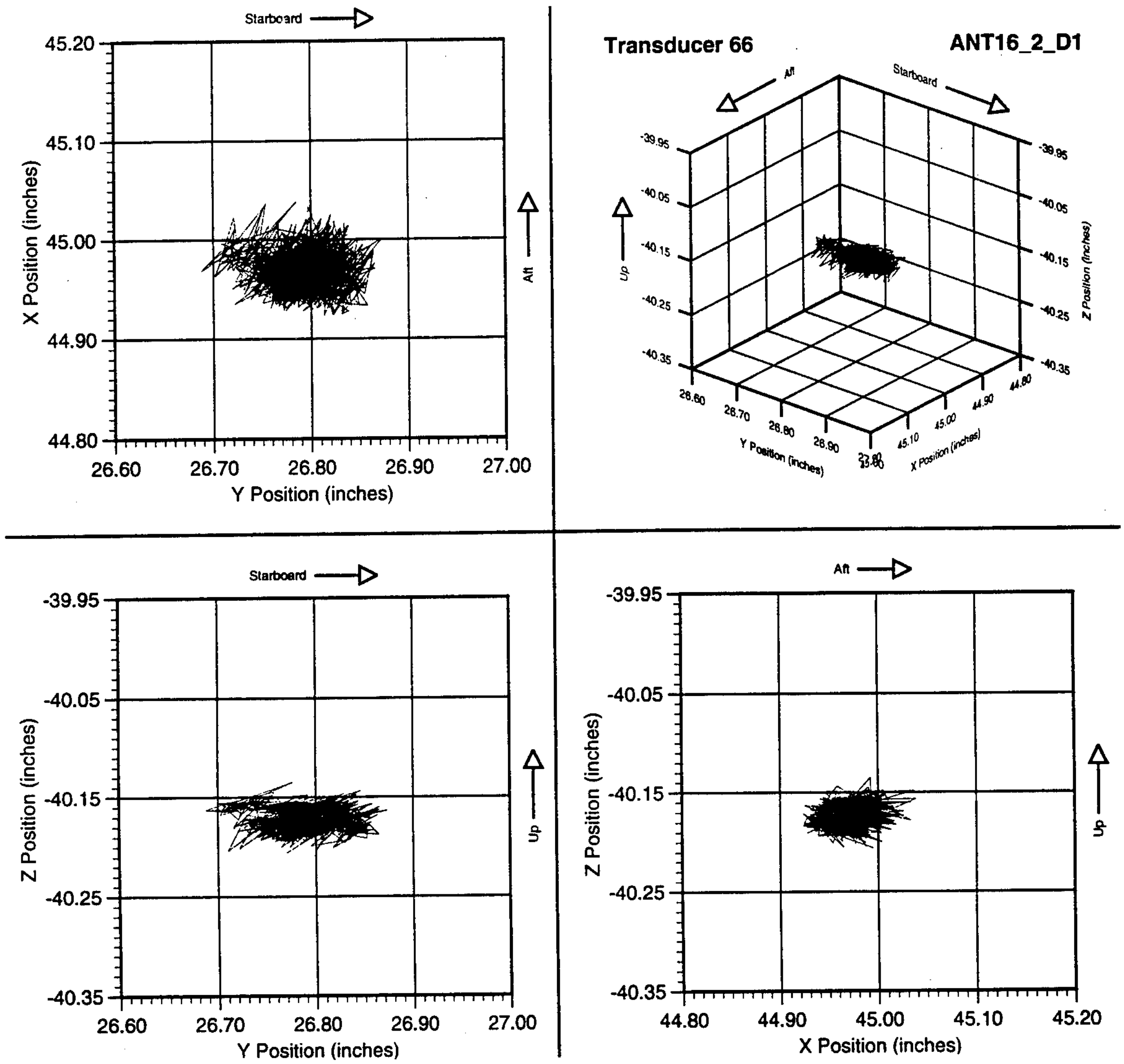
Transducer 66
ANT16_2_D1
Starboard
Aft
Up
X Position (inches)
Y Position (inches)
Z Position (inches)
45.20
45.10
45.00
44.90
44.80
26.60
26.70
26.80
26.90
27.00
-39.95
-40.05
-40.15
-40.25
-40.35

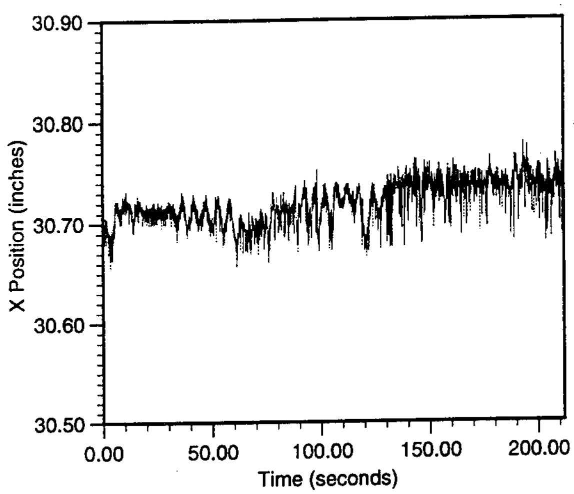

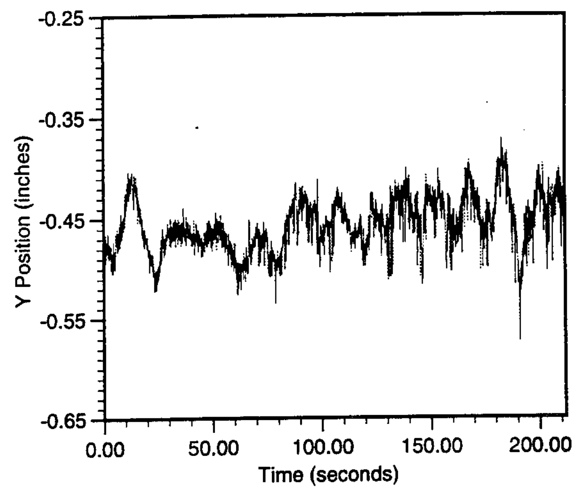

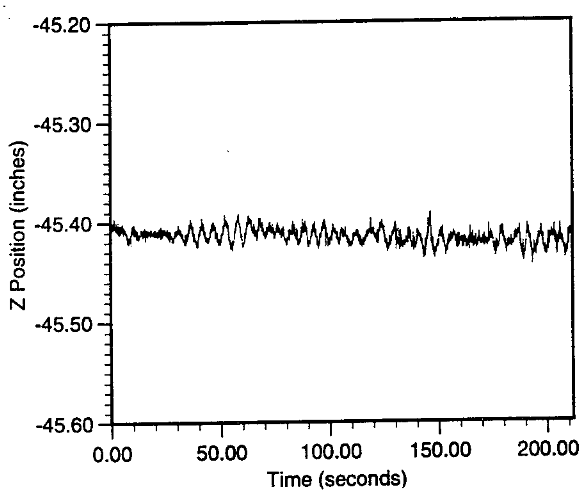

Data Run: ANT16_2_D1
Transducer: 70

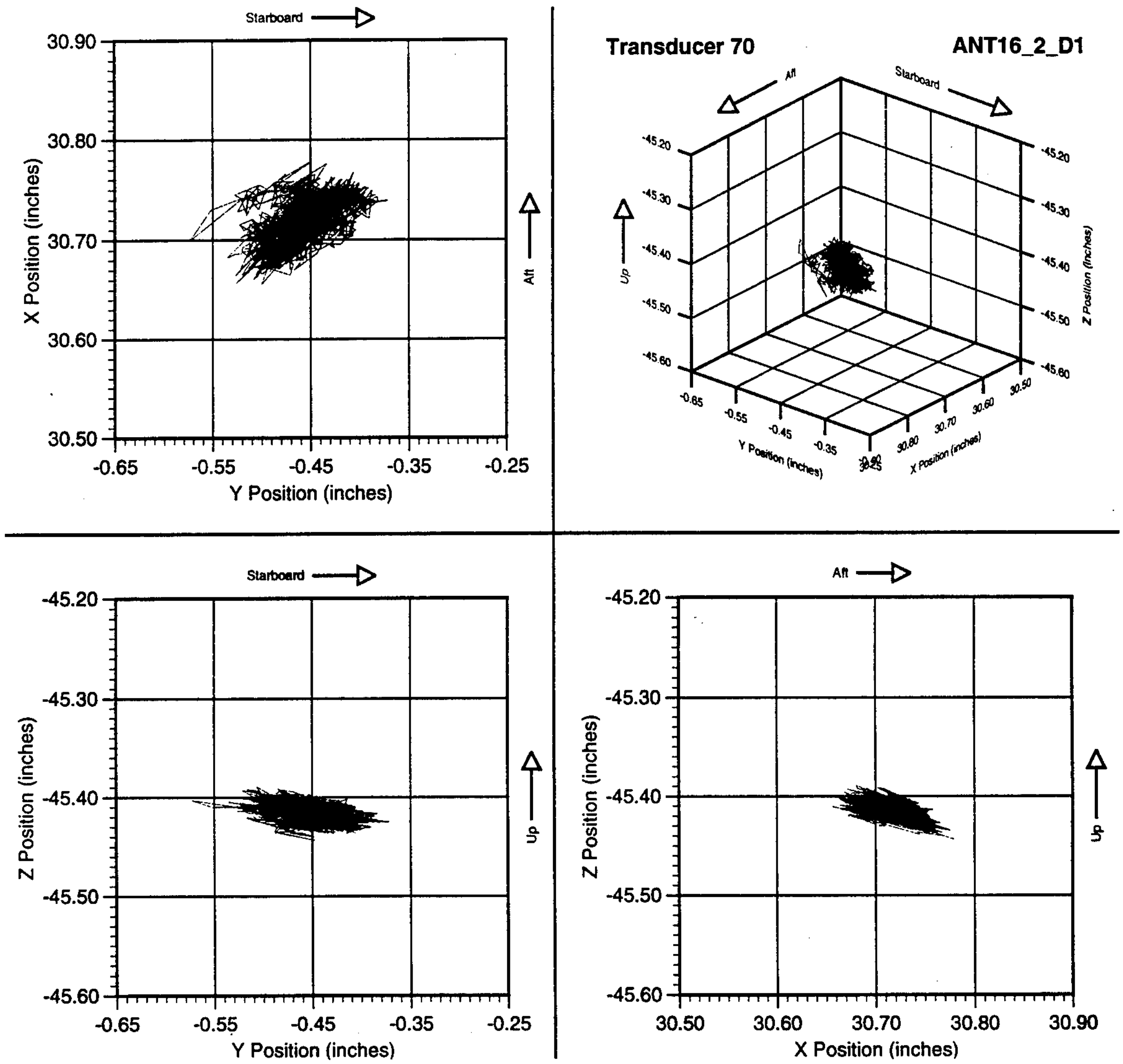
Transducer 70
ANT16_2_D1
Starboard
Aft
Up
X Position (inches)
Y Position (inches)
Z Position (inches)
30.90
30.80
30.70
30.60
30.50
-0.65
-0.55
-0.45
-0.35
-0.25
-45.20
-45.30
-45.40
-45.50
-45.60
30.50
30.60
30.70
30.80
30.90

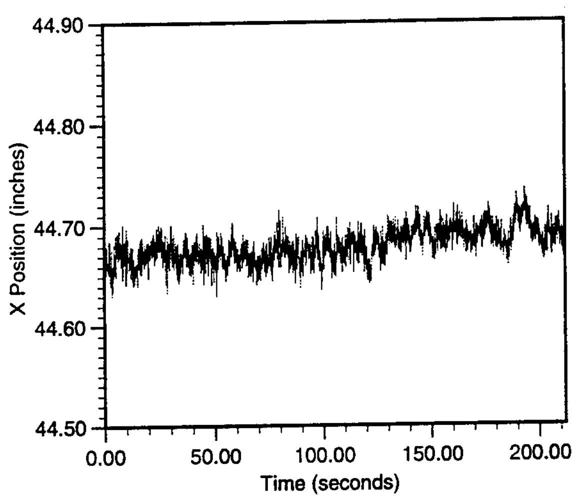

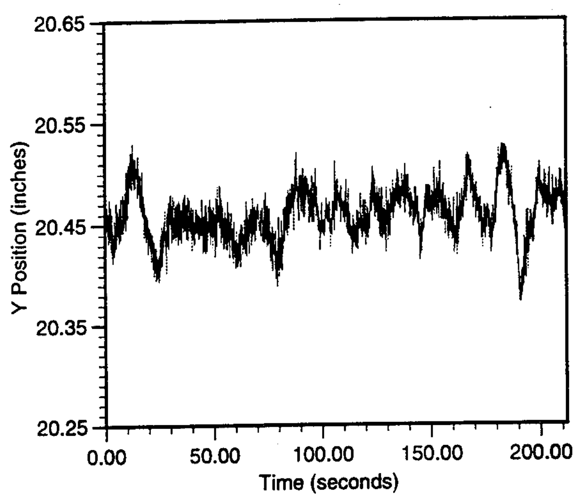

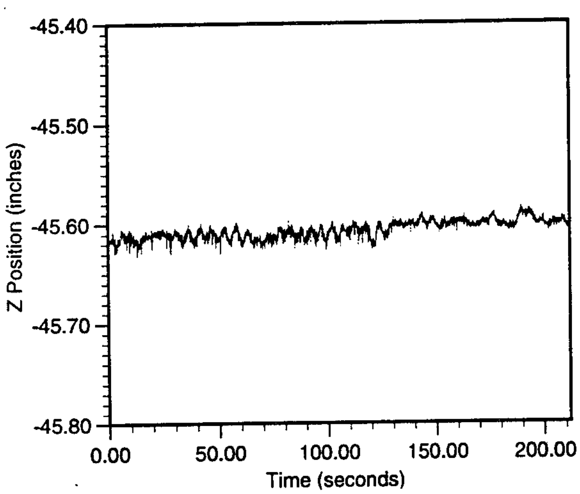

Data Run: ANT16_2_D1
Transducer: 71

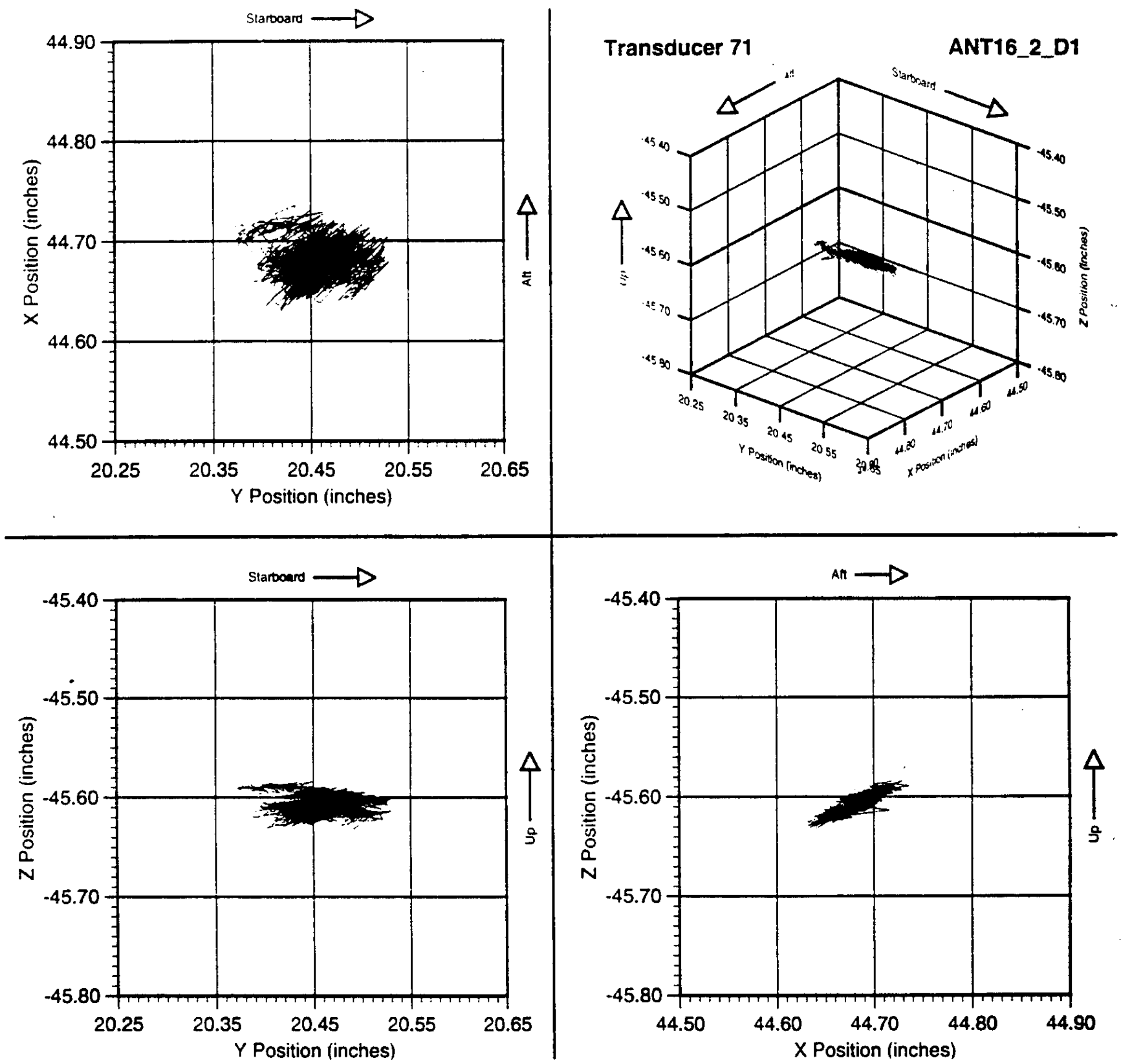

Transducer 71
ANT16_2_D1
Starboard
Aft
Up
X Position (inches)
Y Position (inches)
Z Position (inches)
44.90
44.80
44.70
44.60
44.50
20.25
20.35
20.45
20.55
20.65
-45.40
-45.50
-45.60
-45.70
-45.80

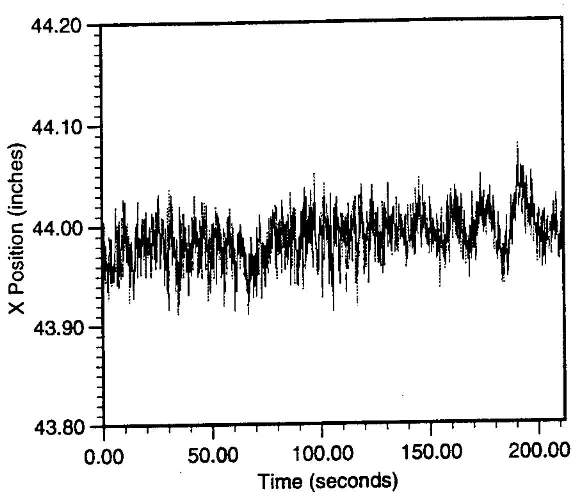

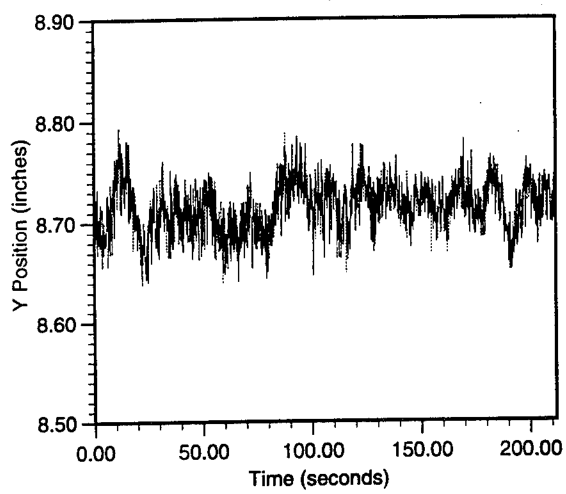

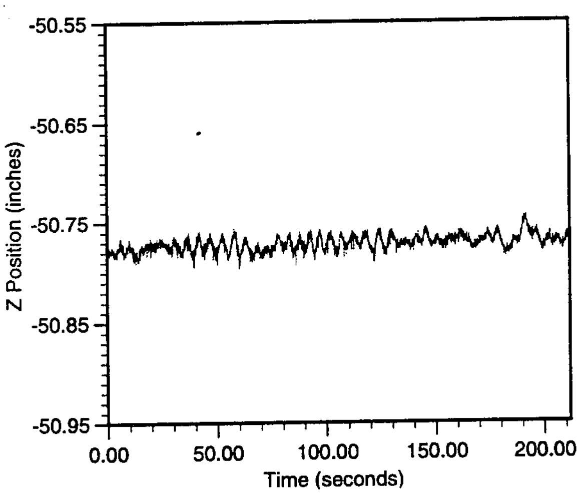

Data Run: ANT16_2_D1
Transducer: 75

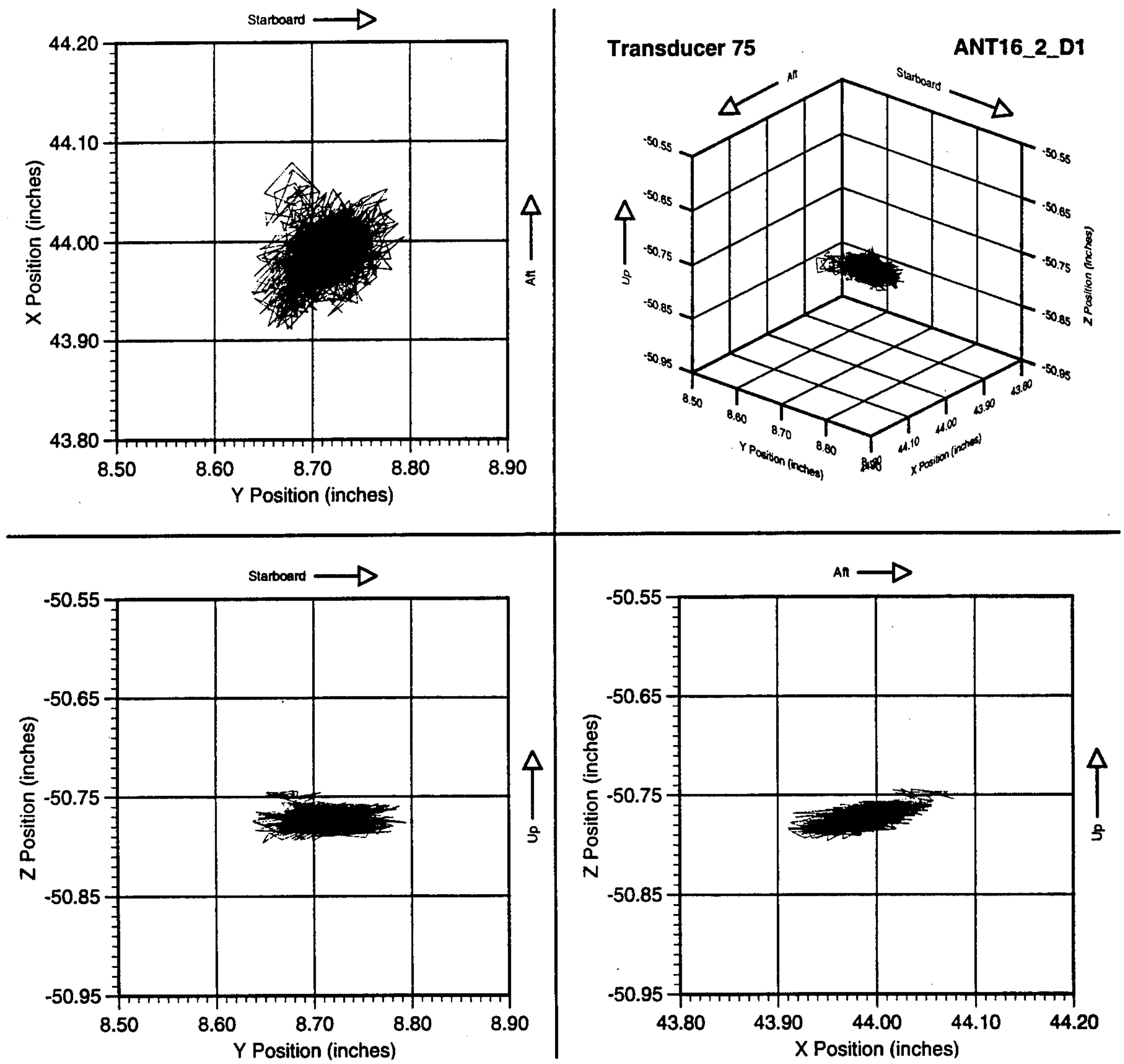
Transducer 75
ANT16_2_D1
Starboard
Aft
Up
X Position (inches)
Y Position (inches)
Z Position (inches)
Starboard
Aft
Up
Aft
Up

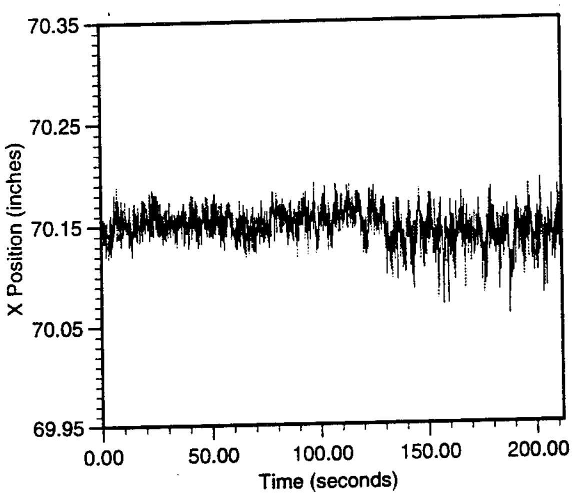

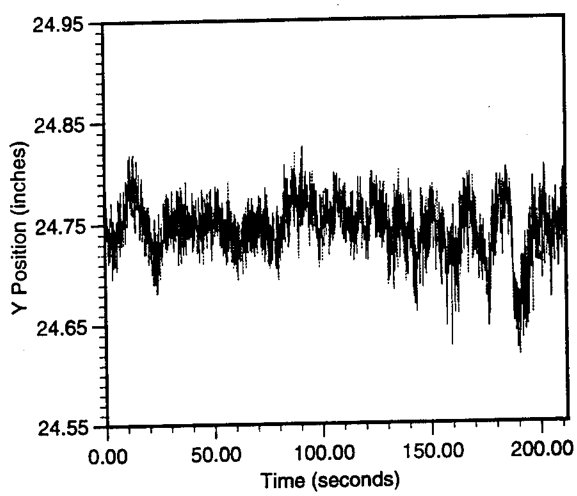

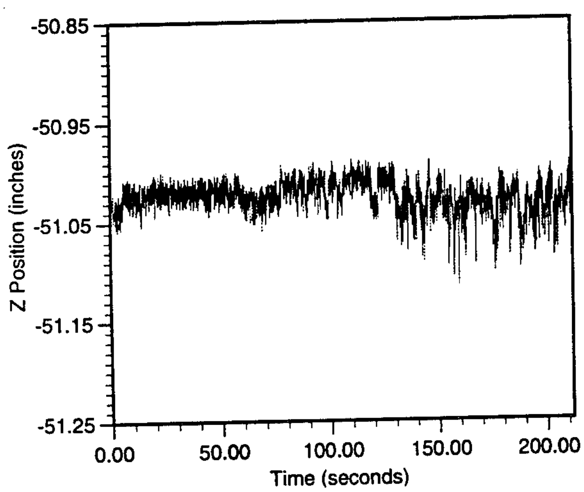

Data Run: ANT16_2_D1
Transducer: 76

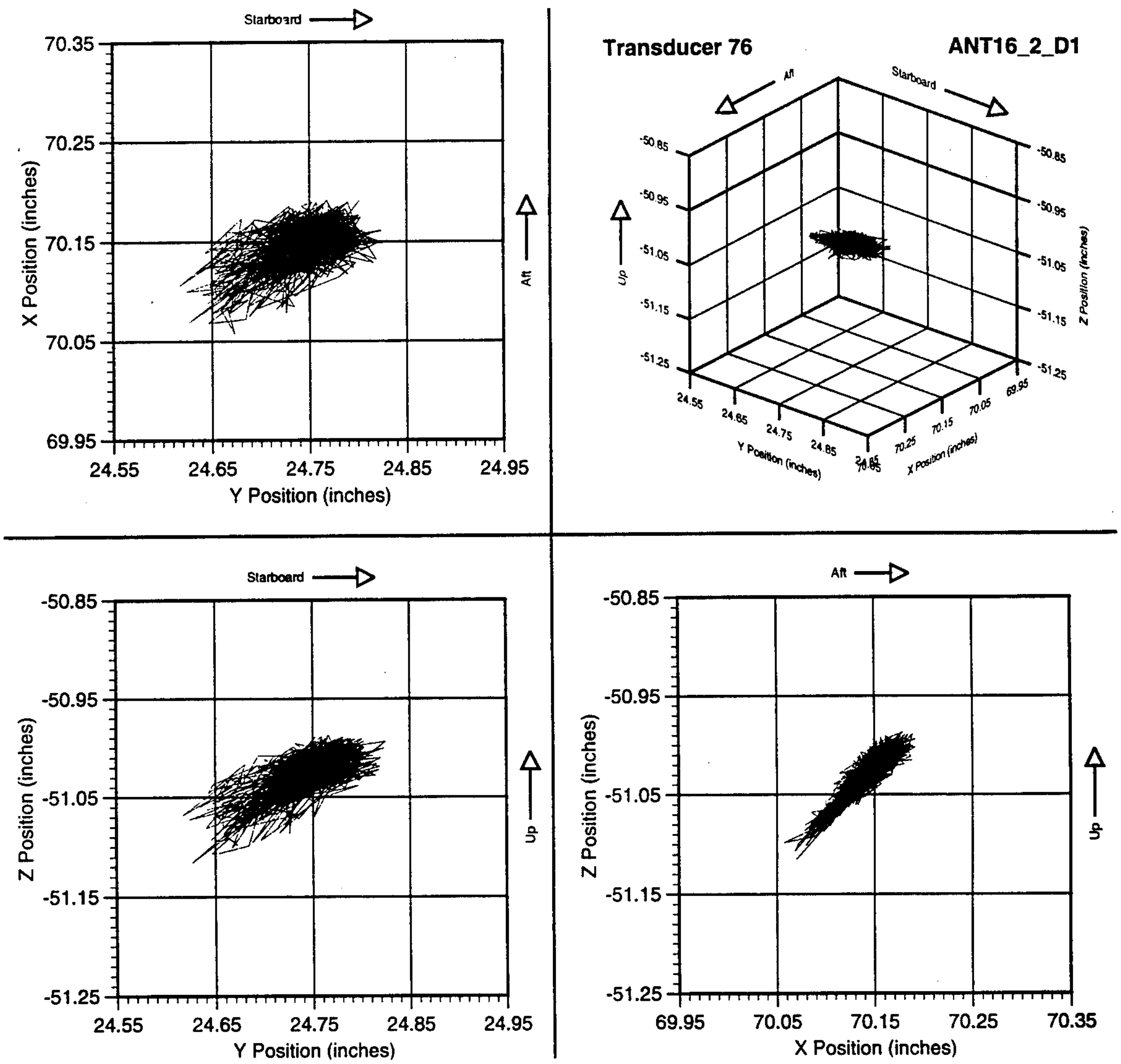
Transducer 76
ANT16_2_D1
Starboard
Aft
Up
X Position (inches)
Y Position (inches)
Z Position (inches)
70.35
70.25
70.15
70.05
69.95
24.55
24.65
24.75
24.85
24.95
-50.85
-50.95
-51.05
-51.15
-51.25

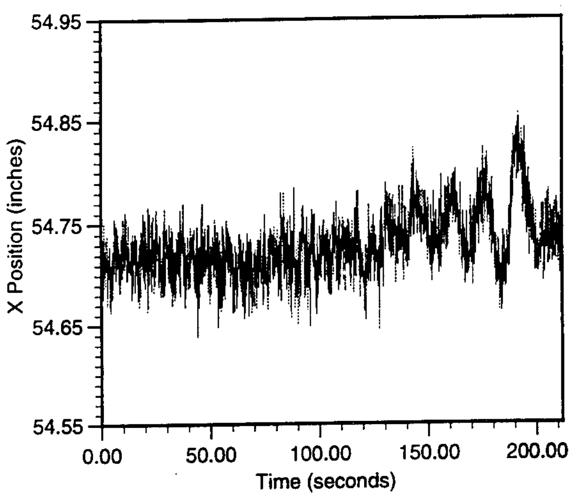

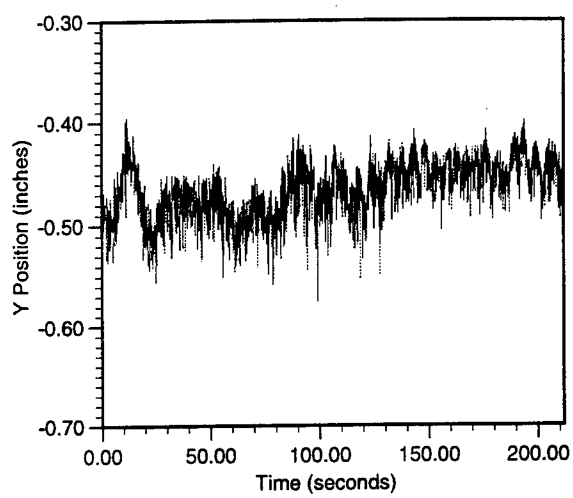

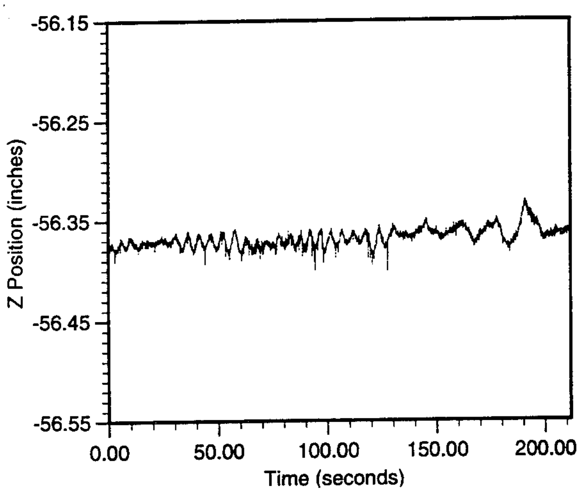

Data Run: ANT16_2_D1
Transducer: 79

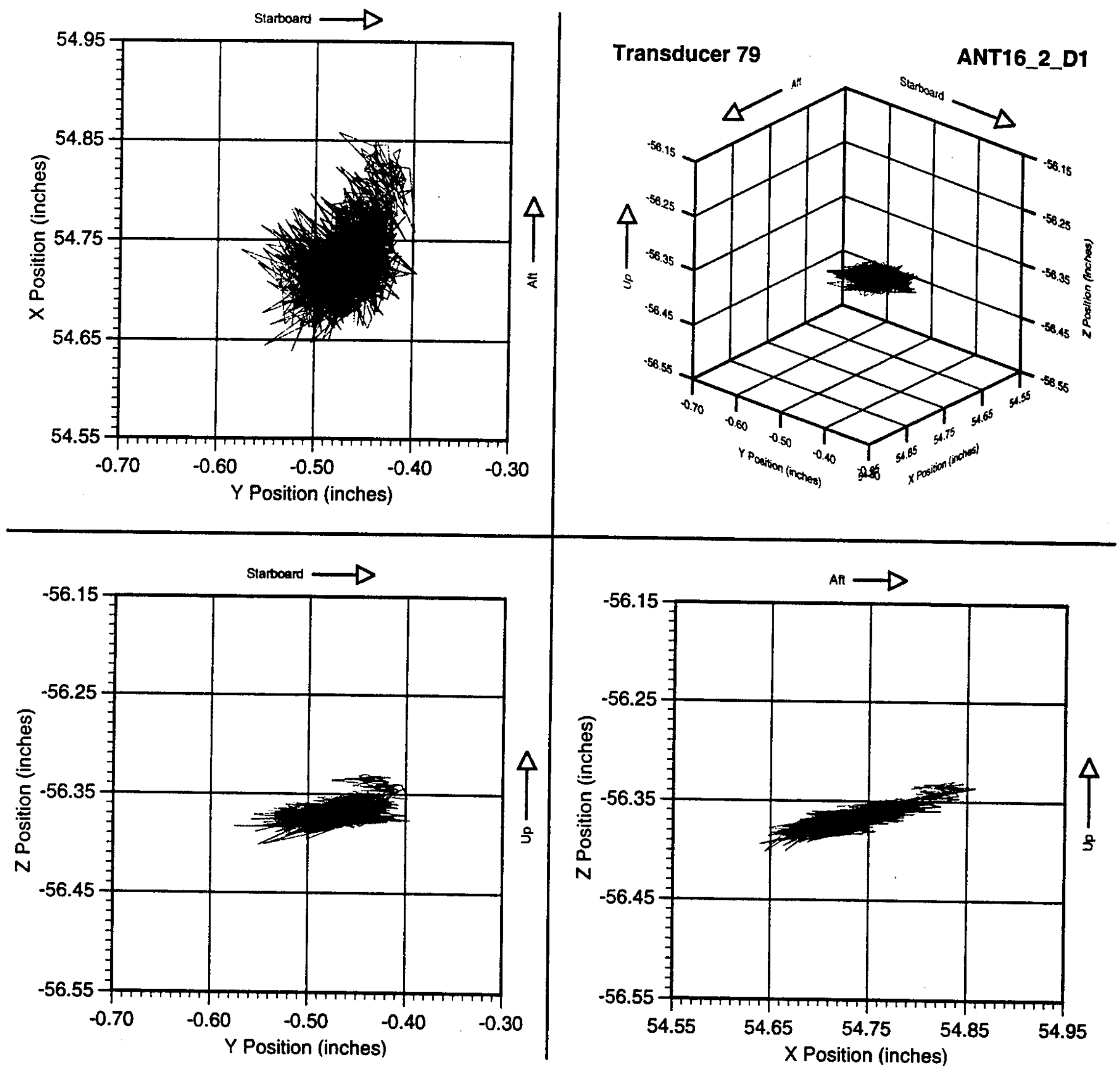
Transducer 79
ANT16_2_D1
Starboard
Aft
Up
X Position (inches)
Y Position (inches)
Z Position (inches)
54.95
54.85
54.75
54.65
54.55
-0.70
-0.60
-0.50
-0.40
-0.30
-56.15
-56.25
-56.35
-56.45
-56.55

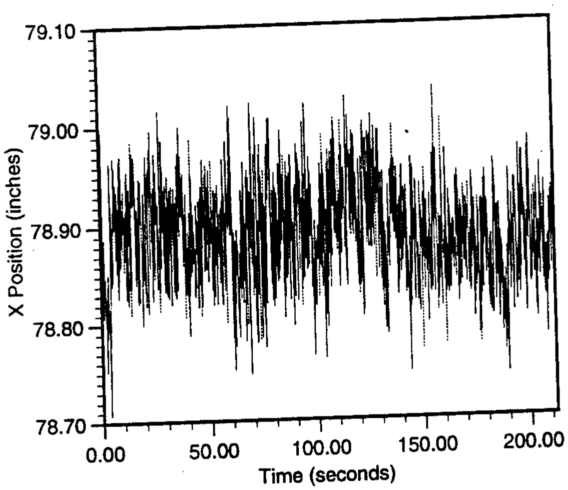

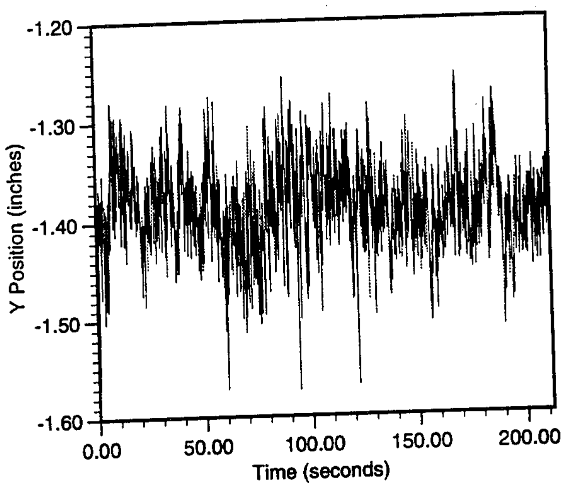

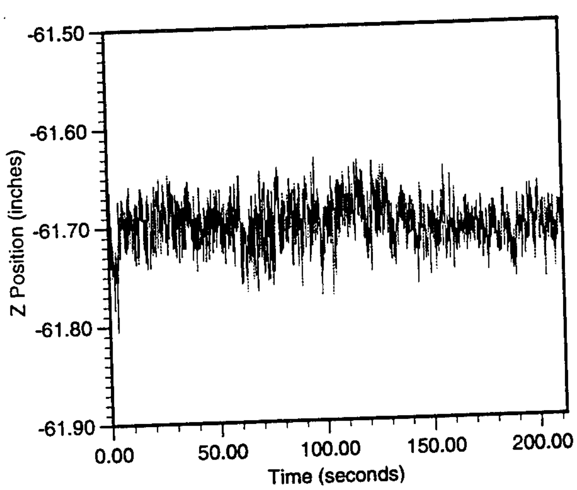

Data Run: ANT16_2_D1
Transducer: 83

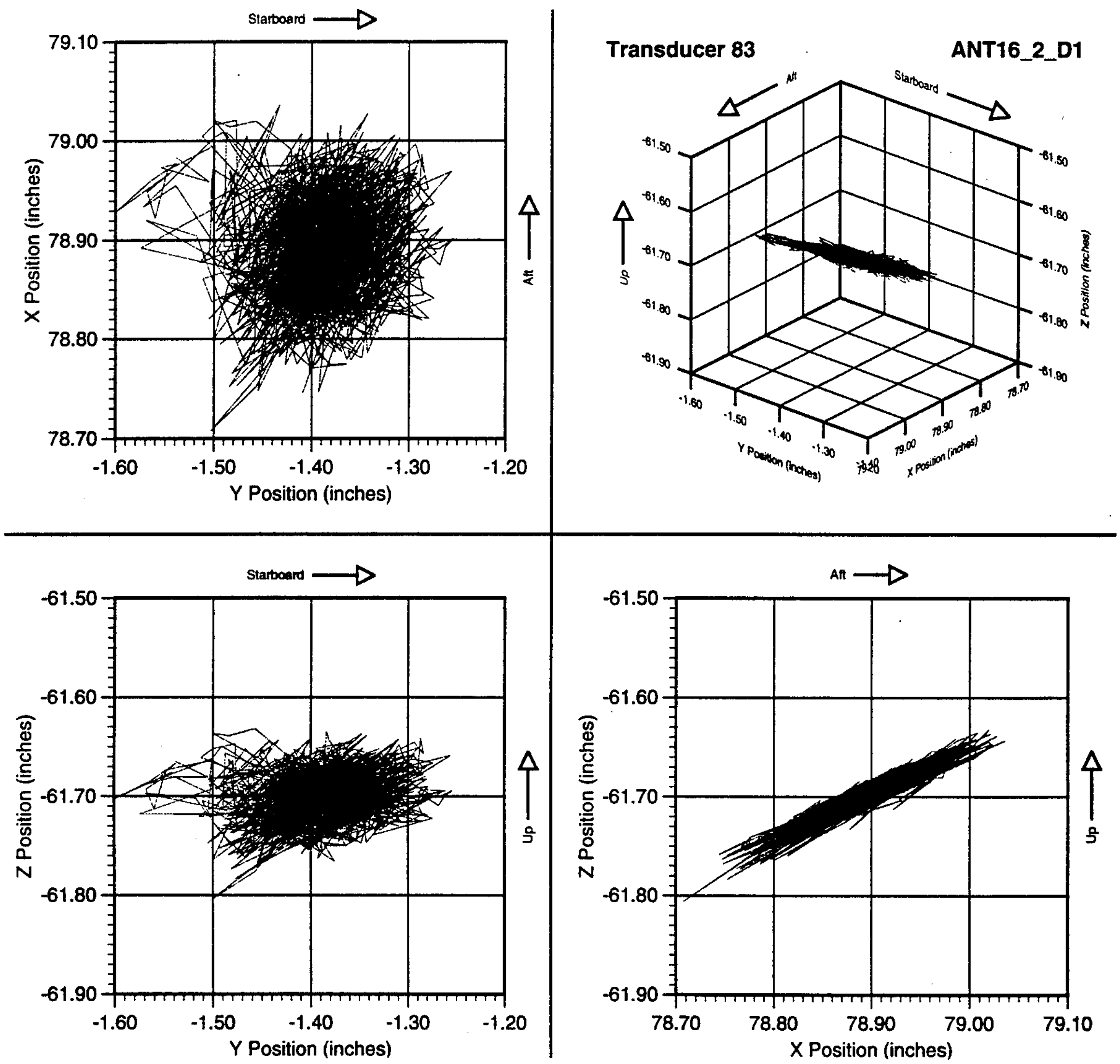
Transducer 83
ANT16_2_D1
Starboard
Aft
Up
X Position (inches)
Y Position (inches)
Z Position (inches)

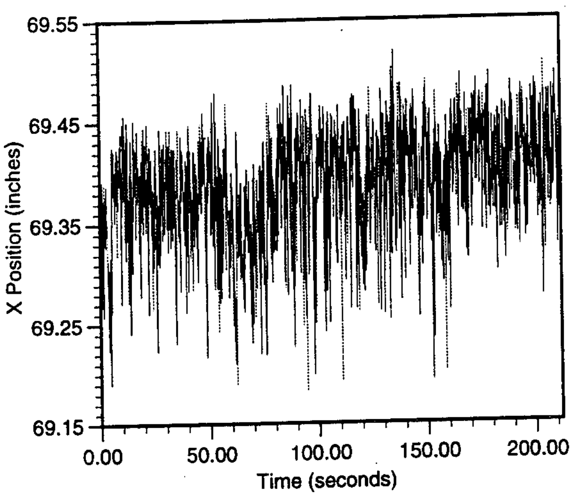

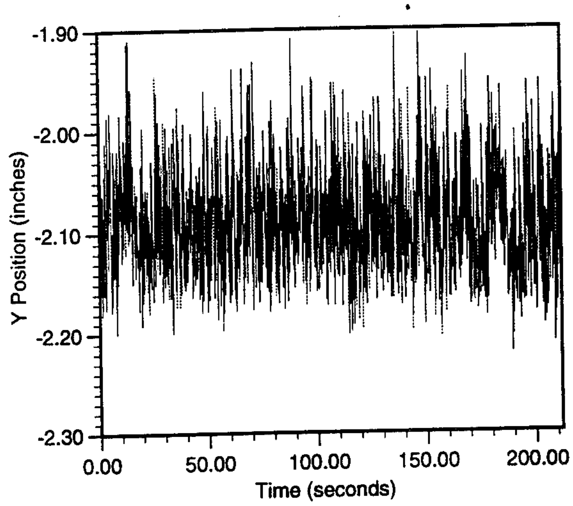

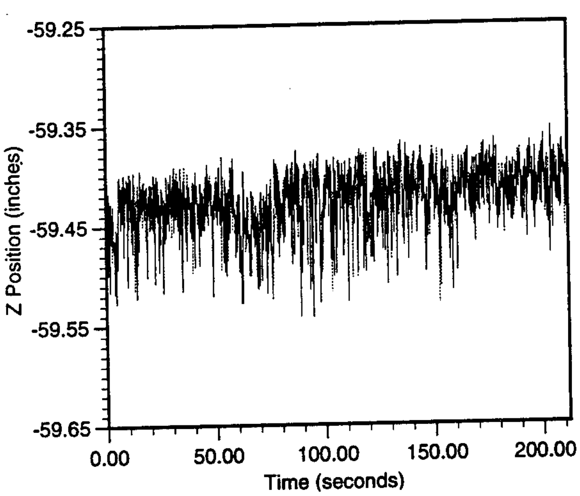

Data Run: ANT16_2_D1
Transducer: 86

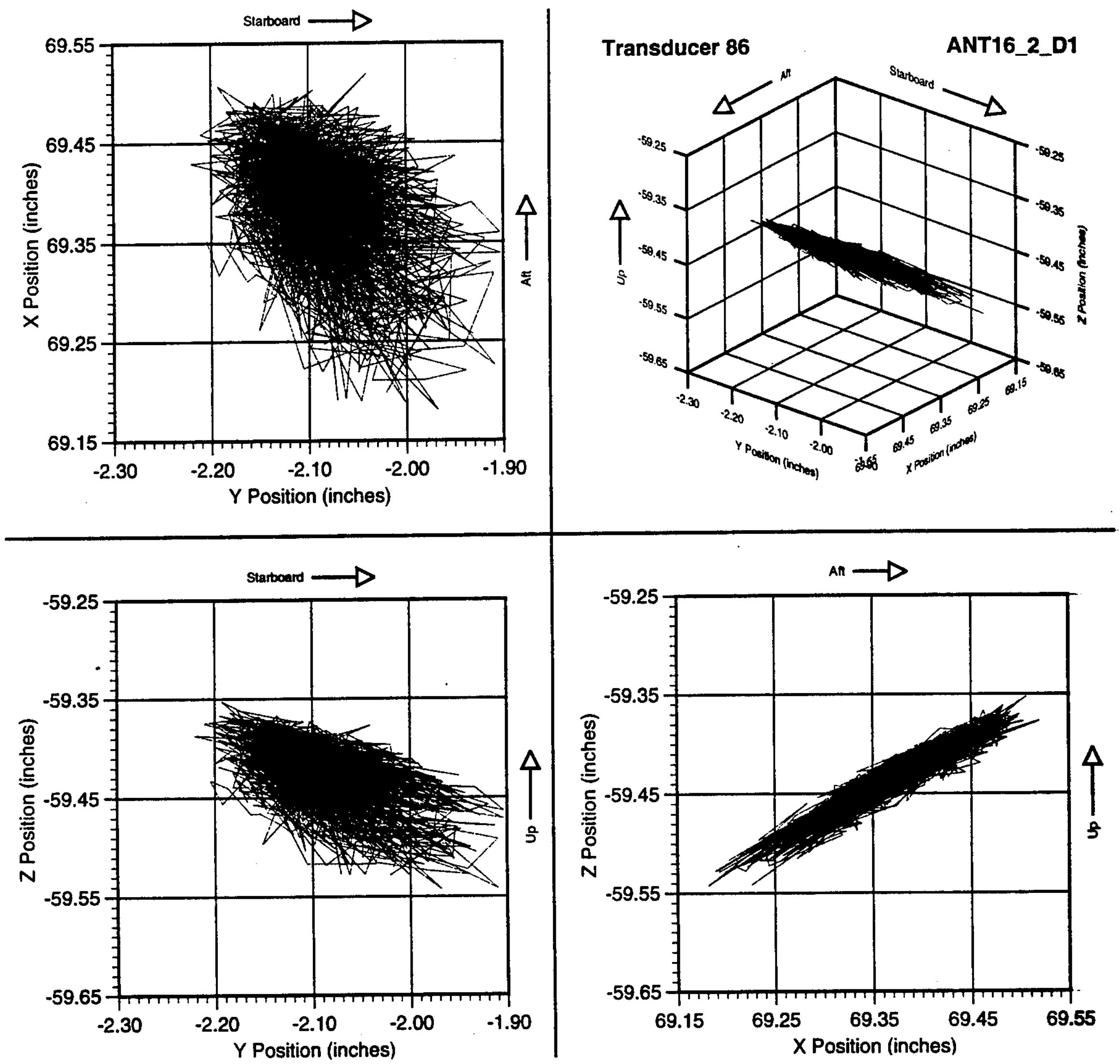
Starboard
69.55
69.45
69.35
69.25
69.15
X Position (inches)
Aft
-2.30
-2.20
-2.10
-2.00
-1.90
Y Position (inches)
Transducer 86
ANT16_2_D1
Aft
Starboard
Up
Z Position (inches)
Y Position (inches)
X Position (inches)
Starboard
-59.25
-59.35
-59.45
-59.55
-59.65
Z Position (inches)
Up
Aft
69.15
69.25
69.35
69.45
69.55
X Position (inches)

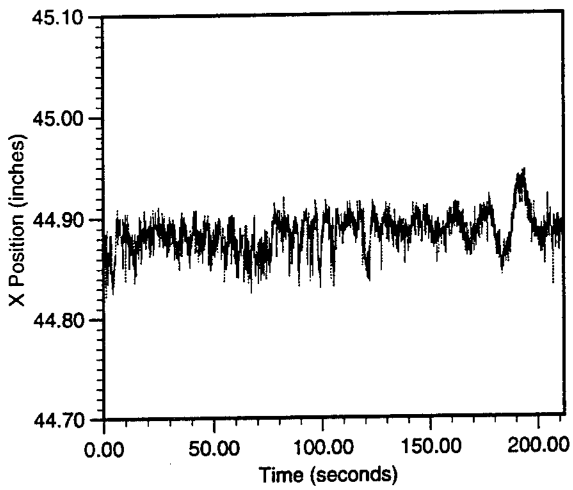

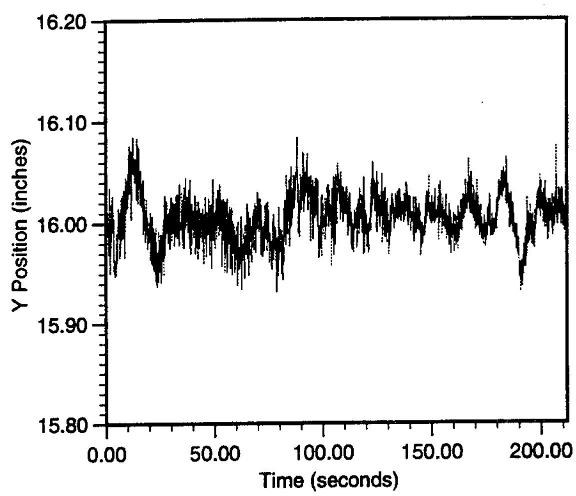

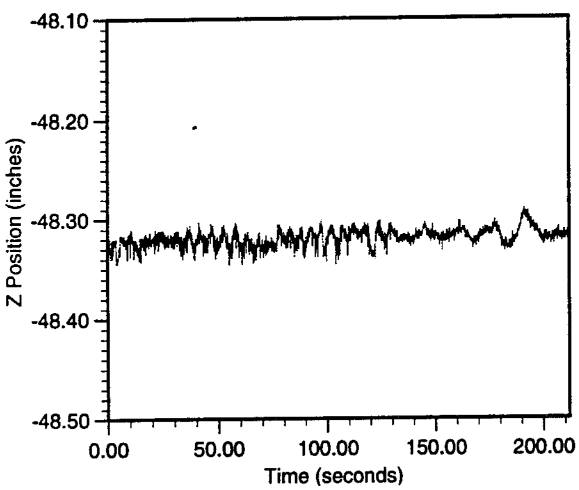

Data Run: ANT16_2_D1
Transducer: 92

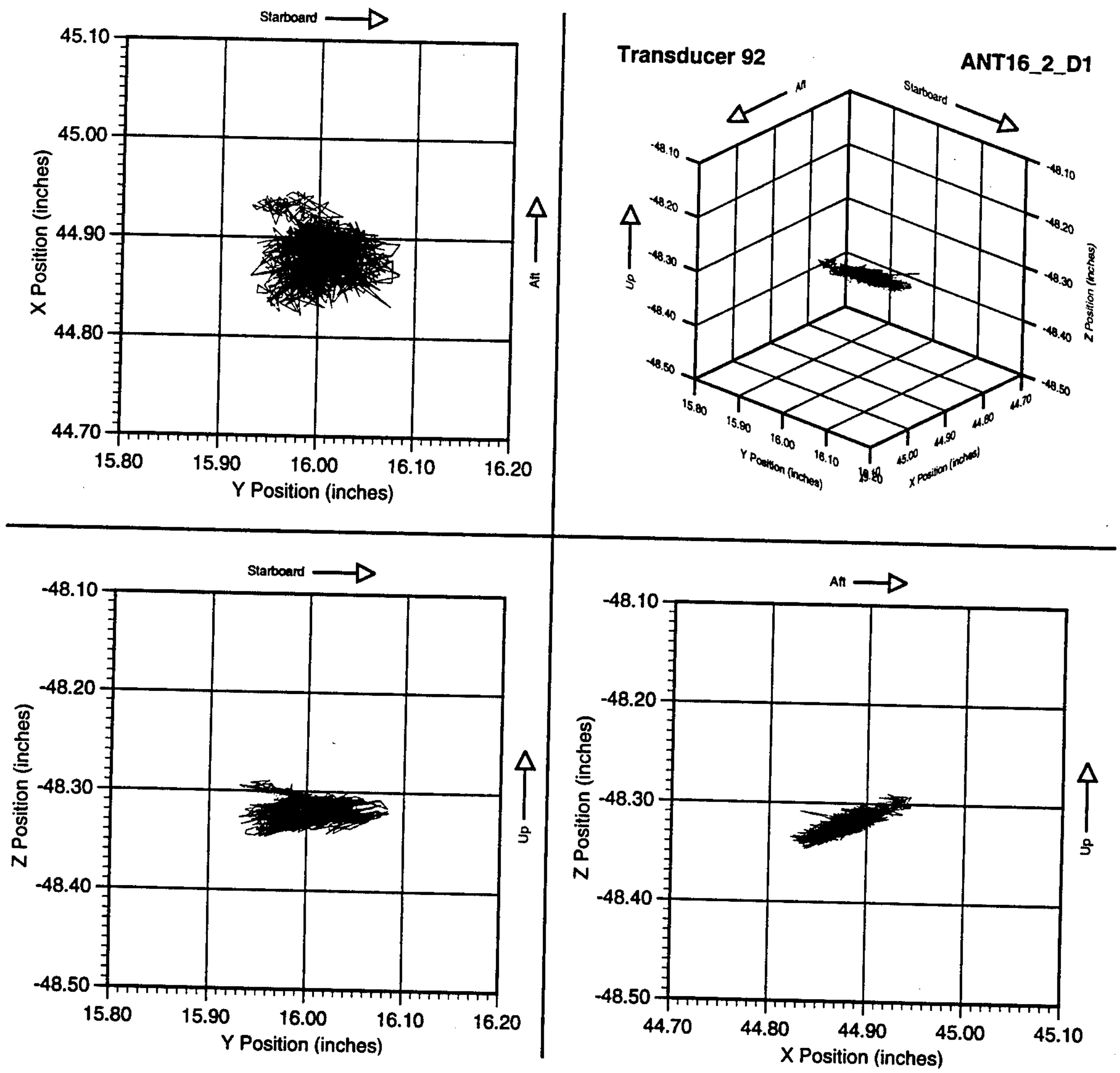
Transducer 92
ANT16_2_D1
Starboard
Aft
Up
X Position (inches)
Y Position (inches)
Z Position (inches)
45.10
45.00
44.90
44.80
44.70
15.80
15.90
16.00
16.10
16.20
-48.10
-48.20
-48.30
-48.40
-48.50

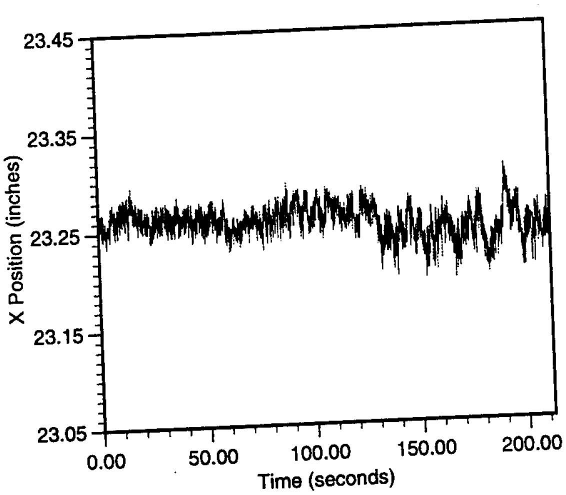

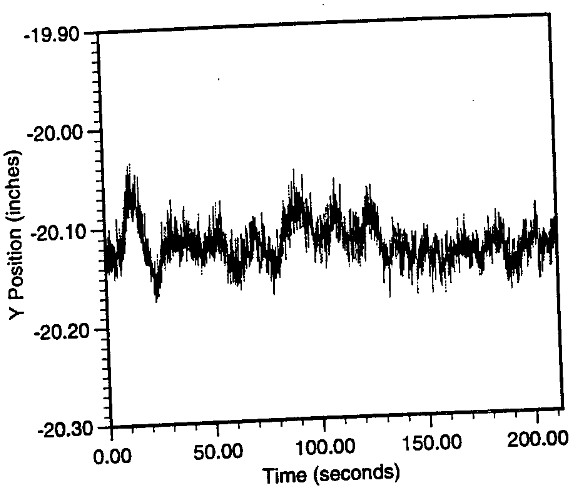

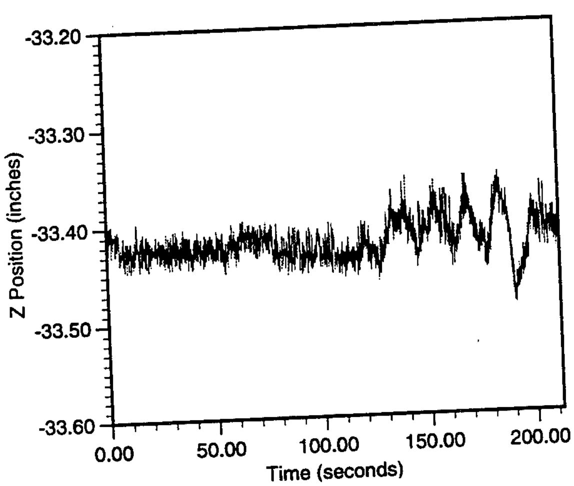

Data Run: ANT16_2_D1
Transducer: 108

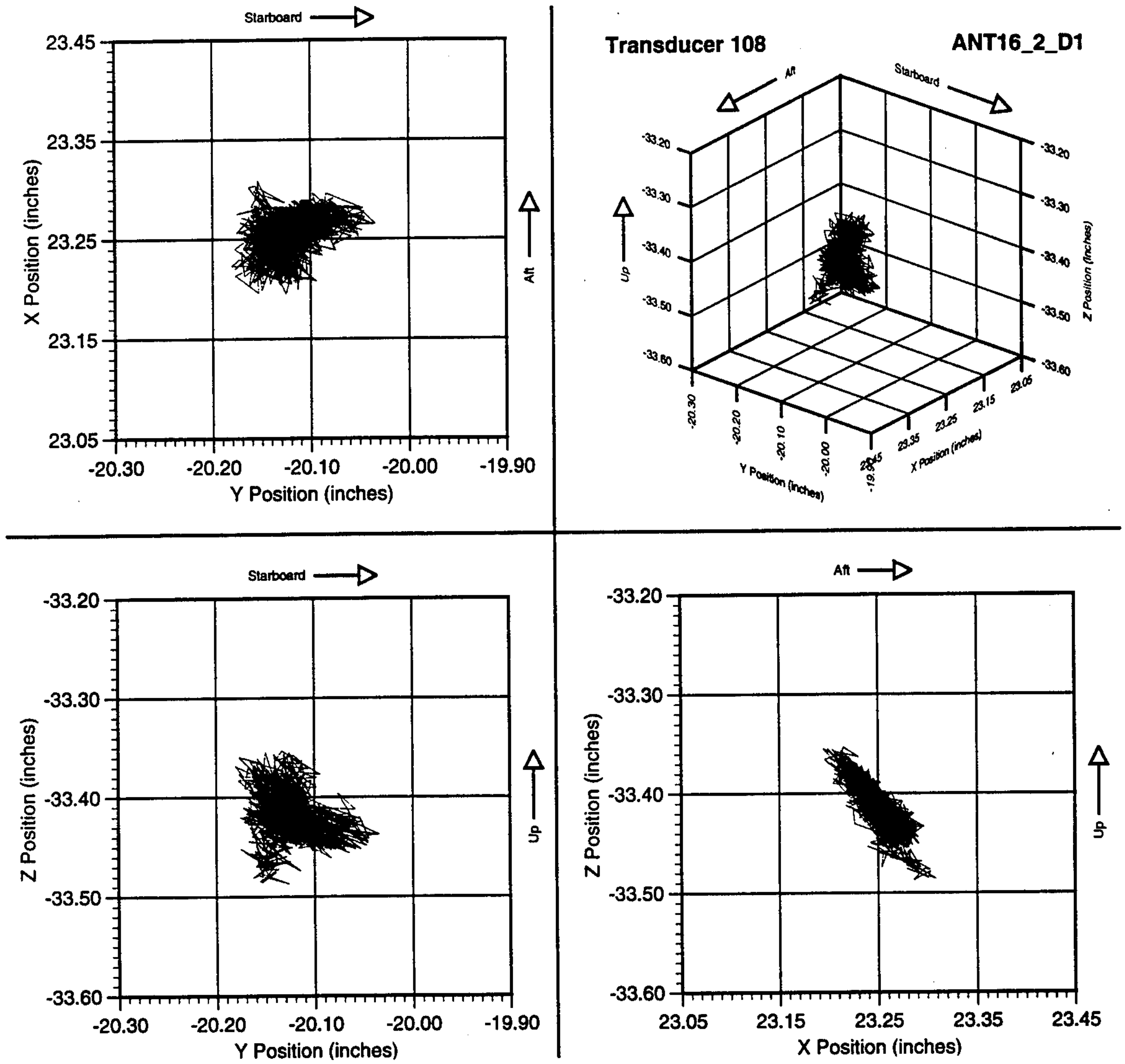
Transducer 108
ANT16_2_D1
Starboard
Aft
Up
X Position (inches)
Y Position (inches)
Z Position (inches)
23.45
23.35
23.25
23.15
23.05
-20.30
-20.20
-20.10
-20.00
-19.90
-33.20
-33.30
-33.40
-33.50
-33.60

Appendix E: Correlation Analysis

E.1 Description

As the pervasiveness of the offset anomalies in the Antigua sea test data became more apparent with continued processing, the prospect of using pitch data from the USS Kauffman to predict vertical displacement in the SRD was investigated. It was intuitively determined that if pitch data could be correlated to existing vertical displacement (Z-axis) data, then a prediction would be possible.

A *graphical* analysis was performed on two data runs. The first analysis was performed on data run ANT16_2_D1 (see Figure E–1), over the time segment used in the UW/APL–NRL comparison. The pitch and Z-axis deflections recorded were quite small. The graphical analysis revealed very little correlation between pitch and the Z-axis data, for the *low* sea state of this data run.

In Figure E–1, the Z-axis data is represented in orange or gray. The orange records correspond to Z-axis records that exhibit *some* correlation with other Z-axis records. The gray records correspond to records that exhibit what appears to be random characteristics.

The second *graphical* analysis was performed on data run CFA2_27D1 (see Figure E–2 & E–3). The sea state was approximately 4 and the ship speed was 4-5 knots. We evaluated an 11.5 second time window that features a large displacement in the data run.This data run showed <u>definite correlation</u> between the pitch and several Z-axis records.

With the promising appearance of this second dataset, a spreadsheet *correlation* analysis was performed. This analysis used a discrete Fourier transform to derive a dominant reference frequency from the pitch data. The amplitude ($\mathbf{A}_p$) and phase (ϕ_p) coefficients from the transform were used to generate an ideal sinusoidal function at the dominant pitch frequency, which was then fit to existing Z-axis deflection data.

The output from the spreadsheet is a linear correlation coefficient (**r**) which specifies the quality of the sinusoidal curve fit. The values of **r** range from 0.0 (no confidence) to 1.0 (high confidence). The output from the spreadsheet also produces a phase angle ($\phi_\mathbf{r}$) which represents the phase difference between the Z-axis deflection and the pitch stimulus.

The spreadsheet correlation analysis is summarized in the legend of Figure E–2. When interpreting the values of **r**, it should be noted that values greater than 0.71 indicate that at least 50% of the random variations in the data records are accounted for in the pitch curve fit. In other words, $\mathbf{r}^2$ represents the percentage of the RMS variations in the data which are accounted for in the correlation process.

In Figure E-2, the Z-axis data is represented in red or gray. The thin-red records correspond to Z-axis records that have a correlation coefficient (**r**) greater than 0.5. The bold-red records correspond to Z-axis records where **r** is greater than 0.71. The gray records correspond to records that have low correlation values. These are records where most of the variation is not correlated.

Figure E–3 demonstrates the relationships of four locations on the SRD and the relationship of the Z-axis acceleration, with pitch. It can be seen from this figure that locations 82, 87 and 106 move upward when pitch indicates downward movement of the bow. Location 70 behaves in an opposite manner implying that the forward part of the SRD moves outward when the bow moves downward.

It should also be noted that this analysis only covers the dynamic component of the data. Any static offsets that may have been present in the data have been subtracted prior to analysis or graphing.

In conclusion, it can be seen from the attached figures that at high sea state and low ship speed, there is a *significant* correspondence between pitch and Z-axis movement in the SRD. When the sea state is low, other factors, such as ship speed, play a larger role in defining vertical movement in the SRD.

E.2 Correlation Analysis Supplement

The discrete Fourier transform is defined as

$$X(f) = T\sum x(t)\, e^{-j\omega t}$$

Where $\omega = 2\pi f_p$

and $T = \Delta t$ (the sample rate)

Using the Euler identity the discrete Fourier transform can be expressed as

$$X(k) = \underbrace{T\left[\frac{\sum x(t)\cos(\omega\{t_i - t_0\})}{n}\right]}_{\text{real}} + \underbrace{jT\left[\frac{\sum x(t)\sin(\omega\{t_i - t_0\})}{n}\right]}_{\text{imaginary}}$$

X(k) can be defined in polar coordinates in terms of an amplitude (A_p) and a phase (ϕ_p).

$$A_p = \sqrt{(\text{real})^2 + (\text{imaginary})^2}$$

$$\phi_p = \operatorname{atan}\left[\frac{\text{imaginary}}{\text{real}}\right]$$

These coefficients are used to develop an estimated sinusoidal function based on the dominant frequency of *pitch* (f_p)

$$X_{est}(t) = bA_p \sin(\omega\{t_i - t_0\} + \phi_p)$$

Where ***b*** is a parameter related to actual spectrum width. We assigned ***b*** a value of 2 for this analysis. The linear correlation coefficient (***r***) is determined from ***X(t)*** and ***X_{est}(t)***

$$r = \sqrt{1 - \frac{\sum (X - X_{est})^2}{\sum X^2}}$$

Fig. E–1 Vertical Deflection Comparison with Pitch and Vertical Acceleration

Data Run ANT16_2_D1 (Time 7.47-28.09 Seconds)
Sea State: 1; Speed: 18-20

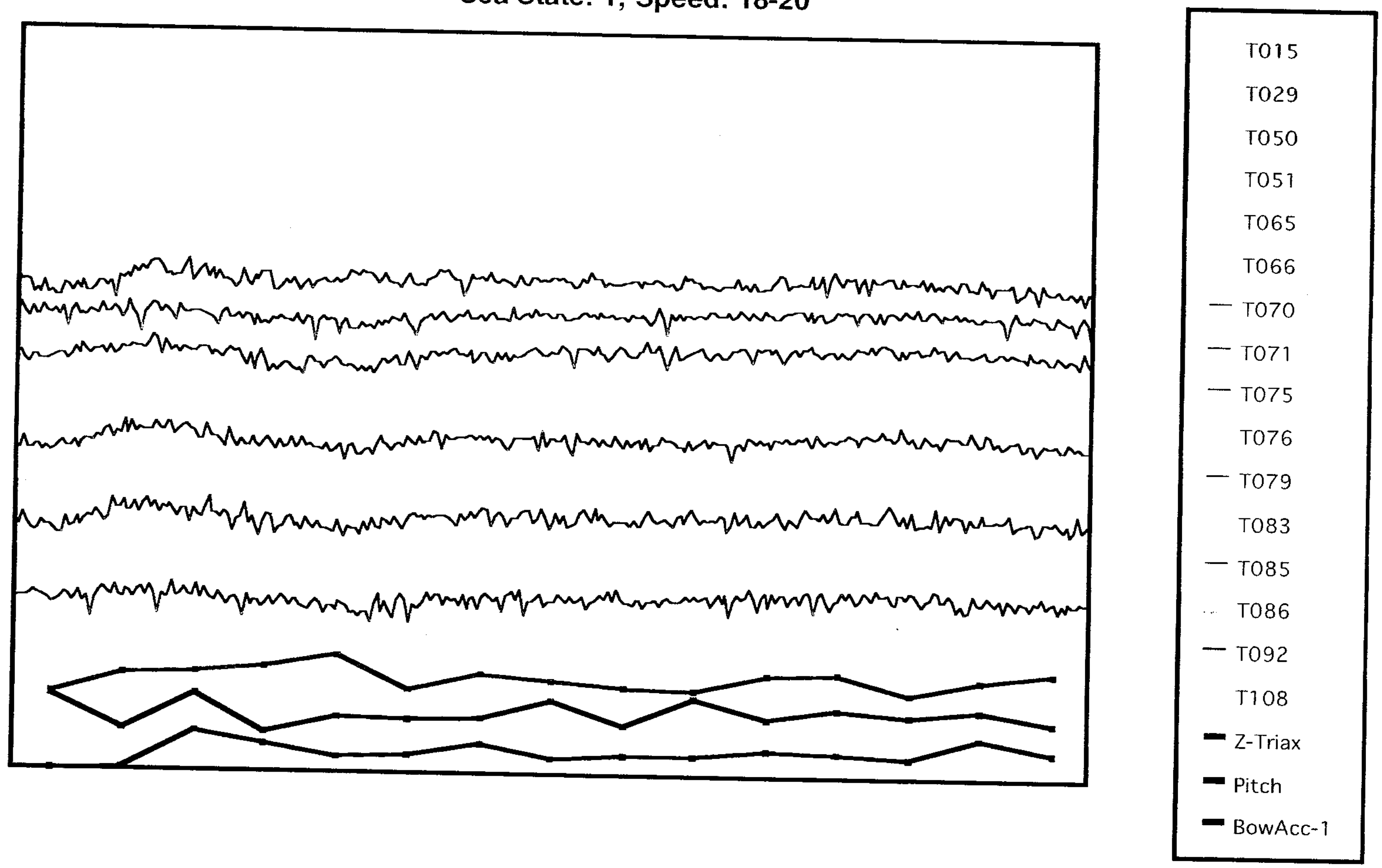

Fig. E–2 Vertical Deflection Comparison with Pitch and Vertical Acceleration

Data Run CFA2_27D1 (Time 124.97-136.64 Seconds)
Sea State 4; Speed 4 kts

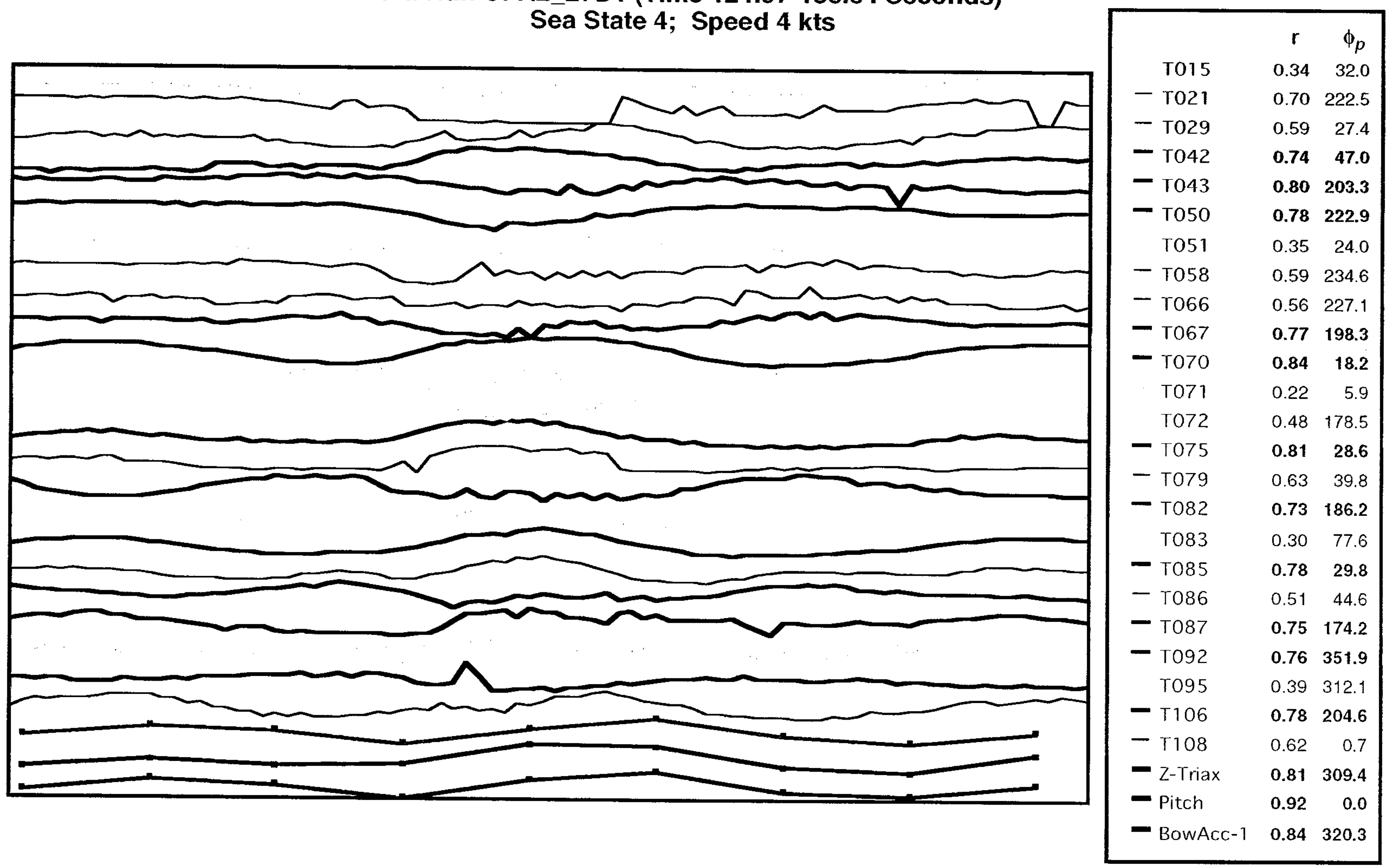

Fig. E–3 Comparisons with Pitch
CFA2_27D1

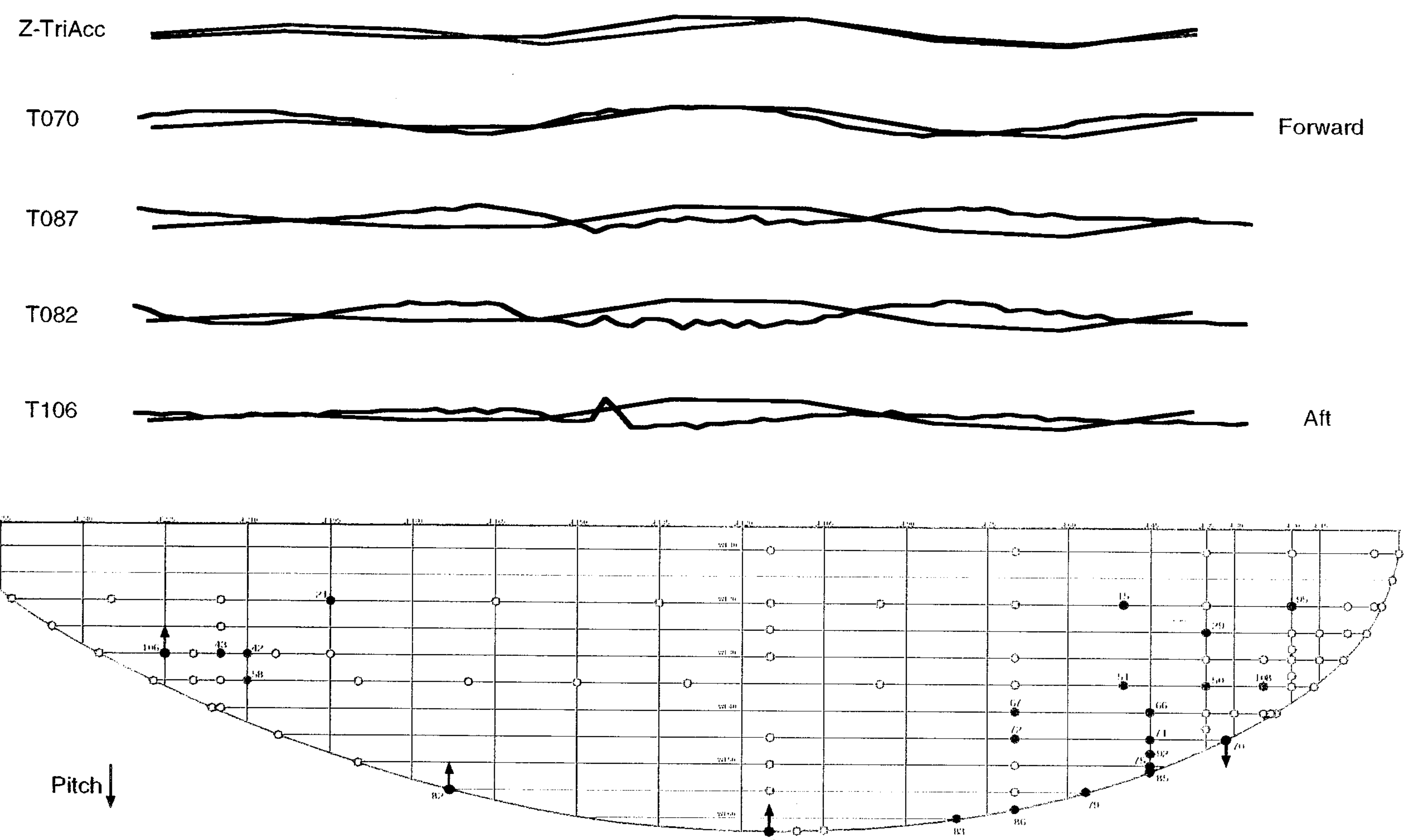

Appendix F: Distance Determination and Coordinate Transformation Algorithms

F.4 Introduction

Each time a transducer on the dome inner surface is electrically driven, the data recorded consists of four acoustic time-of-flight values from the driver transducer to the four hydrophones of a given receiver group. If the speed of sound in the intervening fluid, **c**, is known, then these time-of-flight values can be converted into distances $\mathbf{r_i}$ (for i=1 to 4) such that

$$\mathbf{r_i = c\, t_i}$$

These four distances are used in four groups of three to calculate four different sets of 3-dimensional x,y,z coordinates for the hydrophone. These four sets of coordinate values can then be averaged together for a more exact position determination.

F.5 Distance Determination Algorithm

Any three receiver hydrophones can be considered to form a plane in space and a local coordinate system can be setup (see section F.3) such that the coordinates of these receivers (as shown in figure F-1) are:

$$(0,0,0),\ (\mathbf{a},0,0),\ \text{and}\ (\mathbf{b},\mathbf{c},0)$$

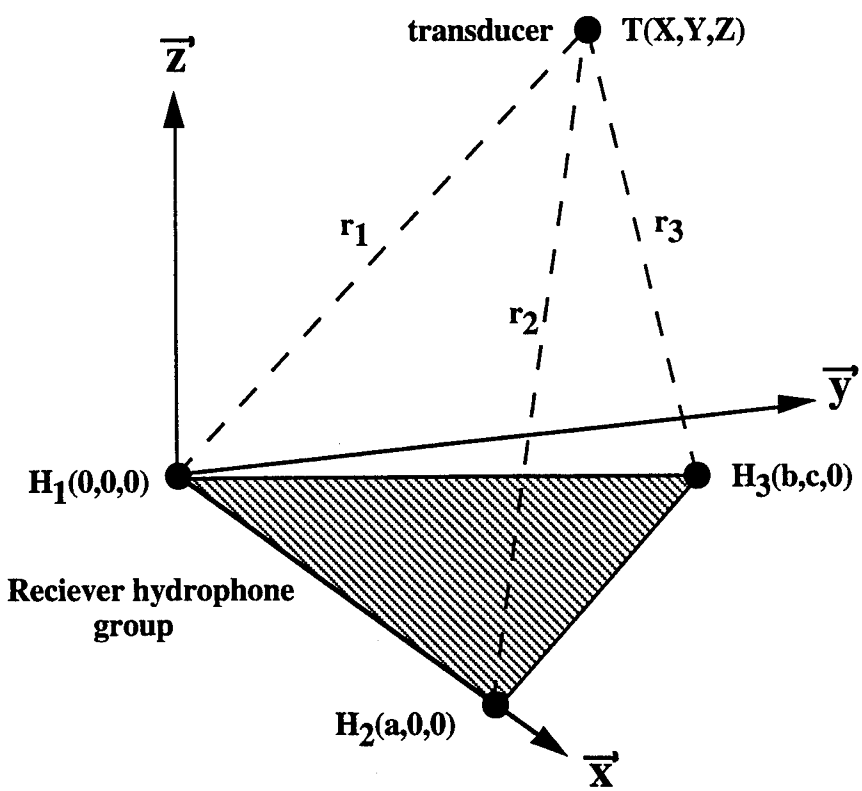

Figure F-1. Distance Determination Algorithm Relationships

Then, by geometry, the position coordinates, (**X,Y,Z**), of any transducer can be determined using the measured time-of-flight values by:

$$\mathbf{X} = \frac{\mathbf{r}_1^2 - \mathbf{r}_2^2 + \mathbf{a}^2}{2\mathbf{a}}$$

$$\mathbf{Y} = \frac{1}{2\mathbf{c}}\left[\mathbf{r}_1^2(1-\frac{\mathbf{b}}{\mathbf{a}})+\mathbf{r}_2^2(\frac{\mathbf{b}}{\mathbf{a}})-\mathbf{r}_3^2+\mathbf{b}^2+\mathbf{c}^2-\mathbf{ab}\right]$$

$$\mathbf{Z} = \sqrt{\mathbf{r}_1^2 - \left(\mathbf{X}^2+\mathbf{Y}^2\right)}$$

F.6 Coordinate Transformation Algorithm

In the SRD case, we have a global coordinate system centered at the top forward center of the dome and oriented along the ship's axis. The positions of all of the receiver hydrophones were measured with respect to this global coordinate system in dry-dock. For a given group of three receivers, let these global coordinate values be

$$\mathbf{H}_1(\mathbf{x}_1^{(0)},\mathbf{y}_1^{(0)},\mathbf{z}_1^{(0)}),\quad \mathbf{H}_2(\mathbf{x}_2^{(0)},\mathbf{y}_2^{(0)},\mathbf{z}_2^{(0)}),\quad \mathbf{H}_3(\mathbf{x}_3^{(0)},\mathbf{y}_3^{(0)},\mathbf{z}_3^{(0)}).$$

We perform a vector translation, shifting the origin of the coordinate system to the point of the first receiver hydrophone, by a vector subtraction of H_1 from all three position vectors. This gives

$$\mathbf{H}_1^{(1)}(0,0,0),\quad \mathbf{H}_2^{(1)}(\mathbf{x}_2^{(1)},\mathbf{y}_2^{(1)},\mathbf{z}_2^{(1)}),\quad \mathbf{H}_3^{(1)}(\mathbf{x}_3^{(1)},\mathbf{y}_3^{(1)},\mathbf{z}_3^{(1)}).$$

where, for example $\mathbf{x}_2^{(1)} = \mathbf{x}_2^{(0)} - \mathbf{x}_1^{(0)}$, $\mathbf{y}_2^{(1)} = \mathbf{y}_2^{(0)} - \mathbf{y}_1^{(0)}$, etc.

A rotation about the $\mathbf{z}^{(1)}$ axis, as shown in figure F-2, is then performed using the transformation matrix

$$\mathbf{A}_{2,\mathbf{z}} = \begin{pmatrix} \cos\varphi_2 & \sin\varphi_2 & 0 \\ -\sin\varphi_2 & \cos\varphi_2 & 0 \\ 0 & 0 & 1 \end{pmatrix}$$

where $\cos\varphi_2 = \frac{x_2^{(1)}}{A_2}$, $\sin\varphi_2 = \frac{y_2^{(1)}}{A_2}$, and $A_2 = \sqrt{x_2^{(1)2} + y_2^{(1)2}}$.

This results in the new coordinates being:

$$\mathbf{H}_1^{(2)}(0,0,0), \quad \mathbf{H}_2^{(2)}(A_2,0,\mathbf{z}_2^{(1)})$$

$$H_3^{(2)}\left(\frac{x_2^{(1)}x_3^{(1)}+y_2^{(1)}y_3^{(1)}}{A_2}, \frac{x_2^{(1)}y_3^{(1)}-x_3^{(1)}y_2^{(1)}}{A_2}, z_3^{(1)}\right)$$

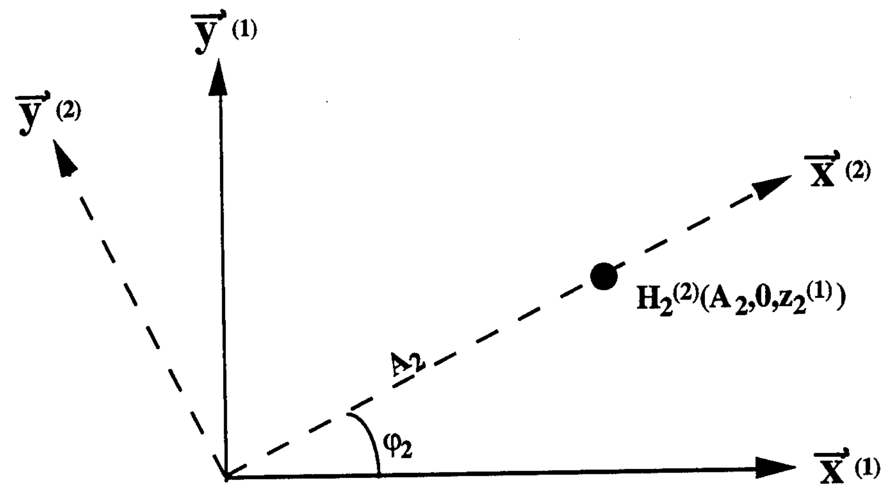

Figure F-2. Rotation About the z Axis.

A second rotation, this time about the $y^{(2)}$ axis, is then done. This matrix is

$$A_{3,y} = \begin{pmatrix} \cos\theta_3 & 0 & \sin\theta_3 \\ 0 & 1 & 0 \\ -\sin\theta_3 & 0 & \cos\theta_3 \end{pmatrix}$$

where $\cos\theta_3 = \frac{x_2^{(2)}}{A_3}$, $\sin\theta_3 = \frac{z_2^{(2)}}{A_3}$, and $A_3 = \sqrt{(x_2^{(2)})^2+(y_2^{(2)})^2+(z_2^{(2)})^2}$. Since

$x_2^{(2)} = A_2$, $y_2^{(2)} = 0$, and $z_2^{(2)} = z_2^{(1)}$, we also have $A_3 = \sqrt{(x_2^{(1)})^2+(y_2^{(1)})^2+(z_2^{(1)})^2}$

Hence, for clarity, we will drop the parenthetical indices on the x, y, and z's whenever they refer to the first (1) system. The coordinates after this second rotation can be shown to have the form:

$$H_1^{(3)}(0,0,0), \quad H_2^{(3)}(A_2,0,0), \text{ and}$$

$$H_3^{(3)}\left(\frac{x_2x_3+y_2y_3+z_2z_3}{A_3}, \frac{x_2y_3-x_3y_2}{A_2}, \frac{A_2^2z_3-(x_2x_3+y_2y_3)z_2}{A_2A_3}\right)$$

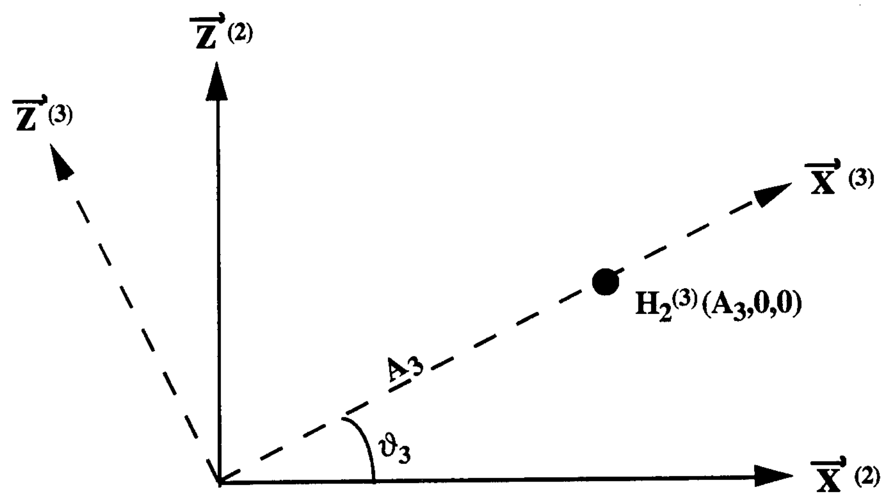

Figure F-3. Rotation About the $y^{(2)}$ Axis.

Finally, we perform another rotation about the $x^{(3)}$ axis having the matrix form:

$$A_{4,x} = \begin{pmatrix} 1 & 0 & 0 \\ 0 & \cos\delta_4 & \sin\delta_4 \\ 0 & -\sin\delta_4 & \cos\delta_4 \end{pmatrix}$$

where $\cos\delta_4 = \frac{y_3^{(3)}}{C_4}$, $\sin\delta_4 = \frac{z_3^{(3)}}{C_4}$, and $C_4^2 = \left(y_3^{(3)2}+z_3^{(3)2}\right)$. This gives us the coordinates

$$H_1(0,0,0)$$

$$H_2(A_3,0,0)$$

$$H_3\left(\frac{x_2x_3+y_2y_3+z_2z_3}{A_3}, C_4, 0\right)$$

as seen in the figure below.

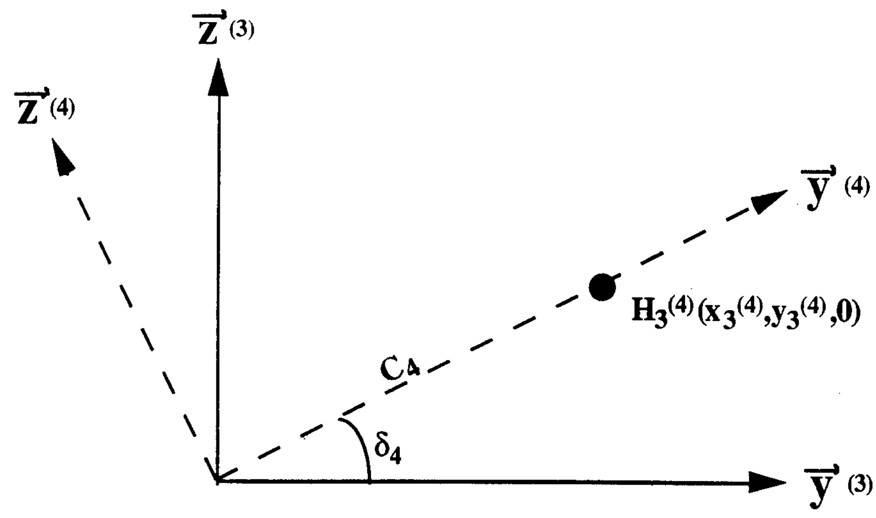

Figure F-4. Rotation About the $x^{(3)}$ Axis.

These are now in the correct coordinate system to use the distance determination algorithm above. Thus to transform into the local correct coordinate system we need to perform a vector translation followed by three rotations

$$\vec{r}' = A_{4,x}A_{3,y}A_{2,z}\vec{r}$$

But, once we have the transducer position in the local coordinate system, we want to transform them back into our global coordinate system to relate them to the positions of all of the other transducers. To do this we invert the matrices and multiply in reverse order

$$\vec{r} = A_{2,z}^{-1}\left(A_{3,y}^{-1}\left(A_{4,x}^{-1}\vec{r}'\right)\right)$$

followed by the vector translation of opposite sign than before.

F.7 Summary

The computer program inputs the receiver hydrophone positions as measured in dry-dock and the groomed time-of-flight readings obtained at sea. For each subgroup of 3 receivers in each of the 10 four hydrophone receiver groups the program calculates all of the above vector translations and rotation matrices and their inverses. Then, in the scan pattern file associated with each data set the program is informed which receiver array was used to record the time-of-flight data for each transducer in the data run. Using the above algorithms the 3 dimensional displacement of each transducer is calculated in the global coordinate system of the SRD.

Appendix G: Failure Mechanism Likelihood Analysis

G.1 Introduction

During the Antigua trial of the Sonar Dome Acoustic Deflection Measurement System, the system behaved in an anomalous manner and much of the data collected was degraded by noise. Following this test, an in-house study was conducted to determine the single most likely or most important cause of the system failure, and to identify all potential contributors to the observed system anomalies.

The following documents the results of this study. It includes system design and procedure alterations and guidelines which will be implemented in future system deployments to ensure in-so-far as possible that a similar failure cannot reoccur.

G.2 Potential Candidate Ratings

Table G-1 presents the results of our post-trial analysis. It lists each mechanism suggested as a potential candidate which might conceivably be responsible for the failures encountered. The likelihood that each might be responsible was evaluated (often subjectively) using the criteria described below, and a relative rating was assigned in four key categories. From these a total was calculated for each candidate, and a relative final rating was obtained by (somewhat arbitrarily) subtracting 8 from this total.

Candidates with a total rating of zero or less are considered highly unlikely, and need not be considered further in this analysis. The bases of the rating factors for candidates with final ratings greater than zero are discussed later in this section.

G.3 Description of the Rating Factors.

The guidelines used in assigning the above ratings are as follows:

- **Observed Precondition:** This score relates to the direct observation of any physical pre–existing conditions related to the potential occurrence of the failure mode. The score ranges from 0, if there was no direct observation of the physical conditions needed, to a score of 5 if the required pre-existing condition was observed. Note that a score of 5 does not assure the failure mode occurred, but only that the pre-existing conditions required to enable the failure were known to be present.

TABLE G-1. Ratings Summary for the Potential Failure Candidate Mechanisms.

	Potential Candidate	Observed Precondition	Concerns re: Design	Consistency with Timing	Consistency with Mode	**(Total- 8)**
	Water Intrusion Due to:					
1	- module seals	0	2	2	5	**1**
2	- sandblasting re: connectors	5	3	2	3	**5**
3	- case corrosion	0	4	1	3	0
	Crosstalk Due to:					
4	- shared cables in cableways	5	2	2	4	**5**
5	- module design	0	1	1	3	(-3)
6	- ship EMI or power	3	2	2	3	**2**
	Mechanical Damage:					
7	- to modules during dome installation	0	2	1	2	(-3)
8	- to dome during deployment	0	0	3	2	(-3)
9	- to cables due to high sea conditions	0	1	3	2	(-2)
	Electrical Damage:					
10	- Burnout from ship operating sonar	5	1	3	2	**3**
11	- Burnout from ship power transients	5	0	2	0	(-1)
12	- Sand-blast contamination of controller hardware	5	1	1	1	0
	Combination Effects:					
	Items 2 and 4	5	4	4	5	**10**
	Items 2 and 6	4	3	4	5	**8**

- **Concerns re: design:** Post-test analysis of the system design with the objective of locating deficiencies has resulted in identifying a number of areas for potential design improvement. The score in this category reflects the relative likelihood that a deficiency in the system or component design, in conjunction with other events and conditions, could potentially lead to the type of failure candidate. A score of 5 indicates the known presence of a design defect which could account for the type of candidate condition described under certain conceivable conditions, while a score of 0 indicates our inability to find any system design feature which could contribute to the candidate occurrence. Note that a score of 5 does not assure the failure mode occurred, but only that a system design feature could potentially result in the occurrence of the failure type if other enabling conditions were present.
- **Consistency with failure timing:** Following a substantial period of satisfactory system operation, the observed failure events occurred rather suddenly and sporadically. The dates and observations are as shown in Table G-2.

TABLE G-2. Observation Log

Date	Location	Acoustic - System Status
Aug. 91 - Jan. 92	CBD full system tests	Fully functioning
May	BFG driver installation	-----
Sept.	Installation on USS Kauffman / Portland Maine	Fully functioning
Oct. 21-22	Shakedown Cruise	Fully functioning; minor adjustment to trigger gain settings needed.
Nov. 4-6	Pierside tests	Major degradation noted: • trigger gain levels off • 4 star modules inactive • DC offsets on signal lines
Nov. 14 - 15	Diagnostic pierside	Initially fully operational. Then degradation progressively reoccurred. (Subset of 32 still operating)
Nov. 16 - 25	Sea Trial	65 locations initially usable, but further progressive degradation during the trial.

The degradation tended to coincide with ship deployment (or immediate preparations for ship deployment) for the Antigua run, but was not observed in the previous Maine Shakedown run. The rating in this category reflects the relative likelihood that the candidate failure mode would occur with this type of timing. For example, a candidate which requires simultaneous catastrophic failures of multiple independent items to produce this timing history would be rated 0, while one which emphasizes a single event leading to the onset of sporadic behavior would be rated 5.

- **Consistency with failure mode:** As indicated in Table G-2, following shipboard installation, some of the triggering levels required adjustment. A few weeks later, prior to beginning the Antigua trial, the levels again required adjustment. This was followed by erratic triggering behavior of some modules, where the number of affected modules increased during the course of the trial. Some modules recovered for periods during the trial. Post analysis of the data strongly suggests well-defined triggering offsets, which would be stable for long periods before transitioning to a new level. The rating in this category reflects the likelihood that the failure candidate could mimic this observed behavior.

G.4 Description of the Candidates.

The candidates with positive final ratings are now discussed, and the intended corrective actions for future system deployments are presented.

- **1. Water intrusion due to module seals:** This candidate assumes failure of the O-ring seals used to close the module containers. A reconsideration of the seal design suggests that a better enclosure could have avoided this concern. Two factors weigh against the likelihood of this candidate. First, it is unlikely that all seals would have failed within the narrow time window observed. Such a failure mechanism is typically associated with a wide distribution of time-to-failures. Secondly, in previous submergence tests of these enclosures, there is no evidence of seal failure. These tests included 24 hr submergence at 60 psi pressure for all modules, and some long term submergence testing at lower pressures.

  While this candidate does not appear responsible for the data anomalies of the Antigua data set, precautionary measures will be taken in all future system designs to remove this issue from contention. These measures will include the use a more rugged enclosure with more robust seals.

- **2. Water intrusion due to sandblasting re: connectors:** This candidate follows from the fact that sandblasting and painting was occurring overhead during the dry–dock installation. Since the ship dry-dock schedule would not permit a suspension of these activities, we were forced to make do with a covering canopy which did not protect the system components from either the airborne grit or epoxy paint.

  This candidate is seen to have a high rating. This reflects our concern that the O-ring seals on the standard underwater electrical connectors have a high probability of having picked up grit, which would lead inevitably to a water path to the electrical leads, resulting in stray electrical coupling paths to all other radiating, or grounded equipment, operating on the ship. While by itself this candidate is not fully consistent with the timing, or mode of failures observed, it will be seen that in conjunction with items 4 or 6 nearly all rating factors are then quite high.

This candidate does appear to be an important contributor to the data anomalies observed. While future system designs will be modified to reduce the impact of contaminants, the most important improvement will be our conviction that system and component installation will not be attempted in the future unless the environment conditions are suitable to the limitations of the hardware.

- **3. Water intrusion due to case corrosion:** This candidate was proposed following the observation that a stainless steel mounting tab was used on the (anodized) aluminum enclosure. It was proposed that this use of dissimilar metals might lead to early failure due to electrolytic corrosion. This candidate is rated low for reasons similar to that of candidate 1. Submergence tests are currently underway to verify this.

  To avoid future concerns, future system designs will particularly avoid the use of dissimilar metals.

- **4. Crosstalk due to shared cables in the cable-ways:** This concern follows from the fact that while new cable-ways were supposed to be installed for our exclusive use, during system installation we encountered considerable resistance from SUPSHIP to install these cable-ways due to dry-dock time constraints. Hence our system cables shared existing cable-ways with other unshielded ship cables. This resulted in many of our cables running parallel and in close proximity to other shipboard cables. These shipboard cables are believed to be associated with the operation of the SQS–56 Sonar, and hence probably were carrying appreciable currents and dynamic signals. Such a condition is highly conducive to crosstalk.

  While this candidate is rated relatively high, by itself it cannot account for the timing of the failures. This candidate would be expected to contaminate the data primarily when the ship is under way. This is consistent with the data. However, since it did not appear on the Maine Shakedown cruise, the system design apparently included appropriate shielding and internal compensation to tolerate the levels of crosstalk present under the conditions of the Maine Shakedown cruise. Hence for this candidate to be a major concern, some new electrical coupling path must appear prior to the Antigua cruise, such as that of Candidate 2 above. Such a combination of events could certainly bypass the internal protections included in the electronic design and have symptoms fully consistent with the observed failure mode and timing.

- **5. Crosstalk due to module design:** This would include any inherent deficiency in the design of the electronic circuitry which would make it susceptible to internal crosstalk or signal coupling. We were unable to locate any such design weakness, and the negative final score indicates a very low probability that this is a contributor.

- **6. Crosstalk due to ship EMI or power:** This concern is similar to that of item 4. By itself, the electronics are judged sufficiently protected from such noise that this would not be an issue, as shown for example in the Maine Shakedown cruise. In conjunction with new electrical leakage paths, however, no electronic circuit can be said to be fully immune.

This candidate has a lower final score than Candidate 4 largely because the levels of induced noise would be expected to be much lower, and hence it would be more likely to be tolerated by the system.

- **7, 8, 9. Mechanical Damage:** This category is uniformly rated low. Upon post-test review, the mechanical design of the components is judged satisfactory to handle all normal ship environmental operating conditions. While unusual ship conditions such as running the dome into an obstruction might damage some components of the system, there were no such unusual occurrences reported by the crew. Minor mechanical failures would not account for the data failures observed.

- **10. Burnout from ship operating sonar in active mode:** The SQS–56 sonar system was frequently shifted to active mode without warning while our system was collecting data. This overpowered our system, and forced a quick manual shutdown on each occurrence While our electronics design includes some protection from large overvoltages, this candidate reflects the concern that the level of protection may not have been sufficient to handle the very large levels encountered. If such damage occurred, the most likely components include the pre–amplifiers and the on-board power supply regulators.

  This candidate is not rated particularly high. Additional clamps will be installed in future systems to remove this concern.

- **11. Burnout from ship power transients:** During the conduct of the tests, some significant fluctuations in the ship-supplied power were observed. The likelihood that these contributed to the system degradation are considered low, due largely to the fact that such fluctuations were anticipated and protections were included in the custom electronic circuitry and commercial equipment.

- **12. Sandblast contamination of controller hardware:** While in dry-dock, sandblasting accidentally occurred in the Sonar Equipment room, severely contaminating our rack-mounted electronics, including computer hardware and storage media. This is certainly a potential source of early equipment failure. However, the type of failures encountered and the results of the diagnostic tests performed in the control room all suggest that this event is not a major contributor to the problems encountered.

Appendix H: Environmental Data

H.1 Introduction

As was previously noted, the environmental data acquisition program, "SEAB7"[2], was not ready on the Maine Shakedown test. The time intervening between the Maine Shakedown and the Antigua trip, was intended for completing the environmental data acquisition software and for fine tuning the deflection measurement system's overall performance.

H.2 Background

When the environmental data acquisition software was ready for testing, FFG–59 was visited in Newport, R.I., on November 4–5, 1992. After energizing the deflection measurement system, it was gradually discovered that a significant degradation in system performance had occurred. This was typified by numerous driver transducer drop–outs and eventually the functional loss of four star modules. The evidence initially indicated that several star modules and/or perhaps a junction box may have become flooded. There was so much concern over pinpointing and correcting the problem that *all* available time was spent on this task rather than checking out the new environmental data acquisition software. Before leaving FFG–59 on November 5, intermittent functionality had been regained from the degraded modules. Since the evidence suggested that the intermittent functionality problem was associated with the electronics *sealed* in the SRD, there was no purpose in staying longer to correct the problem.

On November 14, a pre–Antigua departure checkout was performed on the deflection measurement equipment. All components were functioning nominally. On November 15, prior to the arrival of the sea test personnel, another equipment check revealed that the same components, discovered on November 4–5, had begun to function intermittently again.

After FFG–59's departure, sea test personnel tried exhaustively to collect data in spite of repeated equipment malfunctions. By this time, it had become a certainty that the equipment malfunctions were occurring due to water intrusion into components in the SRD. In many respects, this situation is very similar to the problems NASA has experienced with some of their unmanned exploration vehicles; the malfunctioning deflection measurement equipment was *sealed* in the SRD, and therefore wasn't accessible for repair. The Antigua sea test personnel did all that they could to acquire what data the deflection measurement equipment would functionally permit.

H.3 Post Processing

It wasn't until after the Antigua sea test that the environmental data received close scrutiny. It was then that it was discovered that the environmental sample rate was insufficient for adequate correlation to SRD deflection data. This occurred because the sampling rate of the environmental data acquisition software could not be *accurately* simulated during development in the laboratory. An attempt was made to simulate environmental data collection rates but since similar shipboard hardware was not available in the laboratory, this led to errors in estimating the proper sampling speeds.

The expectation was for the environmental sample rate to be equal to or at least half that of the deflection measurement sample rate. The actual environmental sample rate was between 10 to 15 times slower than the deflection measurement sample rate. This equated to one complete scan of the environmental inputs every 1.3 seconds. If the deflection measurement equipment had been performing properly up to and during the Antigua sea test, this flaw in the environmental data acquisition software would have been detected early and corrected.

When FFG–59 entered dry–dock in January of 1993, the SRD deflection measurement sea test personnel discovered that the starboard side wave height sensor had its electrical connections severed by the heavy seas that the ship had experienced. It was additionally discovered that the acoustic impedance matching foam that had been installed in the cylindrical apertures of both wave height sensors, had become dislodged and pushed up into the apertures, obstructing the acoustic transducers. For this reason, the wave height measurements were either sporadic or non–existent.

In June of 1993, after the Antigua environmental data files had been sent to the UW/APL for FEM evaluation, it was discovered that the pressure data from both pressure transducers was incoherent and was therefore suspected to be corrupted. A survey was conducted of all Antigua data runs, including two pierside runs, and it was noted that in almost every case, the range of pressures, from maximum to minimum, were between 5 and 6 PSI for pressure transducer 1, and 3 to 4 PSI for pressure transducer 2 (see Figure H–1). This wouldn't have caused much concern except that the pierside data runs showed the *same* pressure range as well. The pierside data runs should have exhibited a range difference of no more than 1 PSI.

It was also pointed out by Gordon Chartier of UW/APL that not only was there a 1.5 PSI difference between pressure transducers, after calibration corrections, but the pressure data records didn't correlate well with each other, or with any other environmental record (see Figures H–2 and H–3). There should have been no significant pressure differences between pressure transducers after calibration correction factors had been added. At this point, it became very likely that both pressure transducers had produced unreliable output.

The lack of reliable pressure input information to their FEM limited UW/APL to predicting SRD deflections based upon hydrodynamic loading, or ship speed inputs. This implied that UW/APL could only supply static deflection predictions based on ship speed. They would not be able to accurately predict dynamic deflections based upon sea state.

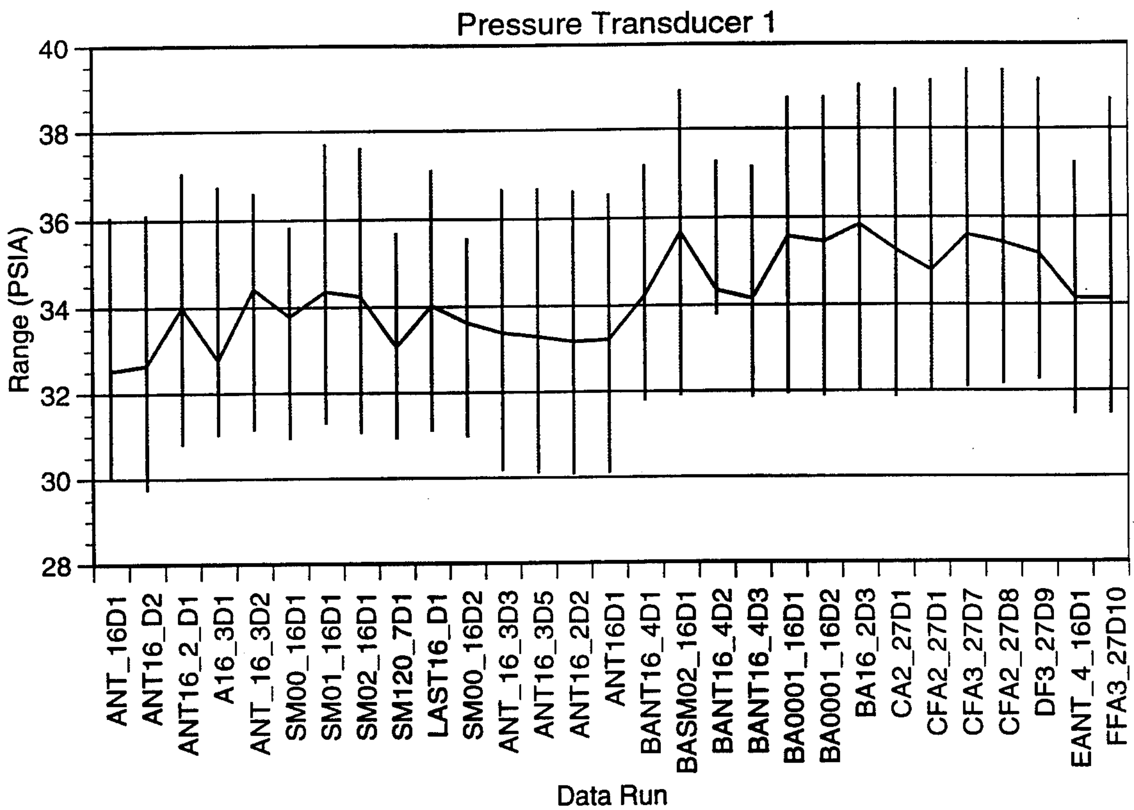

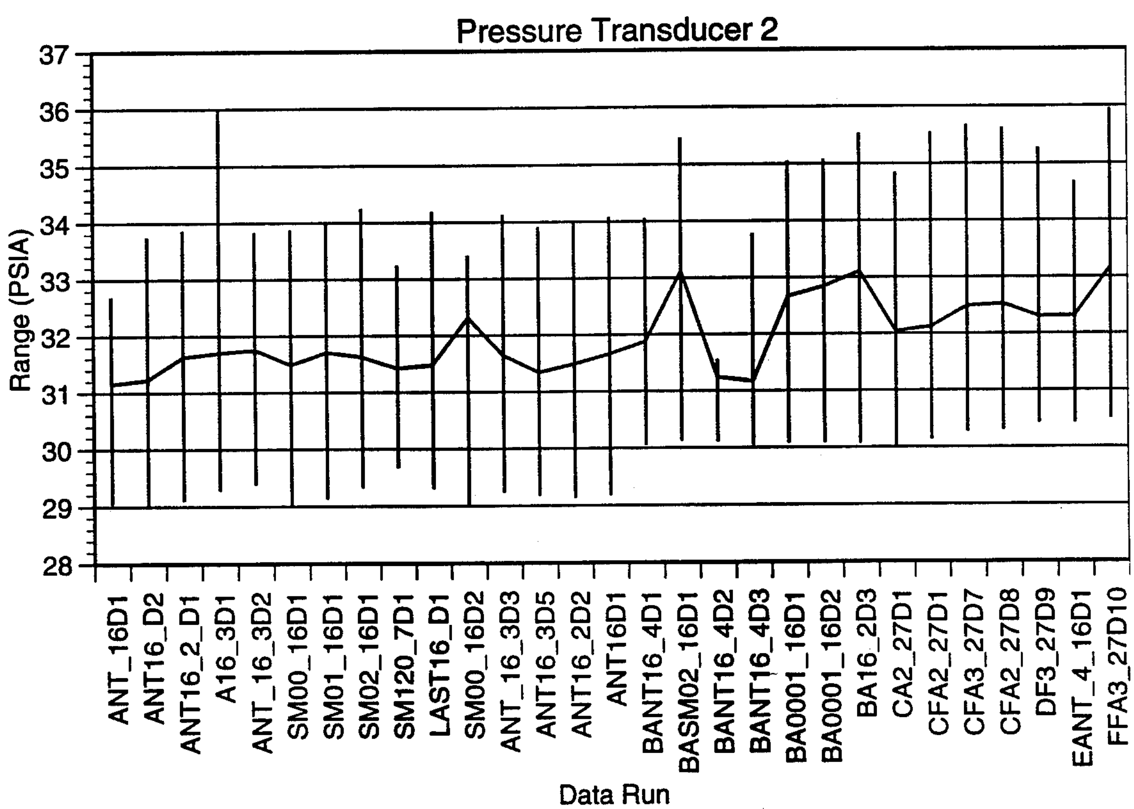

Figure H–1 Pressure Transducer Maximims, Minimums and Averages

Figure H–2 ANT16_2_D1 Environmental Data Profile

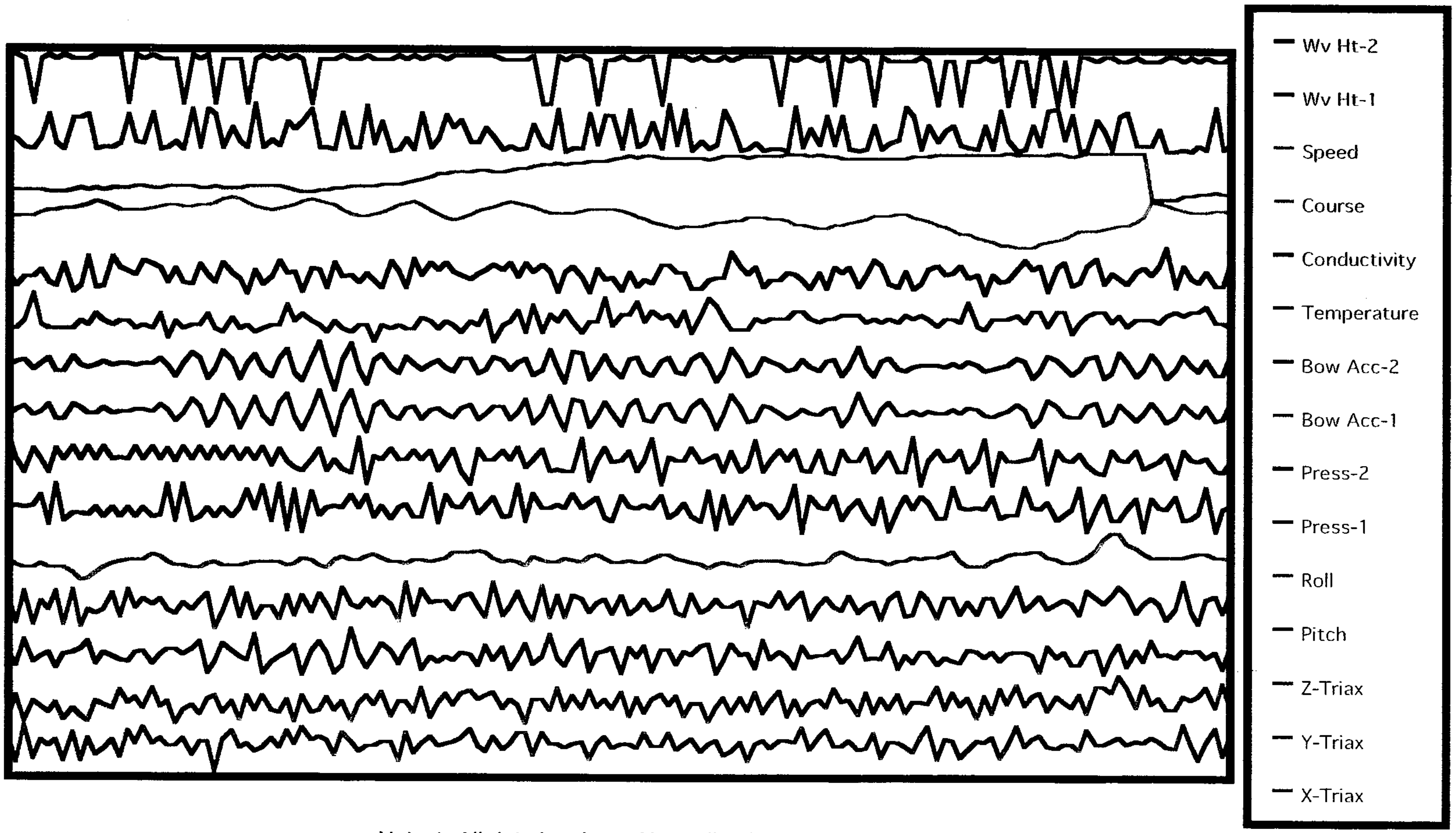

Note 1: All data has been Normalized to a relative scale of **1.**
Note 2:The shaded zone represents the time envelope of the APL comparison.

Figure H–3 ANT_16_3D3 Environmental Data Profile

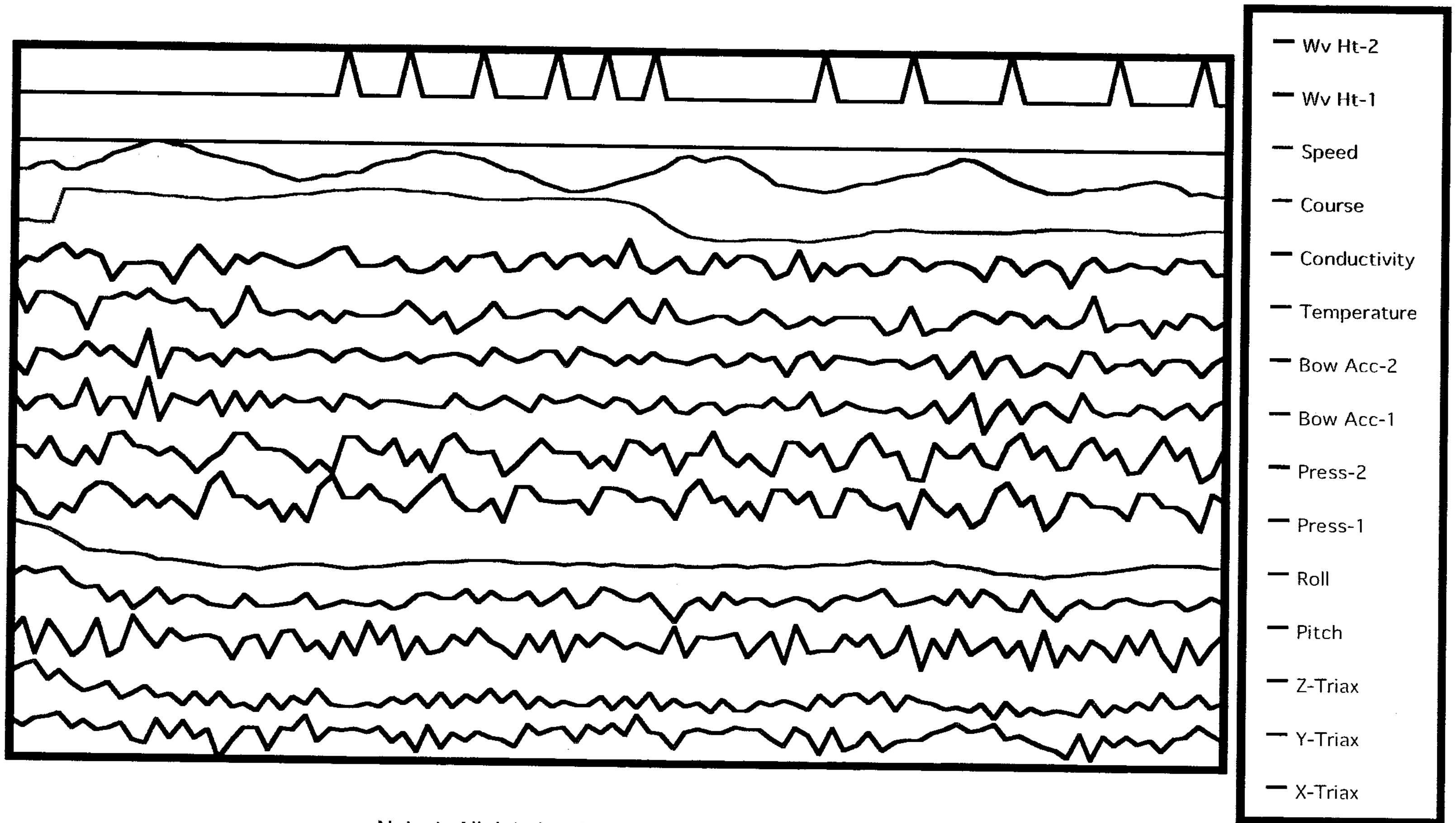

Note 1: All data has been Normalized to a relative scale of 1.
Note 2:The shaded zone represents the time envelope of the APL comparison.